



National Library
of Canada

Acquisitions and
Bibliographic Services Branch

395 Wellington Street
Ottawa, Ontario
K1A 0N4

Bibliothèque nationale
du Canada

Direction des acquisitions et
des services bibliographiques

395, rue Wellington
Ottawa (Ontario)
K1A 0N4

Your file Votre référence

Our file Notre référence

NOTICE

The quality of this microform is heavily dependent upon the quality of the original thesis submitted for microfilming. Every effort has been made to ensure the highest quality of reproduction possible.

If pages are missing, contact the university which granted the degree.

Some pages may have indistinct print especially if the original pages were typed with a poor typewriter ribbon or if the university sent us an inferior photocopy.

Reproduction in full or in part of this microform is governed by the Canadian Copyright Act, R.S.C. 1970, c. C-30, and subsequent amendments.

AVIS

La qualité de cette microforme dépend grandement de la qualité de la thèse soumise au microfilmage. Nous avons tout fait pour assurer une qualité supérieure de reproduction.

S'il manque des pages, veuillez communiquer avec l'université qui a conféré le grade.

La qualité d'impression de certaines pages peut laisser à désirer, surtout si les pages originales ont été dactylographiées à l'aide d'un ruban usé ou si l'université nous a fait parvenir une photocopie de qualité inférieure.

La reproduction, même partielle, de cette microforme est soumise à la Loi canadienne sur le droit d'auteur, SRC 1970, c. C-30, et ses amendements subséquents.

Canada

UNIVERSITY OF ALBERTA

WELL TEST ANALYSIS FOR COMPOSITE RESERVOIRS IN VARIOUS FLOW
GEOMETRIES

BY

MOHAMMED BEN ISSAKA



A thesis submitted to the Faculty of Graduate Studies and Research in partial fulfillment of
the requirements for the degree of DOCTOR OF PHILOSOPHY

IN

PETROLEUM ENGINEERING

DEPARTMENT OF MINING, METALLURGICAL AND PETROLEUM
ENGINEERING

EDMONTON, ALBERTA

SPRING, 1996



National Library
of Canada

Acquisitions and
Bibliographic Services Branch

395 Wellington Street
Ottawa, Ontario
K1A 0N4

Bibliothèque nationale
du Canada

Direction des acquisitions et
des services bibliographiques

395, rue Wellington
Ottawa (Ontario)
K1A 0N4

Votre file *Votre référence*

Votre file *Notre référence*

The author has granted an irrevocable non-exclusive licence allowing the National Library of Canada to reproduce, loan, distribute or sell copies of his/her thesis by any means and in any form or format, making this thesis available to interested persons.

L'auteur a accordé une licence irrévocable et non exclusive permettant à la Bibliothèque nationale du Canada de reproduire, prêter, distribuer ou vendre des copies de sa thèse de quelque manière et sous quelque forme que ce soit pour mettre des exemplaires de cette thèse à la disposition des personnes intéressées.

The author retains ownership of the copyright in his/her thesis. Neither the thesis nor substantial extracts from it may be printed or otherwise reproduced without his/her permission.

L'auteur conserve la propriété du droit d'auteur qui protège sa thèse. Ni la thèse ni des extraits substantiels de celle-ci ne doivent être imprimés ou autrement reproduits sans son autorisation.

ISBN 0-612-10598-9

Canada

University of Alberta

Library Release Form

Name of Author:

Mohammed Ben Issaka

Title of Thesis:

Well Test Analysis for Composite
Reservoirs in Various Flow Geometries

Degree:

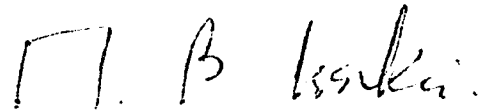
Doctor of Philosophy

Year this Degree Granted:

1996

Permission is hereby granted to University of Alberta Library to reproduce single copies of this thesis and to lend or sell such copies for private, scholarly or scientific research purposes only.

The author reserves all other publication and other rights in association with the copyright in the thesis, and except as hereinbefore provided, neither the thesis nor any substantial portion thereof may be printed or otherwise reproduced in any material form whatever without the author's prior written permission.



7129 Hunterville Rd. NW.

Calgary, Alberta

T2K 4J7

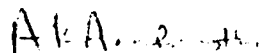
January 26, 1996

THE UNIVERSITY OF ALBERTA
FACULTY OF GRADUATE STUDIES AND RESEARCH

The undersigned certify that they have read, and recommend to the Faculty of Graduate Studies and Research for acceptance, a thesis entitled " WELL TEST ANALYSIS FOR COMPOSITE RESERVOIRS IN VARIOUS FLOW GEOMETRIES" submitted by MOHAMMED BEN ISSAKA in partial fulfillment of the requirements for the degree of DOCTOR OF PHILOSOPHY in PETROLEUM ENGINEERING.



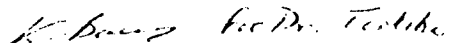
Dr. K. Barron (Chairman)



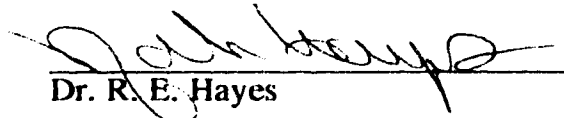
Dr. A. K. Ambastha (Supervisor)



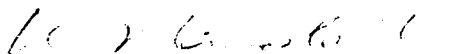
Dr. R. G. Bentsen



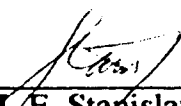
Dr. W. S. Tortike



Dr. R. E. Hayes



Dr. K. Nandakumar



Dr. J. F. Stanislav

DATED: January 21 , 1996

DEDICATION

*To my Mom,
Fati Abalami
and
to the loving memory of my Dad,
Akanbelkum*

ABSTRACT

A composite reservoir is made up of two or more concentric regions with different rock and fluid properties. In well-test analysis for thermal recovery projects, reservoirs have mostly been idealized as radial, composite systems. This idealization is adequate if the reservoir is homogeneous and isotropic, and the well is vertical and not fractured. However, the increasing scope and complexity of thermal recovery projects, as well as, the general heterogeneity of petroleum reservoirs, have necessitated the consideration of different flow geometries other than radial. Steam injection in a fractured well or an anisotropic reservoir, may result in an elliptical swept region. A partially-completed injection well may create a spherically-shaped swept region, while steam injection in a linear or channel reservoir may result in a linear, composite reservoir.

The main objective of this study is to compare, in a comprehensive and systematic manner, the transient pressure and rate behavior of composite reservoirs in radial, elliptical, linear and spherical flow geometries. Normalizing factors to enable comparison of pressure derivative and rate responses for the various flow geometries have been presented. The effect of mobility and storativity ratio on the pseudosteady state behavior of the various composite reservoirs has been investigated. Conditions have been established for the occurrence of pseudosteady state flow for various flow geometries. As well, a generalized pressure derivative is presented that eases the identification of flow regimes characteristic of the various flow geometries. New design and analysis equations based on the generalized pressure derivative have been developed for well testing of composite reservoirs in the various flow geometries. A comparison of the production decline from the various composite reservoirs has also been undertaken. Some type curves for decline curve analysis of linear and radial composite reservoirs are presented.

Finally, a new analytical model for the transient pressure behavior of a three-region composite reservoir with power law property variation in the intermediate region is presented. This model, which accounts for smooth changes in mobility and storativity ahead of the flood front in thermal recovery processes, offers a significant improvement over the sharp-front idealizations of the composite reservoir models currently available.

ACKNOWLEDGEMENTS

I wish to express my sincere gratitude and appreciation to Dr. A. K. Ambastha for his guidance and support throughout this study. Financial support for this work and my graduate studies was provided by a research contract from the Alberta Oil Sands Technology and Research Authority (AOSTRA) and research grants from Chevron Oil Field Research Company, La Habra and NSERC. for which I am very thankful. I would also like to thank Louis Mattar of Fekete Associates Inc., Calgary, for his support and insightful discussions during the writing of this thesis. Finally, I wish to acknowledge the patience, understanding and support of my wife, Esi Toku-Afriyie, and my daughters Fauzia, Sharifah and Janaan during my graduate studies.

TABLE OF CONTENTS

<u>Chapter</u>	<u>Page</u>
1.0 INTRODUCTION	1
2.0 ANALYTICAL SOLUTIONS FOR COMPOSITE RESERVOIRS IN VARIOUS FLOW GEOMETRIES	8
2.1 Introduction	8
2.2 Constant Rate Solutions	10
2.2.1 Radial, Composite Reservoir	10
2.2.2 Elliptical, Composite Reservoir	16
2.2.3 Linear, Composite Reservoir	21
2.2.4 Spherical, Composite Reservoir	25
2.3 Wellbore Storage and Skin	29
2.4 Constant Pressure Solutions	30
2.5 Description of Computer Program	31
2.6 Computational Considerations	33
2.7 Possible Applications	34
3.0 EVALUATION OF THE PSEUDOSTEADY STATE METHOD FOR VARIOUS COMPOSITE RESERVOIRS	41
3.1 Introduction	41
3.2 Comparison of Solutions	45
3.2.1 Radial Reservoir	45
3.2.2 Elliptical Reservoir	46
3.2.3 Linear Reservoir	46
3.2.4 Spherical Reservoir	47
3.3 Discussion of Results	48
3.4 Time Criteria for Pseudosteady State Flow	50

4.0	GENERALIZED PRESSURE DERIVATIVE ANALYSIS OF COMPOSITE RESERVOIRS ..	62
4.1	Introduction ..	62
4.2	Generalized Pressure Derivative ..	63
4.3	Discussion ..	64
4.4	Pressure Derivative Analysis and Design Equations ..	65
4.4.1	Spherical, Composite Reservoir ..	66
4.4.1.1	Analysis and Design Equations ..	66
4.4.1.2	General Discussion ..	70
4.4.2	Linear, Composite Reservoir ..	73
4.4.2.1	Analysis and Design Equations ..	73
4.4.2.2	General Discussion ..	76
4.5	Comparison of Analysis and Design Equations ..	77
5.0	DECLINE CURVE ANALYSIS FOR COMPOSITE RESERVOIRS.....	90
5.1	Introduction ..	90
5.2	Solution Description ..	92
5.3	Comparison of Solutions ..	94
5.3.1	Radial Reservoir ..	94
5.3.2	Elliptical Reservoir ..	95
5.3.3	Linear Reservoir ..	96
5.3.4	Spherical Reservoir ..	97
5.4	General Discussion ..	98
5.5	Decline Curve Analysis ..	100
5.5.1	Comparison of Production Decline Curves ..	101
5.5.2	Decline Curve Analysis for Radial, Composite Reservoirs.....	104
5.5.3	Decline Curve Analysis for Linear, Composite Reservoirs.....	106
6.0	THREE-REGION COMPOSITE RESERVOIR WITH POWER-LAW	

VARIATION IN PROPERTIES	120
6.1 Introduction	120
6.2 Mathematical Development	123
6.3 Verification of Solution	131
6.4 Results and Discussion	132
6.4.1 Effect of Intermediate Region Size	133
6.4.2 Effect of Spectral Exponents	135
7.0 DISCUSSION, CONCLUSIONS AND RECOMMENDATIONS	150
7.1 Discussion	150
7.2 Conclusions	152
7.3 Recommendations	156
References	158
APPENDICES	164
Appendix A: Computer Program for Analytical Solutions for Two-Region, Composite Reservoirs of Various Geometries.	164
Appendix B: Derivation of Diffusivity Equation and Its Solution for the Intermediate Region with Power Law Property Variation	183
Appendix C: Computer Program for Analytical Model of a Three-Region, Composite Reservoir With Power Law Property Variation	187

LIST OF TABLES

		Page
Table 3.1:	Time to the end of pseudosteady state behavior corresponding to the inner region of a linear, composite reservoir.	54
Table 3.2:	Time to the end of pseudosteady state behavior corresponding to the inner region of a spherical, composite reservoir.	55
Table 3.3:	Comparison of conditions for the occurrence of a pseudosteady state period of up to $t_{pN} \approx 0.2$ for various composite reservoirs.	56
Table 4.1:	Flow exponents for some selected flow regimes and geometries.....	79
Table 4.2:	Maximum generalized pressure derivative and the time to maximum derivative for a spherical, composite reservoir	80
Table 4.3:	Time to the beginning of infinite-acting, spherical flow corresponding to the outer region for a spherical, composite reservoir.	81
Table 4.4:	Time to the beginning of infinite-acting, linear flow corresponding to the outer region for a linear, composite reservoir.	82
Table 4.5:	Comparison of analysis equations based on the generalized pressure derivative for composite reservoirs in radial, elliptical, spherical and linear flow geometries.	83
Table 4.6:	Comparison of design equations based on the generalized pressure derivative for composite reservoirs in radial, elliptical, spherical and linear flow geometries.	84

LIST OF FIGURES

	<u>Page</u>
Figure 2.1: Schematic of a two-region, radial, composite reservoir.	36
Figure 2.2: Schematic of a two-region, elliptical, composite reservoir.	37
Figure 2.3: Schematic of a two-region, linear, composite reservoir.	38
Figure 2.4: Schematic of a two-region, spherical, composite reservoir.	39
Figure 2.5: Various geometries and boundary conditions included in the comprehensive model of composite reservoirs.	40
Figure 3.1: Dimensionless semi-log pressure derivative responses for radial, elliptical, linear and spherical, composite reservoirs.	57
Figure 3.2: Dimensionless Cartesian pressure derivative responses for radial, elliptical, linear and spherical, composite reservoirs.	58
Figure 3.3: Comparison of dimensionless semi-log pressure derivative responses for radial and elliptical, composite reservoirs.	59
Figure 3.4: Effect of mobility and storativity ratios on the Cartesian pressure derivative response for a linear, composite reservoir.	60
Figure 3.5: Correlations for the end of pseudosteady state for a linear, composite reservoir.	60
Figure 3.6: Effect of mobility and storativity ratios on the Cartesian pressure derivative response for a spherical, composite reservoir.	61
Figure 3.7: Correlations for the end of pseudosteady state for a spherical, composite reservoir.	61
Figure 4.1: Generalized pressure derivative responses for composite reservoirs	

	in radial, elliptical, spherical and linear flow geometries.	85
Figure 4.2:	Verification of accuracy of the correlation for predicting the maximum generalized pressure derivative for a spherical, composite reservoir.	85
Figure 4.3:	Verification of accuracy of the correlation for predicting the time to the maximum generalized pressure derivative for a spherical, composite reservoir.	86
Figure 4.4:	Verification of accuracy of the correlation for predicting the time to the start of infinite-acting flow in the outer region of a spherical, composite reservoir.	86
Figure 4.5:	Effect of mobility ratio on generalized pressure derivative responses for a spherical, composite reservoir.	87
Figure 4.6:	Effect of storativity ratio on generalized pressure derivative responses for a spherical, composite reservoir.	87
Figure 4.7:	Effect of mobility and storativity ratios on generalized pressure derivative responses for a spherical, composite reservoir.	88
Figure 4.8:	Verification of accuracy of the correlation for predicting the time to the start of infinite-acting flow in the outer region of a linear, composite reservoir.	88
Figure 4.9:	Effect of MF on generalized pressure derivative responses for a linear, composite reservoir.	89
Figure 5.1:	Dimensionless flow rate for composite reservoirs in radial, elliptical, linear and spherical geometries producing at a constant pressure.	109
Figure 5.2:	Dimensionless cumulative production for composite reservoirs in radial, elliptical, linear and spherical geometries producing at a constant pressure.	109

Figure 5.3:	Dimensionless rate responses for closed radial, elliptical, linear and spherical, composite reservoirs producing at a constant pressure. ..	110
Figure 5.4:	Dimensionless cumulative production for closed radial, elliptical, linear, and spherical, composite reservoirs producing at a constant pressure. ..	110
Figure 5.5:	Comparison of dimensionless rate responses for closed radial and elliptical composite reservoirs producing at a constant pressure.	111
Figure 5.6:	Comparison of cumulative production responses for closed, radial and elliptical composite reservoirs producing at a constant pressure. ...	111
Figure 5.7:	Effect of mobility ratio on dimensionless rate responses for a closed, radial, composite reservoir producing at a constant pressure.	112
Figure 5.8:	Effect of mobility ratio on cumulative production responses for a closed, radial, composite reservoir producing at a constant pressure.	112
Figure 5.9:	Effect of storativity ratio on dimensionless rate responses for a closed, radial, composite reservoir producing at a constant pressure.	113
Figure 5.10:	Effect of storativity ratio on cumulative production responses for a closed, radial, composite reservoir producing at a constant pressure.	113
Figure 5.11:	Effect of mobility and storativity ratio on dimensionless rate responses for a closed, radial, composite reservoir producing at a constant pressure.	114
Figure 5.12:	Effect of mobility and storativity ratio on cumulative production responses for a closed, radial, composite reservoir producing at a constant pressure	114
Figure 5.13:	Effect of reservoir size on dimensionless rate responses for a closed, radial, composite reservoir producing at a constant pressure.	115
Figure 5.14:	Effect of reservoir size on cumulative production responses for a closed,	

	radial, composite reservoir producing at a constant pressure.	115
Figure 5.15:	Effect of mobility ratio on dimensionless rate responses for a closed, linear, composite reservoir producing at a constant pressure.	116
Figure 5.16:	Effect of mobility ratio on cumulative production responses for a closed, linear, composite reservoir producing at a constant pressure.	116
Figure 5.17:	Effect of storativity ratio on dimensionless rate responses for a closed, linear, composite reservoir producing at a constant pressure.	117
Figure 5.18:	Effect of storativity ratio on cumulative production responses for a closed, linear, composite reservoir producing at a constant pressure.	117
Figure 5.19:	Effect of mobility and storativity ratio on dimensionless rate responses for a closed, linear, composite reservoir producing at a constant pressure.	118
Figure 5.20:	Effect of mobility and storativity ratio on cumulative production responses for a closed, linear, composite reservoir producing at a constant pressure.	118
Figure 5.21:	Effect of reservoir size on dimensionless rate responses for a closed, linear, composite reservoir producing at a constant pressure.	119
Figure 5.22:	Effect of reservoir size on cumulative production responses for a closed, linear, composite reservoir producing at a constant pressure.	119
Figure 6.1:	Schematic of an infinite three-region, radial, composite reservoir.	140
Figure 6.2:	Schematic of mobility variation with distance for a three-region, radial, composite reservoir.	141
Figure 6.3:	Schematic of storativity variation with distance for a three-region, radial, composite reservoir.	142

Figure 6.4:	Comparison of this study with Fig. 6.46 of <i>Ambastha</i> (1988) solution for an infinitely-large, three-region, composite reservoir.	143
Figure 6.5:	Comparison of this study with Fig. 6.3 of <i>Ambastha</i> (1988) solution for an infinitely-large, two-region, composite reservoir.	143
Figure 6.6:	Comparison of this study with Fig. 2 of Poon (1995) solution for an infinitely-large, two-region, radial, composite reservoir with a fractal outer region.	144
Figure 6.7:	Effect of R_2/R_1 on the semi-log pressure derivative response for an an infinitely-large, three-region, composite reservoir with power law property variation.	145
Figure 6.8:	Effect of R_2/R_1 on the Cartesian pressure derivative response for an an infinitely-large, three-region, composite reservoir with power law property variation.	145
Figure 6.9:	Mobility profile for an infinitely-large, three-region, radial, composite reservoir with power law variation in the intermediate region.	146
Figure 6.10:	Storativity profile for an infinitely-large, three-region, radial, composite reservoir with power law variation in the intermediate region.	146
Figure 6.11:	Effect of θ_1 on the semi-log pressure derivative response for an an infinitely-large, three-region, composite reservoir with power law property variation.	147
Figure 6.12:	Effect of θ_1 on the Cartesian pressure derivative response for an an infinitely-large, three-region, composite reservoir with power law property variation.	147
Figure 6.13:	Effect of θ_2 on the semi-log pressure derivative response for an an infinitely-large, three-region, composite reservoir with power law property variation.	148

Figure 6.14:	Effect of θ_2 on the Cartesian pressure derivative response for an an infinitely-large, three-region, composite reservoir with power law property variation.	148
Figure 6.15:	Effect of equal variations of mobility and storativity on the semi-log pressure derivative response for an infinitely-large, three-region, composite reservoir.	149
Figure 6.16:	Effect of equal variations of mobility and storativity on the Cartesian pressure derivative response for an infinitely-large, three-region, composite reservoir.	149

NOMENCLATURE

a	=	distance to the discontinuity for linear and spherical flow geometries, m
a_D	=	dimensionless distance to the discontinuity for linear and spherical flow geometries = a/r_w for spherical, and a/l for linear
A	=	area of swept (inner) region, m^2 , or constant in Eq. (4.1)
A_j	=	arbitrary constants in the system of equations for radial geometry
A^{2n}	=	terms in the system of equations for elliptical geometry (Eq. (2.66))
b	=	width of a linear composite reservoir, m
b_D	=	dimensionless width of a linear, composite reservoir = b/l
B	=	Formation volume factor, m^3/Sm^3 , or constant in Eq. (4.1)
B_j	=	arbitrary constants in the system of equations for linear geometry
B_{2n}	=	Fourier coefficients of the system of equations for elliptical flow
B^{2n}	=	terms in the system of equations for elliptical geometry (Eq. (2.67))
c_t	=	total compressibility, Pa^{-1}
ce	=	real, even, periodic Mathieu function of integer order
C	=	wellbore storage constant, m^3/Pa , or constant in Eq. (4.3)
Ce	=	modified Mathieu function of first kind of integer order
C_D	=	dimensionless wellbore storage constant
C_j	=	arbitrary constants in the system of equations for spherical geometry
C_{2n}	=	Fourier coefficients of the system of equations for elliptical flow
C^{2n}	=	terms in the system of equations for elliptical geometry (Eq. (2.68))
D_{2n}	=	Fourier coefficients of the system of equations for elliptical flow
D^{2n}	=	terms in the system of equations for elliptical geometry (Eq. (2.69))
E^{2n}	=	terms in the system of equations for elliptical geometry (Eq. (2.70))
F	=	storativity ratio for a two-region reservoir = $(\phi c_t)_1/(\phi c_t)_2$
F_{12}	=	storativity ratio at the discontinuity between regions 1 and 2

	(three-region) = $(\phi_{c1})_1/(\phi_{c1})_2$
F_{13}	= storativity ratio between regions 1 and 3 (three-region) = $(\phi_{c1})_1/(\phi_{c1})_3$
F_{23}	= storativity ratio at the discontinuity between regions 2 and 3 (three-region) = $(\phi_{c1})_2/(\phi_{c1})_3$
F_{ek}	= modified Mathieu function of second kind of integer order
F_{2n}	= Fourier coefficients of the system of equations for elliptical flow
F^{2n}	= terms in the system of equations for elliptical geometry (Eq. (2.71))
G^{2n}	= terms in the system of equations for elliptical geometry (Eq. (2.72))
h	= reservoir thickness, m
$H^{2,n}$	= terms in the system of equations for elliptical geometry (Eq. (2.73))
I_j	= modified Bessel function of first kind of order j
I_ν	= modified Bessel function of first kind of real order
I^{2n}	= terms in the system of equations for elliptical geometry (Eq. (2.74))
k	= permeability, m ²
K_j	= modified Bessel function of second kind of order j
K_ν	= modified Bessel function of second kind of real order
l	= Laplace parameter
L	= fracture half-length, m
m	= arbitrary exponent in the general polynomial equation for dimensionless wellbore pressure, given by Eq.(4.1)
m_c	= Cartesian slope, Pa/s
M	= mobility ratio for a two-region reservoir = $(k/\mu)_1/(k/\mu)_2$
M_{12}	= mobility ratio at the discontinuity between regions 1 and 2 (three-region) = $(k/\mu)_1/(k/\mu)_2$
M_{13}	= mobility ratio between regions 1 and 3 (three-region) = $(k/\mu)_1/(k/\mu)_3$
M_{23}	= mobility ratio at the discontinuity between regions 2 and 3 (three-region) = $(k/\mu)_2/(k/\mu)_3$

- n = flow exponent in the generalized pressure derivative equation
- p = pressure, Pa
- p_D = dimensionless pressure drop
- \bar{p}_D = dimensionless pressure drop in Laplace space
- p_i = initial reservoir pressure, Pa
- p_{we} = wellbore pressure for elliptical flow geometry, Pa
- p_{wl} = wellbore pressure for linear flow geometry, Pa
- p_{wr} = wellbore pressure for radial flow geometry, Pa
- p_{ws} = wellbore pressure for spherical flow geometry, Pa
- p_{wDe} = dimensionless wellbore pressure (elliptical flow) = $2\pi k_I h(p_i - p_{we})/(q\mu_I B)$
- p_{wDl} = dimensionless wellbore pressure (linear flow) = $k_I b h(p_i - p_{wl})/(q\mu_I B)$
- p_{wDN} = dimensionless normalized wellbore pressure for a flow geometry (see Eqs. 3.2, 3.4, 3.7 and 3.12)
- p_{wDr} = dimensionless wellbore pressure (radial flow) = $2\pi k_I h(p_i - p_{wr})/(q\mu_I B)$
- p_{wDs} = dimensionless wellbore pressure (spherical flow) = $4\pi k_I r_w(p_i - p_{ws})/(q\mu_I B)$
- q = injection or production rate, Sm³/s
- q_D = dimensionless injection or production rate
- \bar{q}_D = dimensionless injection or production rate in Laplace space
- q_{De} = dimensionless injection or production rate for elliptical geometry = $q\mu_I B/[2\pi k_I h(p_i - p_{we})]$
- q_{Dl} = dimensionless injection or production rate for linear geometry = $q\mu_I B/[k_I b h(p_i - p_{wl})]$
- q_{Dr} = dimensionless injection or production rate for radial geometry = $q\mu_I B/[2\pi k_I h(p_i - p_{wr})]$
- q_{Ds} = dimensionless injection or production rate for spherical geometry = $q\mu_I B/[4\pi k_I r_w(p_i - p_{ws})]$
- Q = cumulative production or injection, m³

Q_D	=	dimensionless cumulative production or injection
\overline{Q}_D	=	dimensionless cumulative production or injection in Laplace space
Q_{De}	=	dimensionless cumulative production or injection for elliptical geometry
Q_{Dl}	=	dimensionless cumulative production or injection for linear geometry
Q_{Dr}	=	dimensionless cumulative production or injection for radial geometry
Q_{Ds}	=	dimensionless cumulative production or injection for spherical geometry
r	=	radius or radial distance for radial and spherical flow geometries, m
r_D	=	dimensionless distance in radial or spherical geometry = r/r_w
r_{De}	=	dimensionless distance to outer boundary for radial or spherical geometry = r_e/r_w
R	=	discontinuity radius for a two-region, radial composite reservoir, m
R_D	=	dimensionless discontinuity radius for a two-region reservoir = R/r_w
r_{wD}	=	dimensionless wellbore radius (three-region) = r_w/R_1
R_{D2}	=	dimensionless discontinuity radius for region 2 (three-region) = R_2/R_1
R^{2n}	=	terms in the system of equations for elliptical geometry (Eq. (2.76) or (2.80))
S	=	skin factor
t	=	time, s
t_{DA}	=	dimensionless time based on area = $k_{f1}t / [(\phi\mu c_t)_1 A]$
t_{De}	=	dimensionless time for elliptical flow = $k_{f1}t / [(\phi\mu c_t)_1 L^2]$
t_{Dl}	=	dimensionless time for linear flow = $k_{f1}t / [(\phi\mu c_t)_1 l^2]$
t_{Dr}	=	dimensionless time for radial flow = $k_{f1}t / [(\phi\mu c_t)_1 r_w^2]$
t_{Ds}	=	dimensionless time for spherical flow = $k_{f1}t / [(\phi\mu c_t)_1 r_w^2]$
$(t_{DN})_{end}$	=	dimensionless time to the end of infinite-acting flow in the inner region
$(t_{DN})_{max}$	=	dimensionless time to the maximum derivative in the transition region
$(t_{DN})_{II}$	=	dimensionless time to the start of infinite-acting flow in the outer region
T^{2n}	=	terms in the system of equations for elliptical geometry (Eq. (2.77) or (2.81))
V_S	=	swept volume, m ³

x	=	distance in linear flow geometry, m
x_D	=	dimensionless distance in linear flow geometry
x_{eD}	=	dimensionless distance to the outer boundary for linear flow geometry = x_e/l
X^{2n}	=	terms in the system of equations for elliptical geometry (Eq. (2.78) or (2.82))
x, y	=	distances in rectangular coordinate system
Y^{2n}	=	terms in the system of equations for elliptical geometry (Eq. (2.79) or (2.83))
z	=	variable defined in Eq. (2.49)
\bar{z}	=	variable defined in Eq. (2.50)

Greek Symbols

α	=	parameter defined in Eq. (2.59)
α_{ij}	=	terms in the system of equations for radial geometry
β	=	parameter defined in Eq. (2.60)
β_{ij}	=	terms in the system of equations for linear geometry
Δp_s	=	pressure drop due to skin, Pa
Δp_w	=	wellbore pressure drop, Pa
η	=	spatial coordinate in elliptical geometry
λ_{ij}	=	terms in the system of equations for spherical geometry
μ	=	viscosity, Pa-s
ϕ	=	porosity, fraction
θ_1	=	fractal exponent for mobility variation
θ_2	=	fractal exponent for storativity variation
ω	=	diffusivity ratio for a two-region reservoir = $(k/\phi\mu c_t)_1 / (k/\phi\mu c_t)_2$
ω_{12}	=	diffusivity ratio at the discontinuity between regions 1 and 2 for a three-region reservoir = $(k/\phi\mu c_t)_1 / (k/\phi\mu c_t)_2$
ω_{13}	=	diffusivity ratio between regions 1 and 3 for a three-region reservoir

$$= (k/\phi\mu c_f)_i / (k/\phi\mu c_f)_3$$

ξ = spatial coordinate in elliptical geometry

ξ_e = spatial coordinate of outer boundary in elliptical geometry

ξ_w = spatial coordinate of wellbore in elliptical geometry

ξ_o = spatial coordinate of discontinuity boundary in elliptical geometry

Subscripts

D = dimensionless

e = external or outer boundary

e = elliptical flow geometry

i = initial

l = linear flow geometry

N = normalized

r = radial flow geometry

s = spherical flow geometry

t = total

w = wellbore

1 = inner region

2 = outer region for a two-region reservoir or intermediate region
for a three-region reservoir

3 = outer region for a three-region reservoir

2n = periodic

1.0 INTRODUCTION

The pressure transient behavior of composite reservoirs has received considerable attention in the literature. A composite reservoir is made up of two or more regions with different rock and fluid properties. Composite reservoirs may occur naturally, or they may be created artificially. An example of a naturally-occurring composite reservoir is an oil reservoir in communication with an aquifer. Enhanced oil recovery processes such as steam injection, in-situ combustion, polymer flooding and CO₂ miscible flooding provide examples of artificially-created composite reservoirs. Composite reservoirs have also been used to represent reservoirs with a damaged zone around the wellbore (skin) or stimulated wells (*Olarewaju and Lee, 1987a*). In this representation the damaged or stimulated zone becomes the inner region while the rest of the reservoir is the outer region.

To analyze well tests for thermal recovery projects, reservoirs have been idealized mostly as radial, composite reservoirs. A reservoir undergoing steam injection through a fully-penetrating, unfractured, vertical well in a homogeneous, isotropic reservoir may be described as a radial, composite reservoir, consisting of a circular inner steam-swept region and an outer unswept oil region. However, steam injection, in a fractured well or an anisotropic reservoir, may result in an elliptical swept region. A partially-completed injection well may create a spherically-shaped swept region, while steam injection in a linear or channel reservoir may result in a linear, composite reservoir.

Numerous analytical studies of the transient pressure behavior of composite reservoirs have been reported in the literature. While most of these studies have considered radial, composite reservoirs (*Loucks and Guerrero, 1961; Carter, 1966; Bixel and van Poollen, 1967; Eggenschwiler et al., 1980; Olarewaju and Lee, 1987b; Ambastha and Ramey,*

1989), a number of studies have also considered composite reservoirs in other flow geometries. *Bixel et al.* (1963) presented analytical solutions for the buildup and drawdown behavior of composite reservoirs with a linear discontinuity. *Ambastha and Sageev* (1987) and *Poon and Chhina* (1989) have presented analytical solutions for the pressure behavior of linear, composite reservoirs. Analytical solutions of composite reservoirs in an elliptical flow geometry have been presented by *Obut and Ertekin* (1987) and *Stanislav et al.* (1987 and 1992) to approximate the effects of steam injection through a vertically-fractured well. The pressure transient behavior of composite reservoirs in a spherical flow geometry has been presented by *Onyekonwu and Horne* (1983).

To monitor the progress of thermal recovery processes, a knowledge of the swept volume is required. The swept volume will provide, among other things, a measure of the heat loss from the heated zone, and the technical and economic feasibility of the project. *Prats* (1982) has mentioned four of the common methods of estimating the swept volume from thermal recovery projects. These include temperature observation wells, coring, well tests, and mathematical analyses using heat balance.

Among the various methods used to estimate swept volume for thermal recovery projects, well testing has been shown to be relatively quick and inexpensive. Well test data from pressure falloff testing of a steam injection well can be used to estimate the volume of the steam-swept region, based on the pseudosteady state method. The pseudosteady state method, proposed by *Eggenschwiler et al.* (1980), is independent of the shape of the swept region, and is applicable when large mobility and storativity contrasts exist between the swept (inner) and unswept (outer) regions of the reservoir. If the mobility and storativity contrasts are large enough, then it is possible for the swept region to behave like a closed reservoir for a short period of time during the well test. A Cartesian graph of pressure falloff data versus time during this period may yield a straight line, whose slope can be

related to the size of the swept volume. Using an analytical solution for a radial, composite reservoir, *Eggenschwiler et al.* (1980) noted that the mobility contrast between the inner and outer regions of the composite reservoir has to be at least 100 to observe the pseudosteady state flow behavior.

Using Cartesian pressure derivative responses, *Ambastha and Ramey* (1939) established conditions, of mobility and storativity ratio, for the occurrence of pseudosteady state flow for radial, composite reservoirs. *Stanislav et al.* (1992) presented a brief discussion of pseudosteady state flow behavior for an elliptical composite reservoir. To the best of my knowledge, there have been no studies reported in the literature that establish the conditions for the occurrence of pseudosteady state flow for linear and spherical composite reservoirs. A comparison of such conditions for various flow geometries will help in determining when the pseudosteady state method will be appropriate for the estimation of swept volume for thermal recovery projects under various reservoir situations.

Pressure derivatives have been shown to be more sensitive to disturbances in the reservoir than pressure signals, resulting in more detail on derivative graphs than is apparent on pressure graphs. The semi-log pressure derivative, proposed by *Bourdet et al.* (1983), is one of the most widely used pressure derivative functions in well-test analysis. One reason for its popularity is that, for radial reservoirs, the response appears as a horizontal line during the infinite-acting radial flow period, resulting in an easy identification of the flow regime. However, when the semi-log pressure derivative is applied to other flow geometries, such as linear or spherical, the responses are not horizontal, making identification of these flow regimes more difficult. *Jelmert* (1993a and b) has presented a polynomial pressure derivative to simplify the identification of flow regimes for homogeneous reservoirs in other flow geometries. An extension of the theory of the polynomial (or generalized) pressure derivative to the well-test analysis of composite

reservoirs in various flow geometries could yield design and analysis equations based on the derivative responses to augment those based on the pressure responses.

Most composite reservoir models assume a constant flow rate at the well. However, under some testing and production conditions, a constant pressure condition at the well may be more appropriate. A constant pressure condition exists for flowing wells where the surface pressure is controlled. It may also arise in the later stages of a well's history, when the well is drawn down to a constant pressure (*Doe, 1991*). Decline curve analysis is one form of constant-pressure, transient-rate analysis. *Olarewaju and Lee (1987a)* have used production type curves from a constant-pressure, radial, composite model to forecast incremental production from stimulated wells. While production decline curves for radial, composite reservoirs have been discussed fairly well in the literature, the same is not the case for composite reservoirs in elliptical, linear and spherical flow geometries. A comparative study of the production performance of composite reservoirs in the various flow geometries will be a significant addition to the knowledge base of composite reservoir well testing.

Most of the composite reservoir models used to analyze thermal recovery well-test data consist of two regions with different, but uniform, reservoir and fluid properties separated by a sharp interface. In reality, the interface separating the two regions is not sharp. Instead, there is an intermediate region between the inner and outer regions, which is characterized by a sharp decline in mobility and storativity. This has led to the development of three-region, composite reservoir (*Onyekonwu and Ramey, 1986; and Barua and Horne, 1987; Ambastha and Ramey, 1992*), as well as multi-region, composite reservoir solutions (*Acosta and Ambastha, 1994*), to model thermal recovery processes more realistically. In the three-region, composite reservoir model, the intermediate region is represented by a uniform set of mobility and storativity values, that are different from those

in the inner or outer region. In the multi-region, composite reservoir model, the intermediate region is represented by a series of mobility and storativity values that decrease as a step function.

The three-region and multi-region composite reservoir models present some improvements over the two-region composite reservoir model. However, they still have the problem of abrupt changes in mobility and storativity in the intermediate region. Thus, a method that allows for smooth changes in mobility and storativity in the intermediate region will result in a significant improvement over the existing methods. This may be accomplished in a three-region composite reservoir model where the mobility and storativity in the intermediate region are made to decrease in a power law relationship with radial distance.

In the preceding discussion, a brief review of the literature on well test analysis for composite reservoirs in various flow geometries has been presented. A more detailed literature review for individual topics appears in the relevant chapters. Problems with presently available well test analysis models have been pointed out and suggestions for improvement mentioned. Where appropriate, suggestions for the extension of current methods of analysis for homogeneous reservoirs to composite reservoirs have been made. With the present discussion in mind, the main objectives of this study are:

1. To compare, in a comprehensive and systematic manner, the transient pressure behavior of composite reservoirs in radial, elliptical, linear and spherical flow geometries.
2. To establish and compare mobility and storativity conditions for the occurrence of a pseudosteady state flow period of reasonable duration for various flow geometries.

3. To develop a generalized pressure derivative analysis method for composite reservoirs in various flow geometries.
4. To compare production decline curves for composite reservoirs in radial, elliptical, linear and spherical flow geometries.
5. To develop a more realistic three-region composite reservoir model for thermal recovery well test analysis.

Chapter 2 presents the development of the analytical solutions for the transient pressure behavior of two-region, composite reservoirs in radial, elliptical, linear and spherical flow geometries. Solutions with both constant-rate and constant-pressure inner boundary conditions are presented. Wellbore storage and skin effects are included. Possible applications of this model to well-test analysis of composite reservoirs are also discussed. This chapter also presents the algorithm and computer program for the model. The computer program has been written in FORTRAN 77. The Bessel function routines from *IMSL Math Special Functions Library* (1987) were used in the program when needed. Application of this model to integrated well-test analysis for composite reservoirs is explored.

Chapter 3 presents an evaluation of the pseudosteady state method for composite reservoirs in radial, elliptical, linear and spherical flow geometries. The effects of mobility and storativity ratio on the duration of the pseudosteady state period for the various flow geometries are investigated. Normalizing factors to aid in a comparison of the various responses are presented. In Chapter 4, a generalized pressure derivative analysis of well-test data from analytical solutions for the various flow geometries is conducted. Design and analysis equations, based on the generalized pressure derivative, are presented.

Chapter 5 presents a comparison of the injection or production performance of two-region, composite reservoirs in the various flow geometries. Injection or production occurs at a constant pressure, while the outer boundary is considered infinite, closed or at a constant pressure. The effect of mobility and storativity ratios, as well as reservoir size, on the production performances of the various flow geometries are investigated.

Chapter 6 presents an analytical solution for the pressure transient behavior of a three-region, radial, composite reservoir with power law property variation in the intermediate region. Mobility and storativity in the intermediate region decrease as power functions of the radial distance from the first discontinuity boundary. This representation of thermal recovery processes is more realistic than the sharp front idealization of the composite reservoir models currently available. The effects of conductivity indices or fractal exponents for mobility and storativity on the semi-log and Cartesian pressure derivative responses are investigated. Finally, Chapter 7 presents a general discussion and the conclusions of the entire study, as well as recommendations for further studies.

2.0 ANALYTICAL SOLUTIONS FOR COMPOSITE RESERVOIRS IN VARIOUS FLOW GEOMETRIES

2.1 Introduction

Most of the studies of composite reservoirs have considered the reservoir geometry to be radial. *Loucks and Guerrero* (1961) presented analytical solutions for radial, composite reservoirs found using the Laplace transformation. *Carter* (1966) presented solutions for the pressure transient behavior of a closed, radial, composite reservoir with the well producing at a constant rate. *Bixel and van Poolen* (1967) considered the effects of radial discontinuities in composite reservoirs on pressure buildup and drawdown behaviors. They recommended a semi-log type curve matching method to determine the distance to the discontinuity. *Eggenschwiler et al.* (1980) presented an analytical solution in Laplace space for an infinitely-large, two-region, radial, composite reservoir producing at a constant rate, with wellbore storage and skin. *Ambastha* (1988) presented pressure derivative responses for two- and three-region, radial, composite reservoirs with wellbore storage and skin, as well as a thin skin at the discontinuity. The outer boundary of the reservoir was considered to be either infinite, closed or at a constant pressure.

Noting that composite reservoirs are not necessarily radial, *Bixel et al.* (1963) presented solutions for the buildup and drawdown behavior of composite reservoirs with a linear discontinuity. *Ambastha and Sageev* (1987) presented analytical solutions for linear, composite reservoirs including the effects of a thin skin at the discontinuity that may be caused by a partially-communicating fault separating the two regions. *Poon and Chhina* (1989) have also used an analytical model for a linear, composite reservoir to analyze well

test data from a steam injection process where highly permeable communication paths between injection and production wells were observed.

Obut and Ertekin (1987) and *Stanislav et al. (1987)* presented analytical solutions for the transient pressure responses of an infinite-conductivity, vertical fracture in an elliptical, composite reservoir. Recently, *Stanislav et al. (1992)* have presented pressure derivative responses for composite reservoirs in an elliptical flow geometry, including the effects of wellbore storage and skin, as well as a thin skin at the discontinuity.

Onyekonwu and Horne (1983) studied the pressure transient behavior of composite reservoirs in spherical flow geometry. The outer boundary was assumed to be infinite in extent. No wellbore storage or skin effects were considered.

The preceding discussion on composite reservoirs shows that significant studies have been conducted on each of the various flow geometries. However, to the best of my knowledge, no attempt has been made to compare the pressure transient behavior of composite reservoirs in the various flow geometries.

This chapter presents the development of a general analytical pressure transient model for a two-region, composite reservoir. The model encompasses composite reservoirs in radial, elliptical, linear and spherical flow geometries. Wellbore storage and skin effects are included, since these effects are observed in most practical well test data. Solutions with both constant-rate and constant-pressure inner boundary conditions are presented. Constant-rate solutions are developed first in Laplace space for each of the flow geometries. Wellbore storage and skin effects are then added using a method proposed by *van Everdingen and Hurst (1949)*. Subsequently, the constant-rate solutions are converted

to constant-pressure solutions using the well known formula proposed by *van Everdingen* and *Hurst* (1949).

2.2 Constant Rate Solutions

Constant-rate solutions in Laplace space for two-region, composite reservoirs in radial, elliptical, linear and spherical flow geometries are developed first. The following assumptions pertain to the composite reservoirs in all four flow geometries:

1. The formation consists of two discontinuous regions, with homogeneous and isotropic properties on each side of the discontinuity.
2. The front is of infinitesimal thickness, and is considered stationary throughout the test period.
3. Laminar flow of a single phase fluid with slight, but constant, compressibility occurs in each region.
4. Gravity and capillarity effects are negligible.

2.2.1 Radial, Composite Reservoir

In this study, the *Ambastha* (1988) solution is used as a model for the radial, composite reservoir, with some modifications. Wellbore storage and skin at the active well are neglected for now. A constant flow rate at the well is assumed. Also, a thin skin at the discontinuity is not considered. Figure 2.1 shows a schematic of the two-region, radial composite reservoir.

The diffusivity equations, governing fluid flow in a two-region, radial composite reservoir are given by:

$$\frac{1}{r} \frac{\partial}{\partial r} \left(r \frac{\partial p_z}{\partial r} \right) = \left(\frac{\phi \mu c_r}{k} \right)_1 \frac{\partial p_z}{\partial t} \quad \text{for} \quad r_w \leq r \leq R, \text{ and} \quad (2.1)$$

$$\frac{1}{r} \frac{\partial}{\partial r} \left(r \frac{\partial p_z}{\partial r} \right) = \left(\frac{\phi \mu c_r}{k} \right)_2 \frac{\partial p_z}{\partial t} \quad \text{for} \quad R \leq r \leq r_e \text{ (or } < \infty \text{)} . \quad (2.2)$$

In dimensionless form, Eqs. (2.1) and (2.2) become:

$$\frac{1}{r_D} \frac{\partial}{\partial r_D} \left(r_D \frac{\partial p_{D1}}{\partial r_D} \right) = \frac{\partial p_{D1}}{\partial t_D} \quad \text{for} \quad 1 \leq r_D \leq R_D, \text{ and} \quad (2.3)$$

$$\frac{1}{r_D} \frac{\partial}{\partial r_D} \left(r_D \frac{\partial p_{D2}}{\partial r_D} \right) = \omega \frac{\partial p_{D2}}{\partial t_D} \quad \text{for} \quad R_D \leq r_D \leq r_{eD} \text{ (or } < \infty \text{)} . \quad (2.4)$$

Initial conditions:

In dimensionless form, the initial conditions for the two regions are:

$$p_{D1}(r_D, 0) = 0, \text{ and} \quad (2.5)$$

$$p_{D2}(r_D, 0) = 0. \quad (2.6)$$

Inner boundary condition:

Since the flow is laminar, and the rate is constant at the inner boundary (well), Darcy's law is applicable. In dimensionless form, this condition is represented as:

$$\left(\frac{\partial p_{D1}}{\partial r_D} \right)_{r_{D1}} = -1. \quad (2.7)$$

Also, since wellbore storage and skin effects are neglected for now, the dimensionless wellbore pressure is:

$$p_{wD} = p_{D1} \quad \text{for } r_D = 1. \quad (2.8)$$

Conditions at the discontinuity:

At the discontinuity (R_D), it is required that pressures and flow rates be continuous as fluid moves from Region 1 to Region 2. These conditions are expressed as:

$$p_{D1} = p_{D2} \quad \text{for } r_D = R_D, \quad \text{and} \quad (2.9)$$

$$\frac{\partial p_{D2}}{\partial r_D} = M \frac{\partial p_{D1}}{\partial r_D} \quad \text{for } r_D = R_D. \quad (2.10)$$

Outer boundary condition:

The outer boundary may be infinite, closed or at a constant pressure. These conditions are represented as:

$$\text{Infinite:} \quad p_{D2}(r_D, t_{Dr})_{r_D \rightarrow \infty} = 0. \quad (2.11)$$

$$\text{Closed:} \quad \left. \frac{\partial p_{D2}}{\partial r_D} \right|_{r_D = r_{ob}} = 0. \quad (2.12)$$

$$\text{Constant-pressure:} \quad p_{D2}(r_{eD}, t_{Dr}) = 0. \quad (2.13)$$

The dimensionless variables used in Equations (2.3) through (2.13) are defined as follows:

$$p_{D1} = \frac{2\pi k_1 h}{qB\mu_1} (p_i - p_1) . \quad (2.14)$$

$$p_{D2} = \frac{2\pi k_1 h}{qB\mu_1} (p_i - p_2) . \quad (2.15)$$

$$p_{wD} = \frac{2\pi k_1 h}{qB\mu_1} (p_i - p_{wr}) . \quad (2.16)$$

$$t_{Dr} = \frac{k_1}{(\phi\mu c_t)_1} \frac{t}{r_w^2} . \quad (2.17)$$

$$\omega = \frac{(k/\phi\mu c_t)_1}{(k/\phi\mu c_t)_2} . \quad (2.18)$$

$$M = \frac{(k/\mu)_1}{(k/\mu)_2} . \quad (2.19)$$

$$r_D = \frac{r}{r_w} . \quad (2.20)$$

$$r_{cD} = \frac{r_c}{r_w} . \quad (2.21)$$

$$R_D = \frac{R}{r_w} . \quad (2.22)$$

A solution of Eqs. (2.3) and (2.4), subject to the appropriate initial and boundary conditions (Eqs. (2.5) through (2.13)), is carried out in Laplace space. Following the approach of *Ambastha* (1988), and dropping the wellbore storage and skin terms, the dimensionless pressures in Laplace space for Regions 1 and 2 are given in terms of Bessel functions as:

$$\bar{p}_{D1}(r_D, l) = A_1 I_0(r_D \sqrt{l}) + A_2 K_0(r_D \sqrt{l}) \quad \text{for} \quad l \leq r_D \leq R_D \quad (2.23)$$

$$\bar{p}_{D2}(r_D, l) = A_3 I_0(r_D \sqrt{\omega l}) + A_4 K_0(r_D \sqrt{\omega l}) \quad \text{for} \quad R_D \leq r_D \leq r_{eD} \text{ (or } < \infty \text{)}. \quad (2.24)$$

where l is the transformed time variable in Laplace space.

From Eq. (2.8), the dimensionless wellbore pressure in Laplace space is:

$$\bar{p}_{wDr}(l) = A_1 I_0(\sqrt{l}) + A_2 K_0(\sqrt{l}) . \quad (2.25)$$

The constants, A_1 through A_4 , are obtained by solving the system of equations resulting from the use of the boundary condition equations (Eqs. (2.7), and (2.9) through (2.13)).

$$\text{Using Eq. (2.7):} \quad \alpha_{11} A_1 + \alpha_{12} A_2 = \frac{1}{l} , \quad (2.26)$$

$$\text{using Eq. (2.9):} \quad \alpha_{21} A_1 + \alpha_{22} A_2 + \alpha_{23} A_3 + \alpha_{24} A_4 = 0 , \quad (2.27)$$

$$\text{using Eq. (2.10):} \quad \alpha_{31} A_1 + \alpha_{32} A_2 + \alpha_{33} A_3 + \alpha_{34} A_4 = 0, \text{ and} \quad (2.28)$$

$$\text{using Eq. (2.11) or (2.12) or (2.13):} \quad \alpha_{43} A_3 + \alpha_{44} A_4 = 0 . \quad (2.29)$$

The coefficients, α_{ij} , are defined as follows:

$$\alpha_{11} = -\sqrt{l} I_1(\sqrt{l}) . \quad (2.30)$$

$$\alpha_{12} = \sqrt{l} K_1(\sqrt{l}) . \quad (2.31)$$

$$\alpha_{21} = I_0(R_D \sqrt{l}) . \quad (2.32)$$

$$\alpha_{22} = K_0(R_D\sqrt{l}) . \quad (2.33)$$

$$\alpha_{24} = -K_0(R_D\sqrt{\omega l}) . \quad (2.34)$$

$$\alpha_{31} = M\sqrt{l} I_1(R_D\sqrt{l}) . \quad (2.35)$$

$$\alpha_{32} = -M\sqrt{l} K_1(R_D\sqrt{l}) . \quad (2.36)$$

$$\alpha_{34} = -\sqrt{\omega l} K_1(R_D\sqrt{\omega l}) . \quad (2.37)$$

The remaining α 's depend on the specified outer boundary condition. These are given by:

Infinite outer boundary:

Since $I_0(r_D\sqrt{\omega l}) \rightarrow \infty$ as $r_D \rightarrow \infty$, a bounded solution for $\bar{p}_{D2}(r_D \rightarrow \infty, l)$ can be obtained from Eq. (2.24) only if $A_3 = 0$. Consequently, α_{23} , α_{33} , α_{43} in Eqs. (2.27), (2.28) and (2.29) are set to zero. Also $\alpha_{44} = 0$, since $K_0(r_D\sqrt{\omega l}) \rightarrow 0$ as $r_D \rightarrow \infty$, in Eq. (2.29). Thus:

$$\alpha_{23} = \alpha_{33} = \alpha_{43} = \alpha_{44} = 0 . \quad (2.38)$$

Closed outer boundary:

$$\alpha_{23} = -I_0(R_D\sqrt{\omega l}) . \quad (2.39)$$

$$\alpha_{33} = -\sqrt{\omega l} I_1(R_D\sqrt{\omega l}) . \quad (2.40)$$

$$\alpha_{43} = I_1(r_{eD}\sqrt{\omega l}) . \quad (2.41)$$

$$\alpha_{44} = -K_1(r_{eD}\sqrt{\omega l}) . \quad (2.42)$$

Constant-pressure outer boundary:

$$\alpha_{23} = -I_0(R_D \sqrt{\omega l}) . \quad (2.43)$$

$$\alpha_{33} = -\sqrt{\omega l} I_1(R_D \sqrt{\omega l}) . \quad (2.44)$$

$$\alpha_{43} = I_0(r_{eD} \sqrt{\omega l}) . \quad (2.45)$$

$$\alpha_{44} = K_0(r_{eD} \sqrt{\omega l}) . \quad (2.46)$$

To obtain the dimensionless wellbore pressure, and also the pressure derivative, Eq. (2.25) is numerically inverted from Laplace space into real space using the *Stehfest* (1970) algorithm.

2.2.2 Elliptical, Composite Reservoir

The model used for the elliptical, composite reservoir is similar to that of *Stanislav et al.* (1992), with wellbore storage and skin effects being neglected. The reservoir consists of two distinct elliptical regions, as shown in Fig. 2.2. An elliptical swept region is assumed to occur in the presence of an infinite-conductivity, vertical fracture. The vertically-fractured well is located at the center of the inner region, and fully penetrates the formation.

In rectangular coordinates, the two-dimensional diffusivity equations for Regions 1 and 2 are:

$$\frac{\partial^2 p_z}{\partial x^2} + \frac{\partial^2 p_z}{\partial y^2} = \left(\frac{\phi \mu c_f}{k} \right)_z \frac{\partial p_z}{\partial t} \quad \text{and} \quad (2.47)$$

$$\frac{\partial^2 p_z}{\partial x^2} + \frac{\partial^2 p_z}{\partial y^2} = \left(\frac{\phi \mu c_f}{k} \right)_z \frac{\partial p_z}{\partial t} . \quad (2.48)$$

Equations (2.47) and (2.48) can be transformed into elliptic coordinates by use of two variables, z and \bar{z} , defined as:

$$z = x + iy = L \cosh(\xi + i\eta) \quad \text{and} \quad (2.49)$$

$$\bar{z} = x - iy = L \cosh(\xi - i\eta). \quad (2.50)$$

A detailed description of this transformation was presented by *McLachlan* (1947). In elliptic coordinates, Eqs. (2.47) and (2.48) become:

$$\frac{\partial^2 p_1}{\partial \xi^2} + \frac{\partial^2 p_1}{\partial \eta^2} = \frac{L}{2} (\cosh 2\xi - \cos 2\eta) \left(\frac{\phi \mu c_i}{k} \right)_1 \frac{\partial p_1}{\partial t} \quad \text{for} \quad 0 \leq \xi \leq \xi_0, \text{ and} \quad (2.51)$$

$$\frac{\partial^2 p_2}{\partial \xi^2} + \frac{\partial^2 p_2}{\partial \eta^2} = \frac{L}{2} (\cosh 2\xi - \cos 2\eta) \left(\frac{\phi \mu c_i}{k} \right)_2 \frac{\partial p_2}{\partial t} \quad \text{for} \quad \xi_0 \leq \xi \leq \xi_e (\text{or } < \infty). \quad (2.52)$$

where ξ and η are the spatial coordinates in elliptical geometry, and L is the fracture half-length. The parameter ξ_0 is the elliptic distance to the discontinuity boundary, while ξ_e is the elliptic distance to the outer boundary.

In dimensionless form, the diffusivity equation, in elliptic coordinates for Regions 1 and 2 become:

$$\frac{\partial^2 p_{D1}}{\partial \xi^2} + \frac{\partial^2 p_{D1}}{\partial \eta^2} = \frac{1}{2} (\cosh 2\xi - \cos 2\eta) \frac{\partial p_{D1}}{\partial t_{De}} \quad \text{for} \quad 0 \leq \xi \leq \xi_0, \text{ and} \quad (2.53)$$

$$\frac{\partial^2 p_{D2}}{\partial \xi^2} + \frac{\partial^2 p_{D2}}{\partial \eta^2} = \frac{\omega}{2} (\cosh 2\xi - \cos 2\eta) \frac{\partial p_{D2}}{\partial t_{De}} \quad \text{for} \quad \xi_0 \leq \xi \leq \xi_e (\text{or } < \infty). \quad (2.54)$$

The dimensionless wellbore pressure and time for the elliptical reservoir are defined as:

$$p_{wD} = \frac{2\pi k_1 h}{qB\mu_1} (p_i - p_{wc}) . \quad (2.55)$$

$$t_{Dw} = \frac{k_1}{(\phi\mu c_r)_1} \frac{t}{L^2} . \quad (2.56)$$

Other dimensionless variables, as well as the initial and boundary conditions, are similar to those for a radial, composite reservoir.

Equations (2.53) and (2.54) can be put into a form of Mathieu's equation using a separation of variables technique (*McLachlan*, 1947). A solution to these equations is then carried out in Laplace space. The dimensionless pressures in Laplace space for Regions 1 and 2 are given in terms of Mathieu functions as:

$$\bar{p}_{D1}(\xi, \eta) = \sum_{n=0}^{\infty} ce_{2n}(\eta, -\beta) [C_{2n} Ce_{2n}(\xi, -\beta) + F_{2n} Fek_{2n}(\xi, -\beta)] \text{ for } 0 \leq \xi \leq \xi_w, \quad (2.57)$$

$$\bar{p}_{D2}(\xi, \eta) = \sum_{n=0}^{\infty} ce_{2n}(\eta, -\alpha) [B_{2n} Ce_{2n}(\xi, -\alpha) + D_{2n} Fek_{2n}(\xi, -\alpha)] \text{ for } \xi_w \leq \xi \leq \xi_e (\text{or } < \infty), \quad (2.58)$$

The parameters α and β in Eqs. (2.57) and (2.58) include the Laplace space time variable, l , and are defined as:

$$\alpha = \frac{\omega l}{4} . \quad (2.59)$$

$$\beta = \frac{l}{4} . \quad (2.60)$$

Since wellbore storage and skin are neglected, the dimensionless wellbore pressure in Laplace space is given from Eq. (2.57) as:

$$\bar{p}_{wD}(\xi_w, \eta) = \sum_{n=0}^{\infty} ce_{2n}(\eta, -\beta) [C_{2n} Ce_{2n}(\xi_w, -\beta) + F_{2n} Fek_{2n}(\xi_w, -\beta)]. \quad (2.61)$$

By setting $\xi_w = 0$ and $\eta = \pi/2$, Eq. (2.61) becomes a line source solution or the pressure at the fracture face.

The constants B_{2n} , C_{2n} , D_{2n} and F_{2n} , are Fourier coefficients that are obtained by solving the following system of equations resulting from the use of the boundary conditions (Stanislav *et al.*, 1987).

Using the flow rate condition (Darcy's law) at the inner boundary:

$$C_{2n} G^{2n} + F_{2n} H^{2n} = I^{2n}. \quad (2.62)$$

The conditions of pressure and flow rate continuities at the interface boundary yield:

$$C_{2n} A^{2n} + F_{2n} B^{2n} + D_{2n} C^{2n} + B_{2n} R^{2n} = 0, \quad (2.63)$$

$$C_{2n} D^{2n} + F_{2n} E^{2n} + D_{2n} F^{2n} + B_{2n} T^{2n} = 0, \quad (2.64)$$

while the outer boundary condition yields:

$$D_{2n} X^{2n} + B_{2n} Y^{2n} = 0. \quad (2.65)$$

The terms A^{2n} , B^{2n} , C^{2n} , etc., are defined as follows:

$$A^{2n} = Ce_{2n}(\xi_w, -\beta). \quad (2.66)$$

$$B^{2n} = Fek_{2n}(\xi_{in}, -\beta). \quad (2.67)$$

$$C^{2n} = -Fek_{2n}(\xi_{in}, -\alpha). \quad (2.68)$$

$$D^{2n} = Ce'_{2n}(\xi_{in}, -\beta). \quad (2.69)$$

$$E^{2n} = Fek'_{2n}(\xi_{in}, -\beta). \quad (2.70)$$

$$F^{2n} = -\frac{1}{M} Fek'_{2n}(\xi_{in}, -\alpha). \quad (2.71)$$

$$G^{2n} = -Ce'_{2n}(\xi_{in}, -\beta). \quad (2.72)$$

$$H^{2n} = -Fek'_{2n}(\xi_{in}, -\beta). \quad (2.73)$$

$$I^{2n} = \frac{(-1)^n A_0^{2n}}{2\beta}. \quad (2.74)$$

The remaining terms depend on the outer boundary condition.

Infinite outer boundary:

Since $Ce_{2n}(\xi, -\alpha) \rightarrow \infty$ as $\xi \rightarrow \infty$, a bounded solution for $\bar{p}_{D2}(\xi \rightarrow \infty, \eta, l)$ can be obtained from Eq. (2.58) only if $B_{2n} = 0$. Consequently, R^{2n} , T^{2n} , and Y^{2n} in Eqs. (2.63), (2.64) and (2.65) are set to zero. Also, $X^{2n} = 0$ in Eq. (2.65), since $Fek_{2n}(\xi, -\alpha) \rightarrow 0$ as $\xi \rightarrow \infty$ in Eq. (2.58). Thus:

$$R^{2n} = T^{2n} = X^{2n} = Y^{2n} = 0. \quad (2.75)$$

Closed outer boundary:

$$R^{2n} = -Ce_{2n}(\xi_{in}, -\alpha). \quad (2.76)$$

$$T^{2n} = -\frac{1}{M} C e'_{2n}(\xi_{2n}, -\alpha). \quad (2.77)$$

$$X^{2n} = F e k'_{2n}(\xi_{2n}, -\alpha). \quad (2.78)$$

$$Y^{2n} = C e'_{2n}(\xi_{2n}, -\alpha). \quad (2.79)$$

Constant-pressure outer boundary:

$$R^{2n} = -C e_{2n}(\xi_{2n}, -\alpha). \quad (2.80)$$

$$T^{2n} = -\frac{1}{M} C e'_{2n}(\xi_{2n}, -\alpha). \quad (2.81)$$

$$X^{2n} = F e k_{2n}(\xi_{2n}, -\alpha). \quad (2.82)$$

$$Y^{2n} = C e_{2n}(\xi_{2n}, -\alpha). \quad (2.83)$$

2.2.3 Linear, Composite Reservoir

The linear, composite reservoir solution employed in this study is modeled after the *Ambastha and Sageev* (1987) solution. The effect of skin at the discontinuity is, however, neglected. The linear, composite reservoir is rectangular, and considered to be semi-infinite, as shown in Fig. 2.3. Finite outer boundaries are also considered.

The diffusivity equations for the pressure behavior in Regions 1 and 2 are:

$$\frac{\partial^2 p_1}{\partial x^2} = \left(\frac{\phi \mu c_f}{k} \right)_1 \frac{\partial p_1}{\partial t} \quad \text{for } 0 \leq x \leq a, \text{ and} \quad (2.84)$$

$$\frac{\partial^2 p_2}{\partial x^2} = \left(\frac{\phi \mu c_f}{k} \right)_2 \frac{\partial p_2}{\partial t} \quad \text{for } a \leq x \leq x_e \text{ (or } < \infty \text{)}. \quad (2.85)$$

The dimensionless diffusivity equations for Regions 1 and 2 become:

$$\frac{\partial^2 \bar{p}_{D1}}{\partial x_D^2} = \frac{\partial \bar{p}_{D1}}{\partial t_{D1}} \quad \text{for} \quad 0 \leq x_D \leq a_D, \text{ and} \quad (2.86)$$

$$\frac{\partial^2 \bar{p}_{D2}}{\partial x_D^2} = \omega \frac{\partial \bar{p}_{D2}}{\partial t_{D1}} \quad \text{for} \quad a_D \leq x_D \leq x_{eD} \text{ (or } < \infty \text{)}. \quad (2.87)$$

The dimensionless pressure, time and distances are defined, using a characteristic length of unity, as:

$$\bar{p}_{uD1} = \frac{k_z b h}{q B \mu_z} (p_i - p_{u1}). \quad (2.88)$$

$$t_{D1} = \frac{k_1}{(\Phi \mu c_r)_z} \frac{t}{1^2}. \quad (2.89)$$

$$x_D = \frac{x}{1}. \quad (2.90)$$

$$a_D = \frac{a}{1}. \quad (2.91)$$

Other dimensionless variables and boundary conditions are similar to what was presented before for the radial flow geometry.

Transforming Eqs. (2.86) and (2.87) into Laplace space, using the initial conditions, leads to a pair of ordinary differential equations, which can be solved easily. The resulting dimensionless pressures in Regions 1 and 2 in Laplace space are:

$$\bar{p}_{D1}(x_D, l) = B_1 e^{\lambda_{D1} x_D} + B_2 e^{-\lambda_{D1} x_D} \quad \text{for} \quad 0 \leq x_D \leq a_D, \text{ and} \quad (2.92)$$

$$\bar{p}_{D2}(x_D, l) = B_3 e^{a_D \sqrt{l}} + B_4 e^{-a_D \sqrt{l}} \quad \text{for } a_D \leq x_D \leq x_{eD} \text{ (or } < \infty \text{)}. \quad (2.93)$$

Since wellbore storage and skin are neglected for now, the dimensionless pressure at the inner boundary in Laplace space is obtained from Eq. (2.92) by setting $x_D = 0$.

$$\bar{p}_{wD}(l) = B_1 + B_2 \quad (2.94)$$

The constants, B_1 , B_2 , B_3 and B_4 , are obtained by solving the following system of equations resulting from the use of the boundary conditions.

$$\beta_{11} B_1 + \beta_{12} B_2 = \frac{1}{l}. \quad (2.95)$$

$$\beta_{21} B_1 + \beta_{22} B_2 + \beta_{23} B_3 + \beta_{24} B_4 = 0. \quad (2.96)$$

$$\beta_{31} B_1 + \beta_{32} B_2 + \beta_{33} B_3 + \beta_{34} B_4 = 0. \quad (2.97)$$

$$\beta_{43} B_3 + \beta_{44} B_4 = 0. \quad (2.98)$$

The terms, β_{ij} , are defined in the following:

$$\beta_{11} = -\sqrt{l}. \quad (2.99)$$

$$\beta_{12} = \sqrt{l}. \quad (2.100)$$

$$\beta_{21} = e^{a_D \sqrt{l}}. \quad (2.101)$$

$$\beta_{22} = e^{-a_D \sqrt{l}}. \quad (2.102)$$

$$\beta_{24} = -e^{-a_D \sqrt{l}}. \quad (2.103)$$

$$\beta_{31} = \sqrt{l} e^{a_D \sqrt{l}}. \quad (2.104)$$

$$\beta_{32} = -\sqrt{l} e^{-a_D \sqrt{l}}. \quad (2.105)$$

$$\beta_{34} = \frac{\sqrt{\omega l}}{M} e^{-a_D \sqrt{\omega l}}. \quad (2.106)$$

The remaining terms depend on the outer boundary condition.

Infinite outer boundary:

Using the same argument as in the radial and elliptical cases, the infinite outer boundary condition for the linear composite reservoir leads to:

$$\beta_{23} = \beta_{33} = \beta_{43} = \beta_{44} = 0. \quad (2.107)$$

Closed outer boundary: (2.108)

$$\beta_{23} = -e^{a_D \sqrt{\omega l}}. \quad (2.109)$$

$$\beta_{33} = -\frac{\sqrt{\omega l}}{M} e^{a_D \sqrt{\omega l}}. \quad (2.110)$$

$$\beta_{43} = \sqrt{\omega l} e^{a_D \sqrt{\omega l}}. \quad (2.111)$$

$$\beta_{44} = -\sqrt{\omega l} e^{-a_D \sqrt{\omega l}}. \quad (2.112)$$

Constant-pressure outer boundary:

$$\beta_{23} = -e^{a_D \sqrt{\omega l}}. \quad (2.113)$$

$$\beta_{33} = -\frac{\sqrt{\omega l}}{M} e^{u_D \sqrt{\omega l}}. \quad (2.114)$$

$$\beta_{43} = e^{u_D \sqrt{\omega l}}. \quad (2.115)$$

$$\beta_{44} = e^{-u_D \sqrt{\omega l}}. \quad (2.116)$$

2.2.4 Spherical, Composite Reservoir

The *Onyekonwu and Horne* (1983) solution for the pressure behavior of a reservoir with spherically discontinuous properties is used for the spherical, composite reservoir in this study. Figure 2.4 shows a schematic of a spherical, composite reservoir. The reservoir model consists of two concentric spheres, representing the inner and outer regions of the composite reservoir, with the wellbore at the center.

The diffusivity equations for the two regions of the spherical, composite reservoir are:

$$\frac{\partial^2 p_i}{\partial r^2} + \frac{2}{r} \frac{\partial p_i}{\partial r} = \left(\frac{\phi \mu c_i}{k} \right)_i \frac{\partial p_i}{\partial t} \quad \text{for } l \leq r \leq a, \text{ and} \quad (2.117)$$

$$\frac{\partial^2 p_o}{\partial r^2} + \frac{2}{r} \frac{\partial p_o}{\partial r} = \left(\frac{\phi \mu c_o}{k} \right)_o \frac{\partial p_o}{\partial t} \quad \text{for } a \leq r \leq r_e \text{ (or } < \infty \text{)}. \quad (2.118)$$

In dimensionless form, the diffusivity equations become:

$$\frac{\partial^2 p_{Di}}{\partial r_D^2} + \frac{2}{r_D} \frac{\partial p_{Di}}{\partial r_D} = \frac{\partial p_{Di}}{\partial t_D} \quad \text{for } 1 \leq r_D \leq a_D, \text{ and} \quad (2.119)$$

$$\frac{\partial^2 p_{D2}}{\partial r_D^2} + \frac{2}{r_D} \frac{\partial p_{D2}}{\partial r_D} = \omega \frac{\partial p_{D2}}{\partial t_{D2}} \quad \text{for } a_D \leq r_D \leq r_{cD} \text{ (or } < \infty \text{)}. \quad (2.120)$$

The dimensionless pressure and time are defined as:

$$p_{uD} = \frac{4\pi k_l r_w}{qB\mu_1} (p_i - p_{us}). \quad (2.121)$$

$$t_{D2} = \frac{k_l}{(\phi\mu c_r)_l} \frac{t}{r_w^2}. \quad (2.122)$$

The initial and boundary conditions are similar to those for the radial, composite reservoir. A solution of Eqs. (2.119) and (2.120) is accomplished upon transformation into Laplace space. The resulting dimensionless pressures in Regions 1 and 2 are given in Laplace space as:

$$\bar{p}_{D1}(r_D, l) = C_1 \frac{\sinh(r_D \sqrt{l})}{r_D \sqrt{l}} + C_2 \frac{\cosh(r_D \sqrt{l})}{r_D \sqrt{l}} \quad \text{for } 1 \leq r_D \leq a_D, \text{ and} \quad (2.123)$$

$$\bar{p}_{D2}(r_D, l) = C_3 \frac{\sinh(r_D \sqrt{\omega l})}{r_D \sqrt{\omega l}} + C_4 \frac{\cosh(r_D \sqrt{\omega l})}{r_D \sqrt{\omega l}} \quad \text{for } a_D \leq r_D \leq r_{cD} \text{ (or } < \infty \text{)}. \quad (2.124)$$

The dimensionless wellbore pressure in Laplace space is obtained from Eq. (2.123) by setting $r_D = 1$.

$$\bar{p}_{uD}(l) = C_1 \frac{\sinh(\sqrt{l})}{\sqrt{l}} + C_2 \frac{\cosh(\sqrt{l})}{\sqrt{l}}. \quad (2.125)$$

The constants, C_1 , C_2 , C_3 and C_4 , are obtained by solving the following system of equations resulting from the use of the boundary conditions.

$$\lambda_{11}C_1 + \lambda_{12}C_2 = -1. \quad (2.126)$$

$$\lambda_{21}C_1 + \lambda_{22}C_2 + \lambda_{23}C_3 + \lambda_{24}C_4 = 0. \quad (2.127)$$

$$\lambda_{31}C_1 + \lambda_{32}C_2 + \lambda_{33}C_3 + \lambda_{34}C_4 = 0. \quad (2.128)$$

$$\lambda_{43}C_3 + \lambda_{44}C_4 = 0. \quad (2.129)$$

The terms, λ_{ij} , are defined as follows:

$$\lambda_{11} = l \cosh \sqrt{l} - \sqrt{l} \sinh \sqrt{l}. \quad (2.130)$$

$$\lambda_{12} = l \sinh \sqrt{l} - \sqrt{l} \cosh \sqrt{l}. \quad (2.131)$$

$$\lambda_{21} = \sinh(a_D \sqrt{l}). \quad (2.132)$$

$$\lambda_{22} = \cosh(a_D \sqrt{l}). \quad (2.133)$$

$$\lambda_{24} = -\frac{\cosh(a_D \sqrt{\omega l})}{\sqrt{\omega}}. \quad (2.134)$$

$$\lambda_{31} = \cosh(a_D \sqrt{l}) - \frac{\sinh(a_D \sqrt{l})}{a_D \sqrt{l}}. \quad (2.135)$$

$$\lambda_{32} = \sinh(a_D \sqrt{l}) - \frac{\cosh(a_D \sqrt{l})}{a_D \sqrt{l}}. \quad (2.136)$$

$$\lambda_{34} = -\frac{\sinh(a_D \sqrt{\omega l})}{M} + \frac{\cosh(a_D \sqrt{\omega l})}{M a_D \sqrt{\omega l}}. \quad (2.137)$$

The rest of the terms depend on the outer boundary condition.

Infinite outer boundary:

The assumption of an infinitely-large, outer region leads to:

$$\lambda_{23} = \lambda_{33} = \lambda_{43} = \lambda_{44} = 0. \quad (2.138)$$

Closed outer boundary:

$$\lambda_{23} = -\frac{\sinh(a_D \sqrt{\omega l})}{\sqrt{\omega}}. \quad (2.139)$$

$$\lambda_{33} = -\frac{\cosh(a_D \sqrt{\omega l})}{M} + \frac{\sinh(a_D \sqrt{\omega l})}{Ma_D \sqrt{\omega l}}. \quad (2.140)$$

$$\lambda_{43} = \frac{\cosh(r_{eD} \sqrt{\omega l})}{M} - \frac{\sinh(r_{eD} \sqrt{\omega l})}{Mr_{eD} \sqrt{\omega l}}. \quad (2.141)$$

$$\lambda_{44} = \frac{\sinh(r_{eD} \sqrt{\omega l})}{M} - \frac{\cosh(r_{eD} \sqrt{\omega l})}{Mr_{eD} \sqrt{\omega l}}. \quad (2.142)$$

Constant-pressure outer boundary:

$$\lambda_{23} = -\frac{\sinh(a_D \sqrt{\omega l})}{\sqrt{\omega}}. \quad (2.143)$$

$$\lambda_{33} = -\frac{\cosh(a_D \sqrt{\omega l})}{M} + \frac{\sinh(a_D \sqrt{\omega l})}{Ma_D \sqrt{\omega l}}. \quad (2.144)$$

$$\lambda_{43} = \frac{\sinh(r_{eD} \sqrt{\omega l})}{r_{eD} \sqrt{\omega l}}. \quad (2.145)$$

$$\lambda_{44} = \frac{\cosh(r_{eD} \sqrt{\omega l})}{r_{eD} \sqrt{\omega l}}. \quad (2.146)$$

2.3 Wellbore Storage and Skin

The solutions presented so far do not account for wellbore storage or skin effect. To add these effects, new boundary conditions are imposed at the well. Using the radial composite reservoir as an example, the presence of skin at the well is represented as:

$$p_{wD} = p_{mD} - S \left[\frac{\partial p_{mD}}{\partial r_D} \right]_{r_D=1} \quad (2.147)$$

where S is the skin factor.

The wellbore storage condition is represented as:

$$C_D \frac{\partial p_{wD}}{\partial t_D} - \left[\frac{\partial p_{mD}}{\partial r_D} \right]_{r_D=1} = 1, \quad (2.148)$$

where C_D is the dimensionless wellbore storage constant.

The skin factor, S , is defined as:

$$S = \frac{2\pi k h}{q B \mu_i} \Delta p_s, \quad (2.149)$$

where Δp_s is the pressure drop due to skin damage.

The dimensionless wellbore storage constant, C_D , is defined as:

$$C_D = \frac{C}{2\pi h (\phi c_i) r_w^2}. \quad (2.150)$$

where C is the wellbore storage coefficient.

To include the skin and wellbore storage effects into the solution already presented, *van Everdingen* and *Hurst* (1949) developed the problem as a convolution integral. This was solved to yield the dimensionless wellbore pressure including skin and wellbore storage as:

$$\bar{p}_{wD}(l) = \frac{[l \bar{p}_D + S]}{l \{1 + C_D [l \bar{p}_D + S]\}} \quad (2.151)$$

where \bar{p}_D is the dimensionless wellbore pressure in Laplace space without wellbore storage or skin effect.

2.4 Constant Pressure Solutions

Consider the case of a constant pressure inner boundary condition. If a constant pressure condition is imposed at the wellbore, then the injection or production rate must vary with time. Of interest here is the flow rate versus time response for a constant pressure production or injection case. Using Duhamel's principle, *van Everdingen* and *Hurst* (1949) showed that, in Laplace space, the constant-pressure solution is related to the constant-rate solution by the following:

$$\bar{q}_D(l) = \frac{1}{l^2 \bar{p}_{wD}(l)} \quad (2.152)$$

where \bar{q}_D is the Laplace transform of dimensionless rate, q_D , for a constant pressure production condition, and \bar{p}_{wD} is the Laplace transform of the dimensionless wellbore pressure for a constant rate production condition. Thus, the constant pressure solution follows easily, once the constant rate solution is known.

2.5 Description of Computer Program

Figure 2.5 shows various flow geometries and boundary conditions included in this comprehensive model for analysis of composite reservoir well-test data. The computer program for the solutions just described has been written in FORTRAN 77. The complete source code and sample data files are provided in Appendix A. In writing the source code, the following logical sequence has been used:

Main Program: COMPOSITE:

1. Read code for flow geometry via screen.
2. Read name of input data file via screen, and open input file.
The program requires separate input data files to be created for each flow geometry.
3. Depending on the geometry code chosen, the main program calls Subroutine RADDATA, Subroutine ELLDATA, Subroutine LINDATA or Subroutine SPHDATA, for radial, elliptical, linear and spherical geometries, respectively. These subroutines read the necessary input data from the input data file provided.
4. Read the name of output data file via screen, and open output file.
5. Generate a set of time (TD) vector.
6. Call Subroutine INVERT, which numerically inverts the results from Laplace space to real space.

Subroutine INVERT:

Subroutine INVERT uses the Stehfest (1970) algorithm to invert results from Laplace space to real space.

- 6.1 Call Subroutine LAPRAD, Subroutine LAPELL, Subroutine LAPLIN, or Subroutine LAPSPH; depending on the geometry code chosen, to compute the results in Laplace space.

Subroutine LAPRAD

This subroutine computes the dimensionless wellbore pressure and its derivative, or the dimensionless flow rate and cumulative production in Laplace space for the radial flow geometry. These solutions are expressed in terms of modified Bessel functions. Results are returned to INVERT.

Subroutine LAPELL

This subroutine computes the dimensionless wellbore pressure and its derivative, or the dimensionless flow rate and cumulative production in Laplace space for the elliptical flow geometry. These solutions are expressed in terms of real and modified Mathieu functions. Results are returned to INVERT.

Subroutine LAPLIN

This subroutine computes the dimensionless wellbore pressure and its derivative, or the dimensionless flow rate and cumulative production in Laplace space for the linear flow geometry. These solutions are expressed in terms of the exponential function. Results are returned to INVERT.

Subroutine LAPSPH

This subroutine computes the dimensionless wellbore pressure and its derivative, or the dimensionless flow rate and cumulative production in Laplace space for the spherical flow geometry. These solutions are expressed in terms of hyperbolic functions. Results are returned to INVERT.

- 6.2 Invert pressure and Cartesian pressure derivative, or flow rate and cumulative production, to real space and transfer results to main program.
7. Compute semilog pressure derivative or the generalized pressure derivative for the geometry chosen.

8. Write and store results in output file.

2.6 Computational Considerations

For the radial and elliptical geometries, the computational processes involve the calculation of modified Bessel functions of large arguments, especially at small times. This creates an overflow problem, which is eliminated by exponential scaling (*IMSL Math Library*, 1987). For the radial, elliptical and linear geometries, the number of terms in the Laplace inverter, $NL = 8$, was found to be adequate to generate correct results. For the spherical geometry, $NL = 12$, was found to be optimum, even though this choice of NL sometimes led to some instabilities in the computed responses. The results from numerical inversion were verified by comparing with asymptotic analytical solutions for early and late time available in real space for each geometry.

For the elliptical geometry, *IMSL Math Library* (1987) was used to calculate the eigenvalues or characteristic values for the periodic Mathieu functions needed in the solution. To calculate the real and the modified Mathieu functions, subroutines were written based on formulas provided by *McLachlan* (1947). The formulas for modified Mathieu functions are expressed in terms of Bessel functions. Bessel functions of several integer orders are often required. For Bessel functions of multiple integer orders, recurrence relations provided by *Gradshteyn and Ryzhik* (1965) were found to be helpful. Also, it was not possible to generate transient-pressure and rate responses for the elliptical geometry, at dimensionless times, $t_D < 0.1$, due to instabilities in the Mathieu functions at such times.

2.7 Possible Applications

In this study, a general analytical solution for a composite reservoir model has been presented. This model is capable of generating the pressure transient responses for composite reservoirs in radial, elliptical, linear and spherical flow geometries for a constant rate condition, as well as transient-rate responses for a constant pressure injection or production condition.

Reservoirs undergoing a thermal recovery process have been idealized mostly as two-region, radial, composite reservoirs. With this idealization, the size of the inner (swept) region may be determined from pressure falloff test data following constant rate injection, if the mobility and/or storativity ratios between the inner and outer regions are high enough. Situations where the composite reservoir may not be radial, but instead may be elliptical, linear or spherical have been discussed. This model could be used to compare the conditions of mobility and storativity ratios under which the swept volume for these different composite reservoir geometries can be calculated. This model is, however, limited to the analysis of pressure falloff test data after constant rate injection, as opposed to constant pressure injection.

A pressure derivative graph can enhance a pressure signal, and may be more sensitive to disturbances in reservoir conditions. This results in greater detail on a derivative graph than is apparent on a pressure graph. Design and analysis equations based on the logarithmic pressure derivative have been presented for radial, composite reservoirs (*Ambarish and Ramey, 1989*), and to a limited extent, for elliptical, composite reservoirs (*Stooshtay et al., 1992*). Pressure derivatives calculated for the different composite reservoir geometries in this model could be used to develop and compare design and analysis equations for well-test analysis of various composite reservoir flow geometries.

Another application of the model in this study lies in constant pressure injection or in decline curve analysis. From practical considerations, these curves are useful in well performance prediction and rate decline analysis. Constant pressure solutions for radial, composite reservoirs have been presented by *Olarewaju* and *Lee* (1987a and b). To the best of my knowledge, constant pressure solutions for elliptical, linear and spherical, composite reservoirs have not been presented. A comparison of the rate responses in the various flow geometries could be carried out using this model.

This model could also be used in a computerized integrated well-test analysis of composite reservoirs. In this well-test analysis scheme, reservoir parameters are first calculated from well-test data using segmental analysis of straight line portions of the data (*Mattar* and *Santo*, 1995). These parameters then serve as input into an analytical model of the reservoir, which is used to generate synthetic well-test data. The synthetic well-test data are compared to the actual well-test data. The whole procedure may be repeated several times, each time with an improved set of reservoir parameters, until a good match is achieved. If the fit is still not very good, then the reservoir model itself may be altered, and the procedure repeated until there is an acceptable match. The inclusion of wellbore storage and skin effects, as well as accounting for different boundary conditions, makes this model applicable to many practical reservoir-well situations within the context of composite reservoirs.

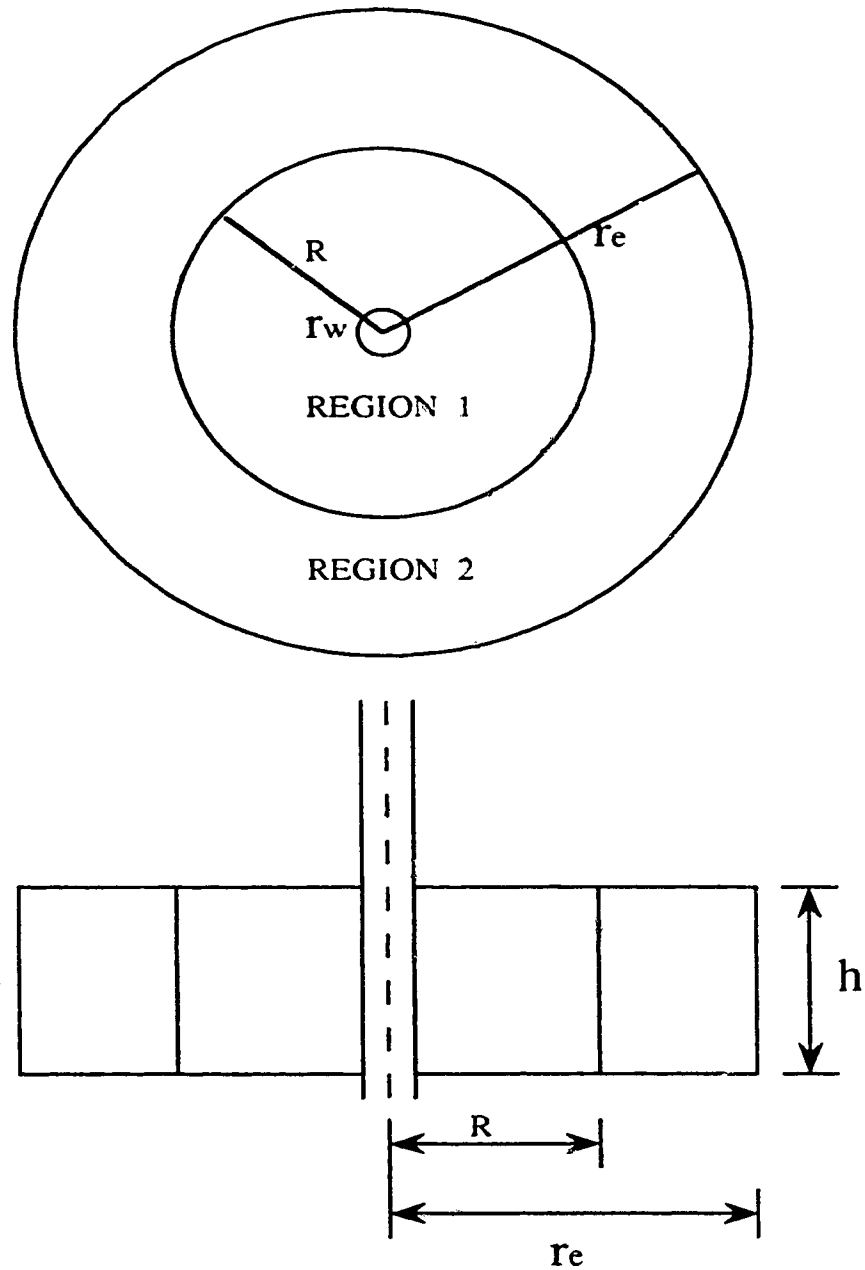


Figure 2.1: Schematic of a two-region, radial, composite reservoir.

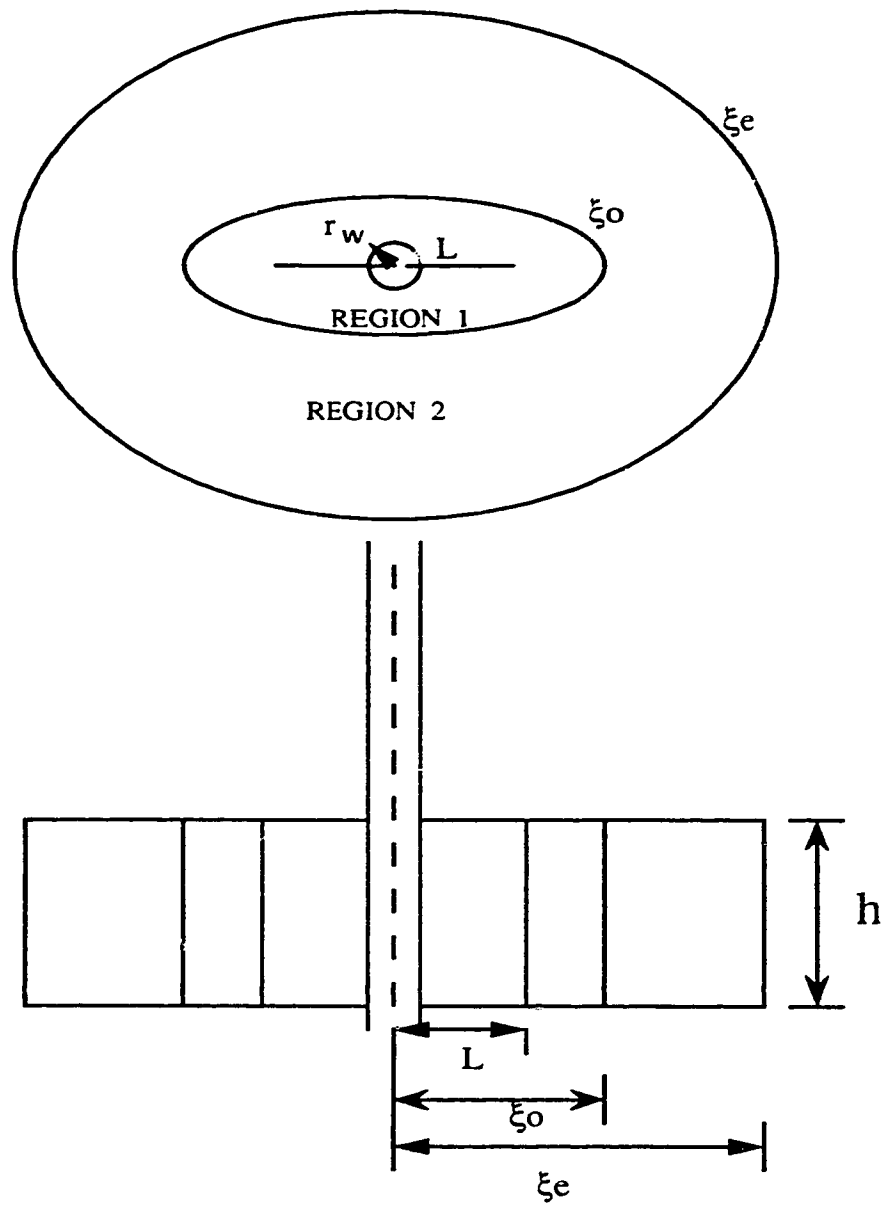


Figure 2.2: Schematic of a two-region, elliptical, composite reservoir.

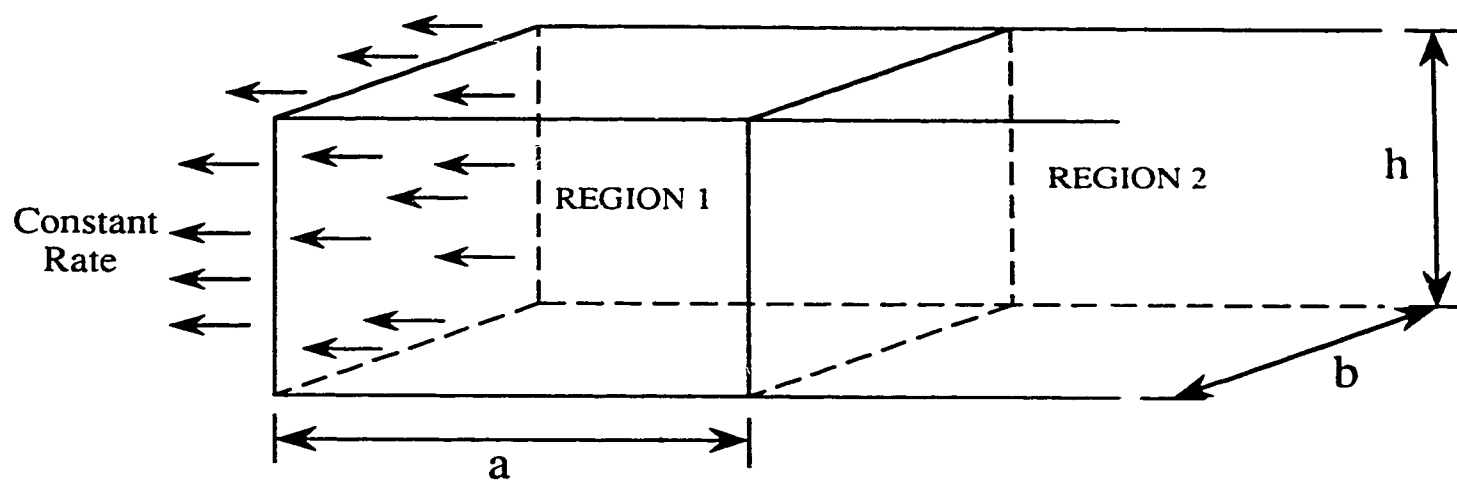


Figure 2.3: Schematic of a two-region, linear, composite reservoir.

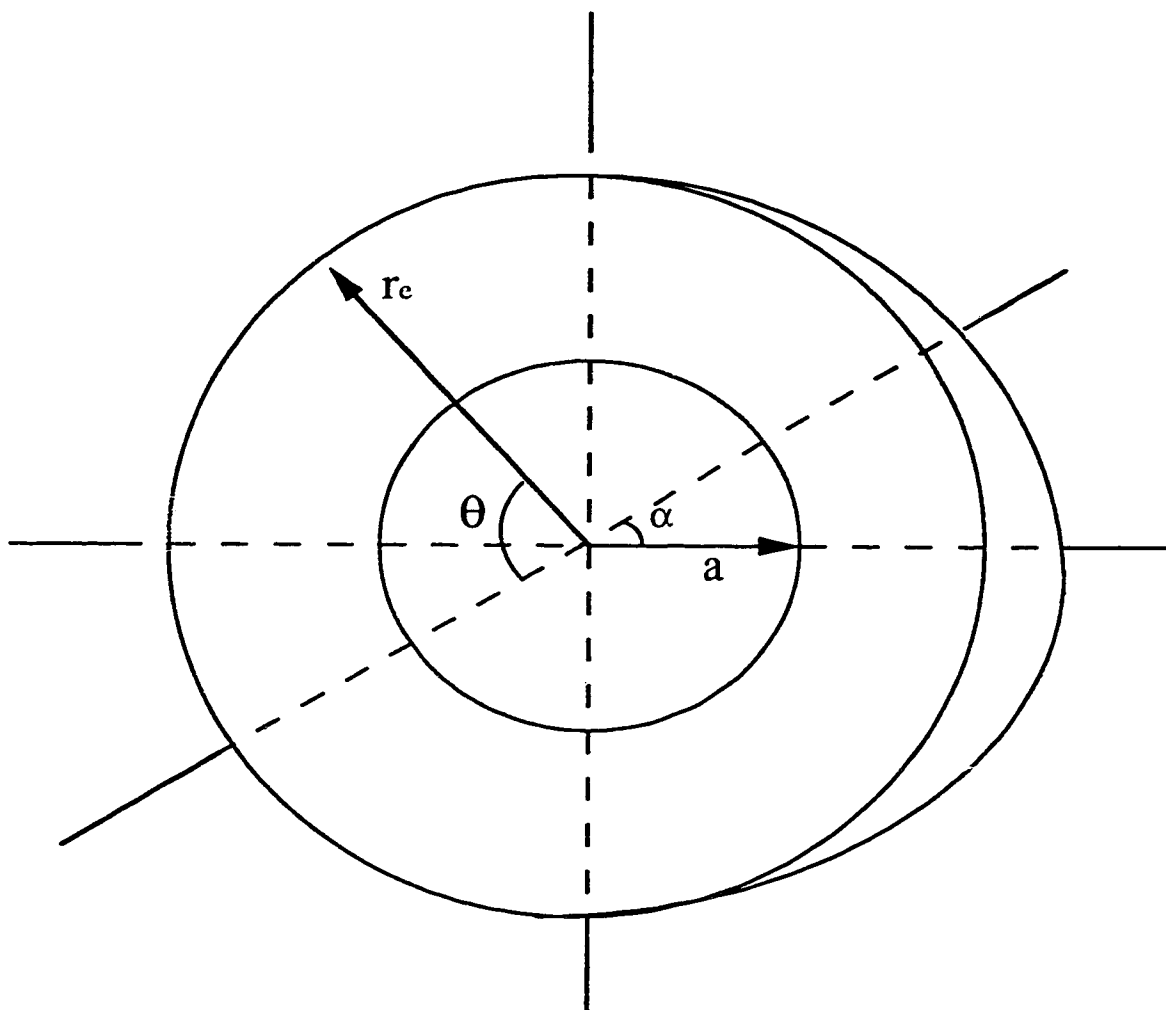


Figure 2.4: Schematic of a two-region, spherical, composite reservoir.

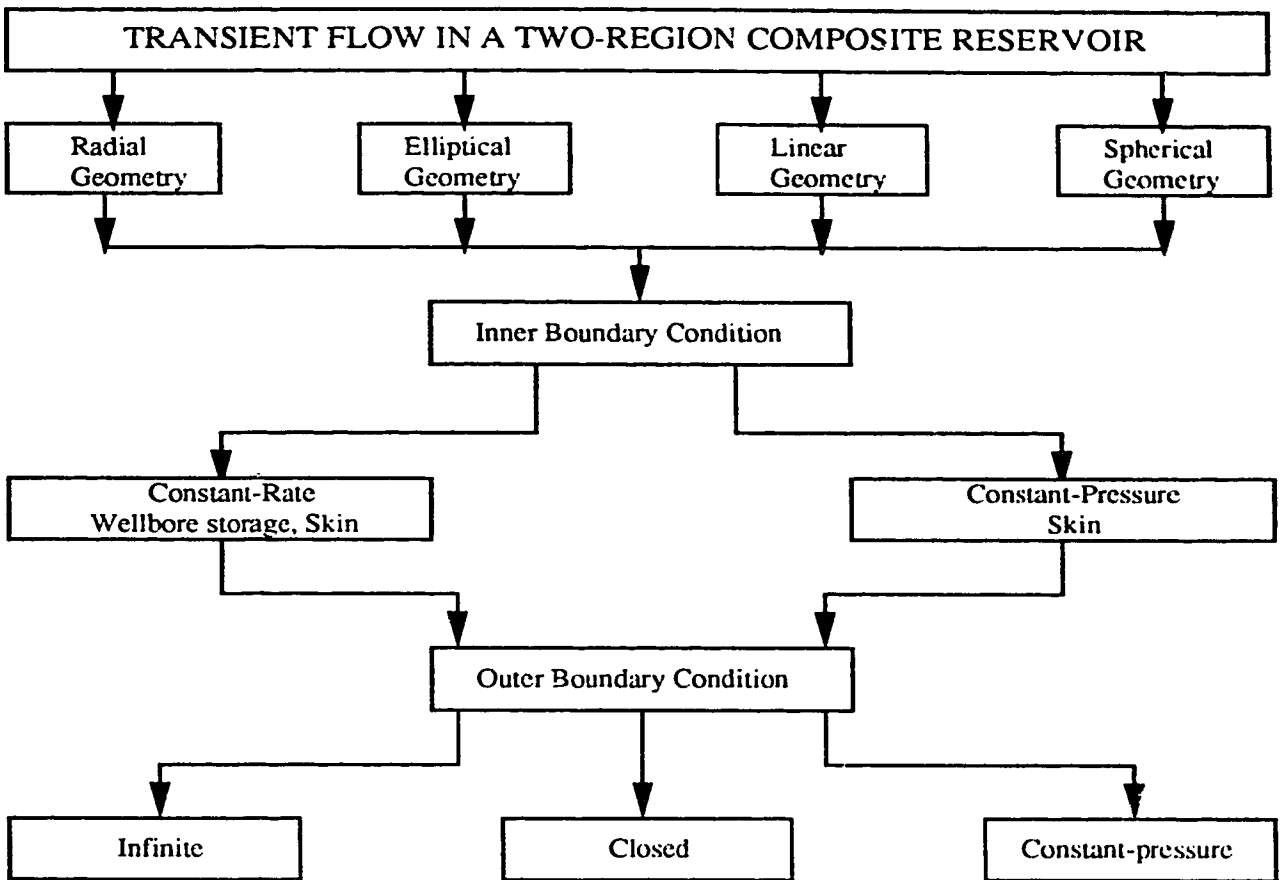


Figure 2.5: Various geometries and boundary conditions included in the comprehensive model of composite reservoirs.

3.0 EVALUATION OF THE PSEUDOSTEADY STATE METHOD FOR VARIOUS COMPOSITE RESERVOIRS

3.1 Introduction

The pseudosteady state method derives from the mobility and storativity contrasts between the inner and outer regions of a composite reservoir. The method was proposed by *Eggenschwiler et al.* (1980) to estimate the volume of the inner region of a radial, composite reservoir. *Eggenschwiler et al.* (1980) observed that if the mobility and storativity contrasts are large, the inner region could behave as a closed reservoir for a short period of time after the end of the first semi-log straight line. A Cartesian graph of pressure versus time during this period may indicate a straight line whose slope, m_c can be related to the swept (inner region) volume, V_s , by:

$$m_c = \frac{qB}{V_s c_f} . \quad (3.1)$$

Several investigators have attempted to confirm the existence of the pseudosteady state period from thermal recovery well-test data. *Walsh et al.* (1981) proposed guidelines for evaluating pressure falloff tests for both steam injection and in-situ combustion wells to determine the swept volume, as well as the heat distribution within the reservoir. They showed that for a steam injection process, accurate determination of the swept volume requires the use of a two-phase effective compressibility, instead of the steam compressibility, for the steam-swept zone. The use of the two-phase compressibility accounts for volumetric changes caused by phase shifts when steam condenses.

Using the *Walsh et al.* (1981) analysis procedure, *Messner and Williams* (1982) analyzed falloff test data from several steamflood projects. Temperature observation wells were included in most of the steam flood projects to aid in verification of the analysis procedure. In addition, *Messner and Williams* (1982) used a fully-implicit, thermal simulator to generate falloff data for a comparative analysis. They concluded that in both the field and the simulated cases, the estimated swept volumes appeared reasonable. There was a difference of about 10% between calculated and actual swept volumes in the simulated cases. Thermal efficiencies were rather low, indicating larger overburden heat losses and more channeling than expected. They stated that the low thermal efficiencies could also be due to the inability of present analysis methods to assess accurately the reservoir heat content ahead of the steam zone. *Messner and Williams* (1982) also found that both field and simulated test results indicated consistently low estimates of the permeability in the swept region. They attributed the low permeability estimates to relative permeability effects.

Further investigations of the applicability of the pseudosteady state method to in-situ combustion projects have been carried out by *Onyekonwu et al.* (1984) and *Da Prat et al.* (1985). *Onyekonwu et al.* (1984) simulated pressure falloff tests of in-situ combustion processes in a one-dimensional, radial reservoir. Analysis of the data using the *Walsh et al.* (1981) procedure yielded calculated swept volumes that were in good agreement with the simulated swept volumes. They, however, found that the swept volume included both the burned volume and the high gas saturation zone ahead of the combustion front. *Da Prat et al.* (1985) applied the pseudosteady state method to the locating of the burning front in an in-situ combustion project in Eastern Venezuela. Two pressure falloff tests were conducted on one air injector. Examination of the falloff data showed that some initial stabilization time was required for the pressure probe to adjust to the ambient temperature. After stabilization, falloff behavior matched theoretical predictions. *Da Prat et al.* (1985)

concluded that the calculated front radius, derived from the burned volume, assuming it to be cylindrical, was consistent with the actual locations of the injector and the producer.

Stanislav et al. (1989) investigated the effect of heat losses on the estimation of swept volume based on the pseudosteady state concept. In analytical solutions of the composite reservoir model for steam injection, the steam zone is assumed to be at a constant temperature. However, heat losses to both the overburden and the underburden can lead to a drop in temperature, resulting in steam condensation. It is, therefore, possible to underestimate the swept volume from analysis of falloff data. *Stanislav et al.* (1989) modified the *Eggenschwiler et al.* (1980) solution to the composite reservoir model by including a term which accounts for heat losses from the steam chamber. They carried out a sensitivity study of the solution to the heat loss term. *Stanislav et al.* (1989) concluded that, under certain conditions, heat losses could have a significant effect on the pressure falloff behavior and dominate the pseudosteady state period. Consequently, they proposed a new analysis procedure for falloff data interpretation, when the heat loss effect is significant.

Fassihi (1988) conducted a study to evaluate the applicability of the pseudosteady state method for estimating swept volume from thermal pressure falloff tests in heterogeneous reservoirs. He used a numerical simulator to simulate injection falloff testing of steamflood and in-situ combustion processes in both radial and two-dimensional (x-y) reservoir models. *Fassihi* (1988) investigated the effect of such parameters as wellbore grid size, non-uniform permeability, layering and oil vaporization, on the estimated swept volume. For steamfloods in relatively homogeneous reservoirs, *Fassihi* (1988) determined that the calculated swept volumes using the pseudosteady state method were in agreement with the simulated volumes. Differences between calculated and simulated swept volumes ranged from 6 to 20 per cent. However, for very heterogeneous reservoirs, there was a very long

transition period that masked the pseudosteady state data, making it impossible to estimate the swept volume.

To determine the swept volume for thermal recovery projects using well test analysis, reservoirs have been idealized as radial, composite reservoirs. However, the increasing scope and complexity of thermal recovery projects, as well as the general heterogeneity of petroleum reservoirs, have necessitated the consideration of different flow geometries, other than radial.

Analytical solutions for the pressure behavior of composite reservoirs of various flow geometries have been presented in the literature. *Ambastha* (1988) presented semi-log and Cartesian pressure derivative responses for two- and three-region, radial, composite reservoirs. A similar study for elliptical, composite reservoirs was presented by *Stanislav et al.* (1992). *Ambastha* and *Sageev* (1987), and *Poon* and *Chhina* (1989) presented analytical solutions for the pressure behavior of linear, composite reservoirs. The pressure transient behavior of composite reservoirs having spherical flow geometry was studied by *Onyekonwu* and *Horne* (1983).

The preceding discussion on composite reservoirs shows that significant analytical studies have been conducted on each of the various flow geometries. However, to the best of my knowledge, no attempt has been made to compare the pressure transient behavior of composite reservoirs in the various flow geometries. Using analytical solutions, this study seeks to compare the pressure behavior of composite reservoirs in radial, elliptical, linear and spherical flow geometries, and, in particular, to establish the conditions under which pseudosteady state flow will occur for each reservoir. Wellbore storage and skin effects are neglected, since their effects, if any, on the pseudosteady state period of all four flow geometries are expected to be the same.

3.2 Comparison of Solutions

Details of the analytical solution used for each of the composite reservoirs was presented in Chapter 2. Schematics of two-region, composite reservoirs in radial, elliptical, linear and spherical flow geometries are presented in Figs. 2.1 through 2.4, respectively. A comparison of the solutions is undertaken by examining the behavior of the dimensionless pressure derivative responses. Both the Cartesian and the semi-log pressure derivatives are considered.

To enable a comparison of the solutions, the dimensionless pressure and time values have to be normalized to account for the different definitions for some of the dimensionless variables in each reservoir. Though not necessary, the radial reservoir solution has been chosen as the reference for the comparison. In addition, the time values for each of the four solutions have been normalized by the area of the inner region of each composite reservoir. Thus, in each reservoir, the results are not affected by the size of the inner region (*Ambastha, 1988; Stanislav et al., 1992*). The normalizing factors for each reservoir are presented in the following.

3.2.1 Radial Reservoir

Since the radial reservoir is the reference, the normalized dimensionless wellbore pressure is equal to the dimensionless wellbore pressure of the radial reservoir.

$$P_{wDv} = P_{wDr} \quad (3.2)$$

The dimensionless variables in Eq. (3.2) and subsequent ones are defined in the Nomenclature.

The normalized time coordinate for the radial reservoir is:

$$t_{DN} = \frac{k_1}{(\phi \mu c_f) r_w^2} \frac{r_w^2 t}{\pi R^2} = \frac{t_{De}}{\pi R_p^2} \quad (3.3)$$

3.2.2 Elliptical Reservoir

Since the dimensionless wellbore pressure for the radial and elliptical reservoirs are equal, by definition,

$$p_{wDN} = p_{wDe} \quad (3.4)$$

The elliptic parameter, ξ_0 , that defines the size of the inner region for the elliptical reservoir is related to the radius of the radial reservoir by (*Stanislav et al.*, 1992):

$$R = \frac{L}{2} e^{\frac{2}{\xi_0}} \quad (3.5)$$

Thus, the normalized time coordinate of the elliptical reservoir becomes:

$$t_{DN} = \frac{L^2}{\pi R^2} t_{De} = \frac{4}{\pi e^{2\xi_0}} t_{De} \quad (3.6)$$

3.2.3 Linear Reservoir

Considering the definitions of dimensionless wellbore pressure for the radial and linear reservoirs, the normalized dimensionless wellbore pressure for the linear reservoir becomes:

$$p_{wDN} = \frac{2\pi}{h_p} p_{wDl} \quad (3.7)$$

The normalizing factor for the time coordinate of the linear reservoir is determined by equating the areas of the inner region for the radial and linear reservoirs.

$$\pi R^2 = ab. \quad (3.8)$$

The normalized time coordinate then becomes:

$$t_{DN} = \frac{1^2}{\pi R^2} t_{DI} = \frac{t_{DI}}{a_D b_D}. \quad (3.9)$$

3.2.4 Spherical Reservoir

Comparing the definitions of dimensionless wellbore pressure for the radial and spherical reservoirs, the normalized dimensionless wellbore pressure for the spherical reservoir becomes:

$$p_{wDN} = \frac{h_D}{2} p_{wDs}. \quad (3.10)$$

Letting $a = R$, and then equating the inner region volumes of the radial and spherical reservoirs, one gets:

$$h_D = \frac{4}{3} a_D. \quad (3.11)$$

Substituting for h_D in Eq. (3.10), the normalized dimensionless wellbore pressure for the spherical reservoir becomes:

$$p_{wDN} = \frac{2}{3} a_D p_{wDs}. \quad (3.12)$$

The normalized time coordinate for the spherical reservoir is:

$$t_{D,u} = \frac{r_w^2}{\pi k h^2} t_{D,s} = \frac{t_{D,s}}{\pi a_D^2}. \quad (3.13)$$

3.3 Discussion of Results

As discussed by *Ambastha* (1988), in the absence of wellbore storage and skin, the parameters that affect the pressure derivative response of an infinitely-large, radial, composite reservoir are the mobility ratio, M ; the diffusivity ratio, ω ; and the dimensionless distance to the discontinuity, R_D . The normalization exercise carried out in the preceding section eliminates the dependence on R_D . The remaining parameters are M and ω . Since, by definition, M is included in ω , a storativity ratio, F , is defined that expresses only the contrast in porosity-compressibility between the inner and outer regions. The storativity ratio is given by:

$$F = \frac{(\phi c_f)_1}{(\phi c_f)_2} = \frac{M}{\omega}. \quad (3.14)$$

Ambastha (1988) presented a sensitivity study for the effect of M and F on the dimensionless semi-log pressure derivative response for radial, composite reservoirs. To compare the pressure derivative responses for the four flow geometries in this study, the values of M and F have been fixed. Figure 3.1 shows a log-log graph of normalized dimensionless semi-log pressure derivative versus normalized time for the four reservoirs. The parameters M and F are 100 and 1000, respectively. The graph shows three clearly defined flow regimes for each case. These flow regimes describe the flow behavior due to the inner region, the discontinuity and the outer region of the various composite reservoirs. The transition between the inner and outer region flow behavior is characterized by unit slope lines of varying lengths for the four flow geometries. A unit slope line, after the inner region flow behavior, on a semi-log pressure derivative graph indicates pseudosteady state behavior. Figure 3.1 shows that, for the same mobility and storativity ratios, the

dimensionless semi-log pressure derivatives for the four flow geometries are identical during pseudosteady state flow for each case. This observation confirms the pseudosteady state method as being independent of the shape of the regularly-shaped swept (inner) region.

Figure 3.1 also shows that pseudosteady state flow starts at the same time for all flow reservoirs. However, the time to the end of pseudosteady state flow varies for different geometrical shapes. The linear flow reservoir shows the longest pseudosteady state period, while the spherical flow reservoir shows the shortest. The radial and elliptical flow reservoirs show the same duration of pseudosteady state flow. Except for the inner region flow behavior, the other pressure derivative characteristics of the radial and elliptical reservoirs seem to be identical.

The responses from the four flow geometries are also compared in Fig. 3.2, which shows a graph of normalized Cartesian pressure derivative versus normalized time for the same parameters as in Fig. 3.1. Once again, three clearly defined flow regimes are shown for each flow geometry. In Fig. 3.2, the transition region between the inner and outer flow regimes is characterized by horizontal lines (zero-slope) of varying lengths. A constant Cartesian pressure derivative, or a horizontal line on a graph of Cartesian pressure derivative versus time, is indicative of pseudosteady state flow. When the responses are normalized by the area of the inner region, as in this study, then the constant Cartesian pressure derivative during pseudosteady state flow should be 2π . Figure 3.2 shows that the linear flow reservoir exhibits the longest pseudosteady state flow period, while the spherical flow reservoir gives the shortest. The radial and elliptical flow reservoirs show the same duration of the pseudosteady state flow period.

A detailed comparison of the responses from radial and elliptical flow reservoirs is shown in Fig. 3.3. The figure shows a log-log graph of normalized dimensionless semi-log pressure derivative versus normalized time for the radial and elliptical reservoirs, with mobility and storativity ratios as cross parameters. The mobility ratio is varied from 1 to 100, while the storativity ratio ranges from 1 to 1000. The effects of mobility and storativity ratios on the semi-log pressure derivative responses for the radial and elliptical, composite reservoirs have been discussed separately by *Ambastha* (1988) and *Stanislav et al.* (1992), respectively. Here, the responses for the two cases are compared. Figure 3.3 confirms the observation made in Figs. 3.1 and 3.2 that the responses for the radial and elliptical reservoirs are identical, except for the inner region responses. Thus, for all practical purposes, thermal well test data for fractured wells can be analyzed using a radial, composite model solution within the context of automated (or automatic) type-curve matching, as long as the early-time linear flow data, due to the presence of the fracture if observed, are excluded from the analysis.

3.4 Time Criteria for Pseudosteady State Flow

To be able to use the pseudosteady state method to determine the swept volume for thermal recovery projects, there should be a means of choosing the correct pseudosteady state Cartesian line. For a well located in the center of a closed drainage region of any regular shape, pseudosteady state behavior may be observed when $t_{DA} > 0.1$, where t_{DA} is based on the drainage area (*Earlougher*, 1977). For a composite reservoir, pseudosteady state behavior should also be observed for $t_{DA} > 0.1$ (t_{DA} based on the area of the inner region), if the mobility and storativity ratios are large enough for the inner region to approximate a closed reservoir. Figures 3.1 and 3.2 show that pseudosteady state behavior is indeed observed for $t_{DN} \geq 0.1$ for all four flow geometries. Recall that the normalized dimensionless time, t_{DN} , is based on the area of the inner region for each composite

reservoir geometry. Since the duration of the pseudosteady state period varies for the different flow geometries, correlations are sought for the time to the end of pseudosteady state flow.

Ambastha (1988) has presented correlations for the time to the end of pseudosteady state flow, based on mobility and storativity ratios, for radial, composite reservoirs. To establish the duration of pseudosteady state flow, *Ambastha* (1988) uses the criteria that the Cartesian pressure derivative be within 2% or 5% of 2π . For the 2% criterion, *Ambastha* (1988) notes that pseudosteady state flow is likely to appear for cases with mobility-storativity product, $MF \geq 10^4$ and $M \geq 10$, if pseudosteady state flow is required to last up to $t_{DA} \approx 0.2$. If the 5% criterion is used, then pseudosteady state behavior is likely to appear for cases with $MF \geq 10^3$ and $M \geq 10$, for pseudosteady state behavior lasting until $t_{DA} \approx 0.2$.

Noting from the previous discussion that the pseudosteady state flow behavior of the elliptical reservoir is identical to the radial reservoir, it follows that, for the elliptical reservoir, pseudosteady state flow lasting up to $t_{DN} \approx 0.2$ occurs for the same conditions as the radial reservoir.

For the linear, composite reservoir, Fig. 3.4 presents Cartesian pressure derivative responses for selected mobility ratios between 1 and 100, and for storativity ratios between 1 and 1000. The transient responses are presented using the correlating parameter, MF , for infinitely-large, linear, composite reservoirs as shown by *Ambastha* and *Sageev* (1987). For pseudosteady state flow to occur, the Cartesian derivative response must be 2π . Fig. 3.4 shows that pseudosteady state flow does occur, the length of which depends on the product of the mobility and storativity ratios. The larger the mobility-storativity product, the longer the duration of the pseudosteady state period.

The normalized dimensionless time, t_{DN} , for the end of the pseudosteady state period, for the linear, composite reservoir, was calculated based on Cartesian pressure derivative deviations of 2% and 5% from 2π . Data for selected cases of mobility and storativity ratios are presented in Table 3.1. Correlations for the time to the end of pseudosteady state flow based on data from Table 3.1 are shown in Fig. 3.5. For the criterion of 2% deviation from 2π , a pseudosteady state period lasting till $t_{DN} \approx 0.2$ is likely for cases of $MF \geq 10^3$. If the 5% criterion is used, then a pseudosteady state period lasting up to $t_{DN} \approx 0.2$ is likely for cases of $MF \geq 10^2$. In Fig. 3.5, the sharp change in trend of the solid curve (2% deviation) just after $MF = 1000$ is due to fact that not enough data were taken. Otherwise the curve should rise smoothly.

For the spherical, composite reservoir, Fig. 3.6 presents Cartesian pressure derivative responses for selected mobility ratios between 1 and 100, and for storativity ratios between 1 and 1000. Figure 3.6 shows that, for the spherical, composite reservoir, the length of the pseudosteady state period is a strong function of the mobility ratio. The storativity ratio has only a mild effect on the duration of the pseudosteady state period. This observation holds true for the radial, composite reservoir, as well (Ambastha, 1988), but is in contrast with the linear, composite reservoir. For the linear, composite reservoir, the length of the pseudosteady state period appears to be equally dependent on both the mobility ratio and the storativity ratio.

Table 3.2 presents selected data used to develop the correlations for the end to pseudosteady state flow for a spherical, composite reservoir. The correlations are shown in Fig. 3.7, for storativity ratios of 100 and 1000. Pseudosteady state behavior was not observed for a storativity ratio of 10. Figure 3.7 shows that for the criterion of 2% deviation from the Cartesian pressure derivative of 2π , a pseudosteady state period lasting

up to $t_{DN} \approx 0.2$ is likely for cases of $MF \geq 10^5$, $M \geq 100$ and $F \geq 100$. If the 5% deviation criterion is used then the required duration of pseudosteady state flow is likely for cases of $MF \geq 10^4$, $M \geq 100$ and $F \geq 100$. Abrupt changes in trend for the three lower curves is due to inadequate data.

The conditions for the time to the end of pseudosteady state flow for the various flow geometries are compared in Table 3.3, for pseudosteady state flow lasting until $t_{DN} \approx 0.2$. This duration of pseudosteady state behavior is considered reasonably long for a proper analysis of the pressure data. For typical reservoir and fluid parameters of a steam injection process ($k=200$ md, $\mu=0.01$ cp, $c_t=0.04$ psi⁻¹, $\phi=0.2$, discontinuity radius =100 ft). $t_{DN} = 0.2$ converts to a pseudosteady state period of about 5 hours. Table 3.3 shows that the conditions for the occurrence of pseudosteady state flow differ for the various flow geometries. The spherical flow geometry requires the highest mobility and storativity contrasts, while the linear flow system requires the least.

Table 3.1: Time to the end of pseudosteady state behavior corresponding to the inner region of a linear, composite reservoir.

MF	t_{DN} for Cartesian slope within 2% of 2π	t_{DN} for Cartesian slope within 5% of 2π
100	0.159	0.195
200	0.169	0.254
500	0.191	0.451
700	0.207	0.594
1000	0.223	0.795
2000	0.286	1.478
5000	0.636	3.533
7000	0.853	4.859
10000	1.164	6.918
20000	2.190	13.660
50000	5.308	34.266
70000	7.380	47.579
100000	10.447	68.031
200000	20.791	135.882
500000	51.981	341.425
700000	72.364	474.082
1000000	103.445	680.310

Table 3.2: Time to the end of pseudosteady state behavior corresponding to the inner region of a spherical, composite reservoir.

M	F	t _{DN} for Cartesian slope within 2% of 2π	t _{DN} for Cartesian slope within 5% of 2π
20 50 70 100 200 500 700 1000	100	0.103 0.118 0.125 0.138 0.191 0.363 0.509 0.704	0.123 0.156 0.234 0.303 0.543 1.272 1.778 2.545
20 50 70 100 200 500 700 1000	1000	0.112 0.143 0.168 0.208 0.342 0.796 1.100 1.541	0.151 0.274 0.358 0.481 0.899 2.225 3.040 4.316

Table 3.3: Comparison of conditions for the occurrence of a pseudosteady state period up to $t_{DN} \approx 0.2$ for various composite reservoirs.

Flow Geometry	Conditions for the occurrence of pseudosteady state for	
	Slope within 2% of 2π	Slope within 5% of 2π
Linear	$MF \geq 10^3$	$MF \geq 10^2$
Radial	$MF \geq 10^4, M \geq 10$	$MF \geq 10^3, M \geq 10$
Elliptical	$MF \geq 10^4, M \geq 10$	$MF \geq 10^3, M \geq 10$
Spherical	$MF \geq 10^5, M \geq 100, F \geq 100$	$MF \geq 10^4, M \geq 100, F \geq 100$

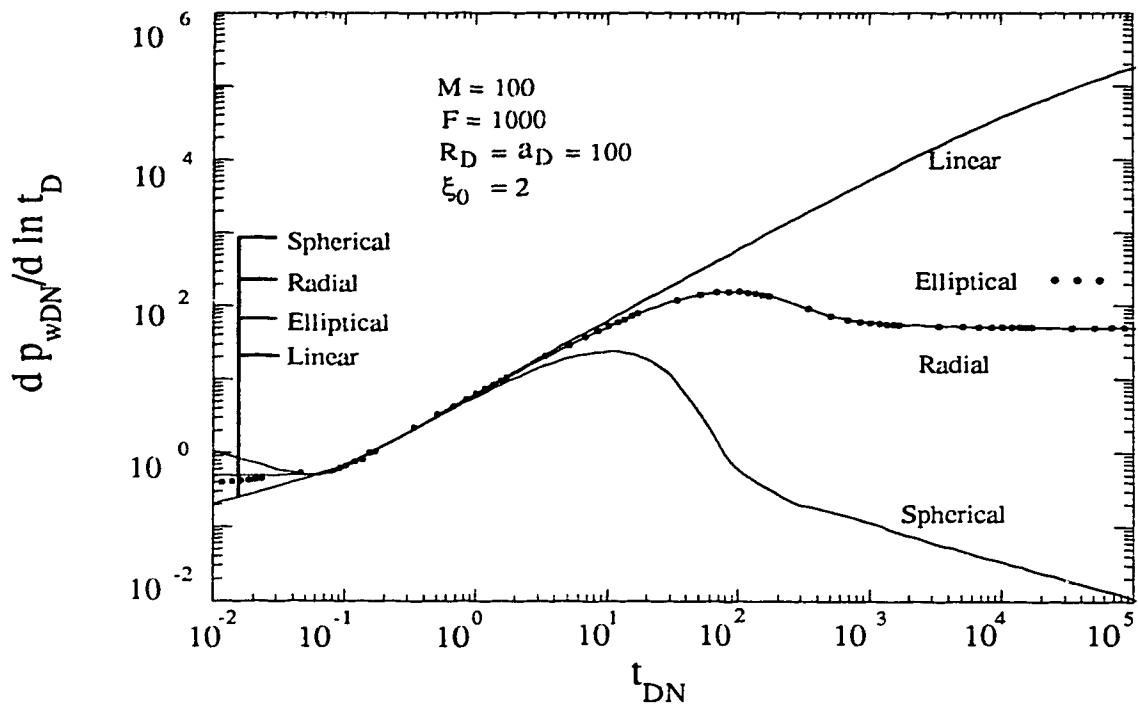


Figure 3.1: Dimensionless semi-log pressure derivative responses for radial, elliptical, linear, and spherical composite reservoirs.

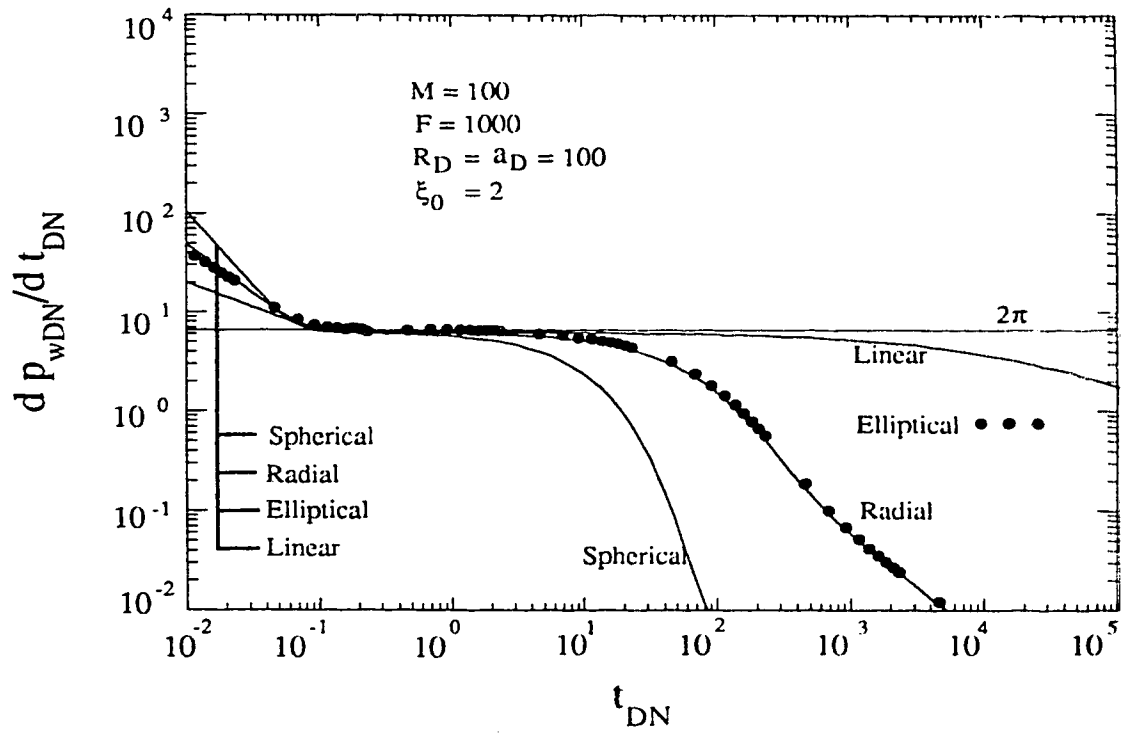


Figure 3.2: Dimensionless Cartesian pressure derivative responses for radial, elliptical, linear and spherical composite reservoirs.

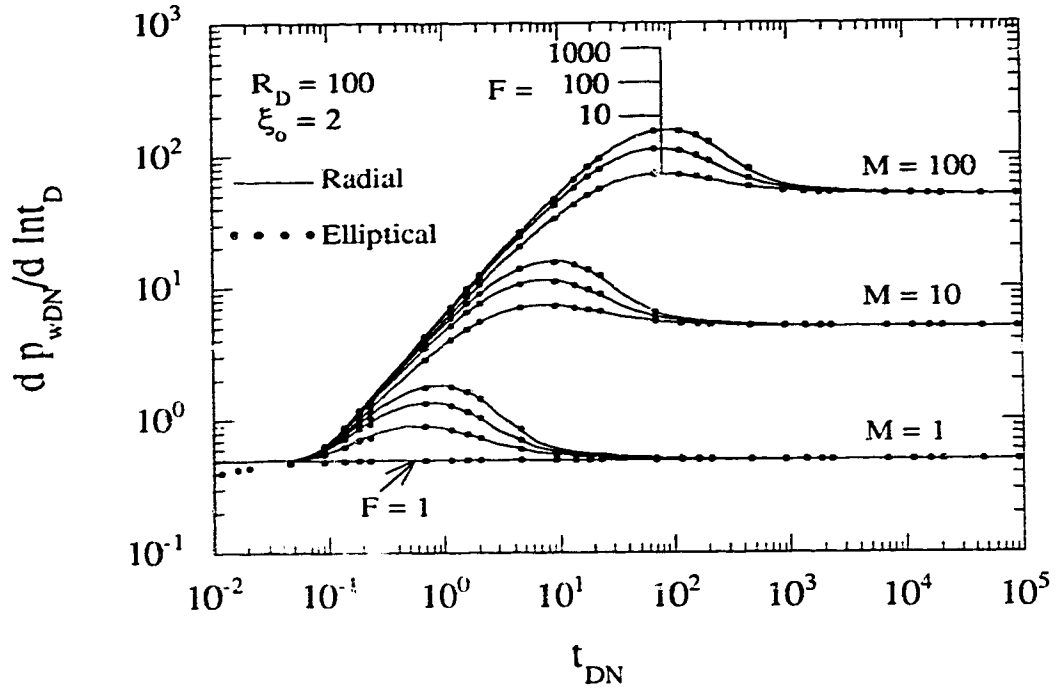


Figure 3.3: Comparison of dimensionless semi-log pressure derivative responses for radial and elliptical composite reservoirs.

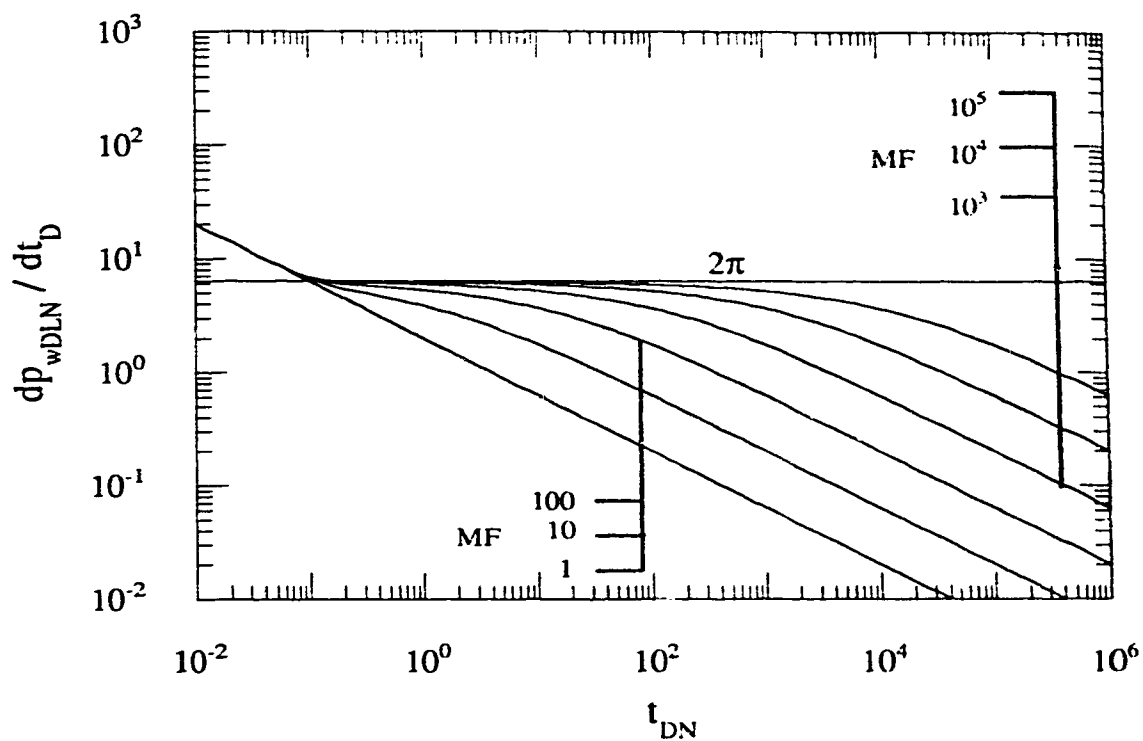


Figure 3.4: Effect of mobility and storativity ratios on the Cartesian pressure derivative responses for a linear, composite reservoir.

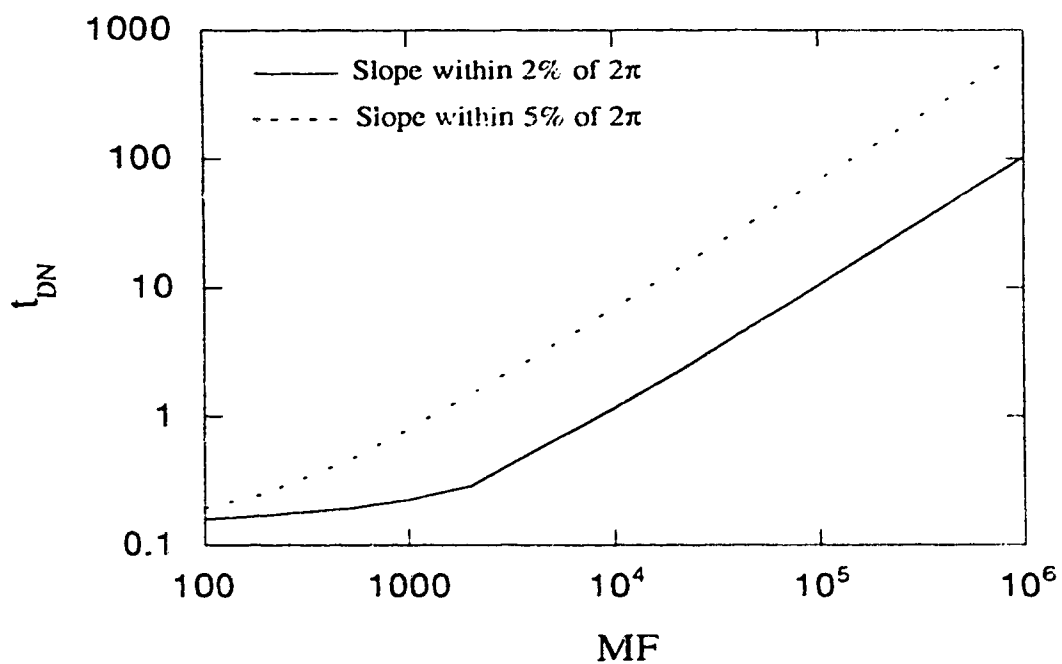


Figure 3.5: Correlations for the end of pseudosteady state for a linear, composite reservoir.

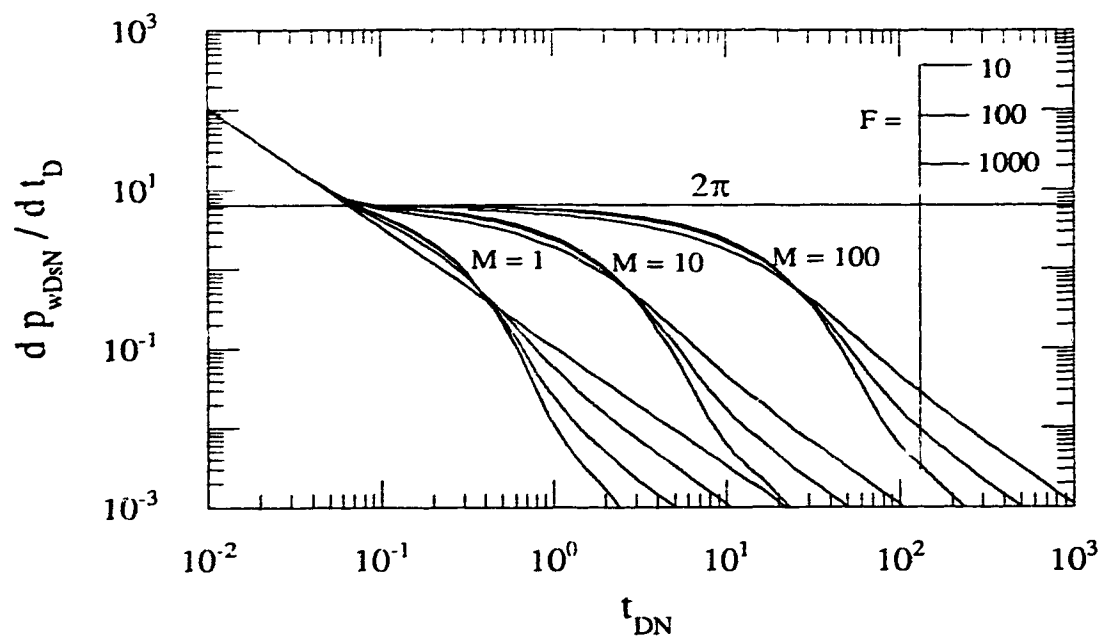


Figure 3.6: Effect of mobility and storativity ratios on the Cartesian pressure derivative responses for a spherical, composite reservoir.

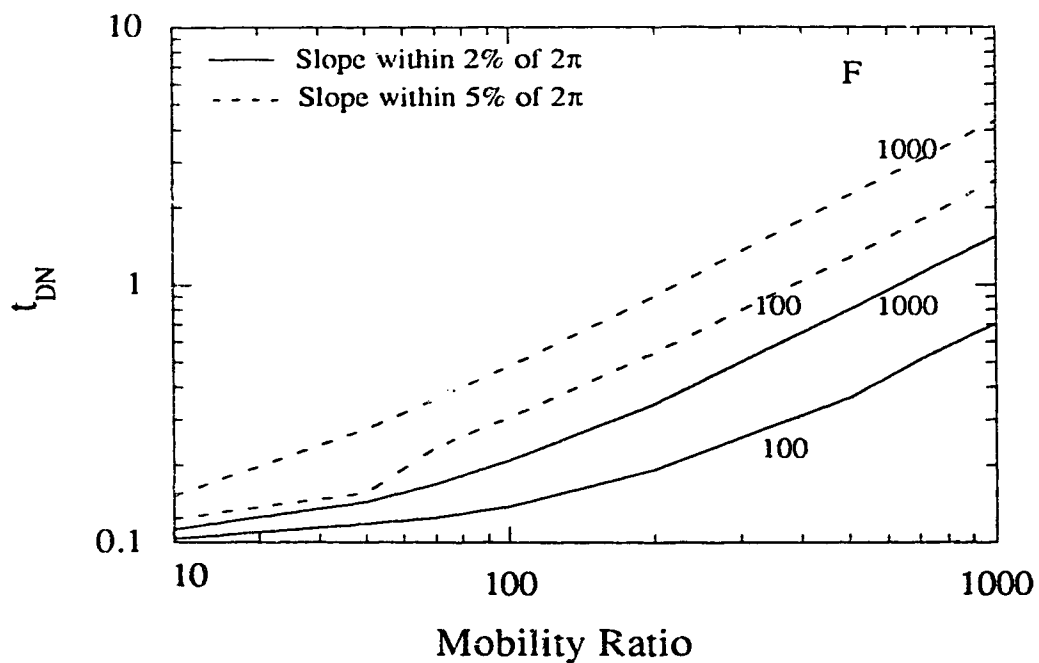


Figure 3.7: Correlations for the end of pseudosteady state for a spherical, composite reservoir.

4.0 GENERALIZED PRESSURE DERIVATIVE ANALYSIS OF COMPOSITE RESERVOIRS

4.1 Introduction

Pressure derivatives have been shown to be more sensitive to disturbances in the reservoir than pressure signals. This results in greater detail on a derivative graph than is apparent on a pressure graph. Pressure derivatives were first introduced by *Tiab and Kumar* (1980), who presented the derivative of pressure with respect to time. Later, *Bourdet et al.* (1983) introduced the semi-log pressure derivative, defined as the derivative of the well pressure with respect to the natural logarithm of time. For radial reservoirs, the semilog pressure derivative response appears as a horizontal line during the infinite-acting radial flow period, resulting in an easy identification of the radial flow regime. As a result, the semilog pressure derivative is widely used in well test analysis of not only homogeneous, but also composite reservoirs.

To analyze well tests for thermal recovery projects, reservoirs have been idealized as composite reservoirs. A reservoir undergoing steam injection may be described as a composite reservoir, consisting of an inner steam-swept region and an outer unswept region. Steam injection in a fractured well may result in an elliptical swept region. For a fully-penetrating, unfractured, vertical well in a homogeneous, isotropic reservoir, the swept region is likely to be radial (circular). A partially-completed injection well may create a spherically-shaped swept region, while steam injection in a linear or channel reservoir may result in a linear, composite reservoir. Analytical solutions for the pressure behavior of composite reservoirs of various flow geometries have been presented in Chapter 2.

When the semi-log pressure derivative is applied to other flow geometries such as linear or spherical, the responses are not horizontal; making identification of these flow regimes more difficult. *Jelmert* (1993a and b) presented a polynomial pressure derivative to simplify the identification of flow regimes for homogeneous reservoirs in other flow geometries. Using analytical solutions, this study extends the theory of the generalized pressure derivative to well-test analysis of composite reservoirs in radial, elliptical, linear and spherical flow geometries. Design and analysis equations, based on the generalized pressure derivative, are presented for well testing of composite reservoirs in various flow geometries.

4.2 Generalized Pressure Derivative

The dimensionless wellbore pressure behavior characteristic of most flow geometries may be represented as a polynomial of the following form:

$$p_{wD} = At_D^m + B, \quad (4.1)$$

where A , B and m are constants that depend on the particular flow geometry.

Upon differentiating Eq. (4.1) with respect to the dimensionless time, t_D , one gets:

$$\frac{d p_{wD}}{d t_D} = mAt_D^{m-1}. \quad (4.2)$$

Equation (4.2) can be simplified and rearranged as:

$$t_D^n \frac{dp_{wD}}{dt_D} = C, \quad (4.3)$$

where $n = 1-m$ and $C = mA$.

Equation (4.3) represents the generalized pressure derivative, in dimensionless form, where the exponent, n , depends on the particular flow geometry. With an appropriate choice of the exponent, n , the generalized pressure derivative becomes a constant, C . Thus, a graph of the derivative versus time will appear as a horizontal line in any coordinate system during the flow period characteristic of that geometry. It is noted that while the dimensionless wellbore during radial flow is not a polynomial of the form in Eq. (4.1), its derivative is. Thus, the theory of the polynomial (generalized) derivative may also be applied to functions whose first derivative is a polynomial (Jelmert, 1993b).

Table 4.1 presents some flow regimes or geometries and their corresponding exponent, n . For $n=1$, the generalized pressure derivative is equivalent to the semi-log pressure derivative of Bourdet *et al.* (1983). The choice of $n=1$ will only lead to a constant derivative, if the flow regime is radial. For linear flow, $n = \frac{1}{2}$, while for spherical flow, $n = \frac{3}{2}$. For $n=0$, the pseudosteady state flow regime, if present, will appear as a horizontal line regardless of the geometry of the composite reservoir. Also, when $n=0$, the generalized pressure derivative is equivalent to the Cartesian pressure derivative proposed by Tiab and Kumar (1980).

4.3 Discussion

The generalized pressure derivative was applied to pressure drawdown data generated from analytical solutions for two-region, composite reservoirs in radial, elliptical, linear and spherical flow geometries. In this chapter, the generalized pressure derivative is used as a means of flow regime identification and is used also to develop equations for the design and analysis of pressure transient data for the various composite reservoirs.

In applying the generalized pressure derivative, flow exponents are chosen for the radial, linear and spherical geometries as per Table 4.1. For the elliptical geometry, which is not shown on Table 4.1, a flow exponent, $n=1$, is chosen on the basis of its similarity with the radial reservoir, as discussed by *Issaka and Ambastha* (1994). Figure 4.1 shows a log-log graph of the generalized pressure derivative versus normalized dimensionless time (t_{DN}) for the four flow geometries. The dimensionless times are normalized by dividing the time values by the cross-sectional area of the inner region of each composite reservoir. This normalization makes the derivative responses independent of the size of the inner region. For this graph, the responses are generated for a mobility ratio, $M=100$, and a storativity ratio, $F=1000$. The generalized derivative responses in Fig. 4.1 show that each of the four geometries indicates three distinct flow regimes. These include an inner region flow regime, where the responses are all horizontal (zero-slope), except for the elliptical reservoir. This is followed by a long transition period during which the effects of the discontinuity are manifested. Pseudosteady state behavior during this period is characterized by slopes equal to the flow exponent, n , chosen for each composite reservoir. Finally, the outer region flow becomes evident, characterized by horizontal lines. The horizontal lines make the identification of the inner and outer region responses for all the geometries much easier than is the case for identification based on the semi-log pressure derivative only. In Fig. 4.1, the responses for the spherical geometry show some irregularities for the outer region flow behavior. These are due to instabilities associated with the numerical inversion of the Laplace space solution. These instabilities are more pronounced as the storativity ratio increases and also for very long times.

4.4 Pressure Derivative Analysis and Design Equations

A detailed discussion of the behavior of the generalized pressure derivative for the various composite reservoirs is presented now. Also presented are well-test analysis equations as

well as empirical design equations for composite reservoirs in the different geometries. *Ambastha and Ramey* (1989) presented detailed discussions of the effect of mobility ratio and storativity ratio on the derivative response for radial, composite reservoirs. In addition, they provided several empirical design equations, as well as a pressure derivative type-curve for radial, composite reservoirs. Due to the similarity of pressure transient responses between the radial and elliptical reservoirs (*Issaka and Ambastha*, 1994, *Stanislav et al.*, 1992), the design equations presented by *Ambastha and Ramey* (1989) for radial systems are considered appropriate for elliptical systems as well. In this study, the discussion will emphasize the spherical and linear, composite reservoirs.

4.4.1 Spherical, Composite Reservoir

In this section, well-test analysis equations, as well as empirical design equations for the start and end of some important flow regimes for spherical, composite reservoirs will be provided. As well, detailed discussions of the effect of mobility and storativity ratios on the generalized pressure derivative responses for the spherical flow geometry will be presented.

4.4.1.1 Analysis and Design Equations

The analysis and design equations will be presented on the basis of the transient generalized pressure derivative responses during the inner region, the transition region, and the outer region flow periods.

Inner region flow:

In the absence of wellbore storage and skin effects, the dimensionless wellbore pressure during infinite-acting spherical flow (*Chatas*, 1966) is given by:

$$p_{wD_s} = 1 - \frac{1}{\sqrt{\pi} t_{D_s}}. \quad (4.4)$$

Differentiating Eq. (4.4) with respect to t_{D_s} , gives the Cartesian derivative:

$$\frac{dp_{wD_s}}{dt_{D_s}} = \frac{t_{D_s}^{-3/2}}{2\sqrt{\pi}}. \quad (4.5)$$

Multiplying both sides of Eq. (4.5) by $t_{D_s}^{3/2}$, the generalized pressure derivative for the spherical reservoir becomes a constant given by:

$$t_{D_s}^{3/2} \frac{dp_{wD_s}}{dt_{D_s}} = \frac{1}{2\sqrt{\pi}}. \quad (4.6)$$

In the analysis of practical well test-data from a pressure falloff test, the first step will be to calculate the Cartesian pressure derivatives, using a differentiation algorithm such as that given by *Bourdet et al.* (1989). The Cartesian pressure derivatives ($\frac{dp_{ws}}{dt_s}$) are then multiplied by $t_s^{3/2}$ to yield the generalized pressure derivative for a spherical reservoir. A constant generalized derivative (a horizontal line) during the early part of the response is indicative of infinite-acting spherical flow. Once the infinite-acting spherical flow period has been identified, a graph of pressure falloff data (p_{ws}) versus reciprocal square root time ($1/\sqrt{t_s}$), on the basis of Eq. (4.4), can be used to obtain an estimate of the mobility, k/μ , in the steam chamber.

The constant generalized pressure derivative from Eq. (4.6) provides another means of determining the properties of the inner region. Using the value of the constant derivative calculated from the pressure falloff data, and the definitions for the dimensionless variables in Eq. (4.6), another estimate of the mobility, k/μ , in the inner region can be obtained. These two estimates must be consistent, and will serve to increase the degree of confidence in the results.

Using the criterion of 2% deviation from $1/2\sqrt{\pi}$, the time to the end of infinite-acting spherical flow corresponding to the inner region is

$$(t_{DNs})_{end} = 0.041. \quad (4.7)$$

The dimensionless time shown in Eq. (4.7) appears to be less than the corresponding value for a radial, composite reservoir. Accounting for the differences in the definitions of normalized dimensionless time, the time to the end of the first semilog straight line for radial, composite reservoirs, given by *Ambastha and Ramey* (1989), becomes 0.056. Thus, infinite-acting flow corresponding to the inner region ends earlier for a spherical reservoir than for a radial reservoir.

Transition region flow:

As shown in Fig. 4.1, for $M = 100$ and $F = 1000$, the transition region derivative response for spherical geometry goes through a maximum value before dropping to an asymptotic value in the outer region. Table 4.2 presents the maximum generalized pressure derivatives and the time to reach the maximum derivative for several combinations of mobility and storativity ratios. The data of Table 4.2 suggest that an approximate correlation for the maximum derivative in the transition region can be given as:

$$(t_{Ds}^{3/2} \frac{dp_{wDs}}{dt_{Ds}})_{max} = (0.189 + 0.021 \log F) M^{1.48}, \quad (4.8)$$

while the time to the maximum derivative is

$$(t_{Ds})_{max} = (0.245 - 0.028 \log F) M. \quad (4.9)$$

Equations (4.8) and (4.9) apply if $M \geq 10$ and $F \geq 10$. The accuracy of Eqs. (4.8) and (4.9) in predicting the maximum generalized derivative and the time to the maximum derivative are verified in Figs. 4.2 and 4.3, respectively. Figures 4.2 and 4.3 compare the predicted values from Eqs. (4.8) and (4.9) to the actual values for the maximum generalized derivative and the time to the maximum derivative, respectively, from Table 4.2. The figures show good agreement, with the accuracy of the correlations increasing as the storativity ratio increases.

Outer region flow:

Onyekonwu and Horne (1983) have shown that at late times the dimensionless wellbore pressure in a spherical, composite reservoir is given by:

$$p_{wDs} = 1 - \frac{1-M}{a_{Ds}} - M \sqrt{\frac{M}{\pi F t_{Ds}}}. \quad (4.10)$$

Upon differentiating Eq. (4.10) with respect to t_{Ds} , one gets

$$\frac{dp_{wDs}}{dt_{Ds}} = \frac{t_{Ds}^{-1/2} M}{2} \sqrt{\frac{M}{\pi F}}. \quad (4.11)$$

Multiplying both sides of Eq. (4.11) by $t_{Ds}^{3/2}$, the generalized pressure derivative response in the outer region of the spherical, composite reservoir becomes

$$t_{Ds}^* \frac{dp_{wDs}}{dt_{Ds}} = \frac{M}{2} \sqrt{\frac{M}{\pi F}} \quad (4.12)$$

Equation (4.12) shows that the outer region derivative response for a spherical, composite reservoir depends on both the mobility ratio and the storativity ratio. From Eq. (4.12), a correlating parameter for the outer region derivative response will be $M \sqrt{\frac{M}{F}}$. It is thus impossible to find individual values of M and F , unless one of the variables is known from a test prior to the thermal recovery process.

Using the criterion of 2% deviation from $\frac{M}{2} \sqrt{\frac{M}{\pi F}}$, the times to the start of the second horizontal line corresponding to the outer region, for various combinations of mobility and storativity ratios, are presented in Table 4.3. The data of Table 4.3 suggest that an approximate correlation for the time to the start of the second horizontal line corresponding to the outer region can be given as:

$$(t_{DS})_H = (25 \log F - 9.4) M. \quad (4.13)$$

A comparison of the predictions of Eq. (4.13) with the actual values from Table 4.3 is shown in Fig. 4.4. Figure 4.4 shows a good agreement, with accuracy increasing with the storativity ratio.

4.4.1.2 General Discussion

Figure 4.5 shows a log-log graph of the generalized pressure derivative $(t_{Ds}^* \frac{dp_{wDs}}{dt_{Ds}})$ versus the normalized dimensionless time (t_{DS}) for a spherical, composite reservoir. The figure shows the effect of mobility ratio on the derivative response for a fixed storativity

ratio, $F = 100$. The derivative response for a homogeneous, spherical reservoir ($M = 1$, $F = 1$) is also shown on Fig. 4.5. The figure shows that all responses form one horizontal line at early times. This indicates infinite-acting flow behavior in the inner region, during which time the effects of the discontinuity are not yet felt. A long transition period follows, during which the derivative responses go through maximum values, before dropping to asymptotic horizontal lines. These horizontal lines represent infinite-acting flow behavior in the outer regions. Here, the separate curves represent the different mobility ratios. The irregularities in the derivative responses just prior to flattening out is the result of numerical instabilities as mentioned earlier. From Fig. 4.5, the mobility ratio is shown to affect strongly the derivative response for spherical flow geometry, similar to the result for radial and elliptical reservoirs (Ambastha and Ramey, 1989, Stanislav *et al.*, 1992). Figure 4.5, however, reveals some significant differences in the derivative responses for spherical and radial, composite reservoirs. For radial reservoirs with $M \geq 1$ and $F \geq 1$, the value of the derivative in the outer region is always greater than, or equal to, the derivative in the inner region (Ambastha and Ramey, 1989). Figure 4.5 shows that this does not necessarily hold true for a spherical reservoir. An examination of Eq. (4.12) shows that for $F > M^3$, the derivative response in the outer region will be less than the response in the inner region. In Fig. 4.5, the response for $M = 1$ and $F = 100$, illustrates the situation where the value of the outer region derivative is less than that of the inner region.

Figure 4.6 shows the effect of storativity ratio on the derivative responses for a spherical reservoir for a fixed mobility ratio, $M = 100$. For storativity ratios greater than unity, each derivative response goes through a maximum value before approaching the asymptotic value characteristic of infinite-acting spherical flow in the outer region. Figure 4.6 also shows that the storativity ratio has very little effect on the derivative response during the transition period leading to the maximum derivative value. The value of the maximum derivative is only slightly affected by the storativity ratio. This behavior is similar to that

shown during the transition period for a radial, composite reservoir, except for one difference. For a radial reservoir, the derivative responses for the different storativity ratios do not cross over during the transition period. However, as shown in Fig. 4.6, the derivative responses for the spherical reservoir do cross over, reversing an earlier trend, where the curve with the highest storativity ratio had the highest derivative. The derivative responses in the outer region show another significant difference between spherical and radial reservoirs. For radial reservoirs of the same mobility ratio, the derivative responses in the outer region form one curve, regardless of the storativity ratio (*Arabastha and Ramey, 1989*). Figure 4.6 shows, however, that for a spherical reservoir, different storativity ratios result in different curves for the outer region. Thus, for a spherical reservoir, the outer region flow behavior is affected by both the mobility ratio and the storativity ratio, which is evident from Eq. (4.12). For a radial reservoir, the outer region flow behavior is affected by only the mobility ratio.

The effect of both mobility ratio and storativity ratio on the generalized pressure derivative for a spherical, composite reservoir is shown on Fig. 4.7. The figure shows derivative responses for selected mobility ratios between 1 and 100, and for storativity ratios between 1 and 1000. Figure 4.7 again shows three clearly defined flow regimes for any combination of M and F , except for the homogeneous case ($M=1$ and $F=1$). The curves corresponding to $F = 1000$ tend to show some discontinuities in trend just before approaching the asymptotic values characteristic of infinite-acting spherical flow in the outer region. This is due to numerical instabilities in computing the derivative response, rather than any reservoir effect. An examination of the outer region derivative responses shows that the response for $M = 10$ and $F = 1000$, on the one hand, and the response for $M = 1$ and $F = 1$, on the other hand, are identical. For these two cases the parameter, $M\sqrt{\frac{M}{F}}$ is 1, making it impossible to obtain independent estimates of the mobility ratio or the storativity ratio.

4.4.2 Linear, Composite Reservoir

This section presents analysis and design equations for well testing of linear, composite reservoirs. In addition, a detailed discussion on the effect of mobility and storativity ratios on the generalized pressure derivative responses for linear flow geometry is presented.

4.4.2.1 Analysis and Design Equations

The analysis and design equations for a linear, composite reservoir are presented on the basis of the transient generalized pressure derivative responses during the inner region, and the outer region flow periods.

Inner region flow:

The dimensionless wellbore pressure during infinite-acting linear flow, in the absence of wellbore storage and skin effects, is given by:

$$p_{wDl} = 2\sqrt{\frac{t_{Dl}}{\pi}}. \quad (4.14)$$

Differentiating Eq. (4.14), with respect to t_{Dl} , gives the Cartesian derivative:

$$\frac{dp_{wDl}}{dt_{Dl}} = \frac{t_{Dl}^{-1/2}}{\sqrt{\pi}}. \quad (4.15)$$

ir becomes a constant given by:

$$(4.16)$$

and (4.14) may be used to provide two separate estimates of the mobility in for a linear, composite reservoir, such as a channel reservoir undergoing These two estimates must agree with each other.

criterion of 2% deviation from $\frac{1}{\sqrt{\pi}}$, the time to the end of infinite- / corresponding to the inner region is

$$(4.17)$$

ndicates that infinite-acting flow in the inner region lasts longer for linear r either spherical or radial geometry.

flow:

: dimensionless wellbore pressure, in the absence of wellbore storage and a linear, composite reservoir is given by

$$(4.18)$$

ifferentiating with respect to t_{D1} , gives:

$$\frac{dp_{wDl}}{dt_{Dl}} = \sqrt{\frac{MF}{\pi}} t_{Dl}^{-1/2}. \quad (4.19)$$

Multiplying both sides of Eq. (4.19) by $t_{Dl}^{1/2}$, the late time generalized pressure derivative for a linear, composite reservoir becomes

$$t_{Dl}^{1/2} \frac{dp_{wDl}}{dt_{Dl}} = \sqrt{\frac{MF}{\pi}}. \quad (4.20)$$

Equation (4.20) shows that the late time derivative response for a linear, composite reservoir depends equally on the mobility ratio and the storativity ratio. The mobility ratio has the same effect on the derivative response as the storativity ratio. Thus, the product, MF can be regarded as a single correlating parameter for infinite, linear, composite reservoirs. Here again it will not be possible to find separate values of M and F from well-test data, unless one of the variables is known from a previous test.

The times to the start of infinite-acting linear flow corresponding to the outer region, for various combinations of mobility and storativity ratios, are presented in Table 4.4. These times are based on the criterion of 2% deviation from $\sqrt{\frac{MF}{\pi}}$. Data from Table 4.4 suggest that an approximate correlation for the start of the second infinite-acting linear flow can be presented as

$$(t_{DlN})_H = 7.45MF. \quad (4.21)$$

Equation (4.21) applies for $M \geq 10$ and $F \geq 10$, and for instances where outer boundary effects do not mask the development of the second infinite-acting linear flow regime. Figure 4.8 shows a comparison of the times predicted using Eq. (4.21), with the actual times from Table 4.4. The figure indicates that Eq. (4.21) generates very accurate

predictions of the time to the start of the second infinite-acting linear flow regime for a linear, composite reservoir.

4.4.2.2 General Discussion

Figure 4.9 presents the effect of the product of mobility ratio and storativity ratio, MF , on the generalized pressure derivative response for a linear, composite reservoir. Derivative responses are presented for selected values of MF between 1 and 100,000. As with all the other flow geometries, Fig. 4.9 shows an early-time horizontal line, indicating infinite-acting linear flow in the inner region. A transition period follows, during which the derivative responses rise steadily due to the effect of mobility and/or storativity ratio. Here, different curves represent different values of MF . The length of the transition period is dependent on the value of MF . As expected, the larger the value of MF , the longer it takes for the transient to cross the discontinuity boundary between the inner and outer regions. Consequently, the transition period is longer. The derivative responses eventually level off to constant values, indicating infinite-acting linear flow corresponding to the outer region. Figure 4.9 shows that MF has a strong effect on the derivative response for linear geometry.

Figure 4.9, however, illustrates one significant difference between linear reservoir, on the one hand, and radial, elliptical and spherical reservoirs, on the other. For radial, elliptical and spherical reservoirs, the derivative responses in the transition region go through maximum values before dropping to asymptotic values in the outer region. Figure 4.9 shows that no such maximum derivatives occur during the transition region for a linear, composite reservoir. Instead, the derivative responses rise steadily through the transition region and eventually level off to asymptotic values in the outer region.

4.5 Comparison of Analysis and Design Equations

In the preceding sections, equations for the design and analysis of pressure transient data for various composite reservoirs, based on the generalized pressure derivative have been presented. Table 4.5 compares the analysis equations for infinite-acting flow corresponding to the inner and outer regions of the various composite reservoirs. As shown in Table 4.5, the value of the generalized derivative in the outer region depends only on mobility ratio, for the radial and elliptical reservoirs. For the spherical and linear reservoirs, however, the derivative is dependent on both the mobility and the storativity ratios. Where possible, reservoir parameters estimated using these equations will add to the degree of confidence in the estimated parameters based on pressure analysis.

Table 4.6 compares the design equations based on the generalized pressure derivative for composite reservoirs in radial, elliptical, spherical and linear flow geometries. Data for the end of infinite-acting flow corresponding to the inner region (second column) indicate that the inner region infinite-acting flow lasts the longest for a linear reservoir. This is followed by a radial reservoir, and then a spherical reservoir. Data for the elliptical reservoir is not available because there is no simple analytical solution in real space (as opposed to Laplace space) for the early time behavior of an elliptical, composite reservoir.

The third and fourth columns of Table 4.6 give the correlations for the maximum derivative in the transition region, and also the times to these maxima. Correlations for the linear reservoir are not available because the derivative response in the transition region shows no maximum. A measure of the length of the transition period can be deduced from the difference between the second column and the fifth column, which is the time to the start of the second infinite-acting flow period corresponding to the outer region. With $M = 100$ and $F = 1000$ (typical values for a steam injection process), the transition period for a radial

reservoir is about five-and-a-half log cycles. For a spherical reservoir this is about five log cycles, while for a linear reservoir, it is seven log cycles. For such long transition periods, it is unlikely that any well test will be conducted long enough to observe the second infinite-acting flow behavior for any composite reservoir.

Table 4.1: Flow exponents for some selected flow regimes and geometries

Flow Regime/Geometry	n
Radial	1
Linear	1/2
Spherical	3/2
Pseudosteady State	0

Table 4.2: Maximum generalized pressure derivative and the time to maximum derivative for a spherical, composite reservoir.

M	F	Maximum derivative, $(t_{Ds}^{3/2} \frac{dp_{vDs}}{dt_{Ds}})_{max}$	Time to maximum derivative, $(t_{DsN})_{max}$
10	10	6.59	2.23
20		17.99	4.78
50		69.56	11.14
70		114.80	15.92
100		195.30	22.28
200		551.20	47.75
500		2172.00	111.40
700		3598.00	159.20
1000		6138.00	222.80
10	100	7.46	1.91
20		20.17	3.98
50		77.79	9.55
70		128.70	12.73
100		218.10	19.10
200		613.90	39.79
500		2421.00	95.49
700		4025.00	127.30
1000		6843.00	191.00
10	1000	7.93	1.59
20		21.47	3.18
50		82.65	7.96
70		136.20	11.14
100		231.70	15.92
200		652.50	31.83
500		2572.00	79.58
700		4259.00	111.40
1000		7270.00	159.20

Table 4.3: Time to the beginning of infinite-acting spherical flow corresponding to the outer region for a spherical, composite reservoir.

M	F	$(t_{D\&N})_{II}$
10	10	143.2
20		254.6
50		636.6
70		954.9
100		1273.0
200		2546.0
500		6366.0
700		8847.0
1000		12315.0
10	100	397.9
20		795.8
50		1910.0
70		2832.0
100		4268.0
200		8753.0
500		20598.0
700		28650.0
1000		42952.0
10	1000	692.3
20		1353.0
50		3403.0
70		5345.0
100		6841.0
200		13254.0
500		32013.0
700		46227.0
1000		66753.0

Table 4.4: Time to the beginning of infinite-acting linear flow corresponding to the outer region for a linear, composite reservoir.

MF	$(t_{DIN})_{II}$
100	755
200	1492
500	3820
700	5372
1000	7371
2000	14960
5000	38970
7000	53050
10000	75120
20000	149200
50000	382000
70000	537200
100000	737100
200000	1496000
500000	3897000
700000	5305000
1000000	7512000

Table 4.5: Comparison of analysis equations based on the generalized pressure derivative for composite systems in radial, elliptical, spherical and linear flow geometries.

Flow Geometry	Generalized Derivative	Value in Inner Region	Value in Outer Region
Radial	$t_{Dr} \frac{dp_{wDr}}{dt_{Dr}}$	$\frac{1}{2}$	$\frac{M^*}{2}$
Elliptical	$t_{De} \frac{dp_{wDe}}{dt_{De}}$	N/A	$\frac{M^{**}}{2}$
Spherical	$t_{Ds}^{3/2} \frac{dp_{wDs}}{dt_{Ds}}$	$\frac{1}{2\sqrt{\pi}}$	$\frac{M}{2} \sqrt{\frac{M}{\pi F}}$
Linear	$t_{Dl}^{1/2} \frac{dp_{wDl}}{dt_{Dl}}$	$\frac{1}{\sqrt{\pi}}$	$\sqrt{\frac{MF}{\pi}}$

* Ambastha and Ramey (1989)

** Stanislav et al. (1992)

Table 4.6: Comparison of design equations based on the generalized pressure derivative for composite systems in radial, elliptical, spherical and linear flow geometries.

Flow Geometry	$(t_{DN})_{rad}$	Maximum Pressure Derivative	$(t_{DN})_{max}$	$(t_{DN})_{II}$
Radial	0.057*	$(0.223 + 0.318 \log F)M^*$	$(0.573 + 0.127 \log F)M^*$	$28.65(1 + \log F)M^*$
Elliptical	N/A	$(0.223 + 0.318 \log F)M$	$(0.573 + 0.127 \log F)M$	$28.65(1 + \log F)M$
Spherical	0.041	$(0.189 + 0.021 \log F)M^{1.48}$	$(0.245 - 0.028 \log F)M$	$(25 \log F - 9.4)M$
Linear	0.061	N/A	N/A	$7.45MF$

* Ambastha and Ramey (1989)

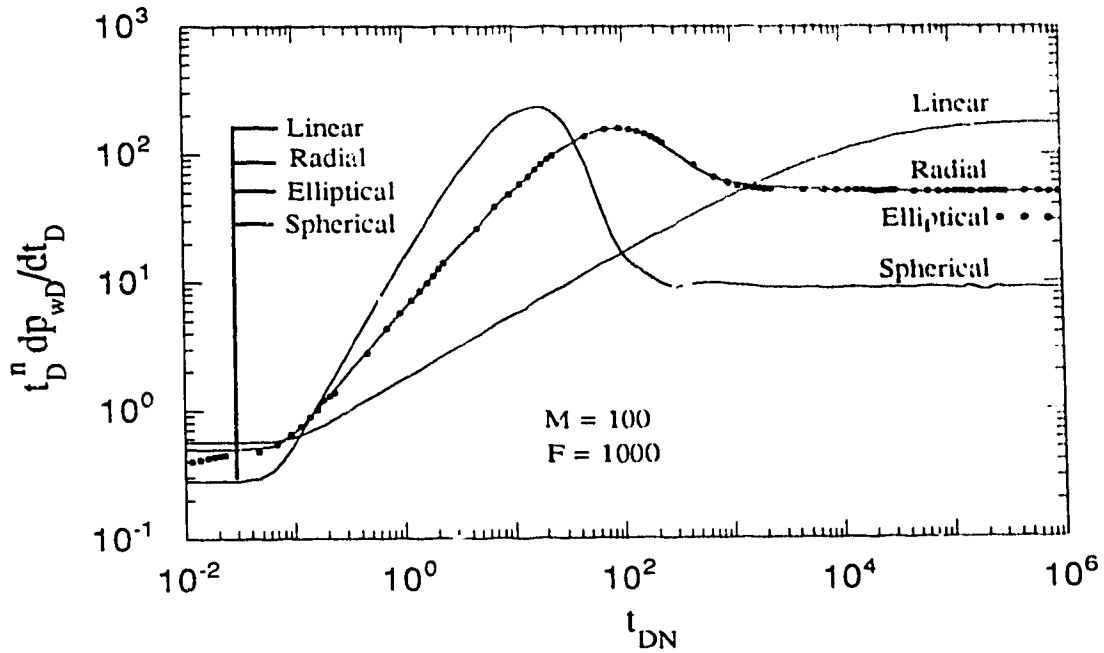


Figure 4.1: Generalized pressure derivative responses for composite reservoirs in radial, elliptical, spherical and linear flow geometries.

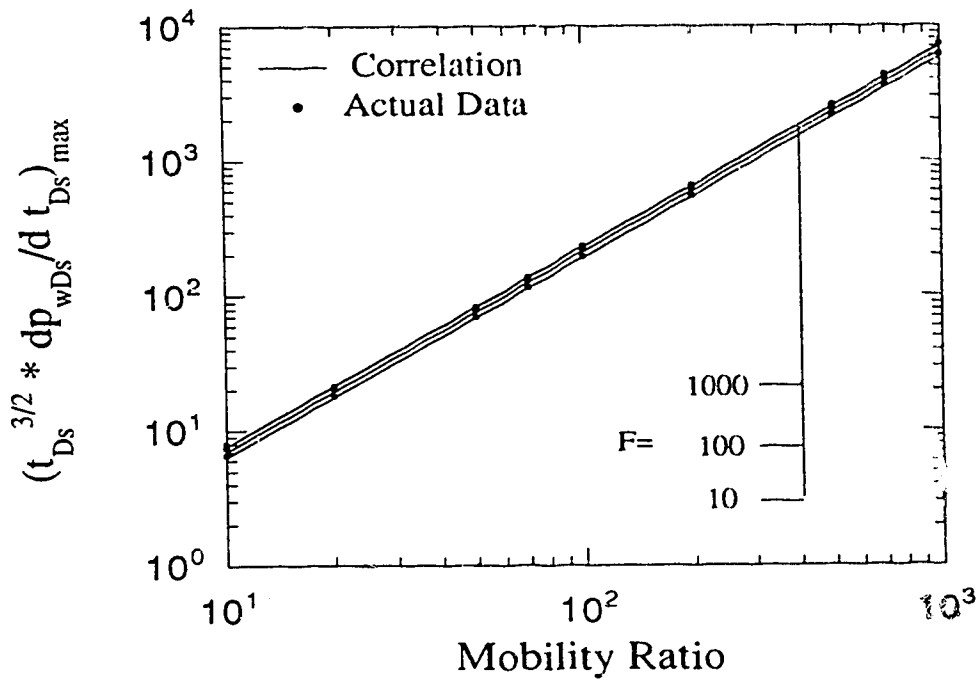


Figure 4.2: Verification of accuracy of the correlation for predicting the maximum generalized pressure derivative for a spherical, composite reservoir.

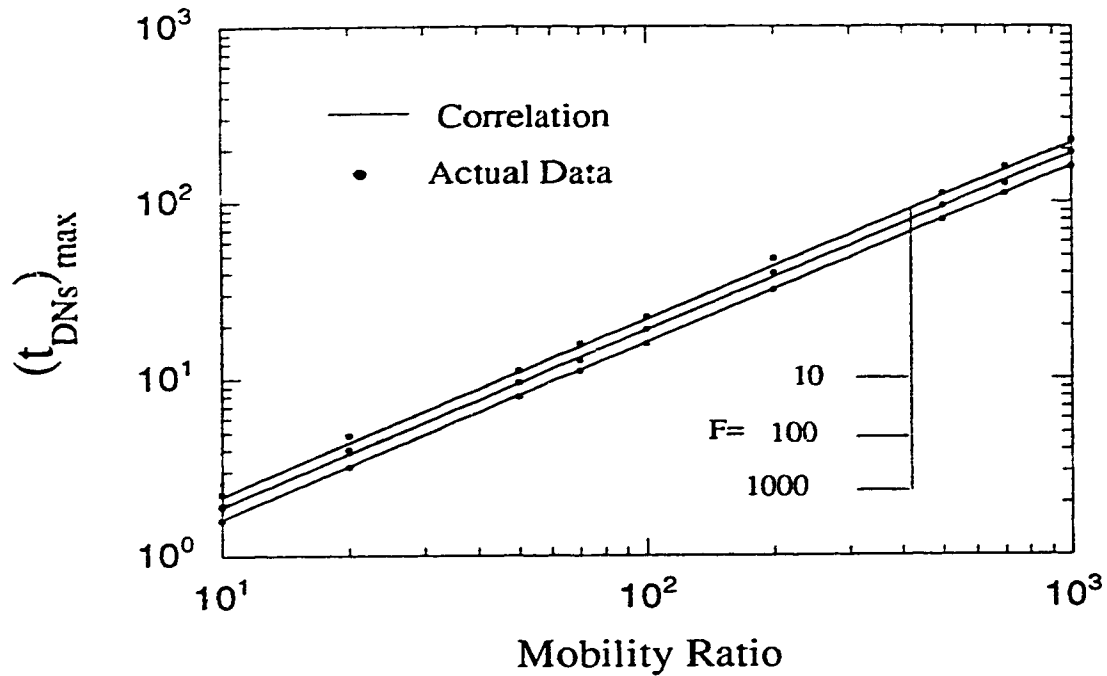


Figure 4.3: Verification of accuracy of the correlation for predicting the time to the maximum generalized pressure derivative for a spherical, composite reservoir.

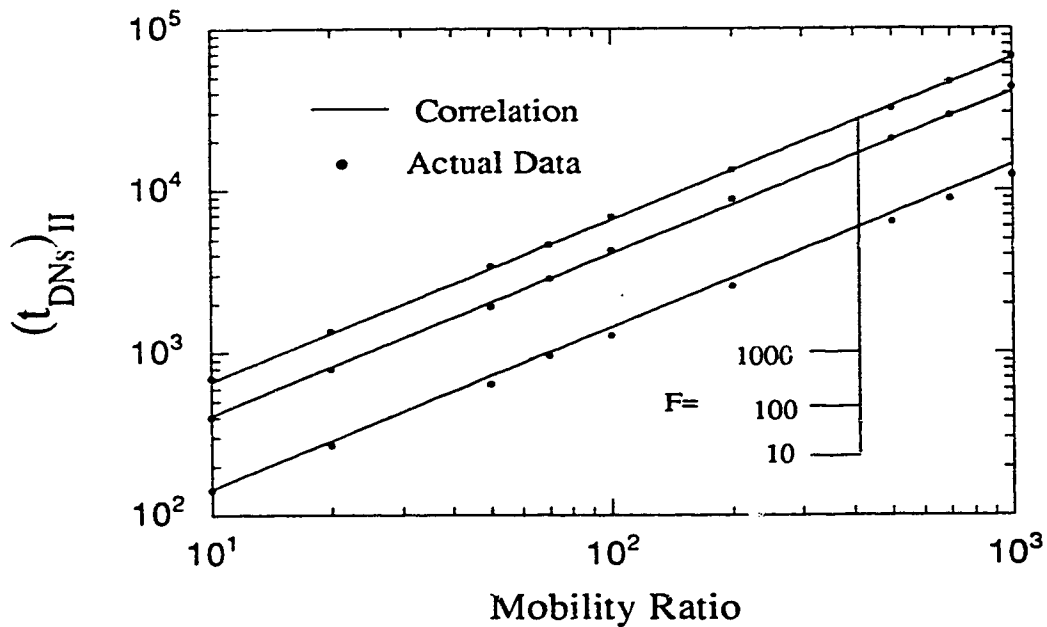


Figure 4.4: Verification of the accuracy of the correlation for predicting the time to the start of infinite-acting flow in the outer region of a spherical, composite reservoir.

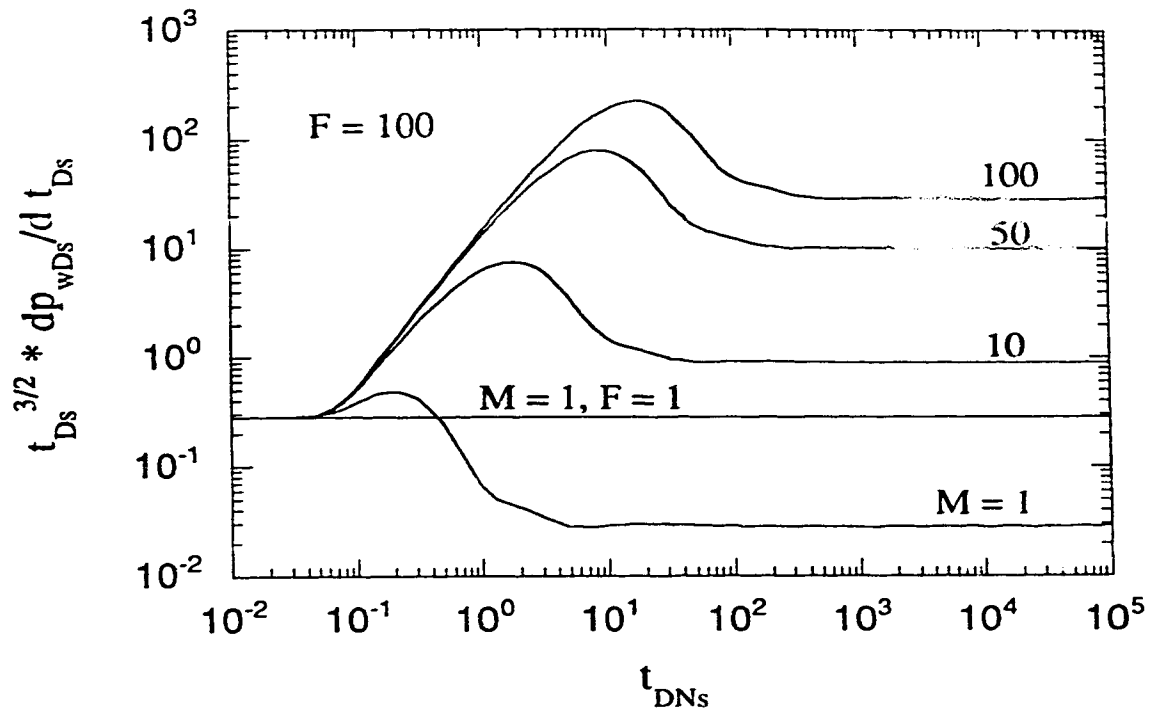


Figure 4.5: Effect of mobility ratio on generalized pressure derivative responses for a spherical, composite reservoir.

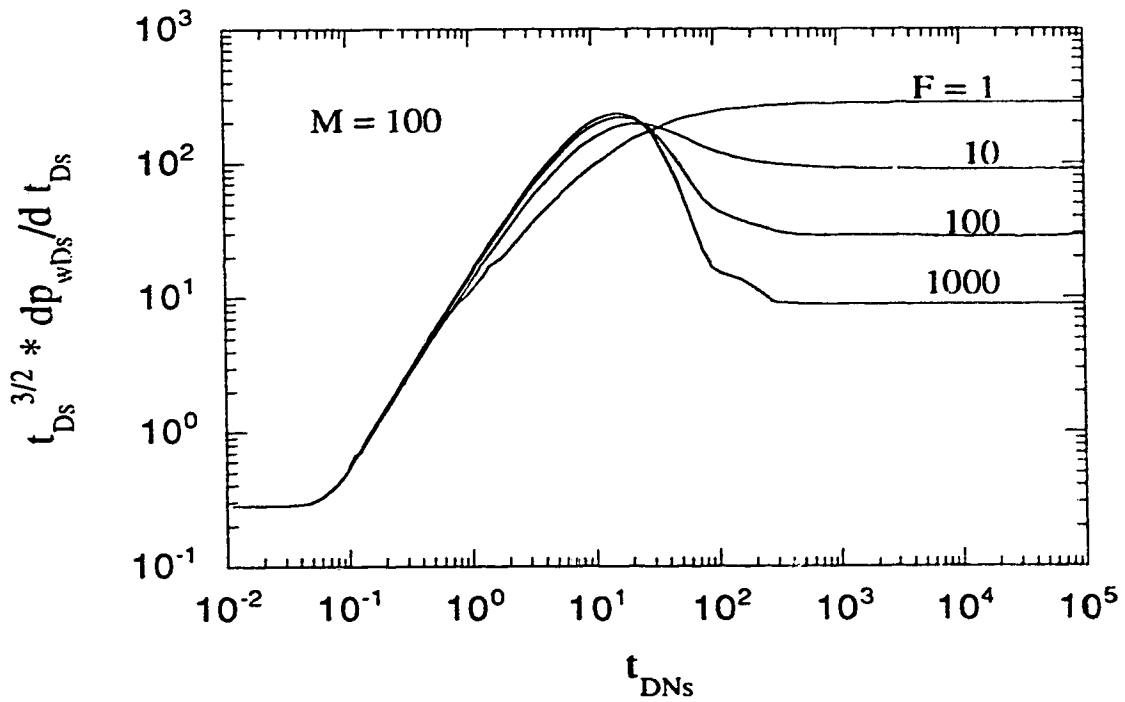


Figure 4.6: Effect of storativity ratio on generalized pressure derivative responses for a spherical, composite reservoir.

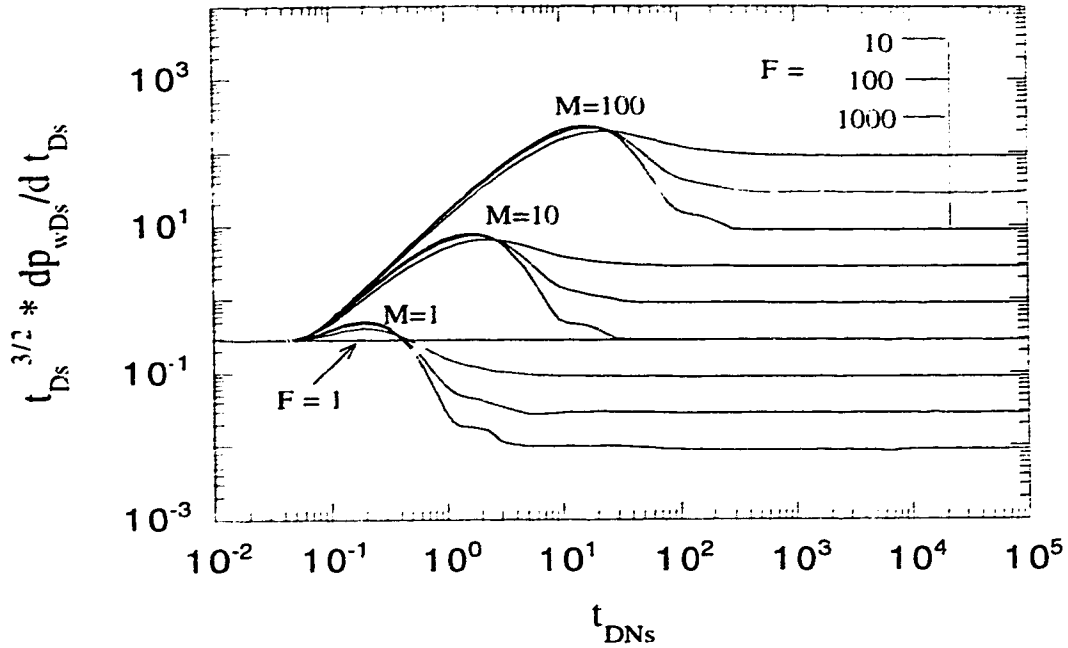


Figure 4.7: Effect of mobility and storativity ratio on generalized pressure derivative responses for a spherical, composite reservoir.

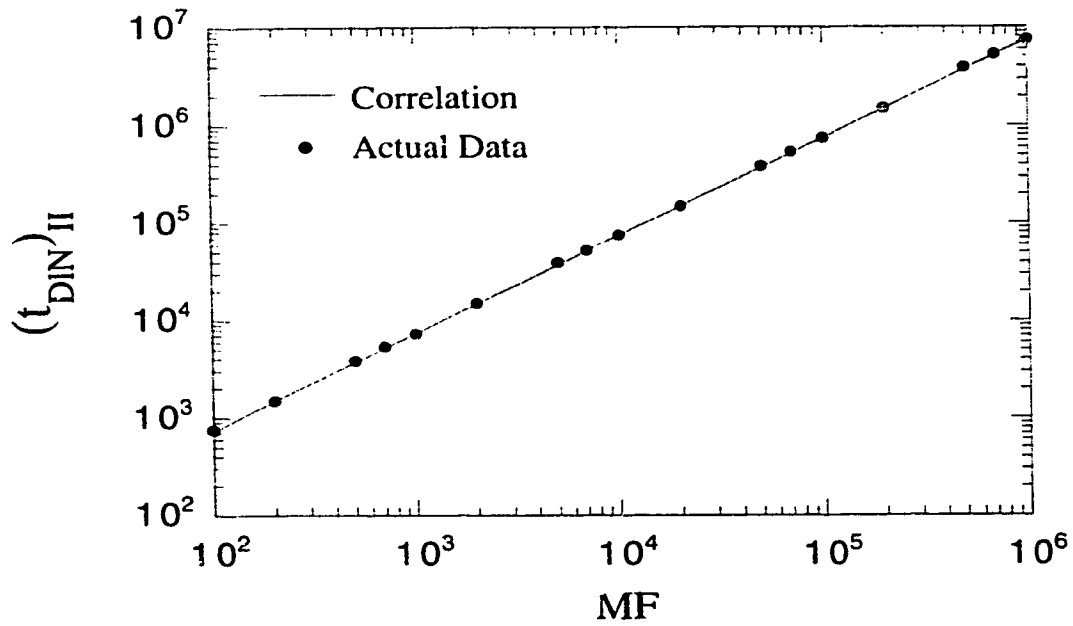


Figure 4.8: Verification of the accuracy of the correlation for predicting the time to the start of infinite-acting flow in the outer region of a linear, composite reservoir.

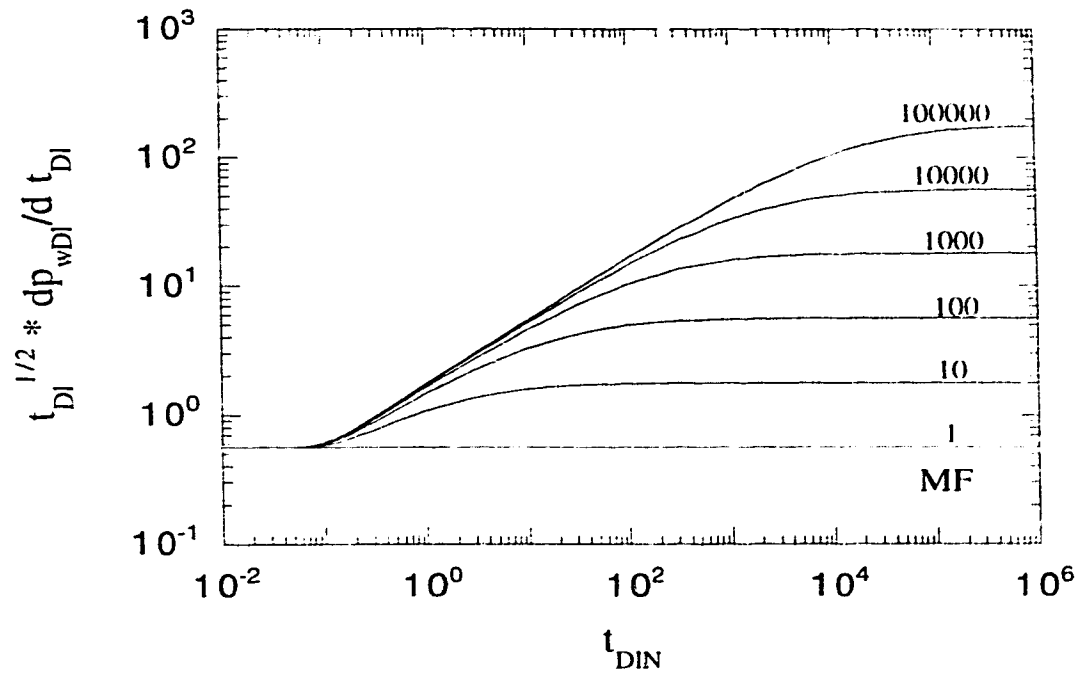


Figure 4.9: Effect of MF on generalized pressure derivative responses for a linear, composite reservoir.

5.0 DECLINE CURVE ANALYSIS FOR COMPOSITE RESERVOIRS

5.1 Introduction

Most well tests conducted in oil reservoirs utilize a constant flow rate at the wellbore. In fact, much of the theory of transient testing in oil reservoirs is based on constant-rate flow or a series of discrete constant-rate flows (*Earlougher, 1977*). However, under some testing and production conditions, a constant pressure condition at the well may be more appropriate. The constant pressure condition exists for flowing wells where the surface pressure is controlled. It may also arise in the later stages of a well's history, when the well is drawn down to a constant pressure (*Doe, 1991*). Decline curve analysis is one form of constant-pressure, transient-rate analysis using both short- and long-term data.

The constant pressure condition at the well may have some advantages over the constant rate condition. For example, in low permeability reservoirs, it may be impossible to maintain flowing well conditions at a constant rate. A constant pressure condition may be the only recourse. Furthermore, because the wellbore is maintained at a constant pressure, there is no transient change in storage in the wellbore. Thus, wellbore storage effects are not a concern. *Uraiet and Raghavan (1980a)* cite the absence of wellbore storage in the constant-pressure condition as one reason why a constant pressure test will be superior to a constant rate test in interference tests whenever wellbore storage effects at the active well influence the observation pressure response. *Doe (1991)* mentions the constant-pressure condition as being well suited to injection testing, since constant-rate methods are handicapped by requiring a knowledge of the permeability beforehand to select a rate. Constant-rate injection is very sensitive to the rate. A rate that is too low will produce no measurable results, while a rate that is too high may cause unintended hydraulic fracturing.

A composite reservoir may occur during steam injection into an oil reservoir or cold water injection into a hot oil reservoir. Alternatively, the injection of cold water into a geothermal reservoir to recover heat for power generation can also create a composite reservoir. In these representations of a composite reservoir, the portion of the reservoir in the immediate vicinity of the wellbore that is occupied by the injected fluid becomes the inner region, while the uninvaded portion of the reservoir becomes the outer region. In the preceding injection processes, the constant-pressure injection condition may be preferable to the constant-rate injection condition.

Composite reservoirs may also be used to represent reservoirs with damaged wells (skin) or stimulated wells (*Olarewaju and Lee*, 1987a). In this representation, the damaged or stimulated zone becomes the inner region, while the rest of the reservoir is the outer region. *Olarewaju and Lee* (1987a) have used production type curves from a constant-pressure radial, composite model to forecast incremental production from the stimulation of damaged wells.

A review of the literature on constant-pressure well testing reveals three main methods of solving the constant-pressure inner boundary problem. The first is a numerical approach using finite differences (*Uraiet and Raghavan*, 1980a and b). The second method, presented by *Cox* (1979), converts constant-rate solutions into constant-pressure solutions without using Laplace transforms. This method involves the expansion of the pressure solution for the constant-rate condition into a pseudosteady-state form and a transient series of negative exponentials. The constant-pressure solution is then obtained directly from the coefficients of the pressure expansion. The third solution scheme uses the Laplace transform technique. The Laplace transform solutions are further divided into two groups. In the first group, use is made of the constant-pressure inner boundary condition, together

with the diffusivity equation and outer boundary condition, to arrive at the solution. An example of this solution scheme, for two-region composite reservoirs, is that presented by *Olarewaju and Lee* (1987a). In the second group of Laplace transform solutions, the constant-rate solution in Laplace space is first sought. Then, using Duhamel's principle, the constant-rate solution is converted into a constant-pressure solution. This solution scheme follows the development first presented by *van Everdingen and Hurst* (1949). In this study, use is made of the *van Everdingen and Hurst* (1949) approach to convert constant-rate solutions for two-region, composite reservoirs of various flow geometries into the constant-pressure solutions.

This chapter presents a comparison of the injection or production performances of two-region, composite reservoirs in radial, elliptical, linear and spherical flow geometries. Injection or production occurs at constant pressure, while the outer boundary is considered infinite, closed or at constant pressure. Wellbore storage effects are neglected, since wellbore storage does not occur during constant bottomhole pressure production or injection. The effect of reservoir size, as well as mobility and storativity ratios, on the production performance of the various flow geometries is investigated.

5.2 Solution Description

The composite reservoirs in this study are all considered to be made up of two regions. Rock and fluid properties in one region of the composite reservoir are considered homogeneous and isotropic, but different from those in the other region. The inner region may be filled with high mobility injected fluid, while the outer region comprises the low mobility oil zone. This situation will be representative of enhanced recovery processes. Alternatively, the inner region may contain low mobility injected fluid, while the outer region is the uninvaded portion of the reservoir. This situation will be representative of

cold water injection into a hot oil reservoir or a geothermal reservoir. In yet another scenario, the inner region could be the damaged or stimulated zone immediately around the wellbore, while the outer region is the oil zone. Injection into, or production from, the composite reservoir occurs at a constant pressure. The model encompasses composite reservoirs in radial, elliptical, linear and spherical flow geometries. Schematics of the two-region, composite reservoirs in radial, elliptical, linear and spherical flow geometries have been presented in Chapter 2.

If a constant pressure condition is imposed at the wellbore, then the injection or production rate must necessarily vary. Here, the flow rate versus time response for constant pressure production or injection is of interest. Using Duhamel's principle, *van Everdingen* and *Hurst* (1949) have shown that, in Laplace space, the constant-pressure solution is related to the constant-rate solution by the following:

$$\bar{q}_D(l) = \frac{1}{l^2 \bar{p}_{wD}(l)} \cdot \quad (5.1)$$

where \bar{q}_D is the Laplace transform of dimensionless rate, q_D , for constant pressure production, and \bar{p}_{wD} is the Laplace transform of the dimensionless wellbore pressure for constant rate production. Thus, the constant pressure solution follows easily, once the constant rate solution is known.

In this study, the constant-rate solutions for two-region, composite reservoirs of various flow geometries in Laplace space are generated first. Subsequently, Eq. (5.1) is used to convert the constant-rate solutions into the constant-pressure solutions. Responses for both the production (injection) rate and the cumulative production (injection) are generated. These responses, which are in Laplace space, are inverted into real space using the numerical inversion algorithm of *Stehfest* (1970).

5.3 Comparison of Solutions

Following the approach outlined in Chapter 3, a comparison of the transient rate and cumulative production responses for composite reservoirs in radial, elliptical, linear and spherical geometries is sought. To facilitate a comparison of the responses, the dimensionless rate and time values have to be normalized, as was done for the transient pressure responses. Here again, the radial reservoir is chosen as the reference for comparison.

The definitions for dimensionless time for the various flow geometries are the same as in Chapter 3. In the following, the normalized dimensionless rate and cumulative production (injection) for each flow geometry is presented.

5.3.1 Radial Reservoir

The dimensionless rate for the radial reservoir is defined as:

$$q_{Dr} = \frac{q(t)\mu_1 B}{2\pi k_1 h(p_i - p_{wr})} , \quad (5.2)$$

where $q(t)$ is the flow rate, which changes with time. All other variables are defined in the Nomenclature.

Since the radial reservoir is the reference, the normalized dimensionless flow rate is the dimensionless flow rate for the radial reservoir.

$$q_{DrN} = q_{Dr} \quad (5.3)$$

The normalized dimensionless time for the radial reservoir is:

$$t_{DrN} = \frac{t_{Dr}}{\pi R_D^2}. \quad (5.4)$$

where R_D is the dimensionless distance to the interface or discontinuity boundary. In Eq. (5.4), the dimensionless time for the radial reservoir was normalized by dividing it by the area of the inner region. *Ambastha* (1988) and *Stanislav et al.* (1992) have shown that normalizing the dimensionless time this way makes the responses independent of the size of the inner region.

Over a given time, t_{Dr} , the cumulative production, Q_{Dr} , for the radial reservoir, may be defined as:

$$Q_{Dr} = \int_0^{t_{Dr}} q_{Dr} dt_{Dr}. \quad (5.5)$$

From Eqs. (5.2) through (5.5), the normalized dimensionless cumulative production for the radial reservoir is

$$Q_{DrN} = \frac{Q_{Dr}}{\pi R_D^2}. \quad (5.6)$$

5.3.2 Elliptical Reservoir

The dimensionless rate for the elliptical reservoir is defined as:

$$q_{Dr} = \frac{q(t)\mu_i B}{2\pi k_1 h(\rho_i - \rho_{we})}. \quad (5.7)$$

A comparison of Eq. (5.7) with Eq. (5.2) shows that the two equations are the same. Thus, the normalized dimensionless rate for the elliptical geometry remains the same

$$q_{DeN} = q_{De}. \quad (5.8)$$

The normalized dimensionless time is:

$$t_{DeN} = \frac{4}{\pi e^{2\xi_o}} t_{De}, \quad (5.9)$$

where ξ_o is the elliptic distance to the discontinuity or interface.

In comparison with Eq. (5.6), the normalized dimensionless cumulative production for the elliptical reservoir is:

$$Q_{DeN} = \frac{4}{\pi e^{2\xi_o}} Q_{De}. \quad (5.10)$$

5.3.3 Linear Reservoir

The dimensionless rate for the linear geometry is defined as:

$$q_{Dl} = \frac{q(t)\mu_i B}{k_1 b h (p_i - p_{wf})}. \quad (5.11)$$

Comparing Eq. (5.11) with Eq. (5.2), the normalized dimensionless rate for the linear reservoir is:

$$q_{DeN} = \frac{b_D}{2\pi} q_{Dl}. \quad (5.12)$$

The normalized dimensionless time is defined as:

$$t_{D,N} = \frac{t_{Dl}}{a_D b_D}, \quad (5.13)$$

where a_D is the dimensionless distance to the discontinuity, while b_D is the dimensionless width of the linear, composite reservoir. Using Eqs. (5.12) and (5.13), together with a definition of Q_{Dl} analogous to Q_{Dr} (Eq. (5.5)), the normalized dimensionless cumulative production rate may be derived as

$$Q_{D,N} = \frac{Q_{Dl}}{2\pi a_D}. \quad (5.14)$$

5.3.4 Spherical Reservoir

For spherical geometry, the dimensionless rate is defined as:

$$q_{Ds} = \frac{q(t)\mu_i B}{4\pi k_i r_w (p_i - p_{ws})}. \quad (5.15)$$

Once again, by comparing with the radial reservoir, the normalized dimensionless rate for the spherical reservoir is:

$$q_{D,N} = \frac{3}{2a_D} q_{Ds}, \quad (5.16)$$

where a_D is the dimensionless distance to the discontinuity.

The normalized dimensionless time for the spherical geometry is given as:

$$t_{D,N} = \frac{t_{Ds}}{\pi a_D^2}. \quad (5.17)$$

For a spherical reservoir, the normalized dimensionless cumulative production may be given as:

$$Q_{D,s} = \frac{3}{2\pi a_D} Q_{D,r} \quad (5.18)$$

5.4 General Discussion

In the discussion that follows, the results obtained for transient flow in two-region, composite reservoirs in radial, elliptical, linear and spherical geometries producing at a constant pressure are presented. The dimensionless production rate (q_D) and the dimensionless cumulative production (Q_D) responses for both the infinite outer boundary and also the closed finite outer boundary conditions are discussed. Wellbore storage and skin effects were neglected in generating the results. After the normalization exercise carried out in the preceding section, the only parameters that affect the transient rate responses are the mobility ratio (M), the storativity ratio (F) and the distance to the outer boundary, if the reservoir is finite.

The transient rate responses for infinite composite reservoirs of the various flow geometries are compared first. The infinite composite reservoir situation may arise in two instances. In the first instance, the reservoir may be physically so large that, within the testing period, the effects of the reservoir boundaries are not felt. Alternatively, the reservoir itself may not be very large. However, the formation may be so tight that the transients take a very long time to reach the outer boundary.

To compare the transient rate responses for the various flow geometries, the values of M and F are fixed. Figure 5.1 presents a comparison of the dimensionless rate responses for

the various flow geometries. The figure is a log-log graph of normalized dimensionless rate versus normalized dimensionless cumulative production for $M = 100$ and $F = 10$. Three transient flow regimes are apparent from the responses for the various flow geometries. The spherical system is less affected by the chosen values of M and F for the time period of interest. The three transient flow regimes describe the flow rate behavior due to the inner region, the discontinuity, and the outer region of the various composite reservoirs.

Figure 5.1 shows that, at the onset of flow, the linear reservoir shows the highest flow rate. This is followed by the elliptical, the radial and the spherical reservoirs, in descending order. Using the concept of restricted entry, fluids in the linear reservoir will encounter the least resistance to flow towards the inner boundary. Thus, it is expected that for the same average reservoir pressure, the flow rate for the linear reservoir will be higher than that for the spherical reservoir, which has the most resistance to flow. As time progresses, the flow rate for all the reservoirs begins to decline gradually, with the linear reservoir showing the fastest decline. Just before the effect of the discontinuity begins to be felt, the flow rates are about the same for all the geometries. Once the effect of the discontinuity is encountered, the flow rates begin to decline sharply, with the linear reservoir showing the sharpest decline. During this transition period, the mobility and storativity contrasts between the inner and outer regions of the composite reservoirs make the inner region behave as a closed reservoir for a short period. Thus, a short pseudosteady state period is encountered, during which the flow rates decline sharply. Once the fluid flow begins to be affected by the outer region, the flow rates resume their normal rate of decline.

Figure 5.1 also shows that the dimensionless rate responses for the radial and elliptical reservoirs are identical after the effects of the discontinuity are felt. In Chapter 3, it was

shown that the transient pressure derivative responses for infinitely-large, two-region, radial and elliptical, composite reservoirs are identical, except for the inner region.

A comparison of the normalized dimensionless cumulative production responses for the various flow geometries is shown in Fig. 5.2. Figure 5.2 shows that, except for the spherical reservoir, the three transient flow regimes are evident from the responses for the various flow geometries. As expected, the linear reservoir shows the highest cumulative production at the onset of flow. With the progression of time, the cumulative production for the other geometries increase faster, surpassing the linear reservoir by a normalized dimensionless time (t_{DN}) of 20. For the chosen values of M and F , the cumulative production response for the spherical reservoir surpasses that for the radial and elliptical reservoirs by $t_{DN} = 50$.

In the rest of this chapter, decline curves for composite reservoirs in radial elliptical, linear and spherical flow geometries are discussed. The decline curves are obtained by generating the transient rate responses for a closed finite outer boundary. Results for cumulative production are also discussed.

5.5 Decline Curve Analysis

Analysis of production decline curves presents a useful tool in forecasting the future production from a well or reservoir. A knowledge of the future production is probably the most important factor in the economic analysis of exploration and production expenditures. Decline curve analysis can be used to estimate the production performance of a stimulated well due to acidizing. A comparison of the production decline curves before and after acid treatment will enable a determination of the technical and economic success of the treatment.

For homogeneous reservoirs, *Fetkovich* (1980) presented an extensive discussion of decline curve analysis using type curves. *Fetkovich* (1980) showed, among other things, how to use production decline type curves to estimate the formation flow capacity (kh) and the porosity-compressibility (ϕc_f). For composite reservoirs, however, *Olarewaju* and *Lee* (1987a) have argued that the conventional homogeneous decline type curves are not appropriate. *Olarewaju* and *Lee* (1987a, b and c) have presented production decline curves for the analysis of transient rate data from radial, composite reservoirs with a damaged or stimulated well. *Turki et al.* (1989) presented rate decline and rate decline derivative type curves for constant-pressure production in a two-region, radial, composite reservoir. They conducted a parametric study of the effects of mobility ratio, storativity ratio and distance to the discontinuity on the rate decline and rate decline derivative for both infinite and finite composite reservoirs.

While production decline curves for radial, composite reservoirs have been presented fairly well in the literature, the same is not case for composite reservoirs in elliptical, linear and spherical flow geometries. In this study, a comparison of the production decline curves from composite reservoirs in radial, elliptical, linear and spherical flow geometries is presented. In addition, a detailed investigation of the effects of mobility and storativity ratios, as well as the reservoir size on the transient rate responses from radial and linear, composite reservoirs is presented.

5.5.1 Comparison of Production Decline Curves

Figure 5.3 compares the dimensionless rate responses for composite reservoirs in radial, elliptical, linear and spherical geometries with closed outer boundaries. The curves for the spherical geometry do not begin at the same time as the other geometries. This is due to

numerical instabilities in inverting the solution from Laplace space at early time. Figure 5.3 is generated for a storativity ratio of $F = 1$, and two mobility ratio values, $M = 1$ and $M = 10$. For radial, linear and spherical composite reservoirs, the ratio of outer boundary distance to the discontinuity boundary distance is 100. Thus, considering the different shapes of the various geometries, the total reservoir volume is different for each geometry. The spherical reservoir has the largest volume, followed by the radial reservoir, and then the linear reservoir. For the elliptical reservoir, the ratio of the outer boundary elliptic distance to the inner boundary elliptic distance (ξ_e/ξ_0) is 3.3. For $\xi_e/\xi_0 = 3.3$, the total reservoir volume for the elliptical and radial geometries is equal. Figure 5.3, once again, shows that the linear reservoir starts with the highest flow rate, while the spherical reservoir has the lowest rate. In Fig. 5.3, the effect of the outer boundary is indicated by a sharp drop in the flow rate towards zero at late times. This reflects true pseudosteady state flow behavior. The figure shows that the effects of the outer boundary are encountered first by the linear reservoir. This is expected, because the linear reservoir has the smallest total volume. The next to show outer boundary effects are the radial and elliptical reservoirs, which do so at the same time. The spherical reservoir, having the largest volume, takes the longest time to encounter the outer boundary effects. In Fig. 5.3, the curves for $M = 1$ and $F = 1$ represent homogeneous reservoirs.

Figure 5.4 compares the dimensionless cumulative production responses for the various flow geometries, for the same reservoir parameters as in Fig. 5.3. Here, outer boundary effects are indicated by the cumulative production responses approaching asymptotic values (i.e., flattening out). As expected, the linear reservoir responses flatten out first, followed by the radial and elliptical reservoir responses. The spherical reservoir responses take the longest time to encounter the outer boundary effects. Figure 5.4 also shows that, as expected, the responses with higher mobility contrasts take a longer time to exhibit the outer boundary effects than the responses with lower mobility contrasts. Focusing on the

responses for the radial and elliptical reservoirs. Fig. 5.4 shows that for homogeneous reservoirs ($M = 1$, $F = 1$), the cumulative production responses are quite different, until the very end when outer boundary effects begin to be felt. The same observation can be made from Fig. 5.3. For composite reservoirs ($M = 10$), however, the responses for the radial and elliptical reservoirs start to become identical, once the effects of the discontinuity boundary are felt. The next two figures present detailed comparisons of the transient rate responses for the radial and elliptical, composite reservoirs.

The dimensionless production rates for the radial and elliptical, composite reservoirs are compared in Fig. 5.5. The figure shows rate responses for selected mobility ratios between 1 and 100, and for storativity ratios of 10 and 100. The rate responses for the homogeneous reservoirs ($M = 1$, $F = 1$) are also shown in Fig. 5.5. Focusing on the rate responses during the transition period, Fig. 5.5 shows that the higher the mobility ratio, the sharper the drop in dimensionless production rate. From the outer region responses, it can be seen that higher mobility and storativity ratios result in lower production rates. Higher mobility and storativity ratios mean a higher pressure drop across the discontinuity boundary. This results in a greater restriction of flow towards the wellbore.

Figure 5.6 compares the cumulative production responses for the radial and elliptical, composite reservoirs. The figure shows that the responses for the two reservoirs are similar for the composite reservoir responses. The homogeneous reservoir responses are not the same. Figure 5.6 shows that the cumulative production for the elliptical reservoir is higher than that for the radial reservoir at the onset of flow. In fact, the cumulative production for the elliptical reservoir continues to remain higher until the effect of the discontinuity boundary is encountered. This observation holds true for the production rate as well (Fig. 5.5). This phenomenon is not surprising, since the elliptical reservoir

represents a vertical fracture at the well. The flow rate to a fractured well should be higher than that to an unfractured well.

In the following sections, a detailed sensitivity study on the effects of mobility and storativity ratios, as well as reservoir size on the dimensionless rate and cumulative production responses for radial and linear, composite reservoirs is presented. For brevity, the radial and linear, composite reservoirs have been chosen as examples for discussion.

5.5.2 Decline Curve Analysis for Radial, Composite Reservoirs

In this section, the effects of mobility and storativity ratios, and also the effect of reservoir size on the dimensionless rate and cumulative production for a closed, radial, composite reservoir producing at a constant pressure are discussed. Figures 5.7 and 5.8 show the effect of mobility ratio on the normalized dimensionless rate and the normalized dimensionless cumulative production responses, respectively. For these figures, the storativity ratio, $F, = 10$. The ratio of the outer boundary distance to the discontinuity boundary distance (r_{eD}/R_D) is 100. The transient rate responses for a homogeneous, radial reservoir ($M = 1, F = 1$) are also shown for comparison.

Figures 5.7 and 5.8 show that all responses initially form one curve. This corresponds to infinite-acting behavior in the inner region, during which time the effects of the discontinuity boundary are not yet felt. Once the discontinuity boundary is encountered, the responses begin to drop sharply. Infinite-acting behavior is resumed once the transients enter the outer region. The figures also show that, the higher the mobility ratio, the larger the drop in rate or cumulative production. Furthermore, the responses for the higher mobility contrasts take a longer time to show the outer boundary effects than the responses for lower mobility contrasts. By definition, a higher mobility ratio means that the outer

region is tighter (less permeable) than the inner region. It stands to reason, then, that the tighter the outer region, the longer it will take for the transients to travel to the outer boundary.

A comparison of Fig. 5.7 with Fig. 5.8 shows that infinite-acting behavior, corresponding to the inner region, ends sooner for the dimensionless rate (Fig. 5.7) than it does for the dimensionless cumulative production (Fig. 5.8). This observation, which is found to hold true in this study on transient rate behavior, has also been found to be true for transient pressure behavior (*Larsen, 1983; Aarstad, 1987*). The explanation for this occurrence is that the derivatives of a function are more sensitive to disturbances in the reservoir than is the underlying function. Note that the dimensionless rate responses in Fig. 5.7 are the derivatives, with respect to time, of the dimensionless cumulative production responses in Fig. 5.8.

Figures 5.9 and 5.10 show the effect of storativity ratio on the normalized dimensionless rate and the normalized dimensionless cumulative production responses, respectively. These responses are generated for a fixed mobility ratio, $M = 10$. The other fixed parameters are similar to those in Figs. 5.7 and 5.8. For composite reservoirs ($M = 10$ and $F > 1$), Figure 5.9 shows four distinct flow regimes. These are, sequentially, infinite-acting flow in the inner region, transition flow due to the discontinuity, infinite-acting flow in the outer region, and pseudosteady state flow due to the closed outer boundary. Figures 5.9 and 5.10 show that transient responses with higher storativity ratios encounter the outer boundary sooner than those with lower storativity ratios. A higher storativity ratio means that the outer region is much less compressible than if the storativity ratio were lower. It follows that transients will travel faster in a less compressible medium than they will in a more compressible medium.

A comparison of Figs 5.7 and 5.8, on the one hand, with Figs. 5.9 and 5.10, on the other, shows that storativity ratio has less effect on the transient rate and cumulative production responses than does mobility ratio. This observation is found to be true also for the transient pressure derivative responses discussed in Chapter 4.

The combined effect of mobility and storativity ratio on the normalized dimensionless rate and the normalized dimensionless cumulative production responses is shown in Figs 5.11 and 5.12, respectively. The figures show transient responses for selected mobility ratios between 1 and 100, and for storativity ratios between 1 and 100. Figure 5.11 shows four clearly defined flow regimes for any combination of M and F , except for $M = 1$. Figure 5.11 could serve as a type curve for decline curve analysis of radial, composite reservoirs. However, such an undertaking might prove to be formidable, since Fig. 5.11 is only for one fixed ratio of $r_{eD}/R_D = 100$.

Figures 5.13 and 5.14 show the effect of reservoir size on the normalized dimensionless rate and the normalized dimensionless cumulative production responses, respectively. These responses are generated for $M = 10$ and $F = 10$, and for selected ratios of r_{eD}/R_D between 50 and 1000. The infinite reservoir responses are also included for comparison. As expected, Figs. 5.13 and 5.14 show that the larger the reservoir size, the longer it takes for the effects of the outer boundary to be felt.

5.5.3 Decline Curve Analysis for Linear, Composite Reservoirs

Here, the effects of mobility and storativity ratios, as well as reservoir size, on the dimensionless rate and cumulative production responses for a closed, linear, composite reservoir with a constant-pressure inner boundary condition are discussed. Figures 5.15 and 5.16 show the effect of mobility ratio on the normalized dimensionless rate and the

normalized dimensionless cumulative production responses, respectively. For these responses, the storativity ratio is fixed at 10, while the ratio of the reservoir length to the length of the inner region (x_{eD}/u_D) is 100. The transient responses are generated for selected mobility ratios between 1 and 100. The response for a linear, homogeneous reservoir ($M = 1, F = 1$) is included for comparison.

Figures 5.15 and 5.16 show that the higher the mobility ratio, the greater the deviation from the homogeneous reservoir response. Also, responses for higher mobility ratios tend to take longer to show the effects of the closed outer boundary than the responses with lower mobility ratios. Furthermore, a comparison of Fig. 5.15 with Fig. 5.16 shows that, once again, infinite-acting behavior in the inner region ends earlier for the dimensionless flow rate response than it does for the dimensionless cumulative production response.

Figures 5.17 and 5.18 show the effect of storativity ratio on the normalized dimensionless rate and the normalized dimensionless cumulative production responses, respectively. These responses are generated for a fixed mobility ratio, $M = 10$. Other fixed parameters are similar to those in Figs. 5.15 and 5.16. Figures 5.17 and 5.18 show that storativity ratio, just as the mobility ratio, has a significant effect on the transient rate and cumulative production responses.

A comparison of Figs 5.15 and 5.16 with Figs. 5.17 and 5.18, respectively, shows that storativity ratio has almost an identical effect on the transient rate and cumulative production responses as mobility ratio. In fact, the responses are identical until the effect of the closed outer boundary begins to be felt. In Chapter 4, it was shown that mobility ratio and storativity ratio had identical effects on the transient pressure derivative responses because, for infinitely-large, linear, composite reservoirs, the correlating parameter is MF .

However, the above observation indicates that MF is not a correlating parameter for finite, linear, composite reservoirs.

The combined effect of mobility and storativity ratio on the normalized dimensionless rate and the normalized dimensionless cumulative production responses is shown in Figs 5.19 and 5.20, respectively. The ratio, $x_eD/a_D = 100$. Transient responses are generated for selected mobility ratios between 1 and 100, and for storativity ratios between 1 and 100. In Fig. 5.19, the irregularity in the curve for $M = 100$, $F = 100$ is due to numerical instabilities, and not reflective of the flow behavior. Figures 5.19 and 5.20 show clearly that MF is not a correlating parameter for finite, linear, composite reservoirs. In these figures, the responses for $M = 10$, $F = 100$ are different from the responses for $M = 100$, $F = 10$, even though, for the two cases $MF = 1000$. Here again, Fig. 5.19 could serve as a type curve for decline curve analysis of linear, composite reservoirs.

Figures 5.21 and 5.22 show the effect of reservoir size on the normalized dimensionless rate and the normalized dimensionless cumulative production responses, respectively. These responses are generated for $M = 10$ and $F = 10$, and for selected ratios, x_eD/a_D , between 10 and 1000. The infinite reservoir responses are also included for comparison. The figures confirm that the larger the reservoir size, the longer it takes for the effects of the outer boundary to be felt. Figures 5.21 and 5.22 could serve as alternative type curves for matching of rate data from linear, composite reservoirs for pre-assumed values of M and F .

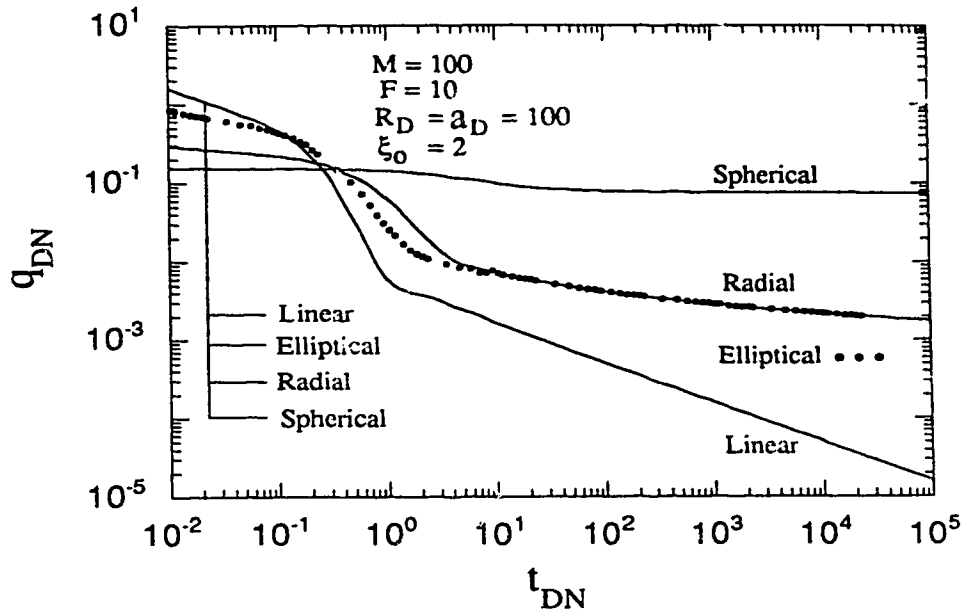


Figure 5.1: Dimensionless flow rate for composite reservoirs in radial, elliptical, linear and spherical geometries producing at a constant pressure.

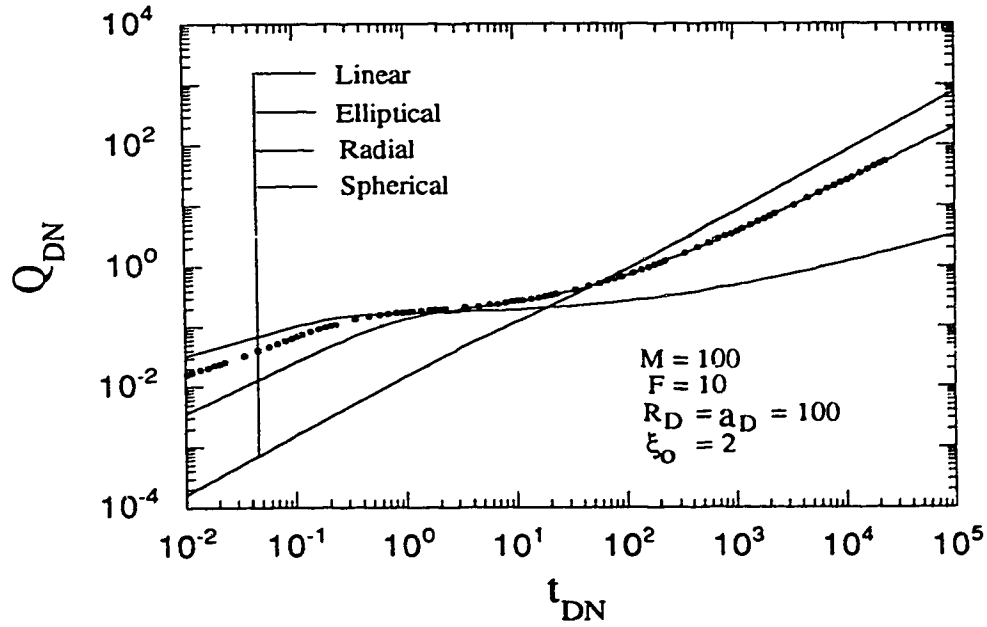


Figure 5.2: Dimensionless cumulative production for composite reservoirs in radial, elliptical, linear and spherical geometries producing at a constant pressure.

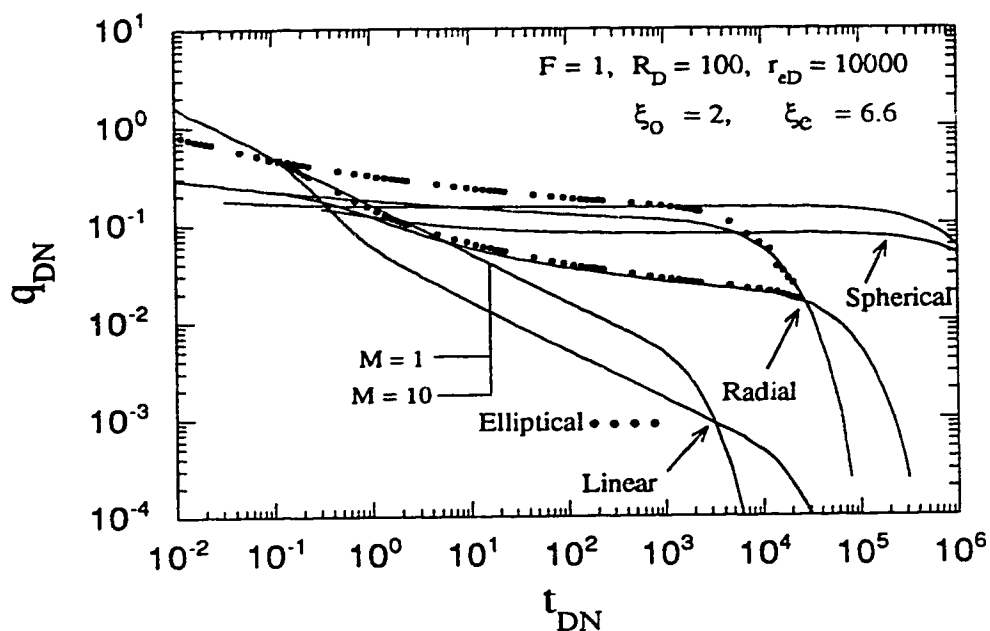


Figure 5.3: Dimensionless rate responses for closed radial, elliptical, linear and spherical, composite reservoirs producing at a constant pressure.

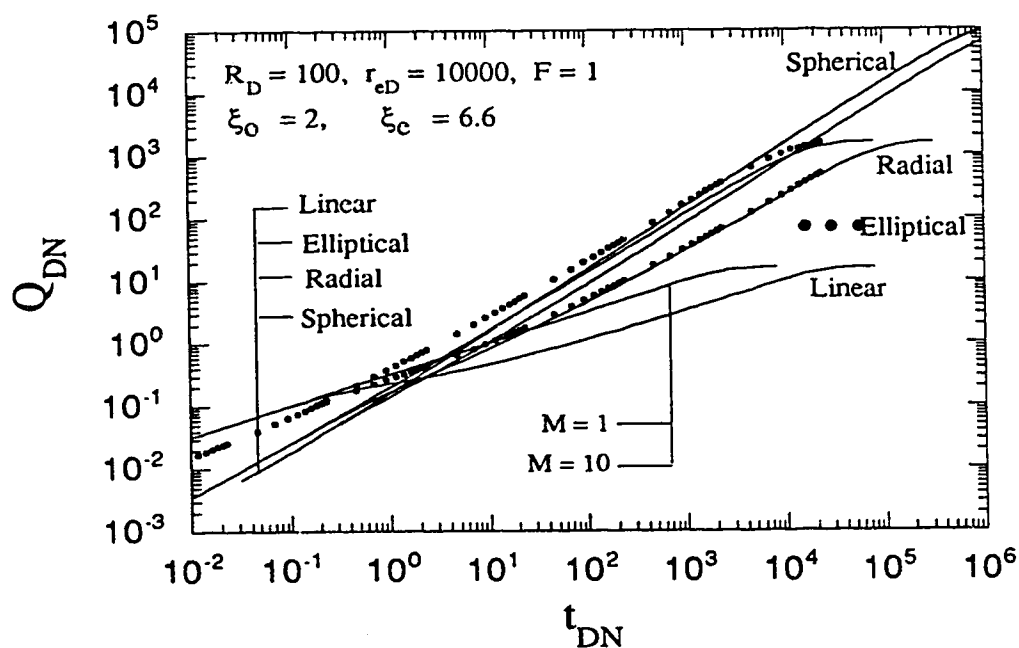


Figure 5.4: Cumulative production responses for closed radial, elliptical, linear and spherical, composite reservoirs producing at a constant pressure.

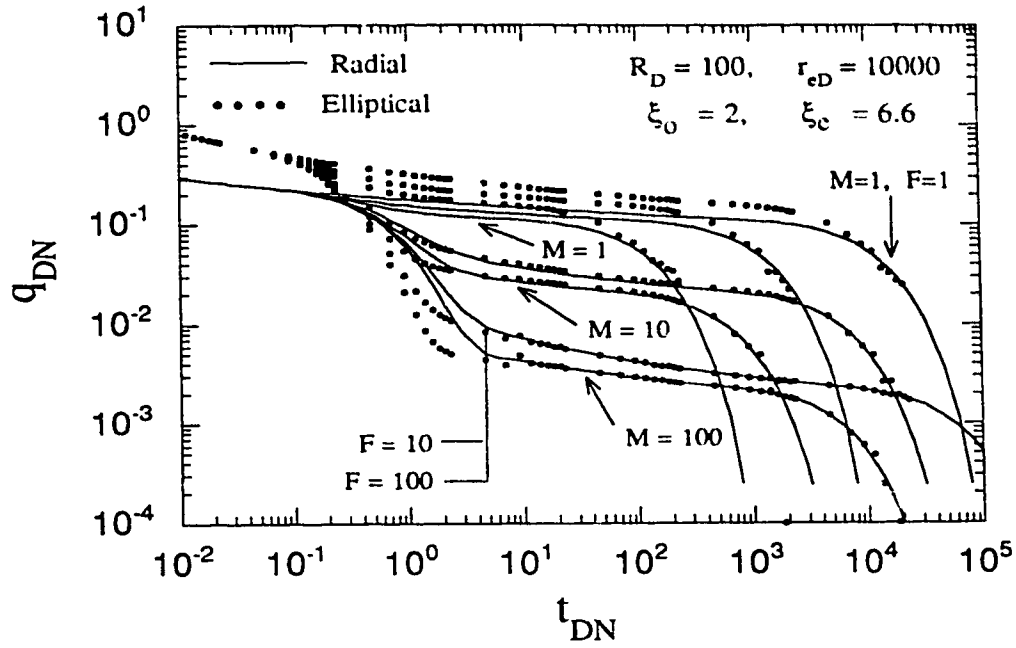


Figure 5.5: Comparison of dimensionless rate responses for closed radial and elliptical composite reservoirs producing at a constant pressure.

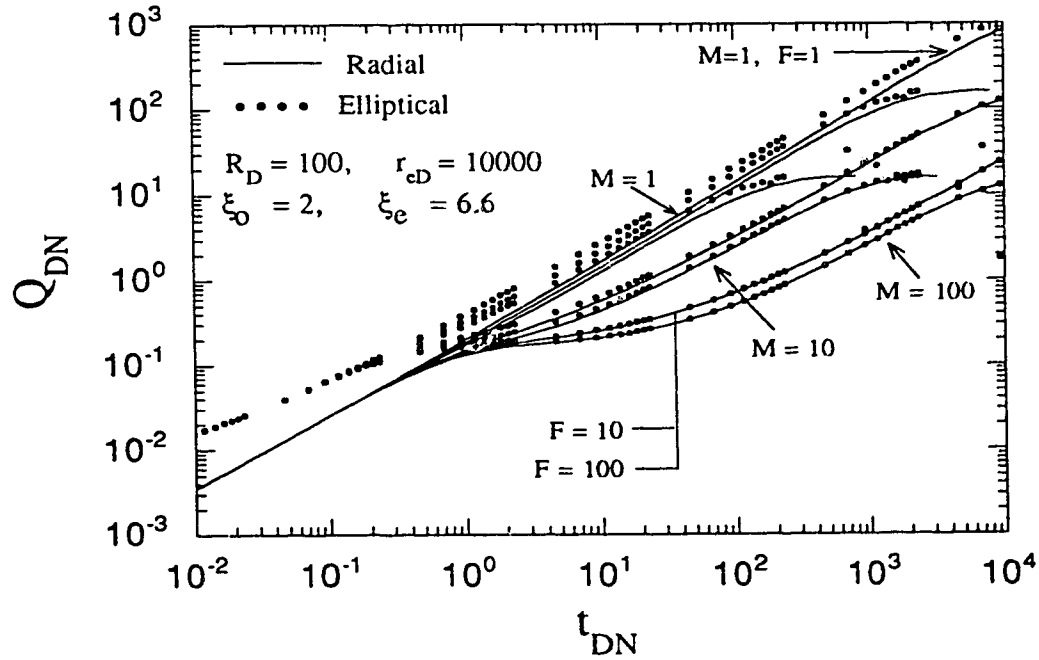


Figure 5.6: Comparison of dimensionless cumulative production responses for closed radial and elliptical composite reservoirs producing at a constant pressure.

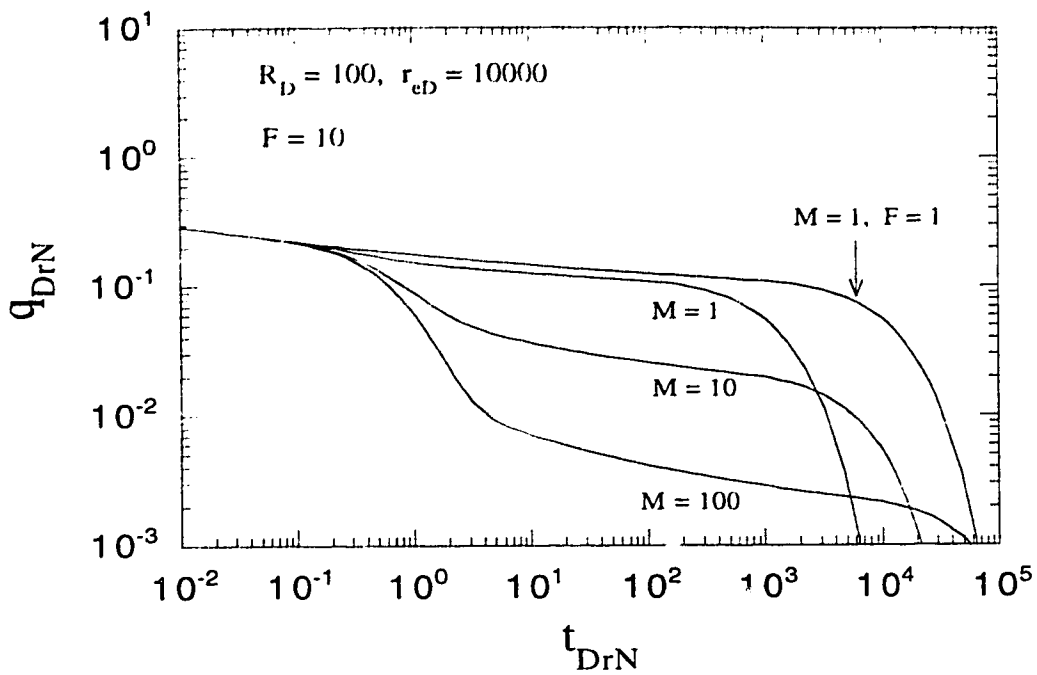


Figure 5.7: Effect of mobility ratio on dimensionless rate responses for a closed, radial, composite reservoir producing at a constant pressure.

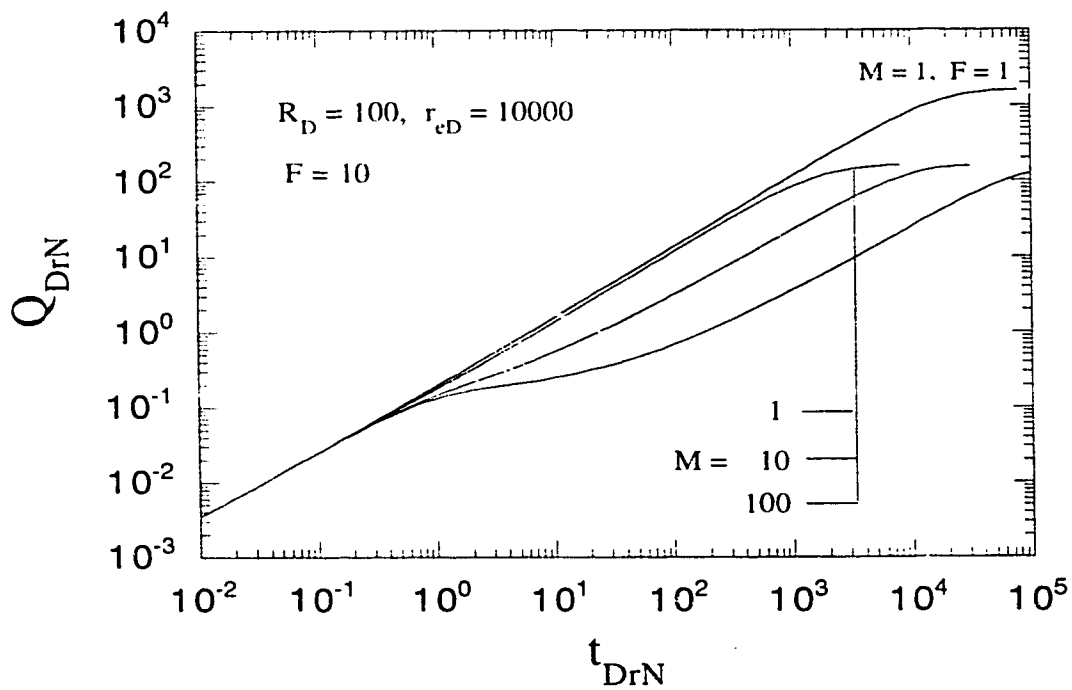


Figure 5.8: Effect of mobility ratio on cumulative production responses for a closed, radial, composite reservoir producing at a constant pressure

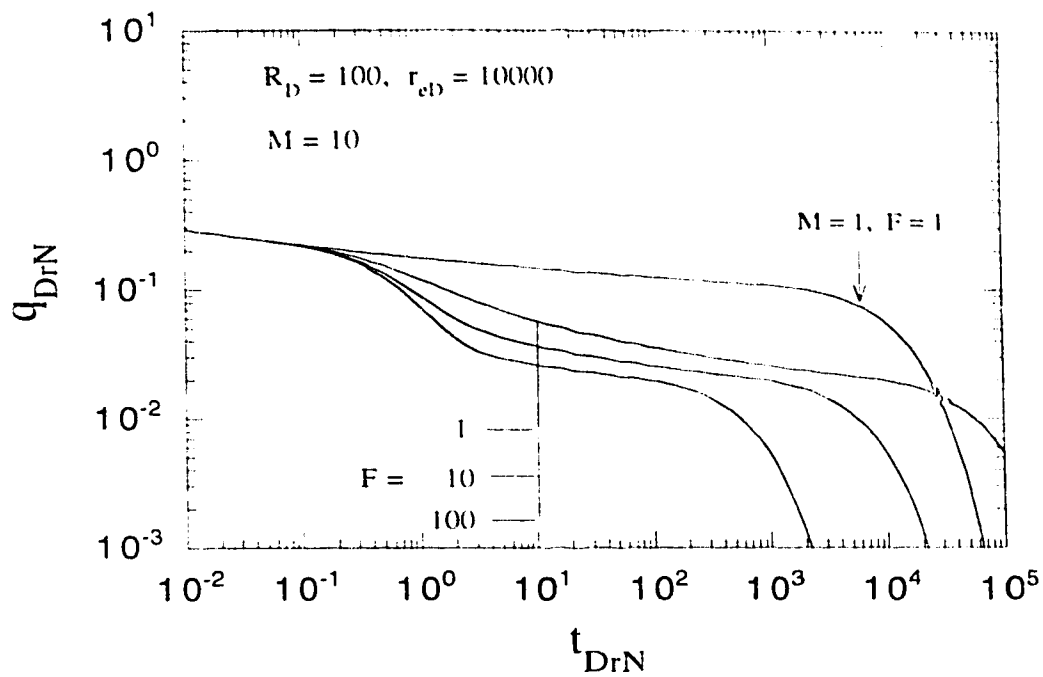


Figure 5.9: Effect of storativity ratio on dimensionless rate responses for a closed, radial, composite reservoir producing at a constant pressure.

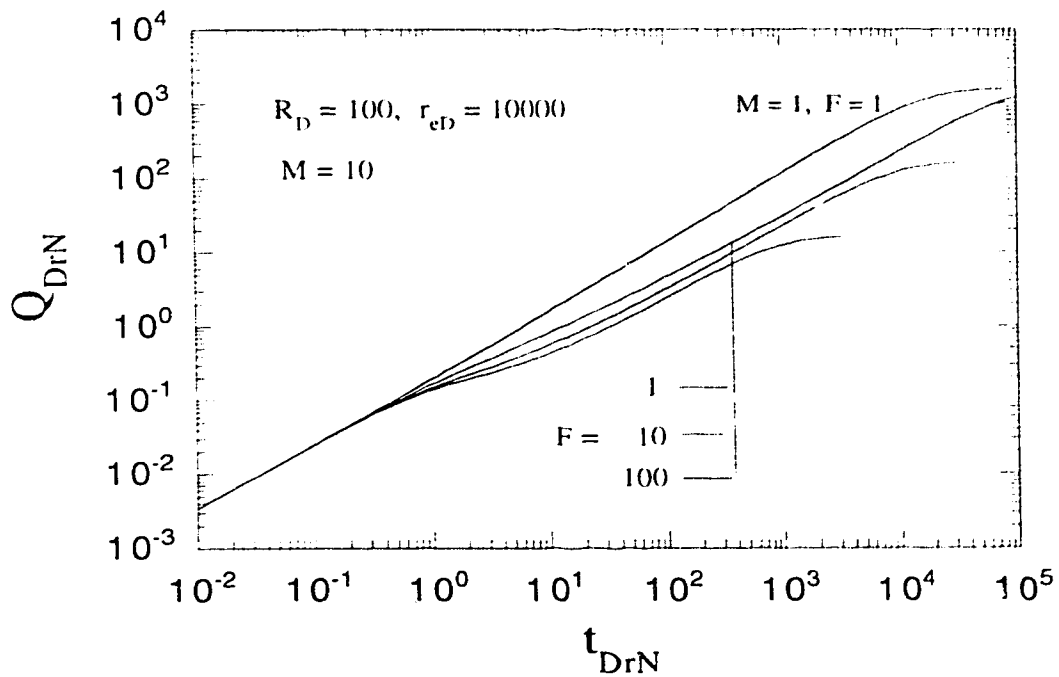


Figure 5.10: Effect of storativity ratio on cumulative production responses for a closed, radial, composite reservoir producing at a constant pressure.

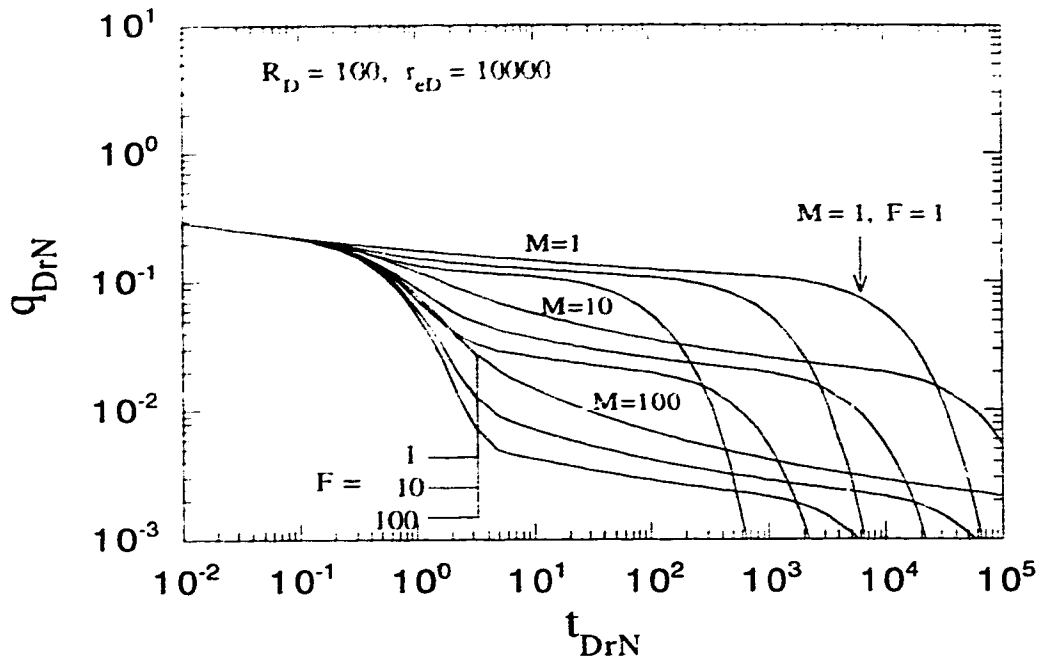


Figure 5.11: Effect of mobility and storativity ratio on dimensionless rate responses for a closed, radial, composite reservoir producing at a constant pressure.

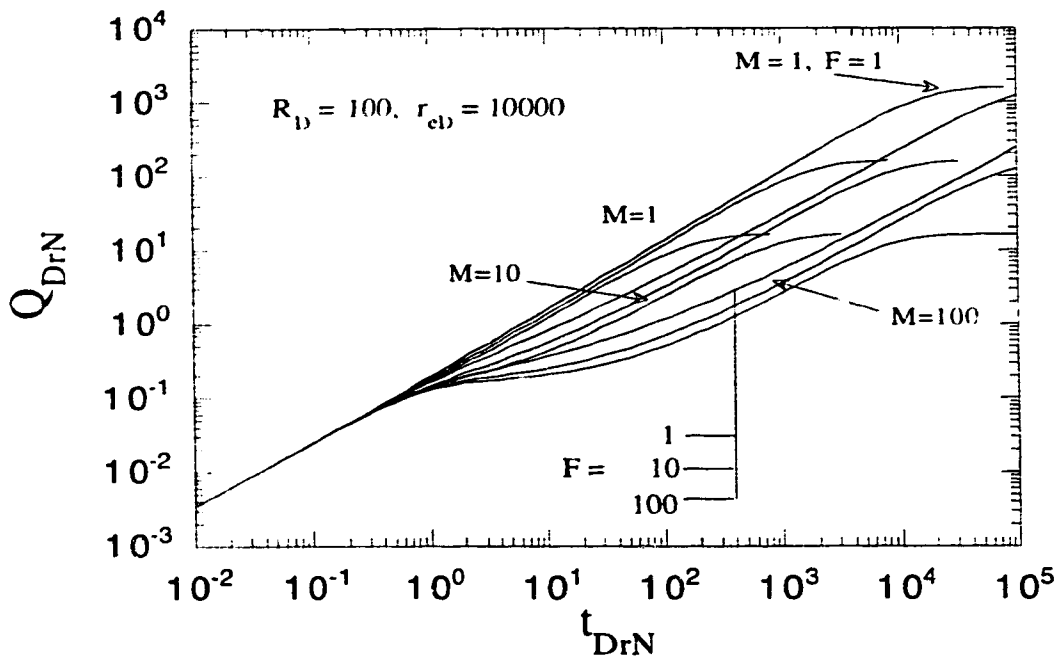


Figure 5.12: Effect of mobility and storativity ratio on cumulative production responses for a closed, radial, composite reservoir producing at a constant pressure.

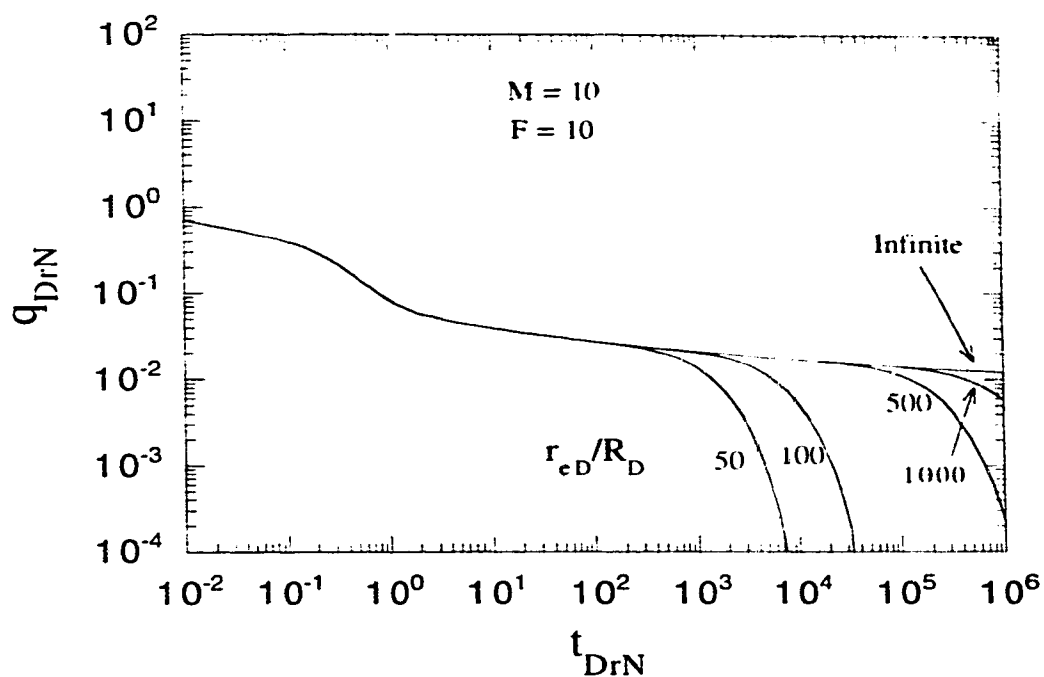


Figure 5.13: Effect of reservoir size on dimensionless rate responses for a closed, radial, composite reservoir producing at a constant pressure.

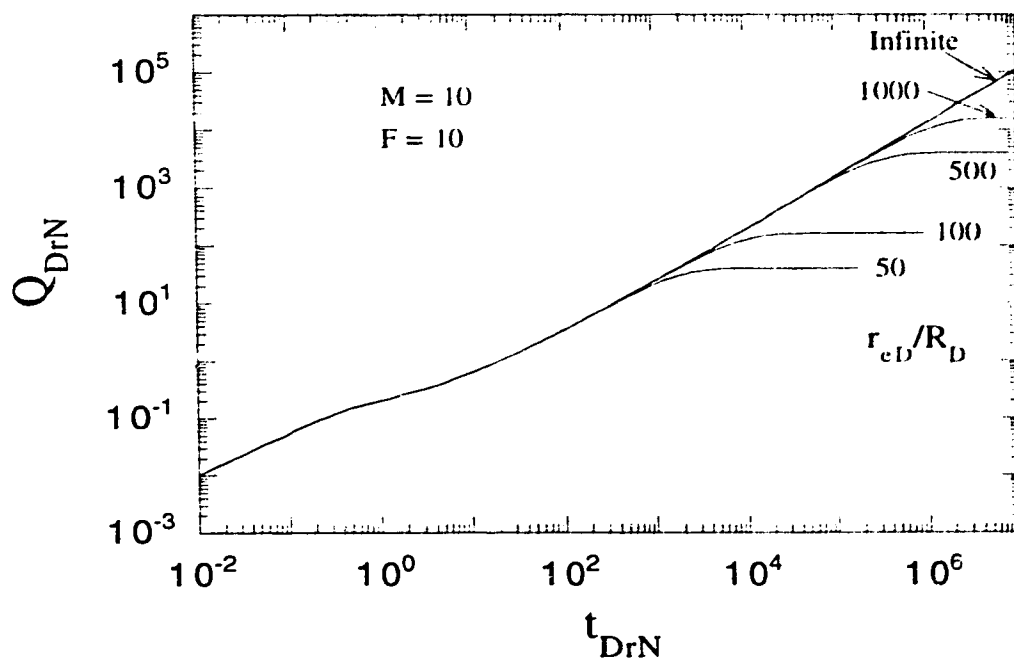


Figure 5.14: Effect of reservoir size on cumulative production responses for a closed, radial, composite reservoir producing at a constant pressure.

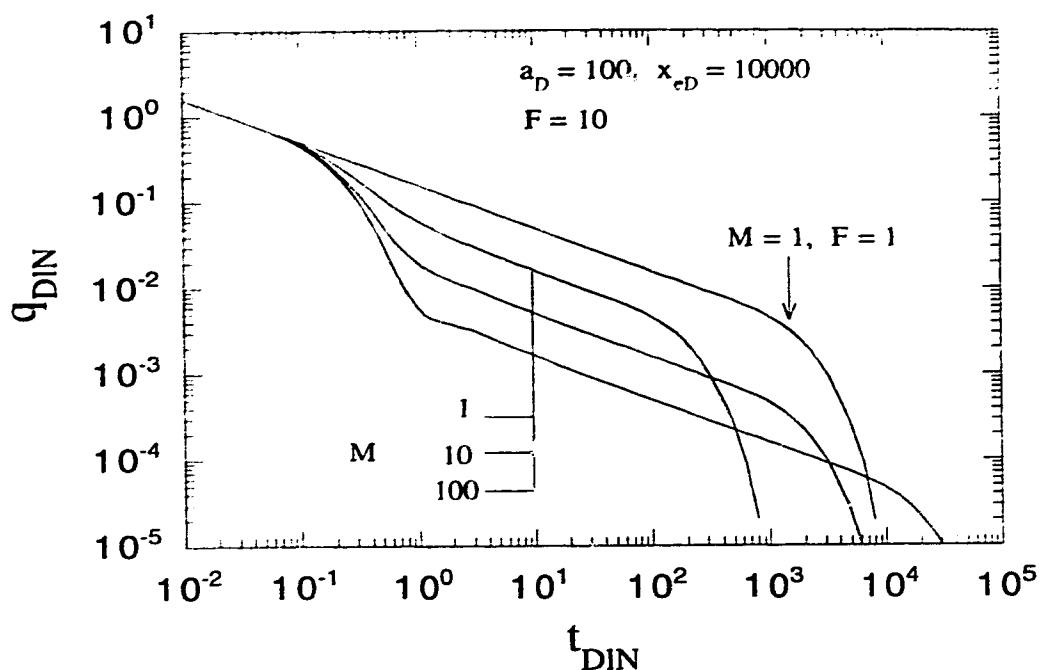


Figure 5.15: Effect of mobility ratio on dimensionless rate responses for a closed, linear, composite reservoir producing at a constant pressure.

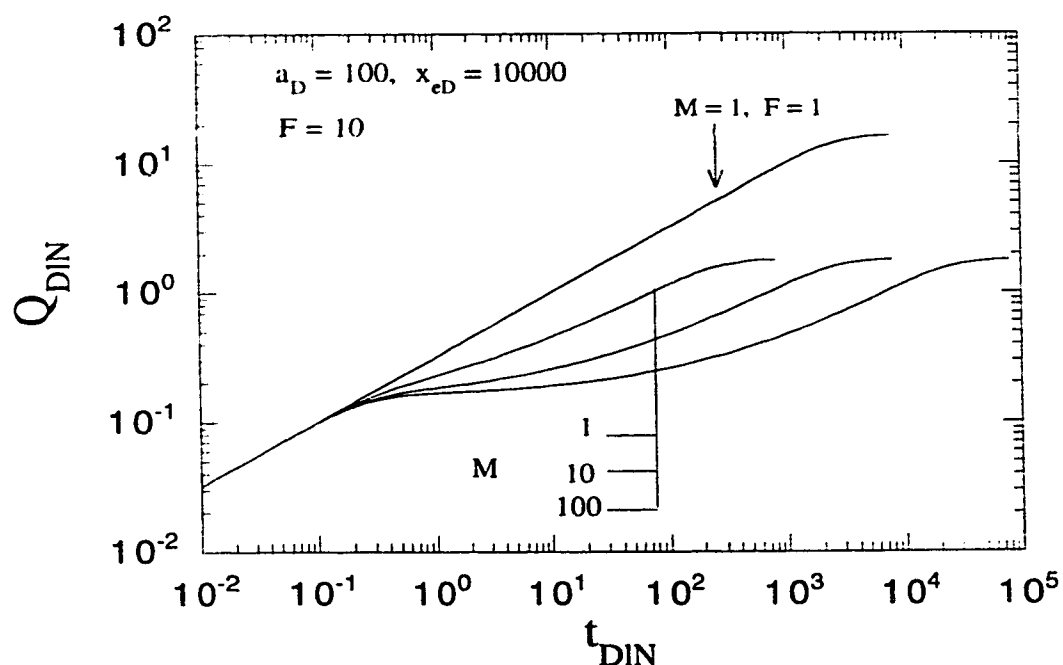


Figure 5.16: Effect of mobility ratio on dimensionless cumulative production responses for a closed, linear, composite reservoir producing at a constant pressure.

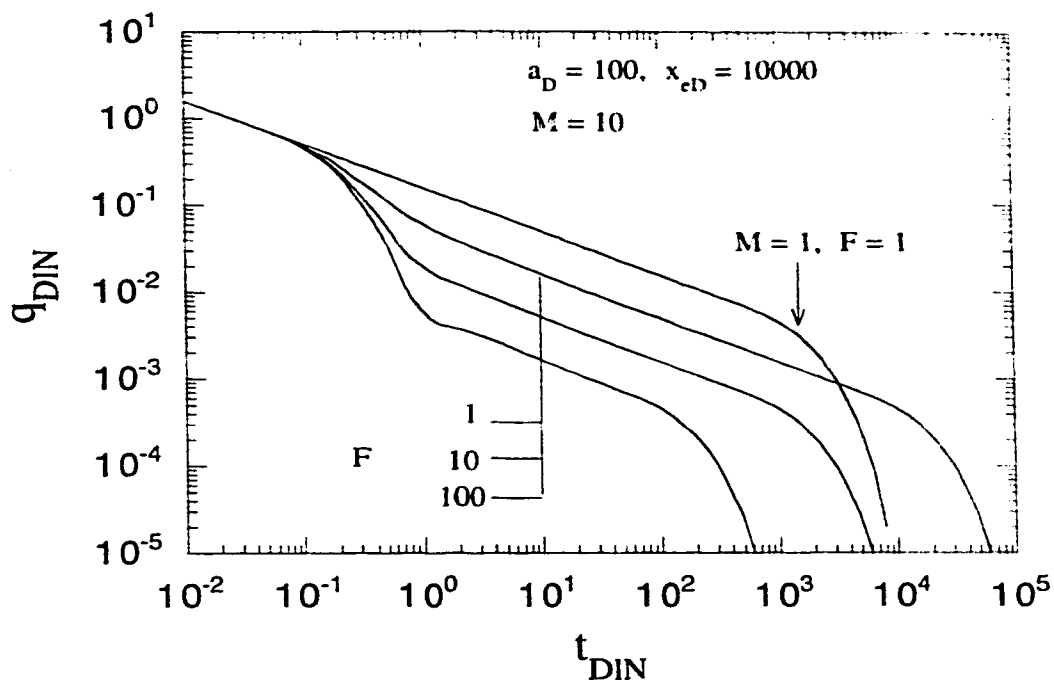


Figure 5.17: Effect of storativity ratio on dimensionless rate responses for a closed, linear, composite reservoir producing at a constant pressure

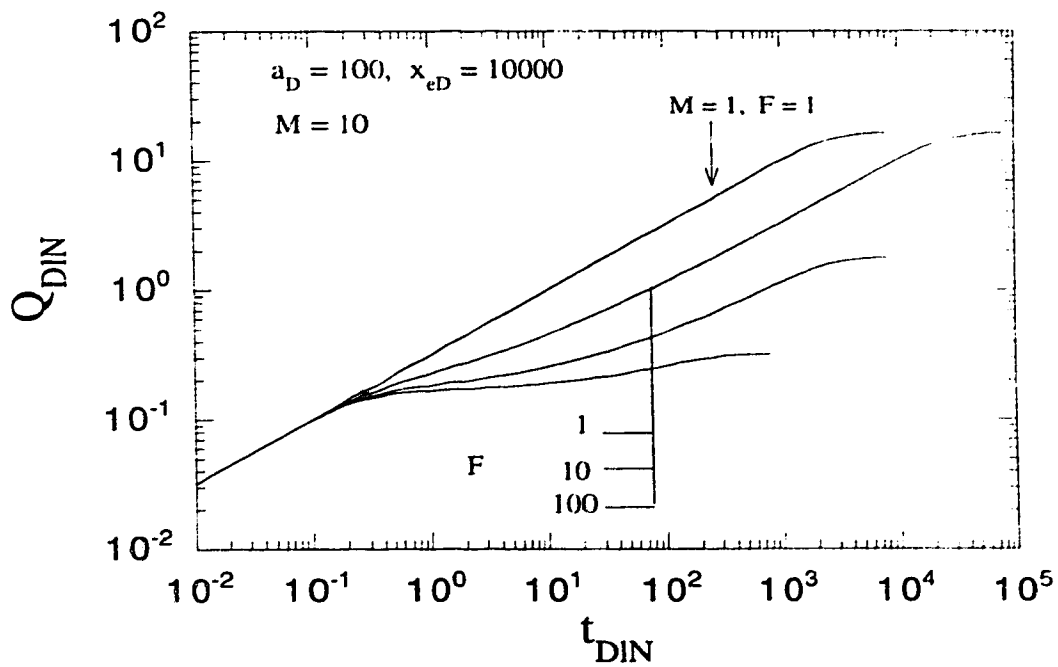


Figure 5.18: Effect of storativity ratio on dimensionless cumulative production responses for a closed, linear, composite reservoir producing at a constant pressure.

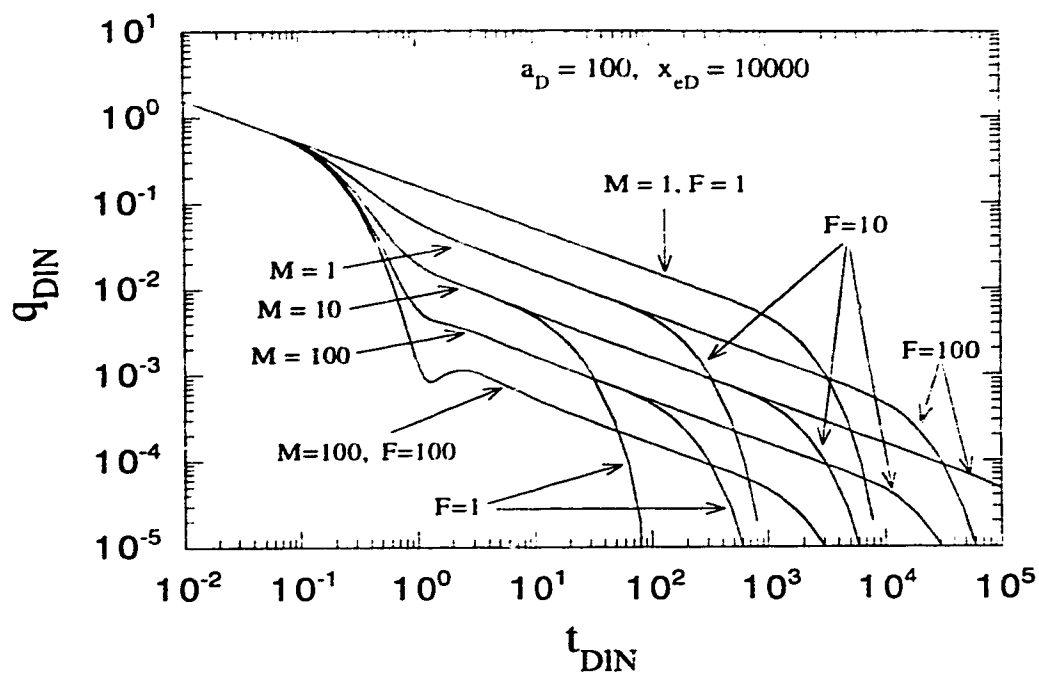


Figure 5.19: Effect of mobility and storativity ratio on dimensionless rate responses for a closed, linear, composite reservoir producing at a constant pressure.

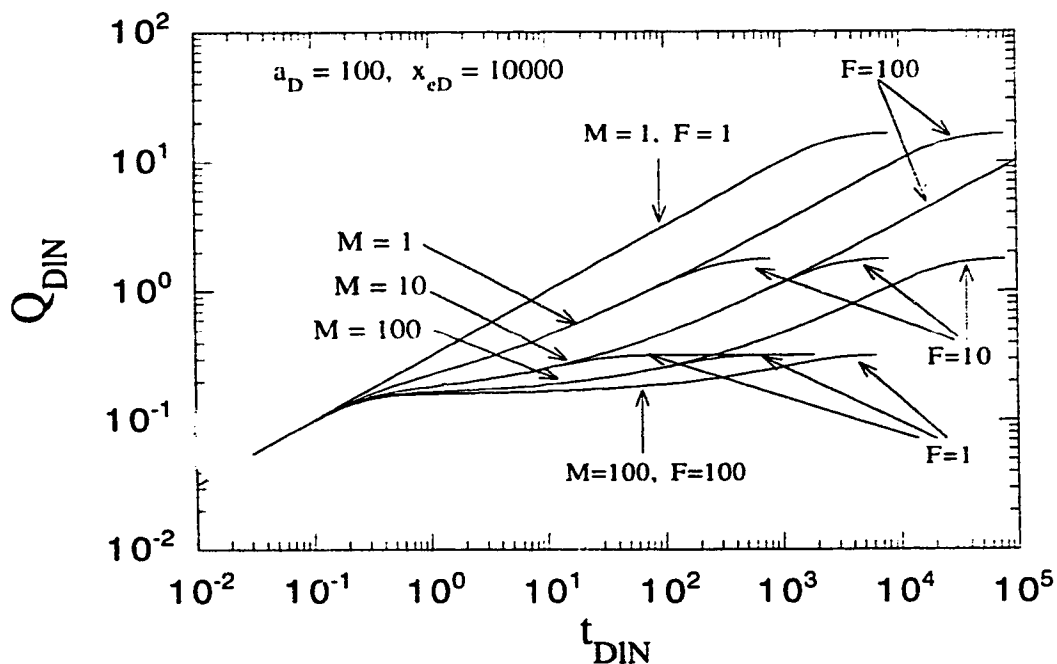


Figure 5.20: Effect of mobility and storativity ratio on dimensionless cumulative production responses for a closed, linear, composite reservoir producing at a constant pressure.

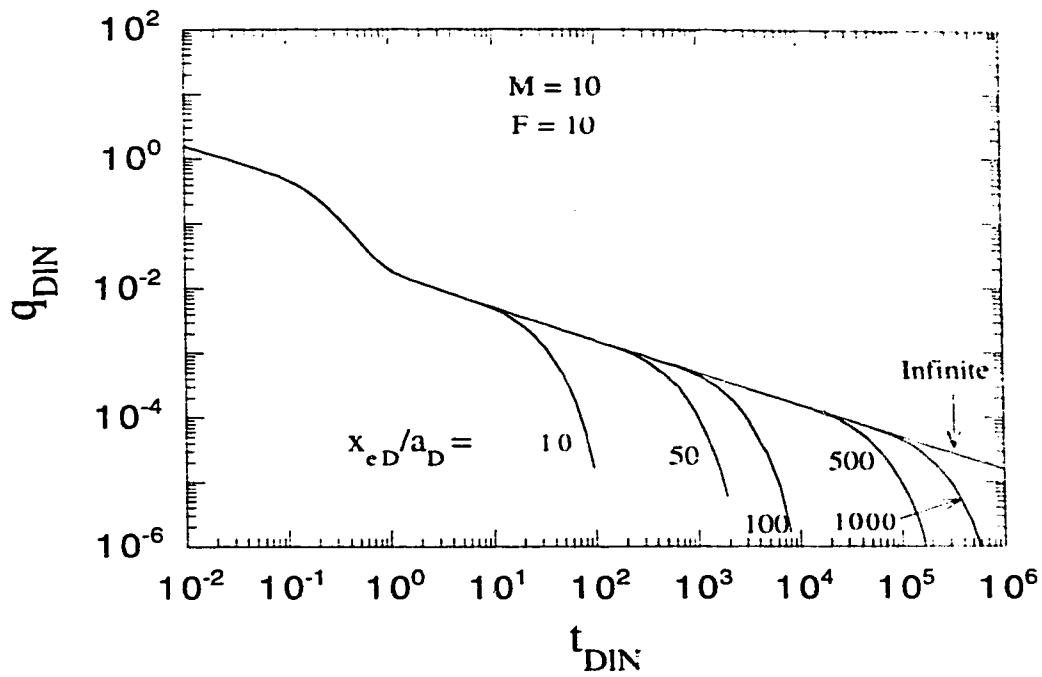


Figure 5.21: Effect of reservoir size on dimensionless rate responses for a closed, linear, composite reservoir producing at a constant pressure.

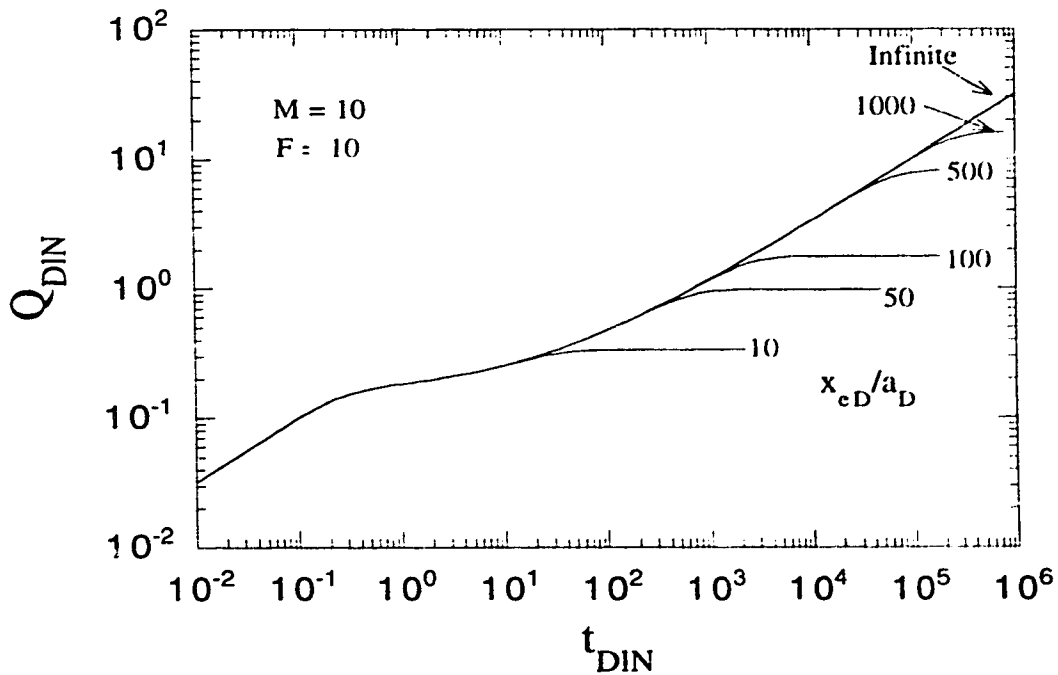


Figure 5.22: Effect of reservoir size on cumulative production responses for a closed, linear, composite reservoir producing at a constant pressure.

6.0 THREE-REGION, COMPOSITE RESERVOIR WITH POWER-LAW VARIATION IN PROPERTIES

6.1 Introduction

Most of the composite reservoir models used to analyze thermal recovery well-test data consist of two regions with different, but uniform, reservoir and fluid properties, separated by a sharp interface. In reality, the interface separating the two regions is not sharp. Instead, there is an intermediate region between the inner and outer regions, which is characterized by a rapid decline in mobility and storativity.

The quest to improve on the two-region, composite models, has led to the development of three-region, composite reservoir models (*Onyekonwu and Ramey, 1986; Barua and Horne, 1987; and Ambastha and Ramey, 1992*). In these models, the intermediate region is represented by a uniform set of mobility and storativity values that lie (in magnitude) between those in the inner region and the outer region.

To represent secondary recovery processes more realistically, analytical multi-region, composite reservoir models have been proposed (*Nanba and Horne, 1989; Abbaszadeh-Dehghani and Kamal, 1989; Bratvold and Horne, 1990*). In these studies, analytical multi-region, composite reservoir models were used to analyze injection and pressure falloff test data following cold water injection, to yield estimates of temperature-dependent mobilities in the flooded and uninvaded regions, as well as oil and water relative permeabilities. *Acosta and Ambastha (1994)* have used a multi-region, composite reservoir model to study the effect of various trends of mobility and storativity variations on thermal recovery well test data. Multi-region, composite reservoir models are made up of more than three regions. The regions between the first and the last make up the intermediate

region. The intermediate region is represented by a series of mobility and storativity values that decrease as some step function of distance from the wellbore.

In recent years, a number of analytical models for the pressure transient behavior of heterogeneous reservoirs have appeared, where the concept of fractal geometry has been used to describe a fracture network (*Chang and Yortsos, 1990; Beier, 1994; Acuña et al., 1995*). Similar analytical models for constant pressure injection or production have been presented by *Barker (1988)* and *Doe (1991)*. The concept of fractal geometry suggests that structures which appear to be completely random can be described within a mathematical framework.

Extending the concept of fractal geometry to composite reservoirs, *Chakrabarty (1993)* presented a two-region, composite reservoir model, where the inner region was assigned a fractal property, while the outer region was homogeneous. The fractal inner region was characterized by declining porosity and permeability, with distance from the wellbore, in a power law relationship. Using semilog pressure derivative responses, *Chakrabarty (1993)* presented a sensitivity study of the model to parameters, such as the size of the inner region, the permeability ratio and the mass fractal dimension.

Recently, *Poon (1995)* has proposed an infinite two-region, radial, composite reservoir model for thermal recovery processes. In this model, the outer region (oil bank) is assigned a fractal property to represent the rapid decline of diffusivity, due to the rapid decline in temperature, ahead of the flood front. The diffusivity in the inner region is constant, while the diffusivity in the outer region decreases in a power law relationship with distance. *Poon (1995)* reported that it was not possible to develop a second semilog straight line corresponding to infinite-acting flow in the outer region, since the rock and fluid properties in the oil bank were not constant (in his model). In reality, however, a

reservoir undergoing thermal recovery is most likely to have three regions. The inner region, which is filled with the injected fluid can be considered homogeneous, with constant mobility and storativity. The intermediate region, which is characterized by rapidly declining temperature, may be assigned a power law variation of properties with distance. The third (outer) region, which is full of cold oil, can be considered homogeneous also, with constant mobility and storativity values that are less than those in the inner region.

This chapter presents an analytical solution for the pressure transient behavior of a three-region, radial, composite reservoir, with a power law variation of properties in the intermediate region. Mobility and storativity in the intermediate region decrease as power law functions of the radial distance from the first discontinuity boundary. This representation of thermal recovery processes is more realistic than the sharp front idealization of the traditional two- and three-region, composite reservoir models. It is also an improvement over the two-region, fractal, composite reservoir model presented by *Poon* (1995), because the model presented in this chapter allows for a homogeneous outer region. The effects of the conductivity indices or fractal exponents and the size of the intermediate region on the transient semi-log and Cartesian pressure derivative responses are investigated.

Figure 6.1 shows a schematic of a three-region, radial, composite reservoir. The outer region is considered to be infinite in extent. The variables R_1 and R_2 are the inner and intermediate region radii, respectively. The intermediate region is characterized by a rapid decline in fluid and rock properties. To make the model more general, mobility and storativity are allowed to vary with different exponents, θ_1 and θ_2 , respectively, in a power law fashion. Figures 6.2 and 6.3 show the mobility and storativity profiles, respectively, for a three-region, radial, composite reservoir. The discontinuities in the mobility and

storativity profiles at R_1 and R_2 are included to make the model more general. A choice of $M_{12} = 1$ and $M_{23} = 1$ removes the discontinuities in the mobility profile, while a choice of $F_{12} = 1$ and $F_{23} = 1$ does the same for the storativity. Wellbore storage and skin effects are included, since these effects are observed in most practical well test data. The constant-rate solution in Laplace space is developed first. Subsequently, the wellbore storage and skin effects are added to the constant-rate solution in Laplace space using a method proposed by *van Everdingen and Hurst*. (1949).

Other assumptions are:

1. The formation is horizontal and of uniform thickness.
2. The fronts are of infinitesimal thickness, and are considered stationary throughout the test period.
3. Laminar flow of a single phase fluid with slight, but constant, compressibility occurs in each region. In the intermediate region, the porosity-total compressibility product changes with distance in a power law fashion.
4. Gravity and capillarity effects are negligible.

6.2 Mathematical Development

For fluid flow in a three-region, radial, composite reservoir with a power law variation of mobility and storativity in the intermediate region, the dimensionless diffusivity equations are given by:

$$\frac{\partial^2 p_{D1}}{\partial r_D^2} + \frac{1}{r_D} \frac{\partial p_{D1}}{\partial r_D} = \frac{\partial p_{D1}}{\partial t_D} \quad \text{for} \quad r_{wD} \leq r_D \leq 1. \quad (6.1)$$

$$\frac{\partial^2 p_{D2}}{\partial r_D^2} + \frac{1-\theta}{r_D} \frac{\partial p_{D2}}{\partial r_D} = \omega_{12} r_D^{\theta-1} \frac{\partial p_{D2}}{\partial t_D} \quad \text{for} \quad 1 \leq r_D \leq R_{D2}, \quad (6.2)$$

where θ_1 and θ_2 are the scaling or spectral exponents in the power law equations for mobility and storativity, respectively. A detailed derivation of Eq. (6.2) and its solution is presented in Appendix B.

$$\frac{\partial^2 p_{D3}}{\partial r_D^2} + \frac{1}{r_D} \frac{\partial p_{D3}}{\partial r_D} = \omega_{13} \frac{\partial p_{D3}}{\partial t_D} \quad \text{for} \quad R_{D2} \leq r_D < \infty. \quad (6.3)$$

Initial conditions:

In dimensionless form, the initial conditions for the three regions are:

$$p_{D1}(r_D, 0) = 0. \quad (6.4)$$

$$p_{D2}(r_D, 0) = 0 \quad \text{and} \quad (6.5)$$

$$p_{D3}(r_D, 0) = 0. \quad (6.6)$$

Inner boundary condition:

Since flow is laminar, and the rate is constant at the inner boundary (well), Darcy's law is applicable. Neglecting the wellbore storage effect for the moment, this condition is represented as:

$$\left(r_D \frac{\partial p_{D3}}{\partial r_D} \right)_{r_D=r_{wD}} = -1. \quad (6.7)$$

Also, since skin effects are neglected for the development of the basic solution, the dimensionless wellbore pressure is:

$$p_{wD} = p_{D1} \quad \text{for } r_D = r_{wD}. \quad (6.8)$$

Conditions at the discontinuities:

At the discontinuities, $r_D = 1$ and R_{D2} ; it is required that pressures and flow rates be continuous as fluid moves from one region to the next. These conditions are expressed as:

$$p_{D1} = p_{D2} \quad \text{at } r_D = 1 \text{ and} \quad (6.9)$$

$$\frac{\partial p_{D2}}{\partial r_D} = M_{12} \frac{\partial p_{D1}}{\partial r_D} \quad \text{at } r_D = 1. \quad (6.10)$$

$$p_{D2} = p_{D3} \quad \text{at } r_D = R_{D2} \text{ and} \quad (6.11)$$

$$\frac{\partial p_{D3}}{\partial r_D} = M_{23} \frac{\partial p_{D2}}{\partial r_D} \quad \text{at } r_D = R_{D2}. \quad (6.12)$$

Outer boundary condition:

The outer boundary is considered to be infinite in extent. This condition is represented as:

$$p_{D3}(r_D, t_D)_{r_D \rightarrow \infty} = 0. \quad (6.13)$$

The dimensionless variables used in the above equations are defined as follows:

$$p_{D1} = \frac{2\pi k_1 h}{qB\mu_1} (p_i - p_1) \quad (6.14)$$

$$p_{D2} = \frac{2\pi k_1 h}{qB\mu_1} (p_i - p_2) \quad (6.15)$$

$$p_{D3} = \frac{2\pi k_1 h}{qB\mu_1} (p_i - p_3) \quad (6.16)$$

$$p_{uD} = \frac{2\pi k_1 h}{qB\mu_1} (p_i - p_u) \quad (6.17)$$

$$r_D = \frac{k_i}{(\phi\mu c_r)_i} \frac{r}{R_i} \quad (6.18)$$

$$F_{12} = (\phi c_r)_1 / (\phi c_r)_2 \quad \text{at } r_D = 1 \quad (6.19)$$

$$M_{12} = \frac{(k/\mu)_1}{(k/\mu)_2} \quad \text{at } r_D = 1 \quad (6.20)$$

$$\omega_{12} = \frac{M_{12}}{F_{12}} \quad \text{at } r_D = 1 \quad (6.21)$$

$$\omega_{13} = \frac{(k/\phi\mu c_r)_1}{(k/\phi\mu c_r)_3} \quad (6.22)$$

$$M_{23} = \frac{(k/\mu)_2}{(k/\mu)_3} \quad \text{at } r_D = R_{D2} \quad (6.23)$$

$$r_D = \frac{r}{R_1} \quad (6.24)$$

$$r_{uD} = \frac{r_u}{R_1} \quad (6.25)$$

$$R_{D2} = \frac{R_2}{R_1} \quad (6.26)$$

A solution of Eqs. (6.1), (6.2) and (6.3), subject to the appropriate initial and boundary conditions (Eqs. (6.4) through (6.13)), is carried out in Laplace space. The dimensionless pressures in Laplace space for the three regions are given in terms of Bessel functions as:

$$\bar{p}_{D1}(r_D, l) = A_1 I_0(r_D \sqrt{l}) + A_2 K_0(r_D \sqrt{l}) \quad \text{for} \quad r_{wD} \leq r_D \leq L, \quad (6.27)$$

$$\bar{p}_{D2}(r_D, l) = A_3 r_D^\gamma I_\gamma(\xi r_D^\beta) + A_4 r_D^\gamma K_\gamma(\xi r_D^\beta) \quad \text{for} \quad L \leq r_D \leq R_{D2}, \quad (6.28)$$

$$\bar{p}_{D3}(r_D, l) = A_5 I_0(r_D \sqrt{\omega_{13} l}) + A_6 K_0(r_D \sqrt{\omega_{13} l}) \quad \text{for} \quad R_{D2} \leq r_D < \infty. \quad (6.29)$$

where l is the transformed time variable in Laplace space.

Other variables introduced in Eq. (6.28) are:

$$\gamma = \frac{\theta_1}{2}. \quad (6.30)$$

$$\beta = \frac{\theta_1 - \theta_2 + 2}{2}. \quad (6.31)$$

$$\nu = \frac{\theta_1}{\theta_1 - \theta_2 + 2}. \quad (6.32)$$

$$\xi = \frac{2\sqrt{\omega_{12} l}}{\theta_1 - \theta_2 + 2} = \frac{\sqrt{\omega_{12} l}}{\beta}. \quad (6.33)$$

From Eq. (6.8), the dimensionless wellbore pressure in Laplace space is:

$$\bar{p}_{uD}(r_{uD}, l) = A_1 I_0(r_{uD} \sqrt{l}) + A_2 K_0(r_{uD} \sqrt{l}). \quad (6.34)$$

The constants A_1 through A_6 are obtained by solving the system of equations resulting from the use of the boundary condition equations (Eqs. (6.7) and (6.9) through (6.13)) in Laplace space.

$$\text{Using Eq. (6.7):} \quad \alpha_{11}A_1 + \alpha_{12}A_2 = \frac{1}{l} \quad (6.35)$$

$$\text{Using Eq. (6.9):} \quad \alpha_{21}A_1 + \alpha_{22}A_2 + \alpha_{23}A_3 + \alpha_{24}A_4 = 0 \quad (6.36)$$

$$\text{Using Eq. (6.10):} \quad \alpha_{31}A_1 + \alpha_{32}A_2 + \alpha_{33}A_3 + \alpha_{34}A_4 = 0 \quad (6.37)$$

$$\text{Using Eq. (6.11):} \quad \alpha_{43}A_3 + \alpha_{44}A_4 + \alpha_{45}A_5 + \alpha_{46}A_6 = 0 \quad (6.38)$$

$$\text{Using Eq. (6.12):} \quad \alpha_{53}A_3 + \alpha_{54}A_4 + \alpha_{55}A_5 + \alpha_{56}A_6 = 0 \quad (6.39)$$

$$\text{Using Eq. (6.13):} \quad \alpha_{65}A_5 + \alpha_{66}A_6 = 0 \quad (6.40)$$

The coefficients, α_{ij} , are defined as follows:

$$\alpha_{1,1} = -r_{u,D}\sqrt{l} I_1(r_{u,D}\sqrt{l}). \quad (6.41)$$

$$\alpha_{1,2} = r_{u,D}\sqrt{l} K_1(r_{u,D}\sqrt{l}). \quad (6.42)$$

$$\alpha_{1,3} = I_0(\sqrt{l}). \quad (6.43)$$

$$\alpha_{1,4} = K_0(\sqrt{l}). \quad (6.44)$$

$$\alpha_{2,3} = -I_v(\xi). \quad (6.45)$$

$$\alpha_{1,4} = -K_v(\xi). \quad (6.46)$$

$$\alpha_{1,1} = -M_{1,2}\sqrt{l} I_1(\sqrt{l}). \quad (6.47)$$

$$\alpha_{1,2} = M_{1,2}\sqrt{l} K_1(\sqrt{l}). \quad (6.48)$$

$$\alpha_{33} = \gamma I_v(\xi) + \beta \xi I_v'(\xi). \quad (6.49)$$

$$\alpha_{34} = \gamma K_v(\xi) + \beta \xi K_v'(\xi). \quad (6.50)$$

$$\alpha_{43} = R_{D2}^\gamma I_v(\xi R_{D2}^\beta). \quad (6.51)$$

$$\alpha_{44} = R_{D2}^\gamma K_v(\xi R_{D2}^\beta). \quad (6.52)$$

$$\alpha_{46} = -K_0(R_{D2} \sqrt{\omega_{13} l}). \quad (6.53)$$

$$\alpha_{53} = -M_{23} [\gamma R_{D2}^{\gamma-1} I_v(\xi R_{D2}^\beta) + \beta \xi R_{D2}^{\gamma+\beta-1} I_v'(\xi R_{D2}^\beta)]. \quad (6.54)$$

$$\alpha_{54} = -M_{23} [\gamma R_{D2}^{\gamma-1} K_v(\xi R_{D2}^\beta) + \beta \xi R_{D2}^{\gamma+\beta-1} K_v'(\xi R_{D2}^\beta)]. \quad (6.55)$$

$$\alpha_{56} = -\sqrt{\omega_{13} l} K_1(R_{D2} \sqrt{\omega_{13} l}). \quad (6.56)$$

The remaining α 's are set to zero upon considering the implications of the infinite outer boundary condition (Eq. (6.13)).

Since $I_0(r_D \sqrt{\omega l}) \rightarrow \infty$ as $r_D \rightarrow \infty$, a bounded solution for $\bar{p}_{D3}(r_D \rightarrow \infty, l)$ can be obtained from Eq. (6.29) only if $A_5 = 0$. Consequently, α_{45} , α_{55} and α_{65} in Eqs. (6.38), (6.39) and (6.40), respectively, are set to zero. Also α_{66} drops out since $K_0(r_D \sqrt{\omega l}) \rightarrow 0$ as $r_D \rightarrow \infty$, in Eq. (6.29). Thus:

$$\alpha_{45} = \alpha_{55} = \alpha_{65} = \alpha_{66} = 0. \quad (6.57)$$

To obtain the dimensionless wellbore pressure, and also the pressure derivative, Eq. (6.34) is inverted numerically from Laplace space into real space using the *Stehfest* (1970) algorithm.

Wellbore Storage and Skin:

The solutions presented so far do not account for wellbore storage or skin effect. To add these effects, new boundary conditions are imposed at the well. The presence of skin at the well is represented as:

$$p_{wD} = p_{Dz} - S \left(r_D \frac{\partial p_{Dz}}{\partial r_D} \right)_{r_D=r_{wD}}. \quad (6.58)$$

In Eq. (6.58), S is the skin factor defined as:

$$S = \frac{2\pi k_f h}{qB\mu_1} \Delta p_s, \quad (6.59)$$

where Δp_s is the pressure drop due to skin damage.

The wellbore storage condition is represented as:

$$C_D \frac{\partial p_{wD}}{\partial t_D} - \left(r_D \frac{\partial p_{Dz}}{\partial r_D} \right)_{r_D=r_{wD}} = 1. \quad (6.60)$$

The dimensionless wellbore storage constant, C_D , in Eq. (6.60) is defined as:

$$C_D = \frac{C}{2\pi h(\phi c_f) R_w^2}, \quad (6.61)$$

where C is the wellbore storage coefficient.

To include the skin and wellbore storage effects in the solution already presented, *van Everdingen and Hurst* (1949) developed the problem as a convolution integral. This was solved to yield the dimensionless wellbore pressure including skin and wellbore storage as:

$$\bar{p}_{wD}(l) = \frac{[l \bar{p}_D + S]}{l \{1 + C_D [l \bar{p}_D + S]\}} \quad (6.62)$$

where \bar{p}_D is the dimensionless wellbore pressure in Laplace space without wellbore storage or skin effect. Appendix C presents the computer program for the analytical solution developed in this section.

6.3 Verification of Solution

The analytical solution presented in the preceding section was verified against other works in the literature which can be considered subsets of this study. If the spectral exponents, θ_1 and θ_2 , are set to zero, then the model presented in this chapter is identical to the three-region, composite reservoir solution presented by *Ambastha* (1988). Figure 6.4 presents a comparison of the semi-log pressure derivative responses generated from this study with those from Fig. 6.46 of *Ambastha* (1988). Figure 6.4 shows an excellent match between the two responses, for different mobility ratios (M_{I2}) between the first and the intermediate regions.

The model response is also compared with the response from a two-region, composite reservoir solution presented by *Ambastha* (1988). To convert the three-region, composite reservoir model of this study into a two-region, composite reservoir, R_{D2} is set equal to unity. Again, θ_1 and θ_2 are set to zero. Figure 6.5 shows a comparison of the semi-log pressure derivative responses generated from this model with similar responses from Fig. 6.3 of *Ambastha* (1988), which was used to show the effect of storativity ratio on the semi-log pressure derivative response for a two-region, composite reservoir. Other parameter values used in this model to generate the responses for comparison are shown on Fig. 6.5. Figure 6.5 shows an excellent agreement between the two sets of responses.

Further verification of the model presented in this chapter is carried out by comparing it with the solution presented by *Poon* (1995), which is for an infinitely-large, two-region, radial, composite reservoir, with a fractal outer region. To generate the two-region, composite reservoir response of *Poon* (1995), using the solution in this study, the dimensionless wellbore radius (r_{wD}) and the first dimensionless discontinuity radius (R_{D1}) are both set equal to 1. The second dimensionless discontinuity radius, $R_{D2} = 100$. Figure 6.6 shows a comparison of dimensionless wellbore pressure response using the model from this chapter with results from Fig. 2 of *Poon* (1995). For this comparison, θ_1 and θ_2 should be equal to 2. However, for θ_2 equal to 2 (in this model), the order of the modified Bessel functions needed in generating the solution is either indeterminate or unity. The modified Bessel functions are required to have fractional order. For the responses in Fig. 6.6, the spectral exponents, θ_1 and θ_2 , are 2 and 1.99, respectively. The figure shows a very good match between the two results, for different dimensionless wellbore storage constants. Thus, the solution presented in this study can be considered validated.

6.4 Results and Discussion

For an infinitely-large, three-region radial, composite reservoir, *Ambastha* (1988) has shown that the parameters that affect the pressure behavior are M_{12} , M_{13} , F_{12} , F_{13} , R_{D1} , and R_{D2} . However, when the intermediate region properties are allowed to vary in a power law fashion, then the spectral exponents for mobility and storativity, θ_1 and θ_2 , are introduced. *Ambastha* (1988), and *Ambastha* and *Ramey* (1992) have presented exhaustive discussions on the effect of the above parameters (except θ_1 and θ_2) on the semi-log pressure derivative responses for three-region composite reservoirs. The effects of these parameters on the responses generated in this study will not be discussed, since they are largely the same as presented by *Ambastha* (1988), and *Ambastha* and *Ramey*

(1992). However, the effect of R_2/R_1 will be discussed in the presence of power law variation of reservoir and fluid properties in the intermediate region. This will be followed by a discussion of the effects of the spectral exponents, θ_1 and θ_2 .

6.4.1 Effect of Intermediate Region Size

Figures 6.7 and 6.8 show the effect of the intermediate region size on the dimensionless semi-log and Cartesian pressure derivative responses, respectively, for a three-region, radial, composite reservoir with power law property variation in the intermediate region. The parameters θ_1 and θ_2 are set equal to unity. The responses shown in Figs. 6.7 and 6.8 are for selected R_2/R_1 ratios of 1.1, 2, 3, 4 and 5. Other parameters are as given on the figures. Fig. 6.7 shows that, at early times, all semi-log pressure derivative responses form one curve, with a constant value of 0.5. This indicates infinite-acting radial flow corresponding to the inner region mobility. During this time, the effect of the radial discontinuities have not yet been felt. At intermediate times, all cases show a sharp rise, due to changing mobility and storativity in the intermediate region. At this time, the responses are different for the different sizes of the intermediate region. Each response goes through a maximum value before approaching a constant value of $M_{1,2}/2$ in the outer region. For the set of parameter values used, Fig. 6.7 shows that the parameter R_2/R_1 has a significant effect on the magnitude of the maximum derivative. However, R_2/R_1 values up to 5 have only a mild effect on the time to the maximum semi-log derivative, and no noticeable effect on the time to the beginning of infinite-acting radial flow corresponding to the outer region mobility. The effect of R_2/R_1 on the semi-log derivative responses shown in Fig. 6.7 is consistent with the effect of R_2/R_1 on the semi-log derivative responses for a three-region, composite reservoir with uniform mobility and storativity in the intermediate region (Ambastha, 1988) for $F_{12} \geq 1$.

Figure 6.7 also shows that the response for $R_2/R_1 = 1.1$ indicates a unit-slope line during the first half of the transition region. For other cases of R_2/R_1 , the slope decreases further from unity as R_2/R_1 increases. A unit-slope line on a log-log graph of semi-log pressure derivative versus time during the transition period implies pseudosteady state behavior due to mobility and/or storativity contrasts. Thus, as R_2/R_1 increases, pseudosteady state behavior becomes less noticeable. This suggests that analysis of well-test data during the transition region will yield increasingly overestimated values of R_1 , as the size of the intermediate region increases. The above observation is also similar to the effect of R_2/R_1 on the semi-log pressure derivative responses for a three-region, composite reservoir with uniform mobility and storativity in the intermediate region presented by *Ambastha* (1988).

Figure 6.8 shows the effect of the intermediate region size on the Cartesian pressure derivative responses for a three-region, composite reservoir with power law variation of mobility and storativity in the intermediate region. At early times, all the responses form one curve with a slope of -1, which is indicative of infinite-acting radial flow corresponding to the inner region mobility. At intermediate times, the responses become different, reflecting the differences in the size of the intermediate region. At late times, the responses form one curve again with a slope of -1, indicating infinite-acting radial flow corresponding to the outer region mobility. Figure 6.8 also shows that at intermediate times, the Cartesian pressure derivative responses begin to flatten out approaching zero-slope. A zero-slope on the graph of Cartesian pressure derivative versus time indicates pseudosteady state behavior due to mobility and storativity contrasts. For pseudosteady state flow corresponding to the inner region, the Cartesian pressure derivative is 2π . Figure 6.8 shows that only the response for $R_2/R_1 = 1.1$ indicates pseudosteady state behavior during the early part of the transition period. For $R_2/R_1 = 2$ through 5, the Cartesian pressure derivative responses in the transition region all fall below 2π . Thus, for the selected parameters, well-test data for $R_2/R_1 = 2$ through 5 will yield overestimated

values of the inner region volume, if analyzed using the pseudosteady state method. *Ambastha* (1988) has presented equations for effective Cartesian pressure derivative and effective time based on average reservoir and fluid properties in the intermediate region. *Ambastha* (1988) showed that the pseudosteady state method would yield the front radius R_2 , if effective properties are used to analyze the data. It should be noted that the use of effective properties may still yield slightly overestimated values of R_2 as the size of the intermediate region increases (*Ambastha*, 1988). Though not considered in this study, an effort should be made to modify the equations for effective properties presented by *Ambastha* (1988) to account for varying mobility and storativity in the intermediate region, so as to make them applicable to the model presented in this study.

6.4.2 Effect of Spectral Exponents

Gefen et al. (1983) have shown that, for a permeable network with fractal properties, the hydraulic diffusivity is governed by a power law relation with distance. This is given as:

$$\left(\frac{k}{\phi\mu c_f}\right) \sim r^{-\theta} \quad (6.63)$$

where θ is the fractal or spectral exponent of the power law relation.

The parameter, θ , is related to the topology of the permeable network, and is generally positive. *Beier* (1994) notes that the value of θ for petroleum reservoirs has not yet been established. For non-composite, heterogeneous reservoirs, *Chang and Yortsos* (1990) have shown that the value of θ can be estimated from the slope of a log-log graph of wellbore pressure drop versus time. This follows from the long-time approximate solution for the pressure behavior of a fractal reservoir given as:

$$\Delta p_{\theta} = C_I r^{\frac{\theta}{\theta+2}} \quad (6.64)$$

where C_I is a constant related to the flow geometry characteristic of the reservoir.

Poon (1995) has conducted a sensitivity study on the effect of θ on the pressure behavior of a two-region, composite reservoir. From the results, *Poon* (1995) concludes that, for all practical purposes, the value of θ should be less than 4. However, this study has found that practical values of θ depend on the reference distance from where the properties begin to vary in a power law relationship with distance. Moreover, mobility and storativity need not vary with the same spectral exponent. Mobility and storativity can vary independently with different spectral exponents. Thus, instead of one value of θ for diffusivity, one should consider two values, θ_1 and θ_2 , for mobility and storativity, respectively.

Figures 6.9 and 6.10 present mobility and storativity profiles, respectively, for a three-region, radial, composite reservoir representative of a thermal recovery process. The first and intermediate dimensionless discontinuity radii are 1 and 5, respectively. In the inner and outer regions, the mobility and storativity are constant. However, in the intermediate region, the mobility and storativity begin to drop. The rate of decline of mobility and storativity in the intermediate region depends on the value of the spectral exponent. From Fig. 6.9, for an intermediate region discontinuity radius of 5, θ_1 cannot exceed 2.86 for the assumed mobility ratio values M_{12} and M_{13} . For $\theta_1 > 2.86$, the mobility at the end of the intermediate region will be less than the mobility in the outer region, which is not physically possible for a thermal recovery process.

Figure 6.10 shows that the restrictions on the practical values of θ_1 for mobility variation also apply to θ_2 for storativity variation. In addition, θ_2 cannot be equal to 2. This

follows from the mathematics of the problem, as evidenced from examining Eq. (6.32) for the variable, ν . The variable, ν , defines the order of the modified Bessel functions, which has to be a fraction. Equation (6.32) shows that for $\theta_2 = 2$, ν is either indeterminate for $\theta_1 = 0$ or equal to unity for non-zero θ_1 . Thus, practical values of θ_1 and θ_2 for a three-region, radial, composite reservoir will depend on the size of the intermediate region, and on specific values of M_{12} , M_{13} , F_{12} , and F_{13} . The effects of θ_1 and θ_2 on the semi-log and Cartesian pressure derivative responses for a three-region, radial, composite reservoir are now discussed.

Figures 6.11 and 6.12 show the effect of θ_1 on the dimensionless semi-log and Cartesian pressure derivative responses, respectively, from an infinitely-large, three-region, radial, composite reservoir. Responses are presented for selected values of θ_1 between 0 and 2, while θ_2 is fixed at 1. Other parameters are shown on the figures. As expected, Fig. 6.11 shows that all semi-log pressure derivative responses form one curve at early times, indicating infinite-acting radial flow corresponding to the inner region mobility. During the transition region that follows, due to mobility and storativity contrasts, the semi-log pressure derivative responses begin to separate, forming distinct curves at about the middle of the transition period. Towards the end of the transition period, the responses for the different cases of θ_1 tend toward one curve again. All responses go through maximums at about the same time before approaching a constant value of $M_{13}/2$. Figure 6.11 shows that θ_1 affects the semi-log pressure derivative response only mildly, and this occurs during the middle of the transition period.

Figure 6.12 shows the effect of θ_1 on the Cartesian pressure derivative responses. At early times, the responses of all cases form one curve with a slope of -1, indicating infinite-acting radial flow corresponding to the inner region mobility. During the transition period, the responses start to flatten out, indicating an approach to pseudosteady state behavior.

Figure 6.12, however, suggests that none of the responses reaches pseudosteady state. This is shown by the fact that all responses during the transition period fall below 2π . Figure 6.12 also shows that the higher the value of θ_1 , the closer the transition region Cartesian derivatives approach 2π . Thus, while all cases will yield overestimated values of R_1 , the overestimation will be less for higher values of θ_1 . Higher values of θ_1 imply larger drops in the mobility of the intermediate region. Also, the higher the mobility contrast, the greater the chance of observing pseudosteady state behavior.

The effects of the spectral exponent for storativity, θ_2 , on the semi-log and Cartesian pressure derivative responses are shown in Figs. 6.13 and 6.14, respectively. The responses are generated for selected values of θ_2 from 0 to 1.99. The mobility spectral exponent, θ_1 , is 1. Figure 6.13 shows the usual early-time flattening of the semi-log pressure derivative response, indicative of infinite-acting, radial flow corresponding to the inner region mobility. During the transition period, the responses for the various cases of θ_2 begin to separate. Each derivative response goes through a maximum at a slightly different time before approaching a constant value of $M_{13}/2$ for the outer region mobility. The magnitude of the maximum derivative is only mildly affected by θ_2 . Figure 6.13 shows that θ_2 has a significant effect on the transition region derivative responses. The larger the value of θ_2 , the closer the derivative response during the transition period approaches a unit-slope. θ_2 also affects the time to the start of infinite-acting, radial flow corresponding to the outer region mobility.

When Fig. 6.13 is compared with Fig. 6.11, one can see that θ_2 tends to have a greater effect on the semilog derivative responses than θ_1 . Thus, for the same spectral exponents, the changing storativity influences the derivative response more than the changing mobility. An examination of Eq. (6.32) might offer an explanation as to why this is so. Equation

(6.32) shows that while θ_1 appears in both the numerator and denominator, θ_2 only appears in the denominator. Thus, θ_2 will affect the value of v more than θ_1 will.

Figure 6.14 shows the effect of θ_2 on the Cartesian pressure derivative responses for a three-region, radial composite reservoir. The figure shows that the transition region derivative responses for all cases fall below 2π . Thus, well-test data analysis for any of these cases will yield overestimated values of R_1 . However, the overestimation will be less for larger values of θ_2 .

Figures 6.15 and 6.16 show the effect of equal values of θ_1 and θ_2 on the semi-log and Cartesian pressure derivative responses, respectively. The responses have been generated for selected equal values of θ_1 and θ_2 between 0 and 1.99. Other reservoir parameters are shown on the figures. A comparison of Figs. 6.13 and 6.14 with Figs. 6.15 and 6.16, respectively, shows that the derivative responses are almost identical. This seems to suggest that the effect of the changing storativity overwhelms the effect of the changing mobility. This might be expected in view of Eq. (6.32).

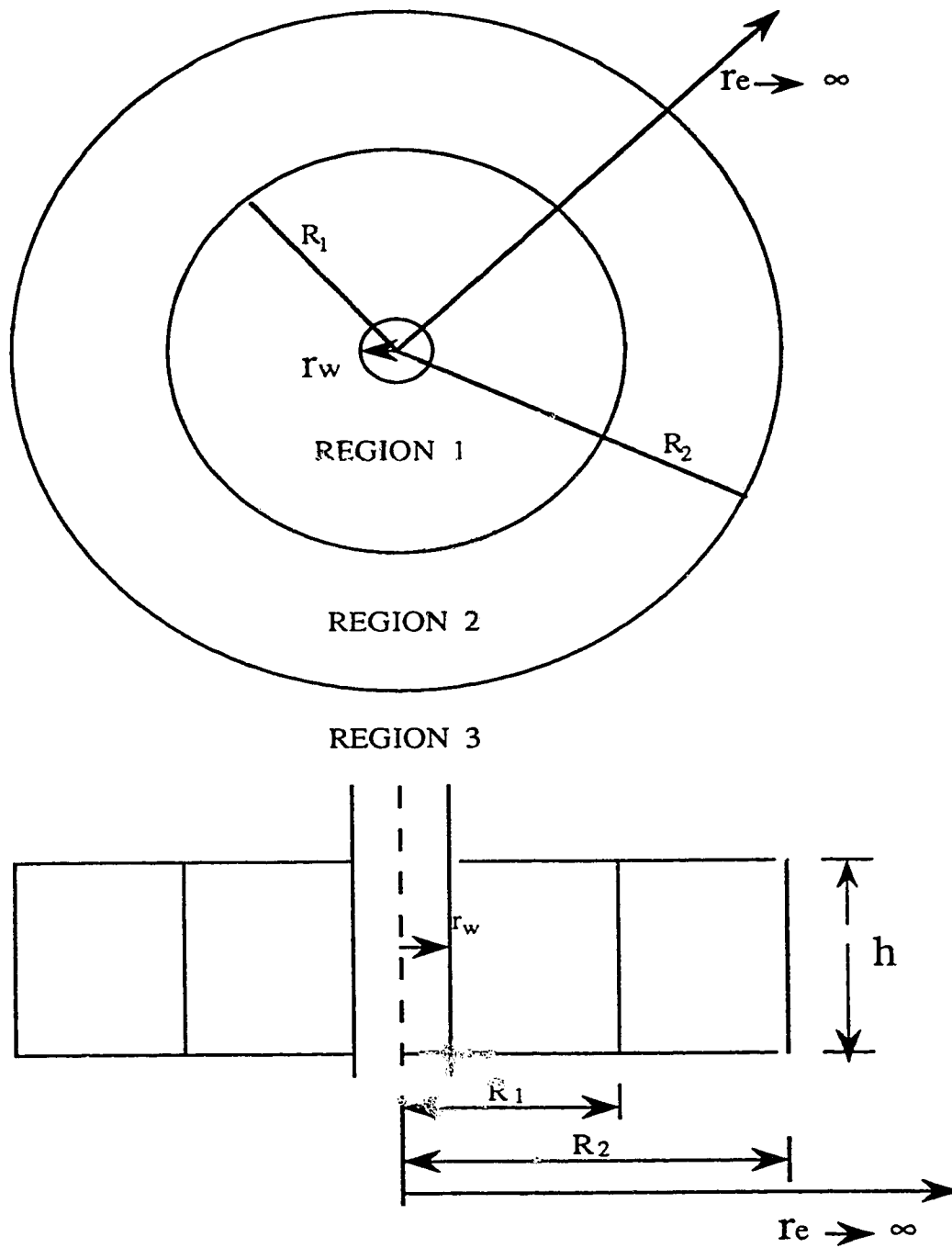


Figure 6.1: Schematic of an infinite three-region, radial, composite reservoir.

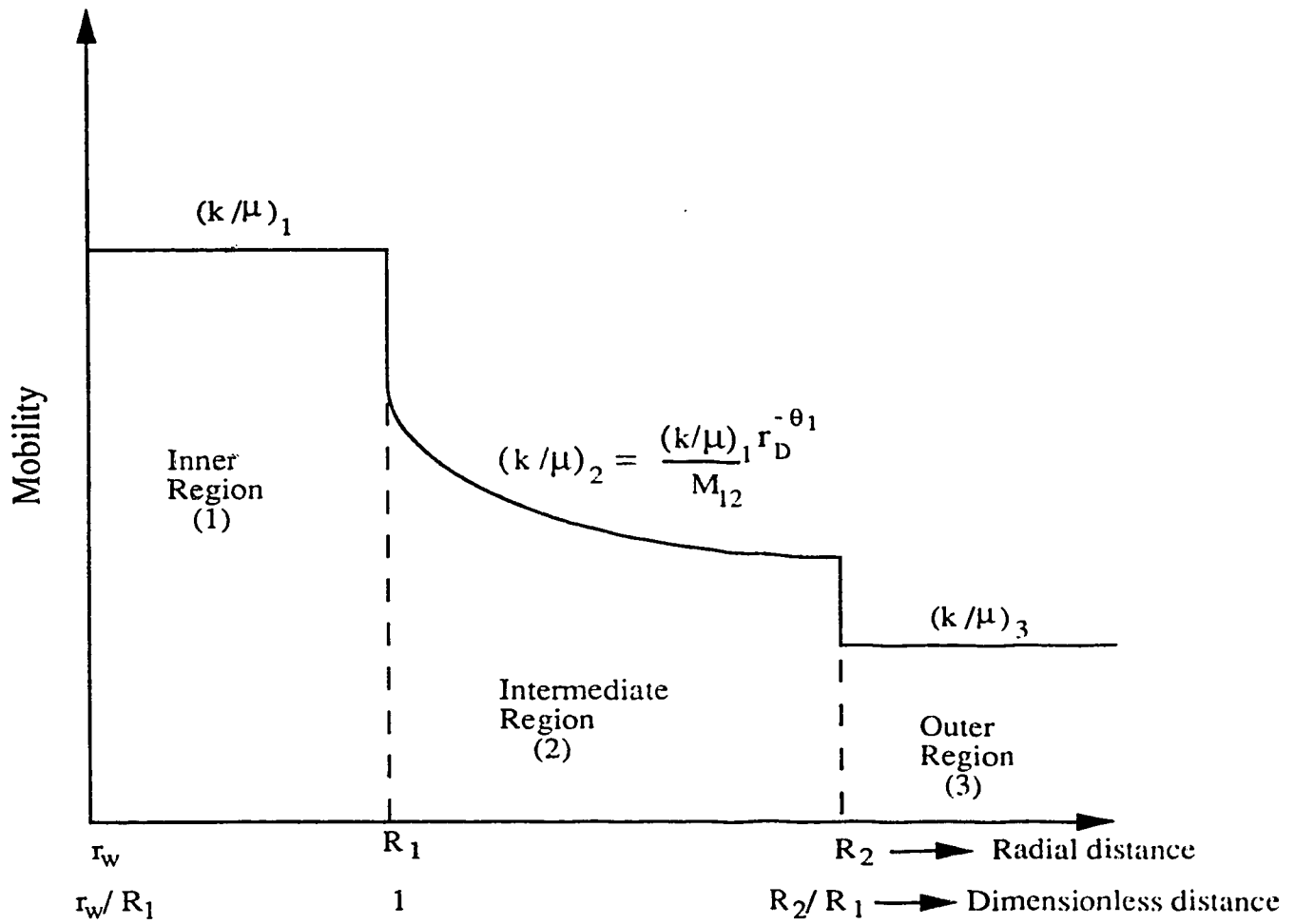


Figure 6.2: Schematic of mobility variation with distance for a three-region, radial, composite reservoir.

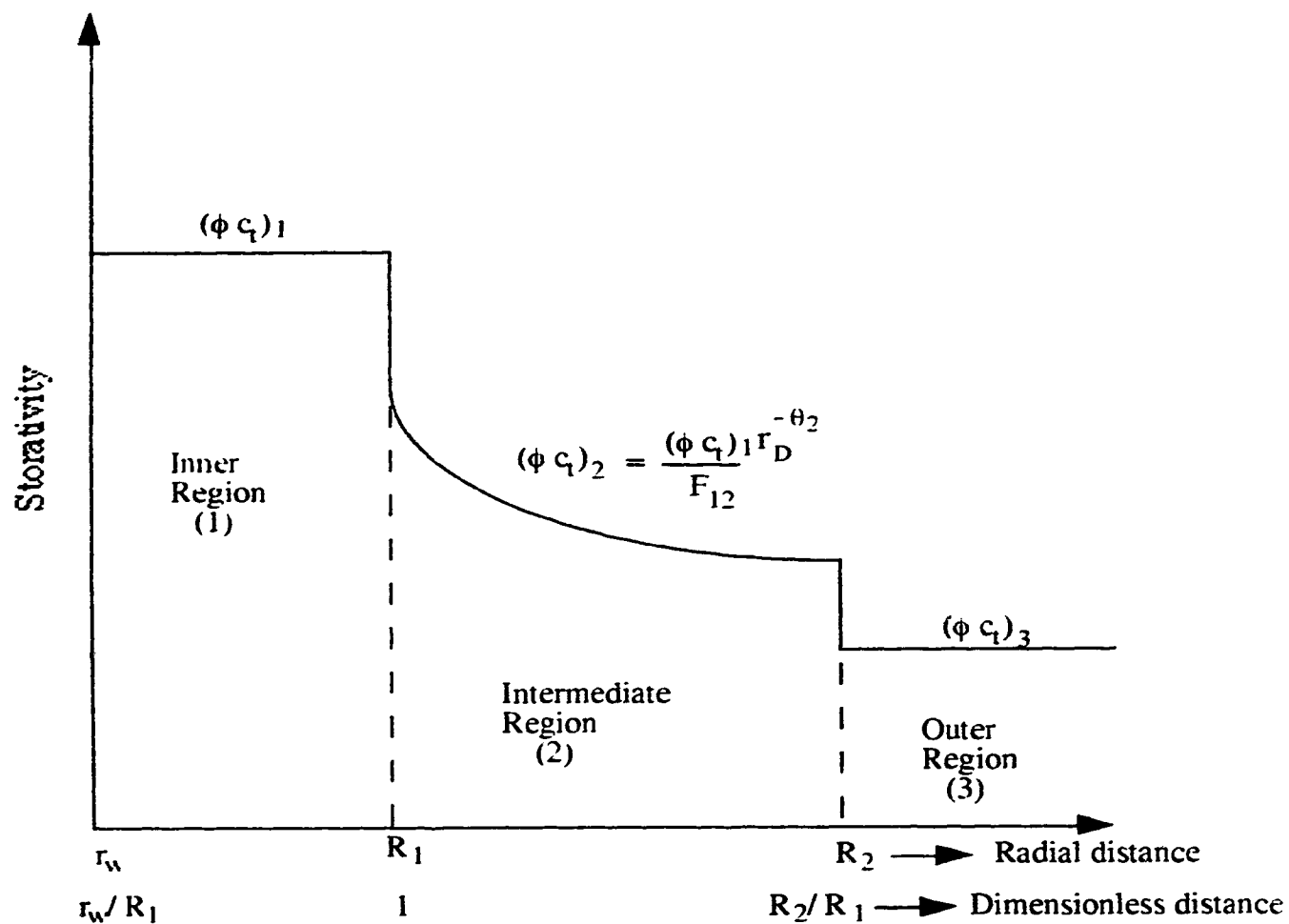


Figure 6.3: Schematic of storativity variation with distance for a three-region, radial, composite reservoir.

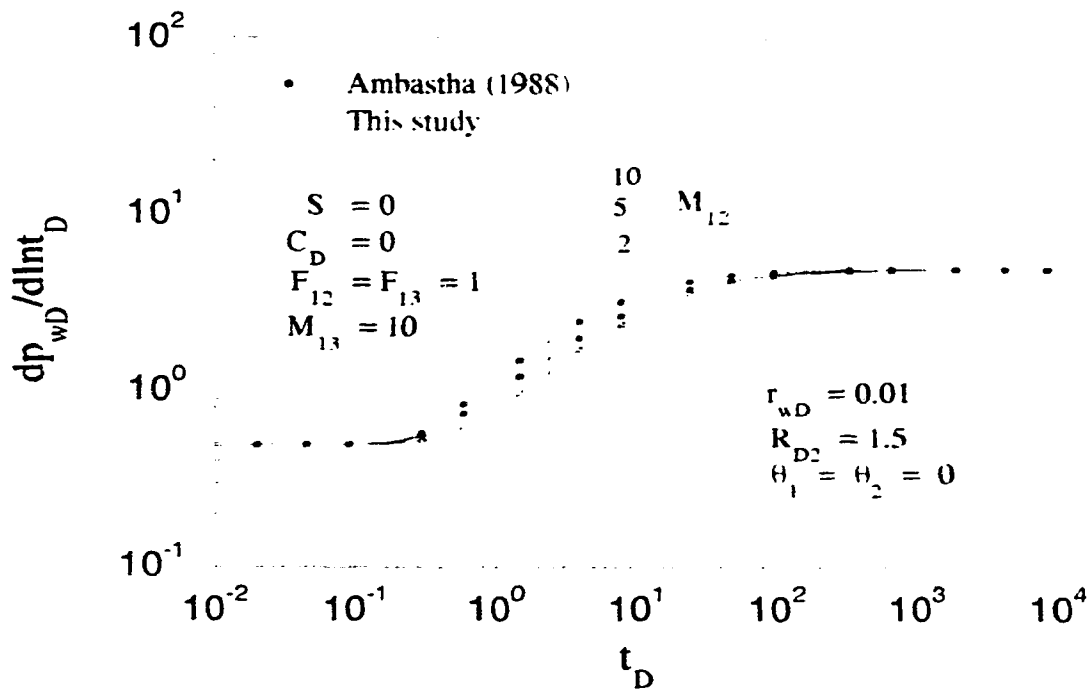


Figure 6.4: Comparison of this study with Fig. 6.46 of Ambastha (1988) for an infinitely-large, three-region, composite reservoir.

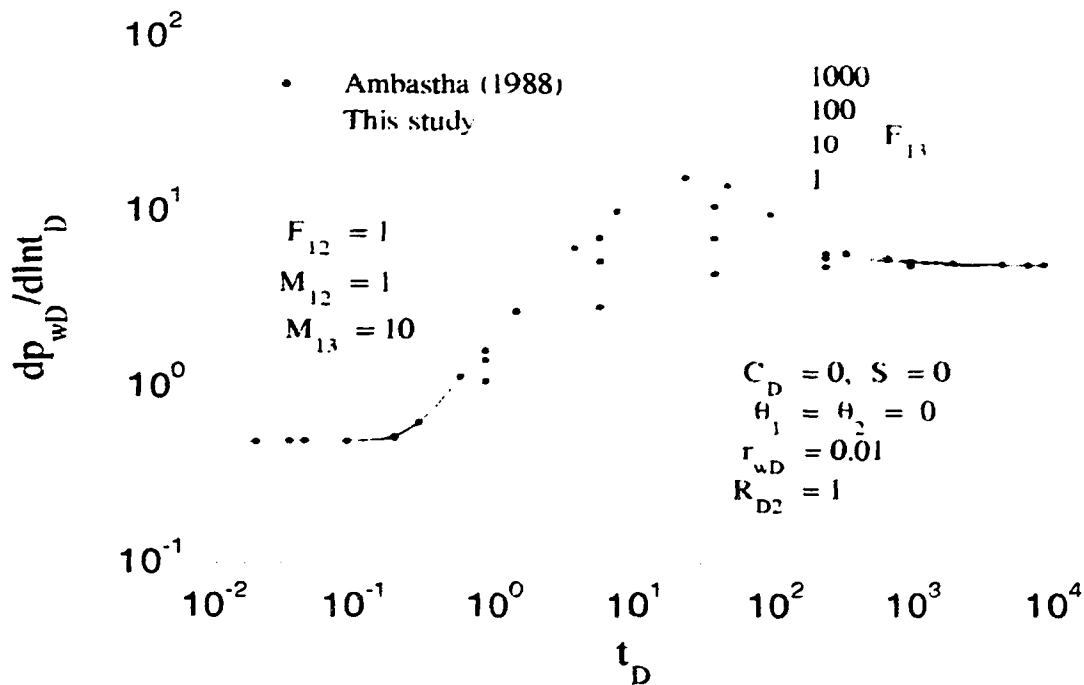


Figure 6.5: Comparison of this study with Figure 6.3 of Ambastha (1988) for an infinitely-large, two-region, composite reservoir.

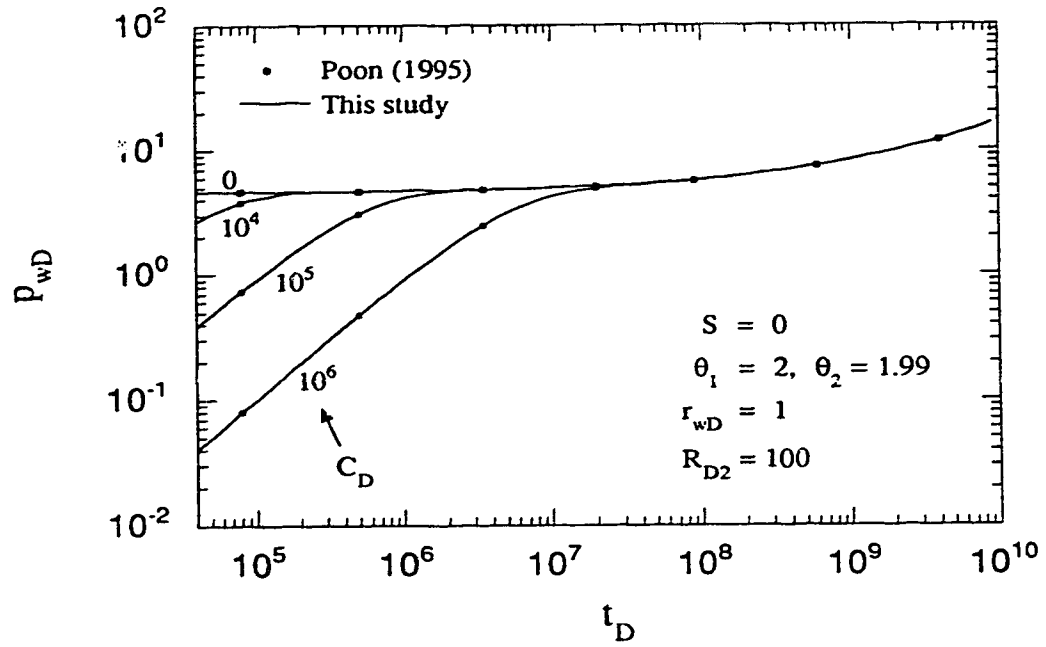


Figure 6.6: Comparison of this study with Fig. 2 of Poon (1995) for an infinitely large, two-region, radial, composite reservoir with a fractal outer region.

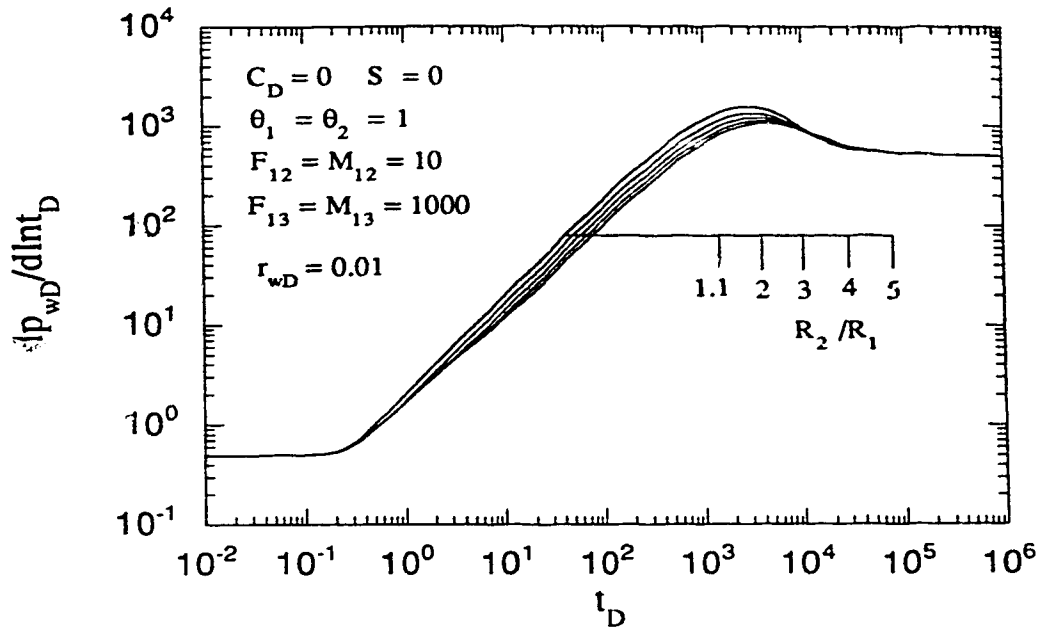


Figure 6.7: Effect of R_2/R_1 on the semi-log pressure derivative response for an infinitely-large, three-region, composite reservoir with power law property variation.

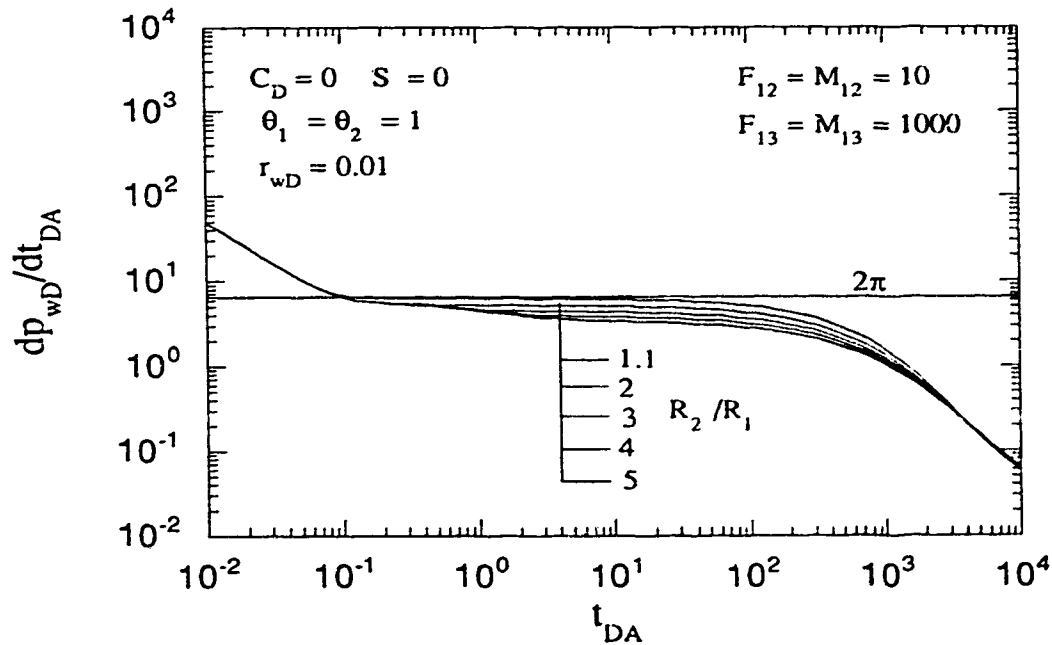


Figure 6.8: Effect of R_2/R_1 on the Cartesian pressure derivative response for an infinitely-large, three-region, composite reservoir with power law property variation.

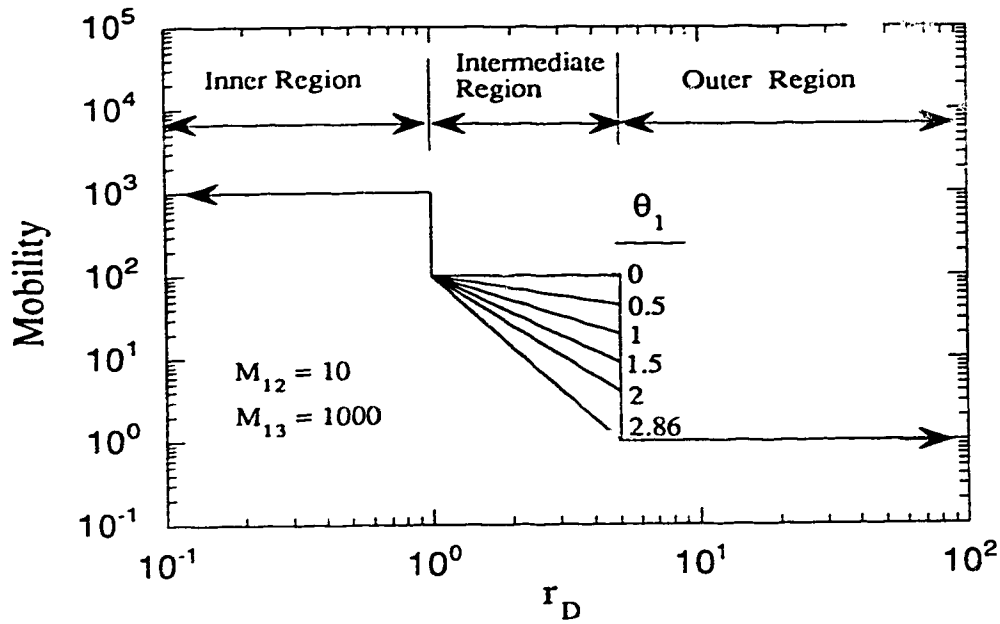


Figure 6.9: Mobility profile for an infinitely-large, three-region, radial, composite reservoir with power law variation in the intermediate region.

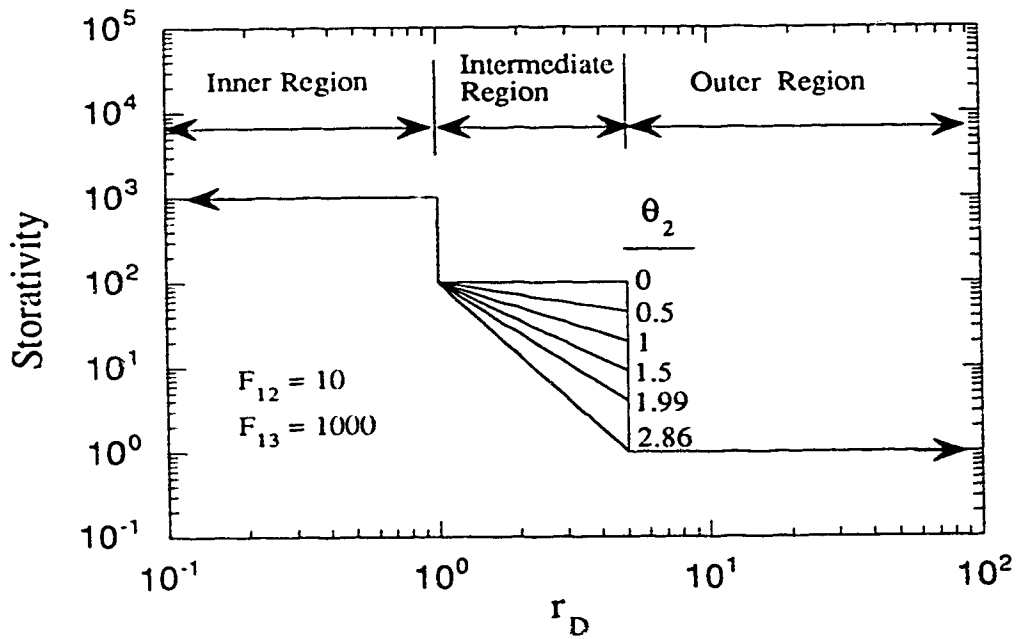


Figure 6.10: Storativity profile for an infinitely-large, three-region, radial, composite reservoir with power law variation in the intermediate region.

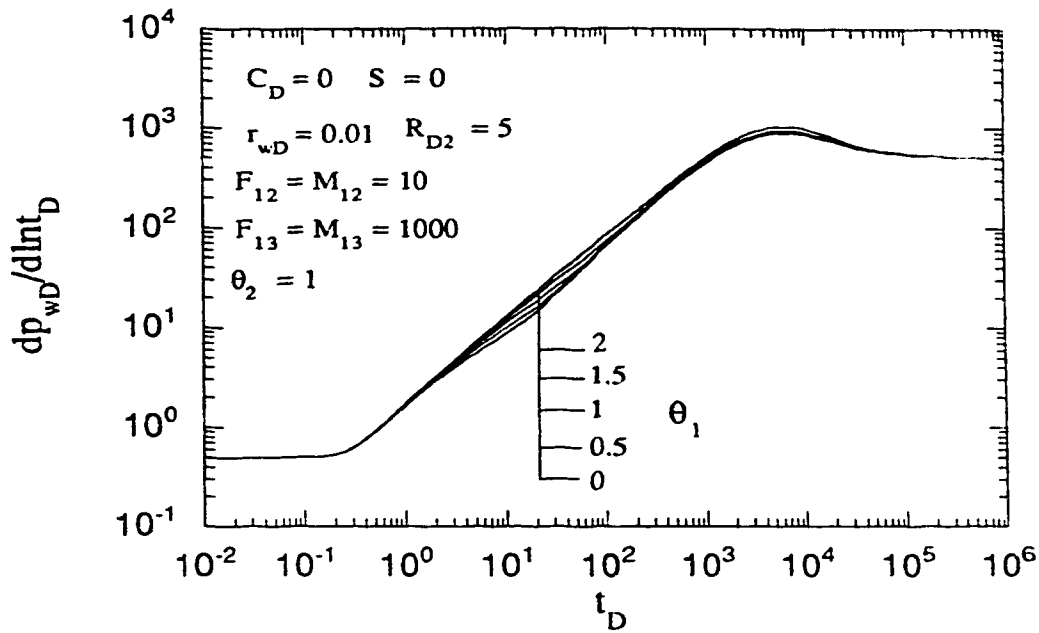


Figure 6.11: Effect of θ_1 on the semi-log pressure derivative response for an infinitely-large, three-region, composite reservoir with power law property variation.

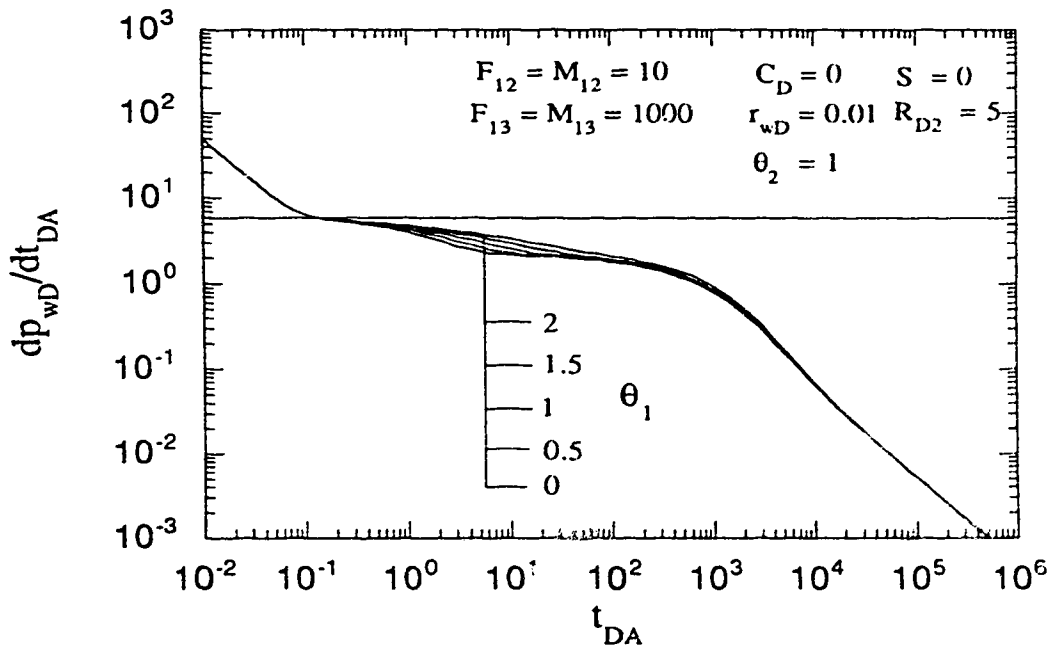


Figure 6.12: Effect of θ_1 on the Cartesian pressure derivative response for an infinitely-large, three-region, composite reservoir with power law property variation.

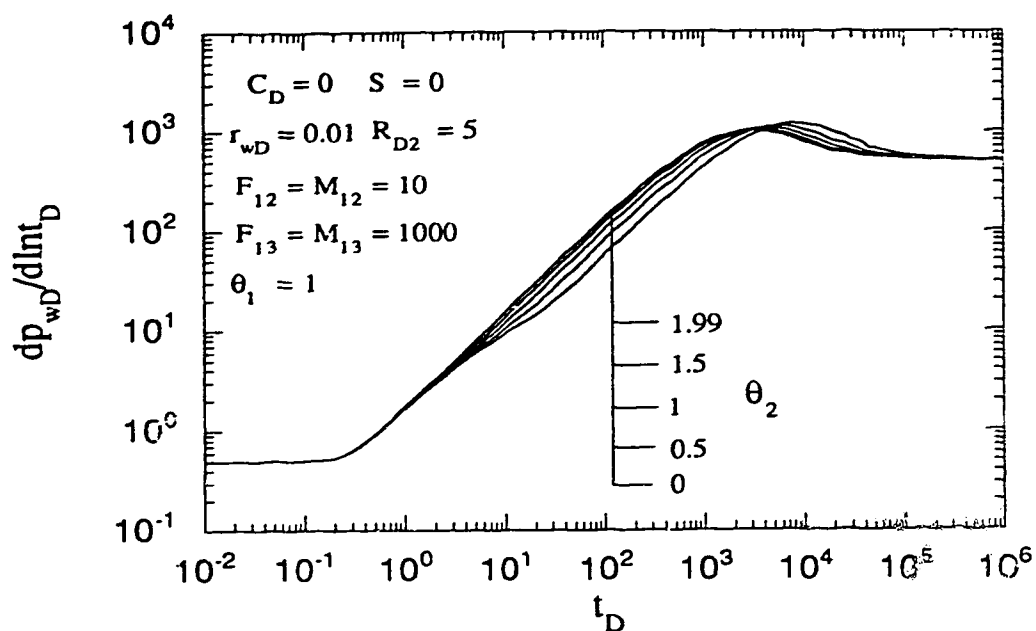


Figure 6.13: Effect of θ_2 on the semi-log pressure derivative response for an infinitely-large, three-region, composite reservoir with power law property variation.

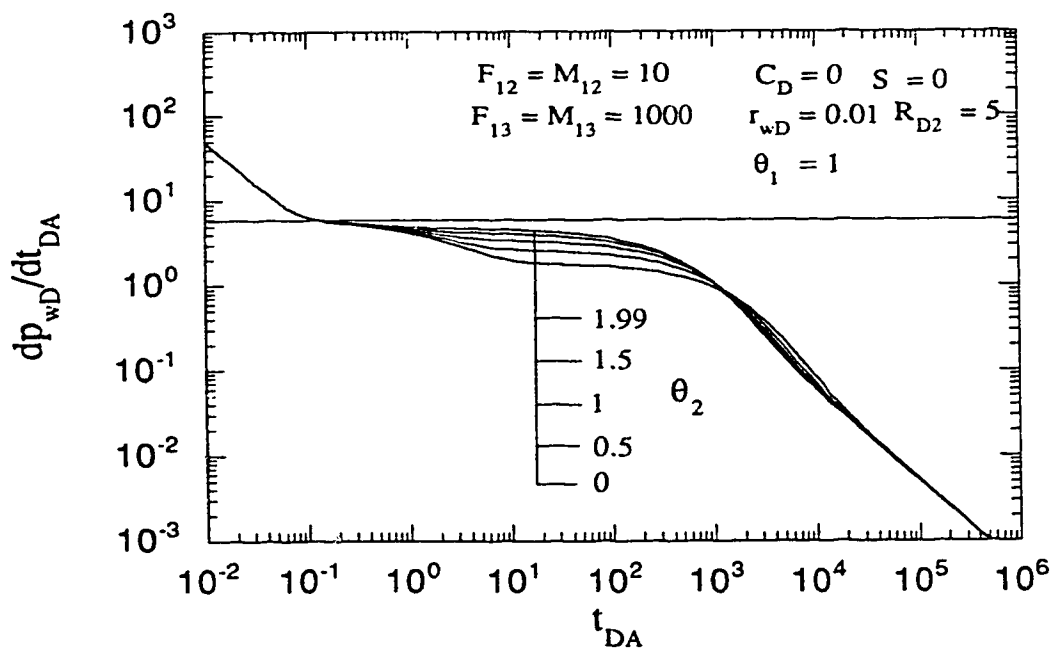


Figure 6.14: Effect of θ_2 on the Cartesian pressure derivative response for an infinitely-large, three-region, composite reservoir with power law property variation.

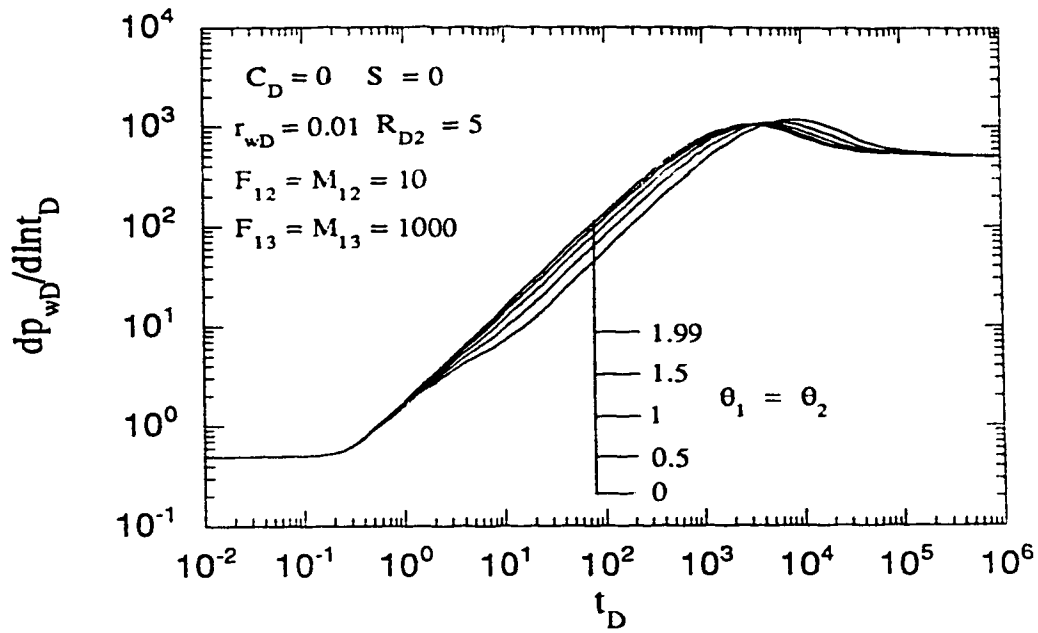


Figure 6.15: Effect of equal variations of mobility and storativity on the semi-log pressure derivative response for an infinitely-large, three-region, composite reservoir.

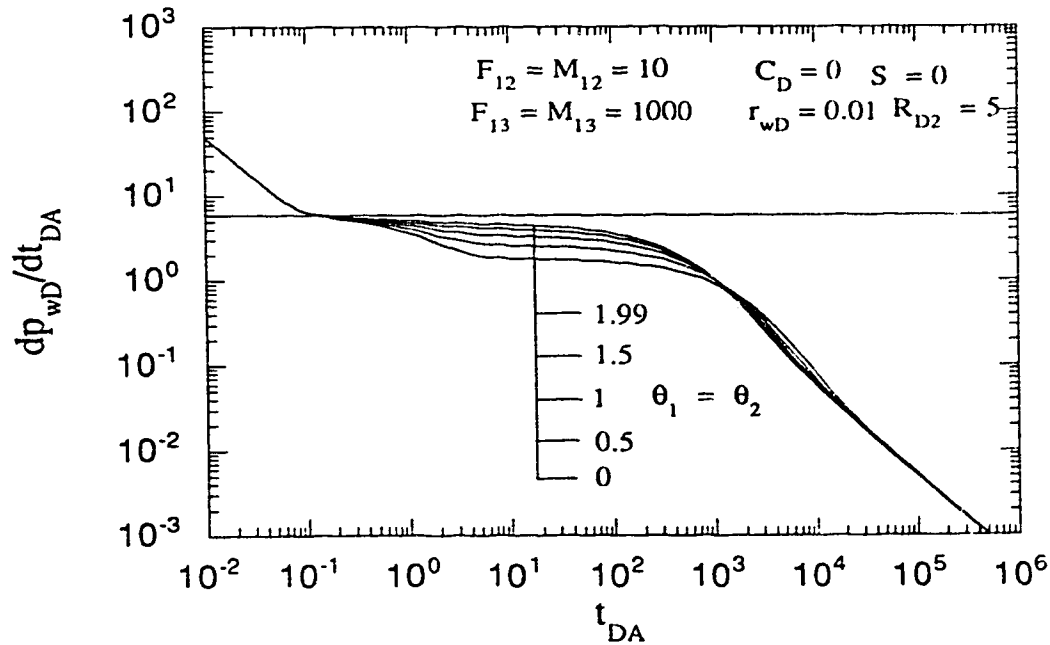


Figure 6.16: Effect of equal variations of mobility and storativity on the Cartesian pressure derivative response for an infinitely-large, three-region, composite reservoir.

7.0 DISCUSSION, CONCLUSIONS, AND RECOMMENDATIONS

7.1 Discussion

This study has presented analytical solutions for two-region, composite reservoirs in radial, elliptical, linear and spherical flow geometries. Both constant-rate and constant-pressure inner boundary conditions have been included. The outer boundary could be infinite or finite, with both closed and constant-pressure conditions. These solutions also include wellbore storage and skin effects, which are found in most practical well-test data. The ultimate goal has been to present a comprehensive study of the transient pressure and rate behavior of composite reservoirs with various flow geometries. A new analytical model for a three-region, composite reservoir with power law property variation in the intermediate region has been presented. The effects of mobility and storativity gradients in the intermediate region on the transient pressure behavior of three-region, composite reservoirs have also been investigated.

Numerous situations exist where a reservoir may not be considered homogeneous. Enhanced oil recovery operations often lead to a situation where the reservoir has a high mobility fluid bank in the immediate vicinity of the wellbore. Alternatively, processes such as the injection of cold water into a hot oil reservoir, or the injection of cold water into a geothermal reservoir to recover energy for power generation, may create a situation where a low mobility fluid bank surrounds the wellbore. Primary recovery processes may have a situation where a portion of the reservoir in the immediate vicinity of the wellbore may have been damaged (lower permeability) during drilling, or may have been stimulated (higher permeability) due to acidization. In all the above situations, the reservoir may be represented as a composite reservoir with two or more discontinuous regions.

The shape of composite reservoirs has mostly been assumed to be radial. However, several situations have been mentioned where the geometry of the reservoir may be elliptical, linear or spherical. While analytical solutions for two-region, composite reservoirs in radial, elliptical, linear and spherical geometries are available in the literature, no attempt has been made to compare the transient pressure and rate behavior of composite reservoirs in the various flow geometries. This study seeks to fill this void, among other things. To facilitate comparison of transient pressure and rate responses for radial, elliptical, linear and spherical flow geometries on an equal footing, normalizing factors have been developed using the radial composite reservoir as the reference. To the best of my knowledge, this is the first time these normalizing factors have appeared in the literature.

The analytical solutions presented in this study have been used to investigate the effect of mobility and storativity ratios on the estimation of the swept (inner region) volume for composite reservoirs in the various flow geometries using the pseudosteady state method. Conditions for the occurrence of pseudosteady state period of a reasonable duration for the various flow geometries have been established and compared. Results from this study confirm that the pseudosteady state method is indeed independent of the geometry of the reservoir for regularly-shaped fronts. However, the duration of pseudosteady state period may be different for different geometries, even if the mobility and storativity ratios are the same.

Equations for a generalized pressure derivative analysis of well-test data from composite reservoirs have been developed to enable easier identification of the principal flow regimes for the various flow geometries. New design and analysis equations based on the generalized pressure derivative for spherical and linear flow geometries have been

developed and compared with those for radial and elliptical flow geometries. Together, these new analysis and design equations constitute a significant addition to well test analysis methods for composite reservoirs. Reservoir parameters estimated using these equations will increase the degree of confidence in the estimated parameters based on pressure analysis.

A comparison of the production performances of two region, composite reservoirs for the various flow geometries has been carried out. Transient rate and cumulative production responses for both infinite and closed, finite reservoirs for the various flow geometries have been discussed and possible type curves for decline curve analysis of radial and linear, composite reservoirs have been presented. Possible applications of this model to computerized integrated analysis of well-test data from composite reservoir testing have been mentioned.

Finally, a new analytical model for the transient pressure behavior of a three-region, composite reservoir with a power law variation of mobility and storativity in the intermediate region has been presented. This model, which accounts for smooth changes in mobility and storativity ahead of the flood front in thermal recovery processes, should serve as an improvement over the sharp-front idealization of the composite reservoir model currently available.

7.2 Conclusions

This study has compared the transient pressure and rate responses for two-region composite reservoirs in radial, elliptical, linear and spherical flow geometries. Among other things, the objectives have been to investigate the effect of mobility and storativity

ratios on the transient pressure and rate responses, as well as, to develop additional design and analysis equations for well-test interpretation of composite reservoir well-test data. The effects of mobility and storativity gradients in the intermediate region on the transient pressure behavior of three-region composite reservoirs have also been investigated. The following conclusions may be drawn from various aspects of this study:

Pseudosteady State Method for Composite Reservoirs

1. Normalizing factors that enable comparison of solutions for composite reservoirs in radial, elliptical, linear and spherical flow geometries have been presented.
2. Time criteria for the start and end of the pseudosteady state flow period for each flow geometry, as functions of mobility and storativity ratios, have been developed to enable the correct choice of the pseudosteady state Cartesian straight line.
3. For the same mobility and storativity ratios, linear flow geometry results in the longest pseudosteady state period, and spherical flow geometry yields the shortest pseudosteady state period. The radial and elliptical flow geometries show the same duration of pseudosteady state.
4. The pressure derivative responses for composite reservoirs in radial and elliptical flow geometries are identical, except for the early-time inner region behavior.
5. The conditions under which a pseudosteady state period of reasonable duration occurs for each of the flow geometries have been established. These criteria will be of help in determining when the pseudosteady state method will be appropriate for the

estimation of swept volumes for thermal recovery projects under various reservoir situations.

Generalized Pressure Derivative Analysis

1. Well-test analysis equations based on the generalized pressure derivative have been presented for composite reservoirs in various flow geometries. Reservoir parameters estimated using these equations will increase the degree of confidence in the estimated parameters based on pressure analysis.
2. New design equations related to specific flow regimes observed in spherical and linear, composite reservoir well tests have been developed and compared with similar equations for radial and elliptical, composite reservoirs.
3. The linear, composite reservoir shows the longest transition period between inner and outer region infinite-acting flow. This is followed by the radial and elliptical, composite reservoirs. The spherical reservoir shows the shortest transition period. This implies that outer region infinite-acting flow is less likely to occur for linear reservoirs than it is for spherical reservoirs.
4. For radial and elliptical reservoirs, the late-time pressure derivative behavior is influenced only by the mobility ratio between the inner and outer regions of composite reservoirs. For linear and spherical reservoirs, however, late-time pressure derivative behavior is governed by both the mobility ratio and the storativity ratio.

Decline Curve Analysis

1. Normalizing factors to enable comparison of transient rate, as well as cumulative production responses, for composite reservoirs in radial, elliptical, linear and spherical flow geometries have been presented.
2. Transient rate and cumulative production responses for radial and elliptical reservoirs are not as identical as is the case for transient pressure derivative responses. Flow rate and cumulative production tend to be higher for elliptical reservoirs than for radial reservoirs, until the effects of the discontinuity boundary are felt. Thereafter, the responses for the two composite reservoirs begin to approach one another.
3. The mobility-storativity product, MF , is not a correlating parameter for transient rate and cumulative production responses from finite, linear, composite reservoirs. However, MF is a correlating parameter for infinitely-large, linear, composite reservoirs.

Three-Region Composite Reservoirs with Power Law Property Variation

1. A new analytical solution has been presented for an infinitely-large, three-region, radial, composite reservoir with a power law variation of mobility and storativity in the intermediate region. This model allows for smooth changes in mobility and storativity, due to rapidly declining temperatures ahead of a flood front in a thermal recovery process.
2. The size of the intermediate region has a significant effect on the magnitude of the maximum semi-log pressure derivative, and a mild effect on the time to the

maximum semi-log pressure derivative. The intermediate region size does not affect the time to the start of infinite-acting radial flow corresponding to the outer region mobility. In the light of the work by *Ambastha* (1988), this conclusion is valid for $F_{I2} \geq 1$.

3. Pseudosteady state behavior is less noticeable as the size of the intermediate region increases. Thus, possible estimates of the swept region volume using the pseudosteady state method may yield increasingly overestimated values as the size of the intermediate region increases.
4. The spectral exponent for mobility variation in the intermediate region, θ_1 , has only a mild effect on the pressure derivative responses for an infinitely-large, three-region, radial composite reservoir.
5. The storativity spectral exponent, θ_2 , significantly affects the pressure derivative responses for a three-region, radial, composite reservoir. When θ_1 and θ_2 assume equal values, the effect of θ_1 on the pressure derivative responses is negligible.
6. Practical values of θ_1 and θ_2 for thermal recovery processes will depend on the distance to the discontinuity boundary of the intermediate region. This value may not be known with certainty, and in fact is one of the parameters being sought from the analysis of well-test data from thermal recovery projects.

7.3 Recommendations

Future studies on well-test analysis of composite reservoirs should address the following:

1. Application of the concept of fractional dimension presented by *Barker* (1988) and *Doe* (1991) to well-test analysis of composite reservoirs needs to be investigated. This concept suggests that, for homogeneous reservoirs, only one diffusivity equation is needed regardless of the geometry of the reservoir. The diffusivity equation contains a parameter, n , which takes on different integer values for the different geometries. The fractional dimension concept has worked well for radial, linear and spherical reservoirs (*Barker*, 1988; *Doe*, 1991). The extension of this concept to elliptical reservoirs needs to be investigated.
2. Extension of the concept of fractional dimension to three-region, composite reservoirs with power law property variation in the intermediate region needs to be studied.
3. An in-depth investigation of the effect of fractal exponents for mobility and storativity on the applicability of the pseudosteady state method to swept volume estimation from thermal recovery processes should be carried out. Effective properties for the pseudosteady state analysis may be calculated using equations, similar to those presented by *Ambastha* (1988), with modifications to account for varying mobility and storativity in the intermediate region.

References

- Aarstad, K.: "Criteria for Determining Times for End of Transient Flow and Start of Pseudosteady State Flow," Engineer Thesis, Stanford University, Stanford, CA (Aug. 1987) 162 pp.
- Abbaszadeh-Dehghani, M. and Kamal, M.M.: "Pressure Transient Testing of Water Injection Wells." *SPE Res. Eng.* (February 1989) 115-124.
- Acosta, L.G. and Ambastha, A.K.: "Thermal Well Test Analysis Using an Analytical Multi-Region Composite Reservoir Model," paper SPE 28422 presented at the Annual Technical Conference and Exhibition of SPE of AIME, New Orleans, Louisiana (Sept. 25-28, 1994).
- Acuña, J.A., Ershagi, I. and Yortsos, Y.C.: "Practical Applications of Fractal Pressure Transient Analysis of Naturally Fractured Reservoirs," *SPE Form. Eval.* (Sept. 1995) 173-179.
- Ambastha, A. K.: "Pressure Transient Analysis for Composite Systems" Ph.D. Thesis, Stanford University, Stanford, CA (Oct. 1988) 193 pp.
- Ambastha, A.K. and Ramey, H.J., Jr.: "Pressure Transient Analysis for a Three-Region Composite Reservoir," paper SPE 24378 presented at the Rocky Mountain Regional Meeting of SPE of AIME, Casper, WY (May 18-21, 1992).
- Ambastha, A.K. and Ramey, H.J., Jr.: "Thermal Recovery Well Test Design and Interpretation," *SPE Form. Eval.* (June 1989) 173-180.
- Ambastha, A. K. and Sageev, A.: "Linear Water Influx of an Infinite Aquifer Through a Partially Communicating Fault," Proceedings of the 12th Geothermal Res. Engg. Workshop, Stanford, CA (Jan. 20-22, 1987).
- Barker, J.A.: "A Generalized Radial Flow Model for Hydraulic Tests in Fractured Rock." *Water Resources Res.* (Oct. 1988) **24**, 1796-1804.

- Barua, J. and Horne, R.N.: "Computerized Analysis of Thermal Recovery Well Test Data," *SPE Form. Eval.* (Dec. 1987) 560-566.
- Beier, R.A.: "Pressure Transient Model for a Vertically Fractured Well in a Fractal Reservoir," *SPE Form. Eval.* (June 1994) 122
- Bixel, H. C., Larkin, B. K. and van Poolen, H. K.: "Effect of Linear Discontinuities on Pressure Buildup and Drawdown Behavior," *J. Pet. Tech.* (Aug. 1963) 885-895.
- Bixel, H. C. and van Poolen, H. K.: "Pressure Drawdown and Buildup in the Presence of Radial Discontinuities," *Soc. Pet. Eng. J.* (Sept. 1967) 301-09.
- Bourdet, D., Ayoub, J. A. and Pirard, Y. M.: "Use of Pressure Derivative in Well-Test Interpretation," *SPE Form. Eval.* (June 1989) 293-301.
- Bourdet, D., Whittle, T. M., Douglas, A. A. and Pirard, Y. M.: "A New Set of Type Curves Simplifies Well Test Analysis," *World Oil* (May 1983) **169**, 95-106.
- Bratvold, R.B. and Horne, R.N.: "Analysis of Pressure Falloff Tests Following Cold Water Injection," *SPE Form Eval.* (Sept. 1990) 293-302.
- Carslaw, H.S. and Jaeger, J.C.: *Conduction of Heat in Solids*, Oxford University Press, London (1959).
- Carter, R. D.: "Pressure Behavior of a Limited Circular Composite Reservoir," *Soc. Pet. Eng. J.* (Dec. 1966) 328-34.
- Chakrabarty, C.: "*Pressure Transient Analysis of Non-Newtonian Power-Law Fluid Flow in Fractal Reservoirs*," Ph.D Thesis, The University of Alberta, Edmonton, AB (April 1993) 175 pp.
- Chang, J. and Yortsos, Y.C.: "Pressure Transient Analysis of Fractal Reservoirs," *SPE Form Eval.* (March 1990) 31-38.

Chatas, A. T.: "Unsteady Spherical Flow in Petroleum Reservoirs" *Soc. Pet. Eng. J.* (June 1966) 102-114

Cox, D.O.: "The Solution of Problems Associated With Constant Well Pressure." paper SPE 8386 presented at the Annual Technical Conference and Exhibition of the SPE of AIME, Las Vegas, NV (Sept. 23-26, 1979).

Da Prat, G., Bockh, A., and Prado, L.: "Use of Pressure Falloff Testing to Locate the Burning Front in the Miga Field, Eastern Venezuela." paper SPE 13667 presented at the California Regional Meeting of SPE of AIME, Bakersfield, CA (March 27-29, 1985)

Doe, T.W.: "Fractional Dimension Analysis of Constant-Pressure Well Tests." paper SPE 22702 presented at the Annual Technical Conference and Exhibition of SPE of AIME, Dallas, TX (Oct. 6-9, 1991).

Earlougher, R. C., Jr.: *Advances in Well Test Analysis*, Monograph Volume 5 of the Henry L. Doherty Series, Society of Petroleum Engineers of AIME, New York (1977).

Eggenschwiler, M., Satman, A., and Ramey, H. J., Jr.: "Interpretation of Injection Well Pressure Transient Data in Thermal Oil Recovery." paper SPE 8908 presented at the California Regional Meeting of SPE of AIME, Los Angeles, CA (April 9-11, 1980).

Fassihi, M. R.: "Evaluation of an Analytic Technique for Estimating Swept Volume From Thermal Pressure Falloff Tests in Heterogeneous Reservoirs." *SPE Form. Eval.* (June 1988) 449-57.

Fetkovich, M.J.: "Decline Curve Analysis Using Type Curves." *J. Pet. Tech.* (June 1980) 1067-1076.

Gefen, Y., Aharony, A., and Alexander, S.: "Anomalous Diffusion in Percolating Clusters," *Physical Review Letters* (1983) **50**(1), 77-80.

Gradshteyn, I.S. and Ryzhik, I.M.: *Table of Integrals, Series, and Products*, (translated by Scripta Technica, Inc.), Academic Press, New York (1965)

IMSL Math Special Functions Library, Users manual, IMSL Math/Library: version 1.0, (1987).

Issaka, M. B. and Ambastha, A. K.: "Evaluation of the Pseudosteady-State Method for Composite Reservoirs in Various Flow Geometries," paper SPE 27907 presented at the Western Regional Meeting of SPE of AIME, Long Beach, CA (March 23-25, 1994).

Jelmert, T. A.: "Theory and Application of Polynomial Type Curves," paper SPE 25876 presented at the Rocky Mountain Regional Meeting of SPE of AIME, Denver, CO (April 12-14, 1993a).

Jelmert, T. A.: "A Note on Flow-Period Diagnostics in Well Testing," *J. Pet. Sc. & Engg.* (1993b) **8**, 329-332.

Larsen, L.: "Limitations on the Use of Single and Multi-Rate Horner, Miller-Dyes-Hutchinson, and Mathews-Brons-Hazebroek Analysis," paper SPE 12135 presented at the Annual Meeting of SPE of AIME, San Francisco, CA (Oct. 5-8, 1983).

Loucks, T. L. and Guerrero, E. T.: "Pressure Drop in a Composite Reservoir," *Soc. Pet. Eng. J.* (Sept. 1961) 170-76.

Mattar, L. and Santo, M.: "A Practical and Systematic Approach to Horizontal Well Test Analysis," *J. Can. Pet. Tech.* (Nov. 1995) 42-46.

McLachlan, N. W.: *Theory and Application of Mathieu Functions*, Oxford University Press, London (1947).

Messner, G. L. and Williams, R. L.: "Application of Pressure Transient Analysis in Steam Injection Wells," paper SPE 10781 presented at the California Regional Meeting of SPE of AIME, San Francisco, CA (March 24-26, 1982)

Nanba, T. and Horne, R.N.: "Estimation of Water and Oil Relative Permeabilities From Pressure Transient Analysis of Water Injection Well Data," paper SPE 19829 presented at the Annual Technical Conference and Exhibition of SPE of AIME, San Antonio, TX (Oct. 8-11, 1989).

- Obut, S. T. and Ertekin, T.: "A Composite Reservoir Solution in Elliptical Flow Geometry," *SPE Form. Eval.* (Sept. 1987) 227-237.
- Olarewaju, J.S. and Lee, W.J.: "Type Curve and Decline Curve Analysis Using Composite Models," paper SPE 17055 presented at the Eastern Regional Meeting of SPE of AIME, Pittsburgh, PA (Oct. 21-23, 1987a).
- Olarewaju, J.S. and Lee, W.J.: "An Analytical Model for Composite Reservoirs Produced at Either Constant Bottomhole Pressure or Constant Rate," paper SPE 16763 presented at the Annual Meeting of SPE of AIME, Dallas, TX (Sept. 27-30, 1987b).
- Olarewaju, J.S. and Lee, W.J.: "A Comprehensive Application of a Composite Reservoir Model to Pressure Transient Analysis," paper SPE 16345 presented at the California Regional Meeting of SPE of AIME, Ventura, CA (April 8-10, 1987c).
- Onyekonwu, M. O. and Horne, R. N.: "Pressure Response of a Reservoir With Spherically Discontinuous Properties," *J. Pet. Tech.* (Nov. 1983) 2127-34.
- Onyekonwu, M.O. and Ramey, H.J., Jr.: "*Interpretation of In-situ Combustion Thermal Oil Recovery Falloff Tests*," SUPRI TR-50, DOE Report No. DOE/SF/11564-14 (March 1984) 140 pp.
- Onyekonwu, M.O., Ramey, H.J., Jr., Brigham, W.E. and Jenkins, R.: "Interpretation of Simulated Falloff Tests," paper SPE 12746 presented at the California Reg. Mtg. of SPE of AIME, Long Beach, CA (April 11-13, 1984)
- Poon, D.: "Transient Pressure Analysis of Fractal Reservoirs," paper CIM 95-34 presented at the Annual Meeting of the Petroleum Society of CIM, Banff, AB (May 14-17, 1995).
- Poon, D and Chhina, H.: "Transient Pressure Analysis of a Linear, Composite Reservoir," paper CIM 89-40-8 presented at the 40th Annual Technical Meeting of the Petroleum Society of CIM, Banff, AB (May 28-31, 1989).
- Prats, M.: *Thermal Recovery*, Monograph Volume 7 of the Henry L. Doherty Series, Society of Petroleum Engineers of AIME, New York (1982) 283 pp.

- Stanislav, J. F., Easwaran, C. V. and Kokal, S. L.: "Analytical Solution for Vertical Fractures in a Composite Reservoir," *J. Can. Pet. Tech.* (Sept., 1987) 51-56.
- Stanislav, J. F., Easwaran, C. V. and Kokal, S. L.: "Interpretation of Thermal Well Falloff Testing," *SPE Form. Eval.* (June 1989) 181-186.
- Stanislav, J. F., Easwaran, C. V. and Kokal, S. L.: "Elliptical Flow in Composite Reservoirs," *J. Can. Pet. Tech.* (Dec. 1992) 47-50.
- Stehfest, H.: "Numerical Inversion of Laplace Transform: Algorithm 368-(d5)," *Communication of ACM* (Jan. 1970) 47-49.
- Tiab, D. And Kumar, A.: "Application of the p'_p Function to Interference Analysis," *J. Pet. Tech.* (August 1980) 1465-70.
- Turki, L., Demski, J.A. and Grader, A.S.: "Decline Curve Analysis in Composite Reservoirs," paper SPE 19316 presented at the Eastern Regional Meeting of the SPE of AIME, Morgantown, WV (Oct. 24-27, 1989).
- Uraiet, A.A. and Raghavan, R.: "Unsteady Flow to a Well Producing at a Constant Pressure," *J. Pet. Tech.* (Oct. 1980a) 1803-1812.
- Uraiet, A.A. and Raghavan, R.: "Pressure Buildup Analysis for a Well Produced at Constant Bottomhole Pressure" *J. Pet. Tech.* (Oct. 1980b) 1813-1824.
- van Everdingen, A. F. and Hurst, W.: "The Application of the Laplace Transformation to Flow Problems in Reservoirs," *Trans., AIME* (1949) **186**, 305-324.
- Walsh, J. W., Jr., Ramey, H. J., Jr., and Brigham, W.E.: "Thermal Injection Well Falloff Testing," paper SPE 10227 presented at the 56th Annual Meeting of SPE of AIME, San Antonio, TX (Oct. 5-7, 1981).

APPENDICES

Appendix A: Computer Program for Analytical Solutions for Two-Region, Composite Reservoirs of Various Geometries

This appendix gives the computer program for the analytical solutions for two-region composite reservoirs in radial, elliptical, linear and spherical geometries used in this study. Description of the program has been given in Chapter 2.

Source Code for Program: COMPOSITE

```
C *****
C .....Source Code for Program: COMPOSITE
C
C   Purpose of this program is to generate the transient-pressure or
C   transient-rate response for a well in a two-region composite
C   reservoir of different flow geometries.
C
C   The flow geometries are Radial, Elliptical, Linear and Spherical.
C
C   Wellbore storage and skin at the well are included.
C
C   Inner boundary (well) may be at constant-rate or constant-
C   pressure.
C
C   Outer boundary may be infinite, closed or at a constant pressure.
C
C *****
C                               Variable Identification List
C *****
C
C   AD  -- dimensionless distance to discontinuity boundary linear and
C         spherical geometries
C   AMOB-- mobility ratio  $(k_1 \mu_2) / (k_2 \mu_1)$ 
C   CD  -- dimensionless wellbore storage constant
C   DIF -- diffusivity ratio  $(k_1 \phi c_t \mu_2) / (k_2 \phi c_t \mu_1)$ 
C   EPSE-- elliptic distance to outer boundary for elliptical geometry
C   EPSO-- elliptic distance to discontinuity boundary for elliptical
C         geometry
C   IBC  -- code for inner boundary condition
C   ICODE-- code for reservoir geometry
C   IOBC-- code for outer boundary condition
C   RD  -- dim. distance to discontinuity boundary for radial geometry
C   RDE  -- dim. distance to outer boundary for spherical geometry
C   RED  -- dim. distance to outer boundary for radial geometry
C   SKIN-- skin factor
C   STO  -- storativity ratio  $(\phi c_{t1} / (\phi c_{t2}))$ 
C   XDE  -- dim. distance to outer boundary for linear geometry
C
C   IMPLICIT REAL*8(A-H,O-Z)
C   DIMENSION TD(20)
C   CHARACTER*12 CDATA
```

```

COMMON M, AMOB, DIF, AD, IBC, ICODE, IOBC, CD, SKIN, STO, RD
+RED, RDE, EPSO, EPSE, XDE
C
C **Accept screen input**
C
WRITE(6,*) 'Enter code for reservoir geometry desired:'
WRITE(6,*) '1 = Radial, 2 = Elliptical,'
WRITE(6,*) '3 = Linear, 4 = Spherical.'
WRITE(6,*) '(1,2,3, or 4) >'
READ(5,*) ICODE
C
WRITE(6,*) 'Enter name of external data file:>'
READ(5,11) CDATA
OPEN(UNIT=7, FILE=CDATA)
C
C Reading input data from file, depending on the geometry code
C
IF (ICODE.EQ.1) THEN
CALL RADDATA(AMOB, RD, CD, SKIN, IBC, IOBC, NC, NTERM,
+STO, TD1, RED)
ELSEIF (ICODE.EQ.2) THEN
CALL ELLDATA(AMOB, CD, SKIN, EPSE, EPSO, IBC, IOBC, NC, NTERM,
+STO, TD1)
ELSEIF (ICODE.EQ.3) THEN
CALL LINDATA(AMOB, CD, SKIN, AD, IBC, IOBC, NC, NTERM,
+STO, TD1, XDE)
ELSE
CALL SPHDATA(AMOB, CD, SKIN, AD, IBC, IOBC, NC, NTERM,
+STO, TD1, RDE)
ENDIF
C
C
WRITE(6,*) 'Enter name of output file:>'
READ(5,11) CDATA
OPEN(UNIT=8, FILE=CDATA)
C
C ** End of screen input **
C
M=777
PI=2.0*ASIN(1.)
C
C Compute diffusivity ratio
DIF=AMOB/STO
C
C Generate the first set of  $t_D$  vector
C
TD(1)=TD1
TD(2)=1.5*TD1
TD(3)=2.*TD1
TD(4)=2.5*TD1
TD(5)=3*TD1
TD(6)=3.1*TD1
TD(7)=4.*TD1
TD(8)=4.5*TD1
TD(9)=5.*TD1
TD(10)=6.*TD1
TD(11)=6.*TD1

```

```

C      TD(13)=9.*TD1
C      -----
C      Generate and print the transient pressure or rate response
C
C
C      DO 1 I=1,NC
C      DO 2 J=1,13
C      SPC=TD(J)
C      IF (IBC.EQ.1) THEN
C          CALL INVERT(SPC,NTERM,PWD,PDP)
C          PDPTD=PD.*SPC
C          WRITE(8,7) SPC, PWD, PDP, PDPTD
C      ELSE
C          CALL INVERT(SPC,NTERM,QDR,QDC)
C          WRITE(8,9) SPC, QDR, QDC
C      ENDIF
2      TD(J)=10.*TD(J)
1      CONTINUE
7      FORMAT(' ',T5,E10.4,T20,E10.4,T35,E10.4,T50,E10.4)
9      FORMAT(' ',T5,E10.4,T20,E10.4,T35,E10.4)
      STOP
      END
C
C      *****
C
C      This subroutine reads data from the input file for the radial flow
C      geometry
C
C      SUBROUTINE RADDATA(AMOB,RD,CD,SKIN,IBC,IOBC,NC,NTERM,
+STO,TD1,RED)
C      IMPLICIT REAL*8 (A-H,O-Z)
C
C          READ(7,*)
C          READ(7,*)
C          READ(7,*)
C          READ(7,*)
C          READ(7,*) IBC
C          READ(7,*)
C          READ(7,*)
C          READ(7,*) IOBC
C          READ(7,*)
C          READ(7,*) CD, SKIN
C          READ(7,*)
C          READ(7,*) AMOB
C          READ(7,*)
C          READ(7,*) STO
C          READ(7,*)
C          READ(7,*) RD
C          READ(7,*)
C          READ(7,*) RED
C          READ(7,*)
C          READ(7,*) NC
C          READ(7,*)
C          READ(7,*) TD1
C          READ(7,*)
C          READ(7,*) NTERM
      RETURN

```

```

      END
C
C *****
C
C This subroutine reads data from the input file for the elliptical
C flow geometry
C
      SUBROUTINE ELLDATA(AMOB,CD,SKIN,EPSE,EPSO,IBC,IOBC,NC,
+NTERM,STO,TD1)
      IMPLICIT REAL*8(A-H,O-Z)
C
      READ(7,*)
      READ(7,*)
      READ(7,*)
      READ(7,*)
      READ(7,*)IBC
      READ(7,*)
      READ(7,*)
      READ(7,*)IOBC
      READ(7,*)
      READ(7,*)CD,SKIN
      READ(7,*)
      READ(7,*)AMOB
      READ(7,*)
      READ(7,*)STO
      READ(7,*)
      READ(7,*)EPSO
      READ(7,*)
      READ(7,*)EPSE
      READ(7,*)
      READ(7,*)NC
      READ(7,*)
      READ(7,*)TD1
      READ(7,*)
      READ(7,*)NTERM
      RETURN
      END
C
C *****
C
C This subroutine reads data from the input file for the linear flow
C geometry
C
      SUBROUTINE LINDATA(AMOB,CD,SKIN,AD,IBC,IOBC,NC,NTERM,
+STO,TD1,XDE)
      IMPLICIT REAL*8(A-H,O-Z)
C
      READ(7,*)
      READ(7,*)
      READ(7,*)
      READ(7,*)
      READ(7,*)IBC
      READ(7,*)
      READ(7,*)
      READ(7,*)IOBC
      READ(7,*)
      READ(7,*)CD,SKIN
      READ(7,*)

```



```

      READ(7,*)AMOB
      READ(7,*)
      READ(7,*)STO
      READ(7,*)
      READ(7,*)AD
      READ(7,*)
      READ(7,*)XDE
      READ(7,*)
      READ(7,*)NC
      READ(7,*)
      READ(7,*)TD1
      READ(7,*)
      READ(7,*)NTERM
    RETURN
  END

C
C
C *****
C
C This subroutine reads data from the input file for the spherical
C flow geometry
C
      SUBROUTINE SPHDATA(AMOB,CD,SKIN,AD,IBC,IOBC,NC,NTERM,
+STO,TD1,RDE)
      IMPLICIT REAL*8(A-H,O-Z)
C
      READ(7,*)
      READ(7,*)
      READ(7,*)
      READ(7,*)
      READ(7,*)IBC
      READ(7,*)
      READ(7,*)
      READ(7,*)IOBC
      READ(7,*)
      READ(7,*)CD,SKIN
      READ(7,*)
      READ(7,*)AMOB
      READ(7,*)
      READ(7,*)STO
      READ(7,*)
      READ(7,*)AD
      READ(7,*)
      READ(7,*)RDE
      READ(7,*)
      READ(7,*)NC
      READ(7,*)
      READ(7,*)TD1
      READ(7,*)
      READ(7,*)NTERM
    RETURN
  END

C
C
C *****
C
      SUBROUTINE LAPRAD(S,PWDL,PDPL)
      IMPLICIT REAL*8(A-H,O-Z)
      EXTERNAL DBSI0E,DBSI1E,DBSK0E,DBSK1E

```

```

COMMON M, AMOB, DIF, AD, IBC, ICODE, IOBC, CD, SKIN, STO, ED
RED, RSE, EPOC, EPOE, RDE
C
C      Radial composite reservoir solution in Laplace space
C      -----
C      We begin by computing the arguments of bessel functions
C
      ARG1=DSQRT(S)
      ARG2=RD*ARG1
      ARG3=DSQRT(DIF)*ARG2
      IF(IOBC.NE.1) ARG4=DSQRT(S*DIF)*RED
C
C      Compute needed bessel functions (exponentially scaled)
C
      A1=DBSI0E(ARG1)
      A2=DBSI0E(ARG2)
C
      B1=DBSI1E(ARG1)
      B2=DBSI1E(ARG2)
C
      D1=DBSK0E(ARG1)
      D2=DBSK0E(ARG2)
      D3=DBSK0E(ARG3)
C
      E1=DBSK1E(ARG1)
      E2=DBSK1E(ARG2)
      E3=DBSK1E(ARG3)
C
      IF(IOBC.EQ.2) THEN
        C11=-DBSK1E(ARG4)
        C22=DBSI1E(ARG4)
      ENDIF
      IF(IOBC.EQ.3) THEN
        C11=DBSK0E(ARG4)
        C22=DBSI1E(ARG4)
      ENDIF
      IF(IOBC.NE.1) THEN
        A3=DBSI0E(ARG3)
        B3=DBSI1E(ARG3)
      ENDIF
C      Calculation of multiplying factors
C
      F1=DEXP(ARG1)
      F2=DEXP(ARG2)
      F3=DEXP(ARG3)
      IF(IOBC.NE.1) THEN
        IF(ARG4.LT.87.) THEN
          F4=DEXP(ARG4)
        ELSE
          F4=DEXP(87.0D+00)
        ENDIF
      ENDIF
C      Computation of coefficients of eqns. For c1,c2 and c3.
C      For finite reservoirs, we have c4 also.
C
      AL11=-ARG1*B1*F1
      AL12=ARG1*E1/F1
      AL21=A2*F2

```

```

AL22=D2/F2
AL23=-D3/F3
AL31=AMOB*ARG1*B2*F2
AL32=-AMOB*ARG1*E2/F2
AL33=DSQRT(S*DIF)*E3/F3
C
  IF(IOBC.NE.1)THEN
    AL24=-A3*F3
    AL34=-DSQRT(S*DIF)*B3*F3
    AL43=C11/F4
    AL44=C22*F4
  ENDIF
C Calculation of c1, c2, and c3
C c4 is also calculated for finite reservoirs
C
  S1=AL21*AL33-AL23*AL31
  S2=AL22*AL33-AL32*AL23
C
  IF(IOBC.EQ.1)THEN
    C2=S1/(S*(AL12*S1-AL11*S2))
    C1=(1.-S*AL12*C2)/S/AL11
    C3=-(AL31*C1+AL32*C2)/AL33
  ENDIF
  IF(IOBC.NE.1)THEN
    S3=AL43/AL44
    S4=AL24*AL31-AL21*AL34
    S5=S1+S3*S4
    S6=AL22*AL34-AL24*AL32
    S7=-AL11*S2+AL12*S1+S3*(AL12*S4+AL11*S6)
    C2=S5/S/S7
    C1=(1.-S*AL12*C2)/S/AL11
    C4=S3*(AL31*C1+AL32*C2)/(AL33-AL34*S3)
    C3=-C4/S3
  ENDIF
C Calculation of transformed solution (constant rate)
C -----
C PWDL = Laplace transform of pwp
C PDPL = Laplace transform of wellbore pressure derivative (dpwp/dtp)
C
  PWDL=C1*A1*F1 + C2*D1/F1
  PDPL=PWDL*S
C
C Adding wellbore storage and skin effects to the constant-rate
C solution
C
  IF (CD.GT.0.OR.SKIN.GT.0) THEN
    PWDL=(S*PWDL + SKIN)/(S*(1 + CD*S*(S*PWDL + SKIN)))
    PDPL=PWDL*S
  ENDIF
C
C Constant pressure inner boundary condition (Duhamel's principle)
C PWDL = Laplace transform of flow rate (QDR)
C PDPL = Laplace transform of cumulative rate (QDC)
C
  IF (IBC.EQ.2) THEN
    PWDL= 1./(S**2*PWDL)
    PDPL=PWDL/S
  ENDIF

```

```

      RETURN
      END
C
C
*****
C
      SUBROUTINE LAPELL(S,PWDL,PDPL)
      IMPLICIT REAL*8(A-H,O-Z)
      EXTERNAL DBSIOE,DBSIE,DBSKOT,DBSKLE
      EXTERNAL CONST,DMATEE,UMACH,DCBJNS,DLSARG
      COMMON M,AMOB,DIF,AD,IBC,ICODE,IOBC,CD,SKIN,STO,RD
      +RED,RDE,EPSO,EPSE,XDE
      DIMENSION AF(50),AA(50),CE(50),P(50)
      DIMENSION CCE(50),CCEP(50),FEK(50),FEKP(50)
C
C      Elliptical composite reservoir solution in Laplace space
C      -----
      NN=3
      EPSW=0.0D+00
      PI=2.0*ASIN(1.)
      ET=PI/2
      SLM1=S/4
      SLM2=DIF*SLM1
      ISYM=0
      IPER=0
      SUML=0.0D+00
      TINY=1.0D-25
C
      DO 3 N=1,NN
         Q=SLM1
         Z=EPSW
C
C      Computing constants and coefficients needed for Mathieu
C      functions
C
         CALL DMATEE(Q,NN,ISYM,IPER,AF)
         CALL COEFF(Q,N,AF,II,AAO,AA)
         CALL P2N(N,AAO,AA,II,P)
C
C      Computing needed Mathieu functions
C
         CALL FNCCE(Z,II,N,AAO,AA,CCE,CCEP)
         CALL FNF EK(Q,Z,II,N,P,AAO,AA,FEK,FEKP)
C
         G2N=-CCEP(N)
         H2N=-FEKP(N)
         HI2N=(-1)**(N-1)*AAO/(2*SLM1)
C
         Z=EPSO
         CALL FNCCE(Z,II,N,AAO,AA,CCE,CCEP)
         CALL FNF EK(Q,Z,II,N,P,AAO,AA,FEK,FEKP)
C
         A2N=CCE(N)
         B2N=FEK(N)
         D2N=CCEP(N)
         E2N=FEKP(N)
C
      Q=SLM2

```

```

      CALL DMATEE(Q,NN,ISYM,IPEP,AF)
      CALL COEFF(Q,N,AF,II,AAO,AA)
      CALL P2N(N,AAO,AA,II,P)
C
      CALL FNCCE(Z,II,N,AAO,AA,CCE,CCEP)
      CALL FNFEK(Q,Z,II,N,P,AAO,AA,FEK,FEKP)
C
      C2N=FEK(N)
      F2N=FEKP(N)/AMOB
      R2N=CCE(N)
      T2N=CCEP(N)/AMOB
C
C      Additional coefficients for closed and constant pressure
C      outer boundary conditions
C
      IF (IOBC.NE.1) THEN
        Z=EPSE
        CALL FNCCE(Z,II,N,AAO,AA,CCE,CCEP)
        CALL FNFEK(Q,Z,II,N,P,AAO,AA,FEK,FEKP)
C
C      Closed outer boundary
C      -----
        IF (IOBC.EQ.2) THEN
          X2N=FEKP(N)
          Y2N=CCEP(N)
        ENDIF
C
C      Constant pressure outer boundary
C      -----
        IF (IOBC.EQ.3) THEN
          X2N=FEK(N)
          Y2N=CCE(N)
        ENDIF
C
        C1=X2N/Y2N
        W2N=C2N - C1*R2N
        Z2N=F2N - C1*T2N
      ENDIF
C
C      Constants for infinite outer boundary
C      -----
      IF (IOBC.EQ.1) THEN
        DENO=G2N*(C2N*E2N - B2N*F2N) + H2N*(A2N*F2N - C2N*D2N)
        CC2N=HI2N*(C2N*E2N - B2N*F2N)/DENO
        FF2N=HI2N*(A2N*F2N - C2N*D2N)/DENO
      ELSE
C
C      Constants for closed and constant-pressure outer boundary
C      conditions
C      -----
        DENO=G2N*(W2N*E2N - B2N*Z2N) + H2N*(A2N*Z2N - W2N*D2N)
        CC2N=HI2N*(W2N*E2N - B2N*Z2N)/DENO
        FF2N=HI2N*(A2N*Z2N - W2N*D2N)/DENO
      ENDIF
C
      Q=SLM1
      CALL DMATEE(Q,NN,ISYM,IPEP,AF)
      CALL COEFF(Q,N,AF,II,AAO,AA)

```

```

      CALL P2N(N,AAO,AA,II,P)
C
      Z=EPSW
      CALL FNCCE(Z,II,N,AAO,AA,CCE,CCEP)
      CALL FNFEK(Q,Z,II,M,P,AAO,AA,FEK,FEKP)
      Z=ET
      CALL FNCE(Z,II,N,AAO,AA,CE)
C
      SUMADD=CE(N)*(CC2N*CCE(N) + FF2N*FEK(II))
      SUML=SUML + SUMADD
      IF (SUMADD.LT.TINY)GO TO 99
3     CONTINUE
C
C     Calculation of transformed solution (constant rate)
C     -----
C     PWDL = Laplace transform of pwD
C     PDPL = Laplace transform of wellbore pressure derivative (dpwD/dtD)
C
99     PWDL=SUML
      PDPL=PWDL*S
C
C     Adding wellbore storage and skin effects to the constant-rate
C     solution
C
      IF (CD.GT.0.OR.SKIN.GT.0) THEN
        PWDL=(S*PWDL + SKIN)/(S*(1 + CD*S*(S*PWDL + SKIN)))
        PDPL=PWDL*S
      ENDIF
C
C     Constant pressure inner boundary condition (Duhamel's principle)
C     PWDL = Laplace transform of flow rate (qDr)
C     PDPL = Laplace transform of cumulative rate (qDc)
C
      IF (IBC.EQ.2) THEN
        PWDL= 1./(S**2*PWDL)
        PDPL=PWDL/S
      ENDIF
      RETURN
      END
C
C
*****
C
      SUBROUTINE LAPLIN(S,PWDL,PDPL)
      IMPLICIT REAL*8(A-H,O-Z)
      COMMON M,AMOB,DIF,AD,IBC,ICODE,IOBC,CD,SKIN,STO,RD
      +RED,RDE,EPSO,EPSE,XDE
C
C     Linear composite reservoir solution in Laplace space
C     -----
      ARG1=AD*DSQRT(S*DIF)
      ARG2=AD*DSQRT(S)
      ARG3=2.*XDE*DSQRT(S*DIF)
      A=DEXP(-ARG1)
      B=DEXP(ARG1)
      D=DEXP(-ARG2)
      E=DEXP(ARG2)
      F=DEXP(-ARG3)

```

```

      G=DSQRT(DIF)/AMOB
C
C      Outer boundary condition
C      -----
C      Infinite outer boundary
C
      IF (IOBC.EQ.1) THEN
        TOP=D*(G-1)
        BOT=S*DSQRT(S)*((D-E) - G*(D+E))
      ENDIF
C      Closed outer boundary
C
      IF (IOBC.EQ.2) THEN
        TOP=-D*((A*F+B) + G*(A*F-B))
        BOT=S*DSQRT(S)*(G*(A*F-B)*(D+E) + (A*F+B)*(D-E))
      ENDIF
C      Constant pressure outer boundary
C
      IF (IOBC.EQ.3) THEN
        TOP=D*((B-A*F) - G*(B+A*F))
        BOT=S*DSQRT(S)*(G*(B+A*F)*(D+E) - (B-A*F)*(D-E))
      ENDIF
C
      C1=TOP/BOT
C
C      Calculation of transformed solution (constant rate)
C      -----
C      PWDL = Laplace transform of pwp
C      PDPL = Laplace transform of wellbore pressure derivative (dpwp/dtD)
C
      PWDL=2*C1 + 1/(S*DSQRT(S))
      PDPL=PWDL*S
C
C
C      Adding wellbore storage and skin effects to the constant-rate
C      solution
C
      IF (CD.GT.0.OR.SKIN.GT.0) THEN
        PWDL=(S*PWDL + SKIN)/(S*(1 + CD*S*(S*PWDL + SKIN)))
        PDPL=PWDL*S
      ENDIF
C
C      Constant pressure inner boundary condition (Duhamel's principle)
C      PWDL = Laplace transform of flow rate (qdr)
C      PDPL = Laplace transform of cumulative rate (qdc)
C
      IF (IBC.EQ.2) THEN
        PWDL= 1./(S**2*PWDL)
        PDPL=PWDL/S
      ENDIF
      RETURN
      END
C
C
C      *****
C
      SUBROUTINE LAPSPH(S, PWDL, PDPL)
      IMPLICIT REAL*8(A-H, O-Z)

```

```
COMMON M, AMOB, DIF, AD, IBC, ICODE, IOBC, CD, SKIN, STO, RD
+RED, PDE, EPSO, EPSE, XDE
```

```
C
C   Spherical composite reservoir solution in Laplace space
C   -----
C       ARG1=DSQRT(S)
C       ARG2=AD*DSQRT(S)
C       ARG3=AD*DSQRT(DIF*S)
C       ARG4=RDE*DSQRT(DIF*S)
C
C       AL11=S*DCOSH(ARG1) - ARG1*DSINH(ARG1)
C       AL12=S*DSINH(ARG1) - ARG1*DCOSH(ARG1)
C
C       AL21=DSINH(ARG2)
C       AL22=DCOSH(ARG2)
C       AL23=-DSINH(ARG3)/DSQRT(DIF)
C       AL24=-DCOSH(ARG3)/DSQRT(DIF)
C
C       AL31=DCOSH(ARG2) - DSINH(ARG2)/ARG2
C       AL32=DSINH(ARG2) - DCOSH(ARG2)/ARG2
C       AL33=-(DCOSH(ARG3) - DSINH(ARG3)/ARG3)/AMOB
C       AL34=-(DSINH(ARG3) - DCOSH(ARG3)/ARG3)/AMOB
C
C   Outer boundary condition
C   -----
C   Infinite outer boundary
C
C       IF (IOBC.EQ.1) THEN
C           A=AL23 - AL24
C           B=AL33 - AL34
C       ENDIF
C
C   Closed outer boundary
C
C       IF (IOBC.EQ.2) THEN
C           AL43=DCOSH(ARG4) - DSINH(ARG4)/ARG4
C           AL44=DSINH(ARG4) - DCOSH(ARG4)/ARG4
C           G=AL43/AL44
C           A=AL23 - AL24*G
C           B=AL33 - AL34*G
C       ENDIF
C
C   Constant pressure outer boundary
C
C       IF (IOBC.EQ.3) THEN
C           AL43=DSINH(ARG4)/ARG4
C           AL44=DCOSH(ARG4)/ARG4
C           G=AL43/AL44
C           A=AL23 - AL24*G
C           B=AL33 - AL34*G
C       ENDIF
C
C       D=AL21*B - AL31*A
C       E=AL22*B - AL32*A
C       F=AL12*D - AL11*E
C
C       C1=E/F
C       C2=-D/F
```



```

C
C Calculation of transformed solution (constant rate)
C -----
C PWDL = Laplace transform of pwp
C PDPL = Laplace transform of wellbore pressure derivative (dpwp/dt)
C
C   PWDL=C1*DSINH(ARG1)/ARG1 + C2*DCOSH(ARG1)/ARG1
C   PDPL=PWDL*S
C
C
C Adding wellbore storage and skin effects to the constant-rate
C solution
C
C   IF (CD.GT.0.OR.SKIN.GT.0) THEN
C     PWDL=(S*PWDL + SKIN)/(S*(1 + CD*S*(S*PWDL + SKIN)))
C     PDPL=PWDL*S
C   ENDIF
C
C Constant pressure inner boundary condition (Duhamel's principle)
C PWDL = Laplace transform of flow rate (qdr)
C PDPL = Laplace transform of cumulative rate (qdc)
C
C   IF (IBC.EQ.2) THEN
C     PWDL= 1./(S**2*PWDL)
C     PDPL=PWDL/S
C   ENDIF
C RETURN
C END
C
C *****
C
C The Stehfest Algorithm
C -----
C
C SUBROUTINE INVERT(TD,NL,PWD,PDP)
C IMPLICIT REAL*8 (A-H,O-Z)
C COMMON M,AMOB,DIF,AD,IBC,ICODE,IOBC,CD,SKIN,STO,RD
C +RED,RDE,EPSE,EPSE,XDE
C DIMENSION G(50),V(50),H(25)
C
C   Now if the array v(i) was calculated previously, the
C   program goes directly to the end of the subroutine to
C   calculate f(s).
C   IF (NL.EQ.M) GO TO 47
C   M=NL
C   DLOGTW=0.6931471805599D+00
C   NH=NL/2
C
C   The factorials of 1 to NL are calculated into g.
C   G(1)=1
C   DO 31 I=2,NL
C     G(I)=G(I-1)*I
31 CONTINUE
C
C   Terms with K only are calculated into array H
C   H(1)=2.0/G(NH-1)
C   DO 36 I=2,NH
C     FI=I

```

```

      IF (I-NH) 34,35,36
34      H(I)=FI**NH*G(2*I)/(G(NH-I)*G(I)*G(I-1))
      GO TO 36
35      H(I)=FI**NH*G(2*I)/(G(I)*G(I-1))
36      CONTINUE
C
C      The terms (-1)**NH+1 are calculated.
C      First the term for I=1
      SN=2*(NH-NH/2*2) -1
C
C      The rest of the SN's are calculated in the main routine
C      The array V(I) is calculated.
      DO 37 I=1,NL
C
C      FIRST SET V(I)=0
      V(I)=0.0
C
C      The limits of K are established.
C      The lower limit for K1=INTEG((I+1/2))
      k1=(i+1)/2
C
C      The upper limit is K2=MIN(I,NL/2)
      K2=I
      IF (K2-NH) 38,38,39
39      K2=NH
C
C      The summation term in V(I) is calculated
38      DO 40 K=K1,K2
      IF (2*K-I) 42,43,42
42      IF (I-K) 41,44,41
41      V(I)=V(I)+H(K)/(G(I-K)*G(2*K-I))
      GO TO 40
43      V(I)=V(I)+H(K)/G(I-K)
      GO TO 40
44      V(I)=V(I)+H(K)/G(2*K-I)
40      CONTINUE
C
C      The V(I) array is finally calculated by weighting
C      according to SN
      V(I)=SN*V(I)
C
C      The term SN changes its sign each iteration.
      SN=-SN
37      CONTINUE
C
C      The numerical approximation is calculated.
C
47      PWD=0.0D+00
      PDP=0.0D+00
      A=DLOGTW/TD
      DO 52 I=1,NL
      ARG=A*I
C      Depending on geometry code, INVERT calls the solution for radial,
C      elliptical, linear or spherical reservoir in Laplace space
C
      IF (ICODE.EQ.1) THEN
      CALL LAPRAD(ARG,PWDL,PDPL)
      ELSEIF (ICODE.EQ.2) THEN

```

```

      CALL LAPELL(ARG,PWDL,PDPL)
    ELSEIF (ICODE.EQ.3) THEN
      CALL LAPLIN(ARG,PWDL,PDPL)
    ELSE
      CALL LAPSPH(ARG,PWDL,PDPL)
    ENDIF
C
      PWD=PWD + V(I)*PWDL
      PDP=PDP + V(I)*PDPL
52  CONTINUE
      PWD=PWD*A
      PDP=PDP*A
48  RETURN
      END
C
C *****
C
C   Coefficient needed in evaluating Mathieu functions
C
      SUBROUTINE COEFF(Q,N,AF,II,AAO,AA)
      IMPLICIT REAL*8 (A-H,O-Z)
      DIMENSION VV(50),FA(50),AF(50),AA(50)
      IF (Q.LT.1.5D-7) THEN
        IF (N.EQ.1) THEN
          AAO=SQRT(2.0)/2.0
          DO 501 I=1,10
            IFAC=I
            CALL FACTORIAL(IFAC,FAC)
RF=FAC
            IFAC=I+1
            CALL FACTORIAL(IFAC,FAC)
            R1F=FAC
            TQ=Q/4
            AFAC=2*TQ**I/RF**2
            BFAC=2*I*(3*I+4)*TQ**(I+2)/R1F**2
            AA(2*I)=(-1)**I*(AFAC-BFAC)*AAO
501      CONTINUE
          ENDIF
          GO TO 502
        ENDIF
        II=50
        VV(1)=AF(N)/Q
        VV(2)=- (4.0/Q)*(1.0-(AF(N)/4.0)+Q**2/(2.0*AF(N)))
        DO 2 I=3,II
          VV(I)=(1.0/Q)*(AF(N)-4.0*(I-1)**2)-(1.0/VV(I-1))
          IF (DABS(VV(I)).GT.DABS(VV(I-1))) GO TO 999
2      CONTINUE
999  II=I-1
      FA(1)=VV(1)
      DO 4 I=2,II
        FA(I)=VV(I)*FA(I-1)
4      CONTINUE
      SUM=2.0D+00
      DO 6 I=1,II
        SUM=SUM+FA(I)**2
6      CONTINUE
      AAO=1.0D+00/DSQRT(SUM)
      DO 8 I=1,II

```

```

      AA(2*I,=FA(I)*AAO
2      CONTINUE
502     RETURN
      END

C
C      *****
C
C      Calculates a constant portion of the formula for Mathieu functions
C
      SUBROUTINE P2N(N,AAO,AA,II,P)
      IMPLICIT REAL*8 (A-H,O-Z)
      DIMENSION AA(50),P(50)
      Z1=0.0D+00
      Z2=1.5707963270D+00
      C1=AAO
      C2=AAO
      DO 10 I=1,II
          C1=C1 + AA(2*I)*DCOS(2*I*Z1)
          C2=C2 + AA(2*I)*DCOS(2*I*Z2)
10      CONTINUE
      P(N)=C1*C2/AAO**2
      RETURN
      END

C
C      *****
C
C      This subroutine evaluates the real, even, periodic Mathieu
C      function of integer order.
C
      SUBROUTINE FNCE(Z,II,N,AAO,AA,CE)
      IMPLICIT REAL*8 (A-H,O-Z)
      DIMENSION AA(50),CE(50)
      SUM=AAO
      DO 12 I=1,II
          SUM=SUM + AA(2*I)*DCOS(2*I*Z)*(-1)**I
12      CONTINUE
      CE(N)=(-1)**(N-1)*SUM
      RETURN
      END

C
C      *****
C
C      This subroutine evaluates the modified Mathieu function of first
C      kind of integer order and its derivative
C
      SUBROUTINE FNCCE(Z,II,N,AAO,AA,CCE,CCEP)
      IMPLICIT REAL*8 (A-H,O-Z)
      DIMENSION AA(50),CCE(50),CCEP(50)
      SUM=AAO
      SUMP=0
      DO 14 I=1,II
          SUM=SUM + AA(2*I)*DCOSH(2*I*Z)*(-1)**I
          SUMP=SUMP+2*I*AA(2*I)*DSINH(2*I*Z)*(-1)**I
14      CONTINUE
      CCE(N)=(-1)**(N-1)*SUM
      CCEP(N)=(-1)**(N-1)*SUMP
      RETURN

```

```

      END
C
C *****
C
C This subroutine evaluates the modified Mathieu function of second
C kind of integer order and its derivative
C
      SUBROUTINE FNFEEK(Q,Z,II,N,P,AAO,AA,FEK,FEKP)
      IMPLICIT REAL*8 (A-H,O-Z)
      DIMENSION AA(50),BSI(50),BK(50),P(50),FEK(50),
+ FEKP(50),BSIP(50),BKP(50),BKE(50)
      EXTERNAL DBSINS,DBSKS,DBSKES
      V1=DSQRT(Q)*DEXP(-Z)
      V2=DSQRT(Q)*DEXP(Z)
      K=II+2
      ZNU=0
      CALL DBSINS(V1,K,BSI)
      IF (V2.GT.1.778E+2) THEN
        DO 320 I=1,K
          BK(I)=0.0D+00
320      CONTINUE
      ELSE
        CALL DBSKS(ZNU,V2,K,BK)
      ENDIF
      SUM=AAO*BSI(1)*BK(1)
      BSIP(1)=BSI(2)*(-V1)
      BKP(1)=-BK(2)*V2
      SUMP=AAO*(BSIP(1)*BK(1) + BSI(1)*BKP(1))
      DO 16 I=2,K-1
        SUM=SUM+AA(2*I-2)*BSI(I)*BK(I)
        BSIP(I)=((I-1)*BSI(I)/V1 + BSI(I+1))*(-V1)
        BKP(I)=((I-1)*BK(I)/V2 - BK(I+1))*V2
        SUMP=SUMP + AA(2*I-2)*(BSIP(I)*BK(I) + BSI(I)*BKP(I))
16      CONTINUE
      FEK(N)=(-1)**(N-1)*P(N)*SUM/3.141592654
      FEKP(N)=(-1)**(N-1)*P(N)*SUMP/3.141592654
      RETURN
      END
C
C *****
C
      SUBROUTINE FACTORIAL(IFAC,FAC)
      IMPLICIT REAL*8 (A-H,O-Z)
      FAC=1
      DO 508 IF=1,IFAC
        FAC=FAC*IF
508      CONTINUE
      RETURN
      END

```

=====

Sample Data Files for Radial, Elliptical, Linear and Spherical Geometries

=====

** Input Data For Composite Reservoir In Radial Flow Geometry

** -----

```

** Enter Code For Inner Boundary Condition (IBC)
** (Constant Rate = 1, Constant Pressure = 2)
1
** Enter Code For Outer Boundary Condition (IOBC)
** (Infinite = 1, Closed = 2, Constant Pressure = 3)
1
** Enter Dimensionless Wellbore Storage, Skin (CD,SKIN)
0.0,0.0
** Enter Mobility Ratio(Region 1/Region 2) (AMOB)
10.
** Enter Storativity Ratio(Region 1/ Region 2) (STO)
10.
** Enter Dimensionless Distance To Discontinuity (RD)
100.
** Enter Dim. Distance To Outer Boundary, If Not Infinite (RED)
100000.
** Enter Number Of Cycles (NC)
8
** Enter First Dimensionless Time (TD1)
100.
** Enter Number Of Terms Needed In Laplace Inverter (NTERM)
8
=====
** Input Data For Composite Reservoir In Elliptical Flow Geometry
** -----
** Enter Code For Inner Boundary Condition (IBC)
** (Constant Rate = 1, Constant Pressure = 2)
2
** Enter Code For Outer Boundary Condition (IOBC)
** (Infinite = 1, Closed = 2, Constant Pressure = 3)
1
** Enter Dimensionless Wellbore Storage, Skin (CD,SKIN)
0.0,0.0
** Enter Mobility Ratio(Region 1/Region 2) (AMOB)
10.
** Enter Storativity Ratio(Region 1/ Region 2) (STO)
10.
** Enter Elliptic Distance To Discontinuity (EPSO)
2.
** Enter Elliptic Distance To Outer Boundary, If Not Infinite (EPSE)
7.907755279d+00
** Enter Number Of Cycles (NC)
7
** Enter First Dimensionless Time (TD1)
0.1
** Enter Number Of Terms Needed In Laplace Inverter (NTERM)
8
=====
** Input Data For Composite Reservoir In Linear Flow Geometry
** -----
** Enter Code For Inner Boundary Condition (IBC)
** (Constant Rate = 1, Constant Pressure = 2)
2
** Enter Code For Outer Boundary Condition (IOBC)
** (Infinite = 1, Closed = 2, Constant Pressure = 3)
2
** Enter Dimensionless Wellbore Storage, Skin (CD,SKIN)
0.0,0.0

```

```

** Enter Mobility Ratio(Region 1/Region 2) (AMOB)
1.
** Enter Storativity Ratio(Region 1/ Region 2) (STO)
1.
** Enter Dimensionless Distance To Discontinuity (AD)
100.
** Enter Dim. Distance To Outer Boundary, If Not Infinite (NDE)
10000.
** Enter Number Of Cycles (NC)
11
** Enter First Dimensionless Time (TD1)
10
** Enter Number Of Terms Needed In Laplace Inverter (NTERM)
5
=====
** Input Data For Composite Reservoir In Spherical Flow Geometry
** -----
** Enter Inner Boundary Condition(IBC)
** (Constant Rate = 1, Constant Pressure = 2)
1
** Enter Outer Boundary Condition(IOBC)
** (Infinite = 1, Closed = 2, Constant Pressure = 3)
1
** Enter Dimensionless Wellbore Storage, Skin (CD,SKIN)
0.0,0.0
** Enter Mobility Ratio(Region 1/Region 2) (AMOB)
1.
** Enter Storativity Ratio(Region 1/ Region 2) (STO)
1.
** Enter Dimensionless Distance To Discontinuity(AD)
100.
** Enter Dim. Distance To Outer Boundary, If Not Infinite (RDE)
10000.
** Enter Number Of Cycles(NC)
10
** Enter First Dimensionless Time(TD1)
100.
** Enter Number Of Terms Needed In Laplace Inverter(NTERM)
12

```

Appendix B

Derivation of Diffusivity Equation and Its Solution for the Intermediate Region with Power Law Property Variation

The diffusivity equation for the intermediate region is given as:

$$\frac{1}{r} \frac{\partial}{\partial r} \left(\left(\frac{k}{\mu} \right)_2 r \frac{\partial p_2}{\partial r} \right) = (\phi c_t)_2 \frac{\partial p_2}{\partial t}. \quad (\text{B-1})$$

Substituting dimensionless variables for pressure and radial distance in Eq. (B-1), one gets:

$$\frac{1}{r_D} \frac{\partial}{\partial r_D} \left(r_D \left(\frac{k}{\mu} \right)_2 \frac{\partial p_{D2}}{\partial r_D} \right) = (\phi c_t)_2 R^2 \frac{\partial p_{D2}}{\partial t}. \quad (\text{B-2})$$

where :

$$p_{D2} = \frac{2\pi k_1 h}{qB\mu_1} (p_i - p_2), \text{ and} \quad (\text{B-3})$$

$$r_D = \frac{r}{R_1}. \quad (\text{B-4})$$

The mobility, $(k/\mu)_2$, and storativity, $(\phi c_t)_2$, in the intermediate region are now allowed to vary in a power law relationship with radial distance from the first discontinuity boundary.

These conditions are represented as:

$$\left(\frac{k}{\mu} \right)_2 = \frac{(k/\mu)_1}{M_{12}} r_D^{-\theta}, \text{ and} \quad (\text{B-5})$$

$$(\phi c_t)_2 = \frac{(\phi c_t)_1}{F_{12}} r_D^{-\theta}, \quad (\text{B-6})$$

where θ_1 and θ_2 are the fractal exponents for the mobility and storativity variations, respectively, in the intermediate region.

Using Eqs. (B-5) and (B-6) in Eq. (B-2), one gets:

$$\frac{1}{r_D} \frac{\partial}{\partial r_D} \left(r_D^{1-\theta_1} \frac{(k/\mu)_1}{M_{12}} \frac{\partial p_{D2}}{\partial r_D} \right) = \frac{(\phi c_r)_1 R_1^2}{F_{12}} r_D^{-\theta_1} \frac{\partial p_{D2}}{\partial t} \quad (\text{B-7})$$

The dimensionless time, t_D , and diffusivity ratio, ω_{12} , are substituted into Eq. (B-7) to get:

$$\frac{1}{r_D} \frac{\partial}{\partial r_D} \left(r_D^{1-\theta_1} \frac{\partial p_{D2}}{\partial r_D} \right) = \omega_{12} r_D^{-\theta_1} \frac{\partial p_{D2}}{\partial t_D} \quad (\text{B-8})$$

where:

$$t_D = \frac{(k/\mu)_1 t}{(\phi c_r)_1 R_1^2}, \text{ and} \quad (\text{B-9})$$

$$\omega_{12} = \frac{M_{12}}{F_{12}}. \quad (\text{B-10})$$

Expanding and rearranging Eq. (B-8) gives the diffusivity equation in the fractal intermediate region as:

$$\frac{\partial^2 p_{D2}}{\partial r_D^2} + \frac{1-\theta_1}{r_D} \frac{\partial p_{D2}}{\partial r_D} = \omega_{12} r_D^{\theta_1-\theta_2} \frac{\partial p_{D2}}{\partial t_D} \quad (\text{B-11})$$

Eq. (B-11), which applies for $l \leq r_D \leq R_{D2}$, is a Bessel equation, whose solution is readily available in Laplace space. Taking the Laplace transform of Eq. (B-11), one gets:

$$\frac{d^2 \bar{p}_{D2}}{dr_D^2} + \frac{1-\theta_1}{r_D} \frac{d\bar{p}_{D2}}{dr_D} = \frac{\omega_{12} l}{r_D^{\theta_1-\theta_2}} \bar{p}_{D2} \quad (\text{B-12})$$

A solution to Eq. (B-12) is obtained by comparing it with the solution for the general Bessel equation. The general Bessel equation in Laplace space is given by Carslaw and Jaeger (1959) as :

$$\frac{d^2 \bar{v}}{dx^2} + \frac{n}{x} \frac{d\bar{v}}{dx} - \frac{q^2}{x^{n-m}} \bar{v} = 0. \quad (\text{B-13})$$

A solution to Eq. (B-13) is:

$$\bar{v} = A x^{-\frac{1}{2}(n-1)} K_v\left(\frac{2q}{m-n+2} x^{-\frac{1}{2}(m-n+2)}\right) + B x^{-\frac{1}{2}(n-1)} I_v\left(\frac{2q}{m-n+2} x^{-\frac{1}{2}(m-n+2)}\right), \quad (\text{B-14})$$

where:

$$v = \frac{1-n}{m-n+2}. \quad (\text{B-15})$$

Comparing Eqs. (B-12) and (B-13) yields:

$$\bar{p}_{D2} \equiv \bar{v}$$

$$r_D \equiv x$$

$$1-\theta_1 \equiv n$$

$$\omega_{D2} \equiv q^2$$

$$1-\theta_2 \equiv m$$

Upon examining Eq. (B-14), the equivalent solution to Eq. (B-12) is:

$$\bar{p}_{D2} = A r_D^\gamma K_v(\xi r_D^\beta) + B r_D^\gamma I_v(\xi r_D^\beta), \quad (\text{B-16})$$

which is the same as Eq. (6.28) in Chapter 6. The parameters γ , β , v , and ξ in Eq. (B-16) are defined by Eqs. (6.30) through (6.33), respectively.

For the present problem, the parameters are M_{12} , M_{13} , F_{12} , F_{13} , r_{wD} , R_{D2} , θ_1 and θ_2 . For thermal recovery operations, however, these parameters have to be chosen in such a way that the mobility ratio, as well as the storativity ratio between the intermediate and outer regions should be greater than or equal to 1.

The mobility ratio is defined as:

$$M_{23} = \frac{(k/\mu)_2}{(k/\mu)_3} \quad \text{at } r_D = R_{D2} \quad (\text{B-17})$$

Substituting Eq. (B-5) into Eq. (B-17) gives:

$$M_{23} = \frac{(k/\mu)_1 R_{D2}^{-\theta_1}}{M_{12} (k/\mu)_3}, \quad (\text{B-18})$$

which can be further simplified to yield:

$$M_{23} = \frac{M_{12}}{M_{12}} R_{D2}^{-\theta_1}. \quad (\text{B-19})$$

Thus, M_{12} , M_{13} , R_{D2} and θ_1 must be chosen in such a manner that $M_{23} \geq 1$.

Similarly, for storativity ratio, the relationship is:

$$F_{23} = \frac{F_{13}}{F_{12}} R_{D2}^{-\theta_1}. \quad (\text{B-20})$$

where:

$$F_{23} = \frac{(\phi c_t)_2}{(\phi c_t)_3} \quad \text{at } r_D = R_{D2} \quad (\text{B-21})$$

Here again, F_{12} , F_{13} , R_{D2} and θ_2 must be chosen in such a manner that $F_{23} \geq 1$.

Appendix C

Computer Program for Analytical Model of a Three-Region, Composite Reservoir With Power Law Property Variation in the Intermediate Region

This appendix gives the computer program for the analytical solution for a three-region infinite, radial, composite reservoir, with a power law variation of mobility and storativity in the intermediate region. The solution has been described in Chapter 6.

Source Code for Program: FRACTAL

```
C *****
C                                     Program Fractal
C
C   THREE-REGION COMPOSITE RESERVOIR WITH POWER LAW
C   PROPERTY VARIATION IN THE INTERMEDIATE REGION
C
C   Purpose of the program is to generate the
C   pressure transient response for a well in
C   a three-region radial composite reservoir,
C   where the intermediate region is represented
C   as a fractal.
C
C   Wellbore storage and skin at the well are neglected.
C
C   Well produces at a constant rate.
C
C   The outer boundary is considered infinite.
C
C *****
C   VARIABLE IDENTIFICATION LIST
C *****
C
C   AMOB12  -- MOBILITY RATIO (K1*MU2)/(K2*MU1)
C   AMOB23  -- MOBILITY RATIO (K2*MU3)/(K3*MU2)
C   CD      -- DIMENSIONLESS WELLBORE STORAGE
C   DIF12   -- DIFFUSIVITY RATIO (K1*PHICTMU2)/K2*PHICTMU1)
C   DIF13   -- DIFFUSIVITY RATIO (K1*PHICTMU3)/K3*PHICTMU1)
C   STO12   -- STORATIVITY RATIO (PHICT1/PHICT2)
C   STO13   -- STORATIVITY RATIO (PHICT1/PHICT3)
C   RWD     -- DIMENSIONLESS WELLBORE RADIUS
C   RD2     -- DIMENSIONLESS DISTANCE TO SECOND DISCONTINUITY
C   SK      -- SKIN FACTOR
C   THETA1  -- SPECTRAL EXPONENT FOR MOBILITY VARIATION
C   THETA2  -- SPECTRAL EXPONENT FOR STORATIVITY VARIATION
C
C   IMPLICIT REAL*8(A-H,O-Z)
C   DIMENSION TD(20)
C   COMMON M,CD,SK,AMOB12,AMOB23,DIF12,DIF13,RWD,RD2,
1  THETA1,THETA2
C
C
C   OPEN(UNIT=7,FILE='frac.d')
```

```

      READ(7,*)
      READ(7,*)
      READ(7,*)CD,SK
      READ(7,*)
      READ(7,*)AMOB12,AMOB13
      READ(7,*)
      READ(7,*)STO12,STO13
      READ(7,*)
      READ(7,*)RWD,RD2
      READ(7,*)
      READ(7,*)THETA1,THETA2
      READ(7,*)
      READ(7,*)NC
      READ(7,*)
      READ(7,*)TD1
      READ(7,*)
      READ(7,*)NTERM
      CLOSE (7)
C
      OPEN(UNIT=8,FILE='frac.o')
C
      M=777
      PI=2.0*ASIN(1.)
C      COMPUTE DIFFUSIVITY RATIO
      AMOB23=(AMOB13/AMOB12)*RD2**(-THETA1)
      DIF12=AMOB12/STO12
      DIF13=AMOB13/STO13
C
C      GENERATE THE FIRST SET OF TD VECTOR
C
      TD(1)=TD1
      TD(2)=1.5*TD1
      TD(3)=2.*TD1
      TD(4)=2.5*TD1
      TD(5)=3*TD1
      TD(6)=3.5*TD1
      TD(7)=4.*TD1
      TD(8)=4.5*TD1
      TD(9)=5.*TD1
      TD(10)=6.*TD1
      TD(11)=7.*TD1
      TD(12)=8.*TD1
      TD(13)=9.*TD1
C
C      -----
C      GENERATE AND PRINT THE TRANSIENT PRESSURE OR RATE RESPONSE
C
      DO 1 I=1,NC
      DO 2 J=1,13
      TIME=TD(J)
      CALL INVERT(TIME,NTERM,PWD,PDP)
      PDPTD=PDP*TIME
      WRITE(8,17)TIME,PWD,PDP,PDPTD
2      TD(J)=10.*TD(J)
1      CONTINUE
17     FORMAT(' ',T5,E10.4,T20,E10.4,T35,E10.4,T50,E10.4)
13     FORMAT(2X,A)
      STOP
      END

```

```

C
C *****
C
SUBROUTINE LAP(S,PWDL,PDPL)
IMPLICIT REAL*8(A-H,O-Z)
DIMENSION B(20),BK(20)
COMMON M,CD,SK,AMOB12,AMOB23,DIF12,DIF13,RWD,RD2,
1 THETA1,THETA2

C
C THREE-REGION RADIAL COMPOSITE SYSTEM SOLUTION IN
C LAPLACE SPACE, WITH POWER LAW PROPERTY VARIATION
C
C SOME PARAMETERS OF POWER LAW RELATION
C
    GAM=THETA1/2.
    BET=(THETA1-THETA2 + 2.)/2.
    XNU=THETA1/(THETA1-THETA2 + 2.)
    XI =DSQRT(S*DIF12)/BET

C
C COMPUTE THE ARGUMENTS OF BESSEL FUNCTIONS
C
    ARG1=DSQRT(S)
    ARG2=RWD*DSQRT(S)
    ARG3=XI
    ARG4=XI*RD2**BET
    ARG5=RD2*DSQRT(S*DIF13)

C
C FACTORS FOR CONVERTING EXPONENTIALLY-SCALED
C BESSEL FUNCTIONS
C
    IF (ARG1.LE.170.) THEN
        F1=DEXP(ARG1)
    ELSE
        F1=DEXP(170.0D00)
    ENDIF
    IF (ARG2.LE.170.) THEN
        F2=DEXP(ARG2)
    ELSE
        F2=DEXP(170.0D00)
    ENDIF
    IF (ARG3.LE.170.) THEN
        F3=DEXP(ARG3)
    ELSE
        F3=DEXP(170.0D00)
    ENDIF
    IF (ARG4.LE.170.) THEN
        F4=DEXP(ARG4)
    ELSE
        F4=DEXP(170.0D00)
    ENDIF
    IF (ARG5.LE.170.) THEN
        F5=DEXP(ARG5)
    ELSE
        F5=DEXP(170.0D00)
    ENDIF

C
C COMPUTE NEEDED BESSEL FUNCTIONS OF INTEGER ORDER
C

```

```

      A1=BESEI0(ARG1)*F1
      A2=BESEI0(ARG2)*F2
C
      B1=BESEI1(ARG1)*F1
      B2=BESEI1(ARG2)*F2
C
      D1=BESEK0(ARG1)/F1
      D2=BESEK0(ARG2)/F2
      D3=BESEK0(ARG5)/F5
C
      E1=BESEK1(ARG1)/F1
      E2=BESEK1(ARG2)/F2
      E3=BESEK1(ARG5)/F5
C
C   COMPUTE NEEDED BESSEL FUNCTIONS OF FRACTIONAL ORDER
C
      NB=2
      IZE=2
C
      IF (XNU.GT.0.) THEN
        ALPHA=XNU
        CALL RIBESL(ARG3,ALPHA,NB,IZE,B,NCALC)
        P1=B(1)*F3
        P2=B(2)*F3
C
        CALL RIBESL(ARG4,ALPHA,NB,IZE,B,NCALC)
        P3=B(1)*F4
        P4=B(2)*F4
C
        CALL RKBESL(ARG3,ALPHA,NB,IZE,BK,NCALC)
        Q1=BK(1)/F3
        Q2=BK(2)/F3
C
        CALL RKBESL(ARG4,ALPHA,NB,IZE,BK,NCALC)
        Q3=BK(1)/F4
        Q4=BK(2)/F4
      ELSE
        P1=BESEI0(ARG3)*F3
        P3=BESEI0(ARG4)*F4
        Q1=BESEK0(ARG3)/F3
        Q3=BESEK0(ARG4)/F4
      ENDIF
C
C   COMPUTE DERIVATIVE OF BESSEL FUNCTIONS OF FRACTIONAL ORDER
C
      IF (XNU.GT.0.) THEN
        P1P= XNU*P1/ARG3 + P2
        Q1P= XNU*Q1/ARG3 - Q2
        P3P= XNU*P3/ARG4 + P4
        Q3P= XNU*Q3/ARG4 - Q4
      ELSE
        P1P=BESEI1(ARG3)*F3
        P3P=BESEI1(ARG4)*F4
        Q1P=-BESEK1(ARG3)/F3
        Q3P=-BESEK1(ARG4)/F4
      ENDIF
C
C   COMPUTATION OF COEFFICIENTS OF EQUATIONS. FOR C1 AND C2

```

```

C      AL11 = -ARG2*B2
      AL12 = ARG2*E2
      AL21 = A1
      AL22 = D1
      AL23 = -P1
      AL24 = -Q1
      AL31 = -AMOB12*ARG1*B1
      AL32 = AMOB12*ARG1*E1
      AL33 = P1*GAM + P1P*BET*XI
      AL34 = Q1*GAM + Q1P*BET*XI
      AL43 = P3*RD2**GAM
      AL44 = Q3*RD2**GAM
      AL46 = -D3
           T1=P3*GAM*RD2** (GAM - 1.)
           T2=P3P*BET*XI*RD2** (GAM + BET - 1.)
      AL53 = -AMOB23*(T1 + T2)
           T1=Q3*GAM*RD2** (GAM - 1.)
           T2=Q3P*BET*XI*RD2** (GAM + BET - 1.)
      AL54 = -AMOB23*(T1 + T2)
      AL56 = -DSQRT(S*DIF13)*E3

C
C      CALCULATION OF C1 AND C2
C
      S1=AL56*AL43-AL46*AL53
      S2=AL56*AL44-AL46*AL54
      S3=(S2*AL23 - S1*AL24)/S2
      S4=(S2*AL33 - S1*AL34)/S2
      S5=-(S4*AL22 - S3*AL32)/(S4*AL21 - S3*AL31)

C
      C1 = S5/((S5*AL11 + AL12)*S)
      C2 = 1./((S5*AL11 + AL12)*S)

C
C      CALCULATION OF TRANSFORMED SOLUTION
C      PWDL = LAPLACE TRANSFORM OF PWD
C
      PWDL= C1*A2 + C2*D2
      PDPL=PWDL*S

C
C      Adding wellbore storage and skin effects to the
C      constant-rate solution
C
      IF (CD.GT.0.OR.SK.GT.0) THEN
          PWDL=(S*PWDL + SK)/(S*(1 + CD*S*(S*PWDL + SK)))
          PDPL=PWDL*S
      ENDIF

C
      RETURN
      END

C
C      *****
C
C      THE STEHFEST ALGORITHM
C      -----
C
      SUBROUTINE INVERT(TD,NL,PWD,PDP)
      IMPLICIT REAL*8 (A-H,O-Z)
      COMMON M,CD,SK,AMOB12,AMOB23,DIF12,DIF13,RWD,RD2,

```



```

1 THETA1,THETA2
  DIMENSION G(50),V(50),H(25)

C
C      NOW IF THE ARRAY V(I) WAS CALCULATED PREVIOUSLY, THE
C      PROGRAM GOES DIRECTLY TO THE END OF THE SUBROUTINE TO
C      CALCULATE F(S).
  IF (NL.EQ.M) GO TO 47
  M=NL
  DLOGTW=0.6931471805599D+00
  NH=NL/2

C
C      THE FACTORIALS OF 1 TO NL ARE CALCULATED INTO G.
  G(1)=1
  DO 31 I=2,NL
    G(I)=G(I-1)*I
31 CONTINUE

C
C      TERMS WITH K ONLY ARE CALCULATED INTO ARRAY H
  H(1)=2.0/G(NH-1)
  DO 36 I=2,NH
    FI=I
    IF (I-NH) 34,35,36
34    H(I)=FI**NH*G(2*I)/(G(NH-I)*G(I)*G(I-1))
    GO TO 36
35    H(I)=FI**NH*G(2*I)/(G(I)*G(I-1))
36 CONTINUE

C
C      THE TERMS (-1)**NH+1 ARE CALCULATED.
C      FIRST THE TERM FOR I=1
  SN=2*(NH-NH/2*2) -1

C
C      THE REST OF THE SN'S ARE CALCULATED IN THE MAIN ROUTINE
C      THE ARRAY V(I) IS CALCULATED.
  DO 37 I=1,NL

C
C      FIRST SET V(I)=0
  V(I)=0.0

C
C      THE LIMITS OF K ARE ESTABLISHED.
C      THE LOWER LIMIT FOR K1=INTEG((I+1/2))
  K1=(I+1)/2

C
C      THE UPPER LIMIT IS K2=MIN(I,NL/2)
  K2=I
  IF (K2-NH) 38,38,39
39  K2=NH

C
C      THE SUMMATION TERM IN V(I) IS CALCULATED
38  DO 40 K=K1,K2
    IF (2*K-I) 42,43,42
42    IF (I-K) 41,44,41
41    V(I)=V(I)+H(K)/(G(I-K)*G(2*K-I))
    GO TO 40
43    V(I)=V(I)+H(K)/G(I-K)
    GO TO 40
44    V(I)=V(I)+H(K)/G(2*K-I)
40 CONTINUE
C

```

```

C          THE V(I) ARRAY IS FINALLY CALCULATED BY WEIGHTING
C          ACCORDING TO SN
          V(I)=SN*V(I)
C
C          THE TERM SN CHANGES ITS SIGN EACH ITERATION.
          SN=-SN
37        CONTINUE
C
C          THE NUMERICAL APPROXIMATION IS CALCULATED.
C
47        PWD=0.0D+00
          PDP=0.0D+00
          A=DLOGTW/TD
          DO 52 I=1,NL
            ARG=A*I
            CALL LAP(ARG,PWDL,PDPL)
            PWD=PWD + V(I)*PWDL
            PDP=PDP + V(I)*PDPL
52        CONTINUE
          PWD=PWD*A
          PDP=PDP*A
48        RETURN
          END

```

=====

Sample Data File for the Three-Region, Radial, Composite Reservoir Program

=====

```

**  DATA FILE FOR A THREE-REGION FRACTAL COMPOSITE RESERVOIR
**  ENTER DIMENSIONLESS WELLBORE STORAGE AND SKIN (CD  and SK)
    0.    0.
**  ENTER MOBILITY RATIOS (1 by 2 and 1 by 3)
    10.   1000.
**  ENTER STORATIVITY RATIOS (1 by 2 and 1 by 3)
    10.   1000.
**  ENTER WELLBORE DISTANCE AND SECOND DISC. DIST. ( RWD and RD2)
    .01    5.
**  ENTER SPECTRAL EXPONENT FOR MOBILITY AND STORATIVITY(Theta)
    2.     1.
**  ENTER NUMBER OF CYCLES
    14
**  ENTER FIRST DIMENSIONLESS TIME
    .01
**  ENTER NUMBER OF TERMS NEEDED IN LAPLACE INVERTER
    8

```